DYNAMIN-MEDIATED MEMBRANE FISSION

Sandrine Morlot

UNIVERSITÉ DE GENÈVE

PARIS DIDEROT

Faculté des Sciences
Département de Biochimie

Matière Condensée et Interfaces
ED 518

Dynamin-Mediated Membrane Fission

THÈSE

présentée et soutenue publiquement le 11 juin 2012

pour l'obtention du

Doctorat de l'Université Paris Diderot - PARIS 7
Doctorat de l'Université de Genève

(spécialités Physique et Biochimie)

par

Sandrine MORLOT

Composition du jury

Président :	Marcos GONZALEZ-GAITAN
Rapporteurs :	Pierre SENS David TARESTE
Examinateurs :	François GALLET Harvey McMAHON
Directeurs de Thèse :	Patricia BASSEREAU Aurélien ROUX

PhysicoChimie Curie, UMR 168

institutCurie
Together, let's beat cancer.

Résumé

La cellule eucaryote est organisée en plusieurs compartiments appelés organelles. Ces organelles et la cellule elle-même sont délimités par des membranes lipidiques qui assurent leur intégrité. Les échanges spécifiques entre organelles requièrent de déformer les membranes pour générer des intermédiaires de transport. La formation de ces intermédiaires à la membrane plasmique, enveloppe de la cellule, s'appelle l'endocytose dont un exemple classique est l'endocytose médiée par la Clathrine. La membrane plasmique est déformée localement en bourgeons par des protéines. Ces bourgeons sont séparés de la membrane plasmique par une étape de fission, qui consiste en la rupture du cou des bourgeons. La fission membranaire est donc une étape clé de l'endocytose pendant laquelle se produit un changement topologique de la surface fermée de membrane. La Dynamine est une protéine dont la fonction a été reliée génétiquement et biochimiquement à la fission membranaire pendant l'endocytose. Des expériences de microscopie électronique ont montré que la Dynamine est capable de déformer les membranes en nanotubes en polymérisant en hélice droite autour de ces tubes. Le rayon externe de l'hélice mesure 50 nm et son pas 13 nm. L'hydrolyse de guanosine triphosphate (GTP) par la Dynamine induit une réduction du rayon (40 nm) et du pas de l'hélice (9 nm), mettant en évidence un mécanisme de constriction. Cette activité est observable en temps réel *in vitro* : en attachant une microbille au polymère de Dynamine, un mouvement de rotation de la bille autour du tube lipidique est observable après injection de GTP et consécutivement à la torsion produite par la constriction. Cependant la constriction générée par la Dynamine ne suffit pas pour produire de la fission. En effet des reconstructions 3D de l'hélice de Dynamine ont montré que le tube de membrane reste stable aprés constriction. L'objet de cette thèse est d'étudier les paramètres mécaniques et énergétiques de l'activité de la Dynamine conduisant à la fission membranaire.

Dans un premier temps, la dynamique de la constriction générée par la Dynamine est étudiée en suivant la rotation de plusieurs billes attachées le long d'un même tube membranaire recouvert de Dynamine. Ces expériences nous ont permis de quantifier précisemment l'activité de torsion le long du polymère de Dynamine. Le nombre de rotations est linéaire avec la position sur l'hélice. La vitesse de rotation diminue de manière exponentielle. Le profil des vitesses de rotation le long du tube est sinusoidal. Le temps caractéristique d'amortissement de la vitesse de rotations augmente avec la racine carée de la longueur du tube. Ces mesures expérimentales sont en accord avec un modèle hydrodynamique décrivant la dynamique des déformations de tubes de membrane décorés de Dynamine. En effet, il a été prédit qu'à des échelles de temps observables, la dynamique de la constriction générée par la Dynamine est dominée par la friction entre la membrane lipidique et l'hélice protéique. Le comportement diffusif attendu est bien vérifié expérimentalement. Cette étude permet de donner une description quantitative de la dynamique de constriction de la Dynamine. En particulier, il est démontré que la constriction se déroule à l'échelle de 100 ms alors que les événements de fission prennent 1 à 10 s. Ce constat nous a menés à étudier le mécanisme de fission membranaire plus en détails.

Dans un second temps, la localisation et la cinétique du processus de fission membranaire ont été étudiées à l'aide d'un montage expérimental combinant pince optique, micropipettes et microscopie confocale. Une vésicule géante unilamellaire (GUV) est maintenue dans une micropipette fixant ainsi sa tension membranaire. Un nanotube de lipides est extrait de la GUV à l'aide d'une bille micrométrique piégée dans une pince optique. Le rayon du nanotube est calculé à partir de la tension de membrane et de la force exercée pour maintenir le tube. Les rayons obtenus varient de 10 à 100 nm. Une seconde micropipette injecte localement près du tube de la Dynamine et du GTP. La polymérisation de la Dynamine sur le tube de membrane est suivie par imagerie confocale de fluorescence. La fission du tube est observée quelques secondes après le début de la polymérisation en présence de GTP. En absence de GTP ou en présence d'un analogue non hydrolysable (par exemple $GTP\gamma S$), la Dynamine polymérise mais ne casse pas le tube, confirmant ainsi que la fission membranaire requiert l'hydrolyse de GTP. J'ai constaté que le taux de fission est plus élevé dans les régions membranaires les plus courbées: aux interfaces bille-tube et tube-GUV. Plus précisemment, la fission du tube se produit à l'interface entre le polymère de Dynamine et la portion libre du tube de membrane. Cette localisation suggère que la fission est favorisée par l'énergie élastique liée à la différence de courbure entre la partie recouverte de Dynamine et la partie libre. Un modèle à une barrière d'énergie a été déduit de ce constat. La barriére energétique de fission est calculée comme la différence d'energie élastique entre un état intermédiaire d'hémifission et un état initial où le tube est partiellement recouvert de Dynamine. Ce modéle prédit la dépendance du temps de fission avec les paramètres élastiques de la membrane (tension et rigidité). Ces prédictions ont été vérifiées expérimentalement: le temps de fission moyen décroit quand la tension augmente (*in vitro* et *in cellulo*) et quand la rigidité diminue. Ce modèle prend également en compte le couple exercé par la Dynamine pour contraindre le tube. Ce couple, évalué entre 730 et 1100 pN.nm à l'aide de pinces magnétiques, réduit la barrière énergétique de fission, évaluée autour de 70 $k_B T$.

Ce travail de thèse a permis d'élaborer un modèle de fission membranaire. La constriction générée par la Dynamine permet de réduire la barrière énergétique de la fission membranaire mais ne suffit pas à elle seule pour provoquer la rupture du tube. En effet il faut réunir plusieurs paramètres pour assurer la fission. Les propriétés élastiques de la membrane jouent notamment un rôle primordial dans le mécanisme de fission. Ces prérequis pour la fission concordent avec les observations faîtes dans la cellule et peuvent être généralisés à d'autres mécanismes de fission.

Abstract

The eucaryotic cell is organized in several compartments named organelles. These organelles and the cell itself are delimited by lipid membranes. The fission of these membranes is required for the vesicular traffic between organelles. Endocytosis is the mechanism of vesicular traffic from the plasma membrane towards other organelles inside the cell. Dynamin is a guanosine triphosphatase implicated in vesicle scission during Clathrin-mediated endocytosis. It polymerizes into a helix at the neck of endocytic buds. Upon guanosine triphosphate hydrolysis (GTP), conformational changes modify the helical structure: the inner radius of the Dynamin-coated tube decreases from 10 to 5 nm and the helical pitch reduces from 13 to 9 nm. These modifications show that fission proceeds through a constriction mechanism. The dynamics of Dynamin constriction is investigated by attaching microbeads along Dynamin-coated tubes and by monitoring the beads' rotations after GTP addition. I found that the deformation of Dynamin helices is highly concerted and damped by the friction between membrane and Dynamin. However constriction is not enough to trigger fission. To further understand the fission reaction, Dynamin polymerization and fission are studied on lipid nanotubes extruded from Giant Unilamellar Vesicles. My work shows that fission occurs at the edge of the Dynamin helix, where the membrane is strongly curved. A statistical analysis of fission time reveals that the fission reaction can be modelled by a single step rate-limiting energy barrier. The fission time dependence on membrane tension, membrane rigidity and torque is established theoretically and validated experimentally. Dynamin torque is evaluated between 730 and 1100 pN.nm. The relevance of the tension dependence is confirmed *in vivo*. This work allows to give a quantitative picture of the energy landscape of Dynamin-mediated fission: the height of the energy barrier of fission is estimated around 70 $k_B T$.

Remerciements

Au cours de cette thèse, j'ai eu la chance de côtoyer deux mondes bien différents: les physiciens de la montagne Sainte Geneviève et les biologistes des Alpes suisses. Un déménagement en milieu de thèse est souvent une épreuve difficile. En ce qui me concerne, le bilan est plus que positif. Ce fut l'occasion de rencontres enrichissantes tant sur le plan scientifique qu'humain.

Je remercie en premier lieu mes deux directeurs de thèse: Aurélien Roux et Patricia Bassereau. Vous avez tout mis en oeuvre pour que ma thèse se déroule au mieux malgré la "séparation". Patricia, tu as suivi mon travail en me donnant toujours de bons conseils. Partager ton bureau aura été une expérience très instructive! Aurélien, tu m'a confié un beau projet avec le juste dosage entre encadrement et liberté. Tu as su rendre contagieux ton enthousiasme et ta passion pour la recherche. Merci également à vous deux pour m'avoir envoyée vers des destinations de rêves lors de conférences et de collaborations scientifiques: l'Utah, l'Australie, la Corse, la côte est des Etats-Unis, la Californie, la Suisse!

Cette thèse n'aurait pas abouti sans l'aide des théoriciens qui ont su donner du sens à mes expériences. Martin Lenz m'a accompagnée dès le début dans l'aventure de la Dynamine. Luis Dinis nous a rejoint en route. Tous les deux ont fortement contribué à me faire franchir la barrière énergétique de la thèse. Je remercie également Jean-François Joanny et Jacques Prost pour leur fructueuse participation. J'ai également eu le plaisir d'intéragir avec Marius Klein et Giovanni Cappello qui ont développé avec brio un montage expérimental permettant de mesurer le couple de la Dynamine. Je tire mon chapeau à John Manzi et Frédéric Humbert pour m'avoir fourni en protéines avec une grande efficacité (je parle de Dynamine bien sûr).

Je remercie les membres du jury pour avoir pris le temps d'évaluer mon travail et s'être déplacés pour assister à ma soutenance: Marcos Gonzalez-Gaitan, François Gallet, Harvey McMahon, Pierre Sens et David Tareste.

Les collègues de labo aussi bien à Paris qu'à Genève furent une deuxième famille pour moi. Je dois beaucoup à Benoit Sorre et Nicolas Chiaruttini pour leur expertise en microscopie et surtout leur amitié, aligner des miroirs dans le noir, c'est plus sympa avec des copains! Nico, merci aussi pour avoir relu ce manuscrit. Merci Mahassine et Sophie pour les longues discussions aux Pantalon/Mayflower/Bombardier et les séances de stepmania. Mon éternelle gratitude revient à Sylvain qui fut l'un des premiers à m'accueillir sur Suisse. Double big up à Ludwig qui connaît les deux faces de mon doctorat. Ah Alice ma chère voisine, que serais-je sans toi? Je tiens aussi à rendre hommage à l'ADIC, en particulier à Ana, Aurèle et Maxime avec qui j'ai partagé beaucoup de bons momments pour préparer les congrès YRLS, la retraite en Angleterre et les soirées! Et un grand merci à Gil, Pierre, Saleem, Darius, Bidisha, Clément, Alessia, Thomas, Alice, Coline, Ayako, François, Matthias, Karine, Valentina, Alejandro, Guillaume, Manu, Sabine, Carole, Sarah, Charlotte, Chrystelle, Laurent, Auxi, Aurélie, Natasha.

Enfin je remercie les amis et la famille qui m'ont soutenue pendant ces quatre années. Tout d'abord, un grand merci à toute la bande de Nogent: Juliette, Célie, Malo, Keke, Tino, Vincent, Guillaume, Annabelle, Emilie, Romary... merci pour les fabuleux weekends à la campagne, les bons repas, les concerts, et surtout les cours de ski, maintenant j'impressionne presque les Suisses (euh en fait non...). Pour David, Résistance! Jess et Tibo, vous êtes maintenant presqu'autant experts que moi en Dynamine mais préparez-vous pour mon prochain thème! Arrivent ensuite les amis suisses et savoyards en particuliers les grimpeurs, les nageurs du Rhone et les plongeurs, vous m'avez fait prendre l'air (et l'eau) quand j'en avais grandement besoin. Pour terminer, je remercie Evelyne, Marc-Antoine et mes parents, cette thèse vous est dédiée.

Contents

List of Notations

ATP	adenosine triphosphate
BSE	bundle signalling element
CME	clathrin-mediated endocytosis
DIC	differential interference contrast
DRP	dynamin-related proteins
GED	guanosine triphosphatase effector domain
GTP	guanosine triphosphate
GTPγS	guanosine 5'-O-(gamma-thio)triphosphate
GUV	giant unilamellar vesicle
Γ	torque (in N.m)
J	mean curvature
K	Gaussian curvature
κ	bending rigidity modulus (in J or $k_B T$)
k_B	Boltzmann constant, $k_B = 1.38\ 10^{-23} J.K^{-1}$
l_d	liquid-disordered
l_o	liquid-ordered
NFA-GalCer	non-hydroxylated fatty acid galactoceramide
P	pressure (in Pa)
PC	phosphatidylcholine
PH	pleckstrin homology
PIP_2	phosphatidylinositol 4,5-bisphosphate
PRD	prolin rich domain
PS	phosphatidylserine
R_c	radius of the constricted Dynamin-coated tube
R_i	tube radius of the hemifission state
R_u	radius of the unconstricted Dynamin-coated tube
σ	membrane tension (in $N.m^{-1}$)
SM	sphingomyelin
T	temperature (in K)
τ_f	fission time (in s)
TGN	Trans-Golgi Network
ω	rotation speed (in $rad.s^{-1}$)

Chapter 1

General Introduction

Lipid membranes are essential to the eucaryotic cell since they delimit the cellular compartments, named organelles, and ensure their specificity. Membranes are auto-sealable, thus their rupture is unfavourable energetically. However communication between organelles is necessary for the cell survival and requires specific exchanges of materials. Membrane fission is a mandatory step to generate vesicles during intracellular traffic. Dynamin is a guanosine triphosphatase implicated in membrane fission in many cellular processes. In particular, Dynamin is required for vesicle release during Clathrin-mediated endocytosis. It polymerizes into a helix at the neck of endocytic bud. Structural data show a constriction of the helix upon GTP hydrolysis. It suggests that Dynamin converts the chemical energy of GTP hydrolysis into mechanical work which would lead eventually to fission. The details of this mechanism remain largely unravelled so far and have been investigated during this thesis.

The first three chapters (chapters 2 to 4) constitute an introduction to the field of Dynamin-mediated fission. In chapter 2, two fundamental properties of biological membranes are introduced: self-assembling and their ability to deform. I will at the same time describe the Clathrin-mediated endocytosis: a Dynamin-dependent cellular mechanisms which requires membrane remodelling at different stages. A physical model of membrane is then explained in chapter 3. The theory developed by Canham and Helfrich allows to correlate the energy of a membrane to its shape. Experiments testing this theory will be detailed: the micropipette aspiration and the nanotube extrusion. Chapter 4 reviews the main properties of Dynamin. Finally, I present a review we published in FEBS Letters in 2009 to summarize the current knowledge about membrane fission and underline what remains not understood in this mechanism.

Chapters 5 and 6 detail the results obtained during this thesis. A quantitative description of Dynamin constriction is presented in chapter 5. Chapter 6 explains how the membrane shape regulates Dynamin-mediated fission. In particular our experiments demonstrate that fission occurs at a precise location: at the edge of the Dynamin polymer. A model of fission is deduced from this observation and predicts how the fission time depends on membrane tension, membrane rigidity and Dynamin torque. These predictions have been tested experimentally.

Finally in Chapter 7 the results of this thesis are discussed under four perspectives. First Dynamin mechanochemical properties are analysed under the light of the studies of classical molecular motors. Dynamin-mediated fission is then compared to the fission induced by phase-separation. From this comparison, some general features of the fission mechanism are emphasized. Then the similarities and differences between fission and fusion will be highlighted. Finally the results obtained from the *in vitro* study of fission will be confronted to *in vivo* data.

Chapter 2

Biological Membranes

Eucaryotic cells are organized in several specialized compartments named organelles. These organelles as well as the cell itself are delimited by membranes. In this chapter, I will describe these biological membranes. They constitute barriers to solutes thanks to the self-assembling property of lipids, the major structural components of biological membranes[1] which will be introduced in the part 2.1 of this chapter. Biological membranes are also very dynamic. Due to the fact that they isolate cellular compartments from each other, membranes participate in a mechanism of intense and specific exchanges between organelles, called vesicular traffic that will be detailed in section 2.2. Emphasis will be put on a mechanism which requires Dynamin, the Clathrin-mediated endocytosis, and on its specific role during synaptic vesicles recycling.

2.1 Lipids: The Building Block Of Membranes

Biological membranes are made of lipids which are amphiphilic molecules containing a hydrophilic head and a hydrophobic backbone. In aqueous environment, amphiphilic molecules tend to self-assemble to minimize interactions between hydrophobic groups and water molecules, leading to structures like micelles or bilayers. The thickness of these bilayers is around 4-5 nm for pure lipid membranes and up to 7 nm for biological membranes due to protein insertions. The main lipid constituants of eucaryotic biological membranes are glycerophospholipids, sphingolipids and sterols.

2.1.1 Glycerophospholipids

Glycerophospholipids are lipids with two hydrocarbon tails and a polar head composed of a glycerol, a phosphate group and a polar group. Usually one of the hydrophobic tail is saturated

[1] It is worth noticing that proteins are also present in large amount in membranes: from 25% to 75% (in mass) in the specific case of mitochondrial membranes. Plasma membranes contain around 50% (in mass) of proteins [3]. Ion channels, pumps, transporters and ligand-receptors are examples of transmembrane proteins. They will not be described in this study as they do not participate in membrane fission.

whereas the other one has at least one cis-double bond. The length of the tail varies from 14 to 24 carbon atoms. Phosphatidylcholine (PC) is the major component of most eucaryotic cellular membranes. Its headgroup is a choline (see Fig.2.1. PC). It self-organizes into fluid planar bilayer. Whereas PC is globally neutral, phosphatidylserine (PS) has a net negative charge due to the serine group at its polar head (see Fig.2.1. PS). This lipid is restricted to the cytosolic leaflet of membranes. Phosphatidylinositols (PtdIns) and its phosphorylated derivates like phosphatidylinositol 4,5-bisphosphate (PIP_2) (see Fig.2.1. PIP2), although present in limited amount in membranes (below 1% of the total phospholipids), constitute an interesting class of glycerophospholipids as their metabolism (phosphorylation and dephosphorylation) is involved in signalling pathways and membrane traffic [27].

2.1.2 Sphingolipids

Sphingolipids derivate from ceramides (see Fig.2.1. Ceramide). They have two saturated or trans-unsaturated hydrocarbon tails which make their hydrophobic core more rigid. Compared to glycerophospholipids, sphingolipids are longer and thus thicken membranes.
Sphingomyelin (SM) is the most abundant sphingolipid in mammalian cells. Like PC, SM carries a choline at its hydrophilic head (see Fig.2.1. SM). The plasma membrane, boundary of the cell, is particularly rich in sphingomyelin. For instance in red blood cell, around 18% of the total lipid weight is due to sphingomyelin [3, 147].

2.1.3 Sterols

Sterols are non polar lipids with a single hydrocarbon tail. They do not form bilayers by themselves but insert within membranes at the upper part region of hydrophobic chains. Cholesterol (see Fig.2.1. Cholesterol) is the major sterol in mammalian cells. Like sphingomyelin, cholesterol is enriched in plasma membranes. It represents 23% of the total lipid weight in red blood cell plasma membranes.

Membranes are not only structural elements of the cell. Indeed as membranes are impermeable to solutes, selective exchanges through the membrane and between organelles must take place via specific mechanisms. Exchanges through the membrane occur via transmembrane proteins like channels and pumps. Exchanges between organelles are enabled by vesicular traffic.

2.2 Vesicular Traffic

Cellular compartments are not static. Indeed lipids and proteins are synthesized in a place sometimes distant from their target location. For example, sphingolipids are synthesized in the Golgi apparatus but the plasma membrane is enriched in these lipids. Secretory proteins

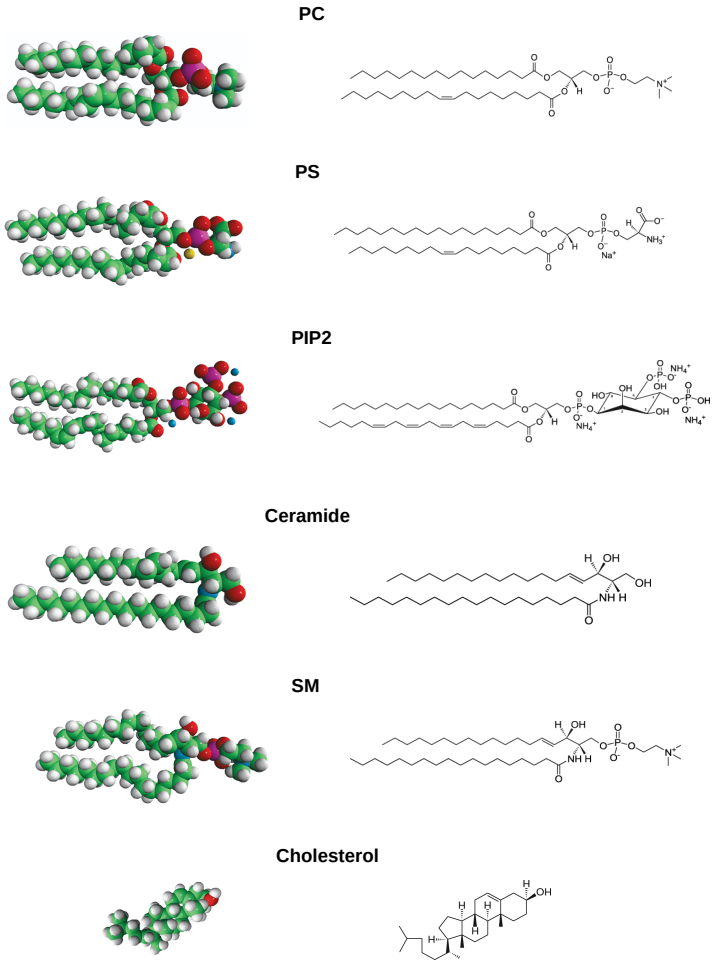

Figure 2.1: Chemical structure of some lipids. From top to bottom: phosphatidylcholine (PC), phosphatidylserine (PS), phosphatidylinositol(4,5)-bisphoshate (PIP2), ceramide, sphingomyelin (SM) and cholesterol. Adapted from Avanti Polar Lipid website *http* : *//avantilipids.com/*.

are synthesized in the endoplasmic reticulum but need to be exported outside the cell. Thus dynamic and well-organized exchanges must take place between organelles [147]. A major way to transport material from one organelle to another is vesicular traffic: a lipid vesicle is generated from the donor membrane, transported toward the acceptor membrane and fused.

2.2.1 General Features Of Vesicular Transport

As organelles are specialized compartments, there are different types of vesicular traffic involving specific sets of proteins (see Fig.2.2.A. and [14]). For instance, transport from the Golgi apparatus to the endoplasmic reticulum is mediated by the COat Protein complex I (COPI) [62] and the reverse route by the COat Protein complex II (COPII) [65]. Clathrin proteins are involved in transport from the plasma membrane and from the trans-Golgi network (TGN).

All these pathways are very distinct as they involve different proteins, different lipids, different cellular localization, different dynamics. However all vesicular transports can be described by three common successive steps (see Fig.2.2.B. and [112]):

1. Deformation and fission of the donor membrane to generate the vesicle:
   The donor membrane is deformed into a bud by specific protein complexes such as COPI, COPII and Clathrin mentionned above. Membrane fission occurs to separate the vesicle from the donor membrane. There are different fission processes. For instance Dynamin is required in fission of clathrin-coated bud at the plasma membrane. ESCRT (Endosomal Sorting Complex Required for Transport) complex is involved in the fission of the intralumenal vesicles of the multivesicular body [99]. Sar1, a small GTPase protein, has been implicated in COPII vesicle scission [81]. From this diversity of proteins involved in fission, it seems that no universal protein machinery drives membrane scission *in vivo*.

2. Transport from the donor membrane to the acceptor membrane:
   The vesicle either diffuses to its target or is actively transported through the cell by molecular motors, like kinesins and myosins, which "walk" along the filaments of the cytoskeleton: microtubules and actin filaments [145].

3. Fusion of the vesicle with the acceptor membrane:
   SNARE (N-ethylmaleimide-sensitive factor attachment protein receptors) proteins are responsible both for targeting the vesicles to its acceptor membrane and for mediating the fusion of the two compartments. Contrary to proteins mediating fission, this family of proteins is well conserved in the different transport pathways [133].

This thesis focuses on the first step, which can be in turn subdivided into five substeps: initiation, cargo selection, budding, fission and uncoating. These steps are further explained through the particular example of Clathrin-mediated endocytosis (see Fig.2.4).

2.2.2 Clathrin-Mediated Endocytosis

Transport from the plasma membrane towards other organelles inside the cell is called endocytosis. Different endocytic pathways exist: caveolae, phagocytosis, macropinocytosis. The most well-characterized endocytic pathway is mediated by the Clathrin protein.

1. Initiation
   Clathrin-mediated endocytosis (CME) is initiated by a module of proteins: FCHo, EPS15 and intersectin [57]. They bind to the membrane via interactions with PIP_2. These nucleator proteins sculpt the membrane to generate the initial deformation which will lead to the endocytic vesicle.

2. Cargo Selection and Budding
   Nucleator proteins recruit another group of proteins: the adaptor proteins. AP2 and AP180 are the most described adaptor proteins [129]. They select the cargo molecules which need to be internalized. Ligand-bound receptors, such as the transferrin receptor or the epidermal growth factor (EGF) receptor, are typical cargoes involved in CME. Adaptor

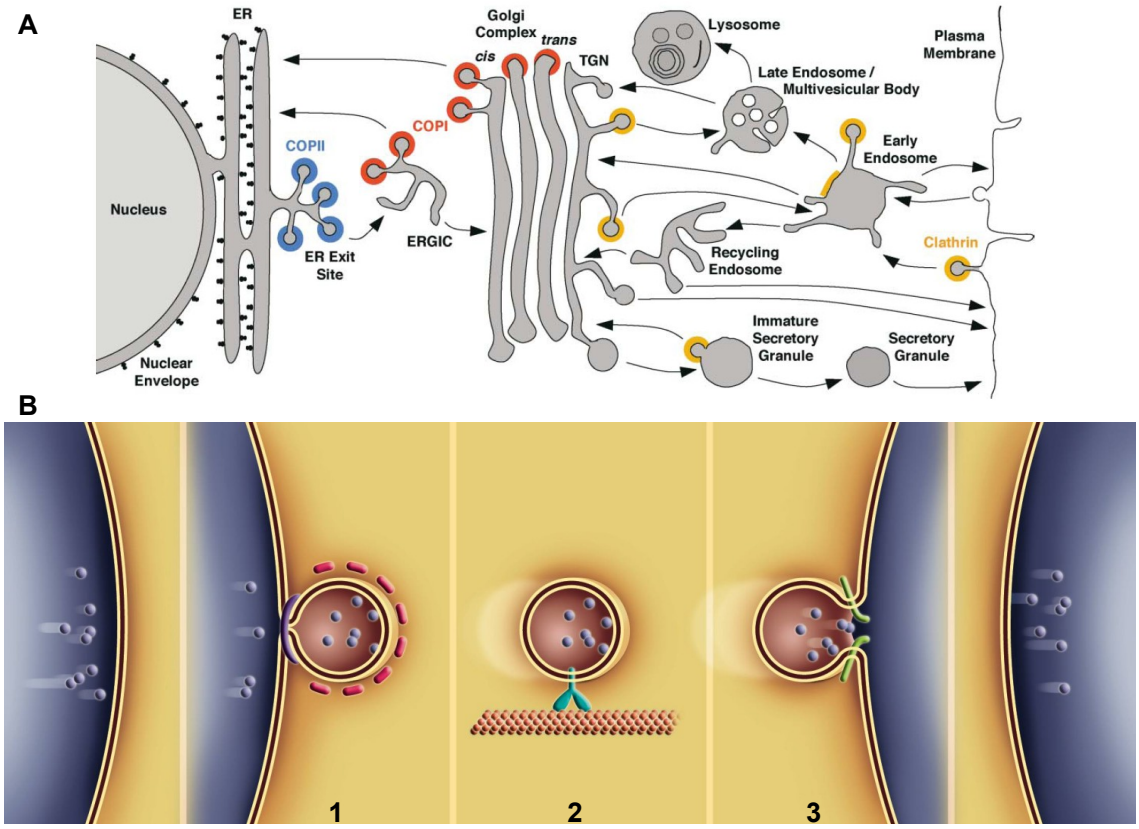

Figure 2.2: A. Sketch representing the main trafficking pathways in eucaryotic cells. Arrows indicate the directions of vesicular transport from the donor organelle to the acceptor organelle. In blue, red and yellow, specific localization of (respectively) COPII-, COPI- and Clathrin-mediated pathways. From Bonifacio and Glick, Cell 2004. B. Sketch of the three main steps during vesicular traffic: 1. membrane budding initiated by coat proteins (red) and vesicle scission triggered by fission proteins (purple) 2. vesicle transport by molecular motors along cytoskeleton structures 3. specific targeting and fusion of the vesicle with the acceptor membrane mediated by SNARE proteins (green). From Roux *et al*, Pour la Science 2007

proteins also directly interact with the plasma membrane especially with PIP_2. Adaptor proteins recruit Clathrin at the plasma membrane. Clathrin is a large protein composed of three heavy chains and three light chains forming together a triskelion. Clathrin triskelia polymerize into pentagons and hexagonal structures which in turn assemble into a lattice forming a spherical cage [44] (see Fig.2.3). Clathrin assembly allows to deform the membrane into a spherical bud while concentrating cargoes in the bud (through their mutual interactions with adaptor proteins). The size of this Clathrin-coated bud varies, depending on cargoes' sizes, from 35 to 200 nm outer diameter [90]. The neck linking the bud to the plasma membrane is then covered by proteins containing a Bin-Amphiphysin-Rvs (BAR) domain: Amphiphysin [152] and Endophilin [110]. Like the nucleator proteins in the initial step of CME, Amphiphysin and Endophilin bind and deform the membrane. They enable the formation of a thin membrane tube linking the Clathrin-coated bud to the plasma membrane.

3. Fission

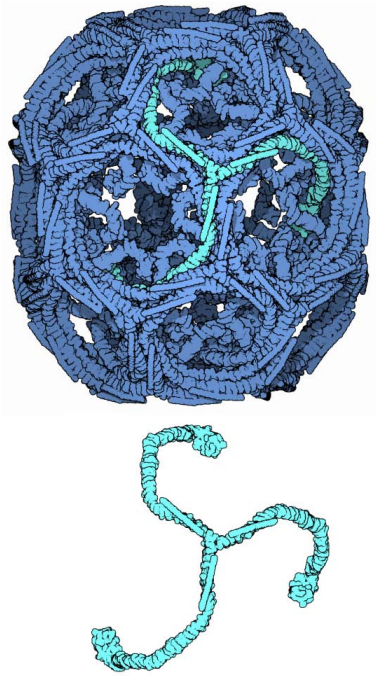

Figure 2.3: Structure of a Clathrin triskelion (bottom) and of a cage of Clathrin (top). From Protein Data Bank, April 2007 Molecule of the Month by Graham T. Johnson and David Goodsell

The release of the vesicle from the plasma membrane is mediated by the Dynamin protein which has been proposed to be recruited to the neck by Amphiphysin [153]. The crucial step of Dynamin-mediated membrane fission constitutes the main interest of the work presented in this thesis. This mechanism will be detailed in the following chapters.

4. Uncoating
   When the vesicle is detached from the plasma membrane, Clathrin rapidly depolymerizes with the help of other proteins: the ATPase Heat Shock Cognate protein 70 (Hsc70) [118] and Auxilin [144]. Auxilin proteins first bind to the vesicle within the Clathrin lattice and thereby destabilize the cage. Then they recruit Hsc70 which fully depolymerize Clathrin upon ATP hydrolysis [43]. In addition to Auxilin and Hsc70 activity, the dephosphorylation of PIP_2 lipids also participates in Clathrin removal [27, 69]. Indeed Synaptojanin, a phosphoinositide phosphatase, is recruited by Endophilin at late stage of CCP maturation [100]. As this phosphatase hydrolyzes PIP_2, the level of PIP_2 decreases only after fission when the released vesicle is no more connected to the plasma membrane which contains a reservoir of PIP_2. The depletion of PIP_2 would promote the dissociation of the coat proteins from the membrane and help recruiting Auxilin.

During CME, several protein-protein and protein-lipid interactions must by coordinated at the right time and the right location. This well orchestrated sequence of proteins recruitments and membrane deformations [139, 90] takes place in every eucaryotic cells in a constitutive manner. In some specialized cells, CME plays also an essential role such as in neurons where a highly dynamic endocytic activity is required to recycle synaptic vesicles.

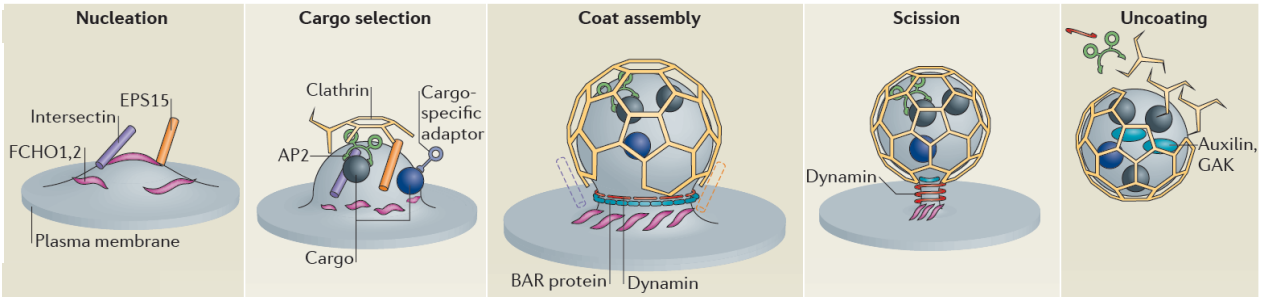

Figure 2.4: Sketch of the five steps of Clathrin-mediated endocytosis with the main proteins involved in the process. From McMahon and Boucrot, Nature Reviews Molecular Cell Biology 2011

2.2.3 Synaptic Vesicle Recycling

The synapse is the junction between a presynaptic neuron and a postsynaptic neuron (see Fig.2.5). At this connection, chemical signals are transmitted via neurotransmitters molecules (glutamate, acetylcholine, Gamma-AminoButyric Acid (GABA)...). At the presynaptic neuron, neurotransmitters are confined inside vesicles. These synaptic vesicles are then released in the synapse by exocytosis, a process where vesicles fuse with the plasma membrane and release their contents outside the cell. The released neurotransmitters then bind to specific receptors located at the plasma membrane of the postsynaptic neurons. In the presynaptic region, the exocytic machinery like the SNARE proteins involved in fusion and the excess membrane added to the plasma membrane during exocytosis are recycled through CME [59]. This recycling is very intense as there can be up to thousands synaptic vesicles in a presynaptic neuron. Indeed CME in neurons occurs within 10 to 25 s [156, 66] which is faster than in non neuronal cells (around 1 minute [139]).

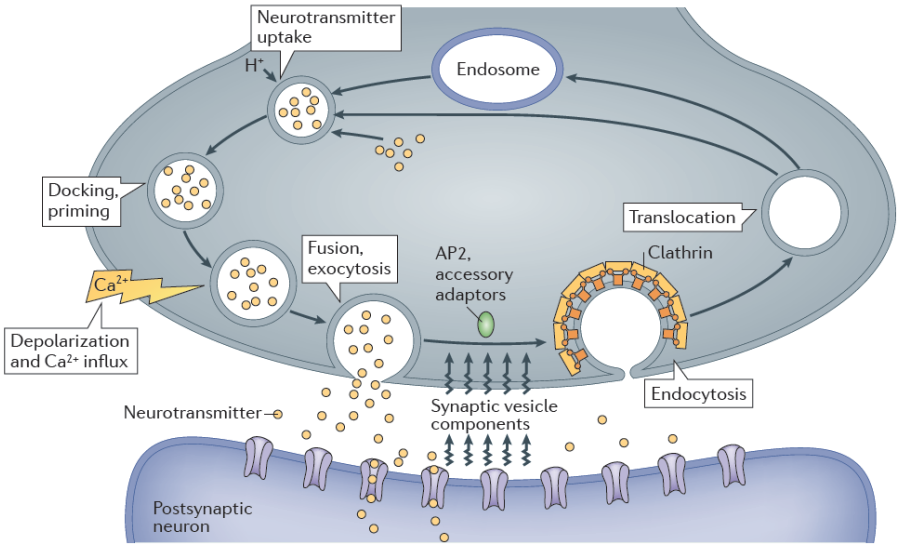

Figure 2.5: Sketch illustrating synaptic vesicles recycling. From McMahon and Boucrot 2011, Nature Reviews Molecular Cell Biology

Clathrin-mediated endocytosis and its specific role during synaptic vesicles recycling are good

examples highlighting the spatial and temporal coordination of different cellular mechanisms remodelling the membrane. Thus biological membranes conciliate two important mechanical properties: self-assembling to ensure the organelle's integrity and a propensity to deform under external forces to enable dynamic vesicular transport. To better understand their mechanical properties, biological membranes have been studied by physicists.

Chapter 3

Physics Of Membrane

In this chapter, I will explain how membranes have been modelled by physicists. The shape of a membrane determines its energy as it will be explained in 3.1. Thus deforming a membrane changes its energy. Experiments modifying the membrane shape, such as micropipette aspiration and nanotube extrusion, have been designed to probe membrane mechanics and will be detailed in 3.2. Finally I will give energetic considerations about membrane fission in the last part of this chapter 3.3.

3.1 Theoretical Description Of A Membrane

Membranes are traditionally modelled as homogeneous fluid thin sheets. In most cases, their thickness (a few nm) is negligible compared to the length scale of their surface (a few μm). If this approximation is satisfied, any membrane deformation can be decomposed into three elementary deformations: stretching, shearing and bending as depicted in Fig.3.1 [37]. Describing these deformations enables to calculate the elastic energy of the membrane.

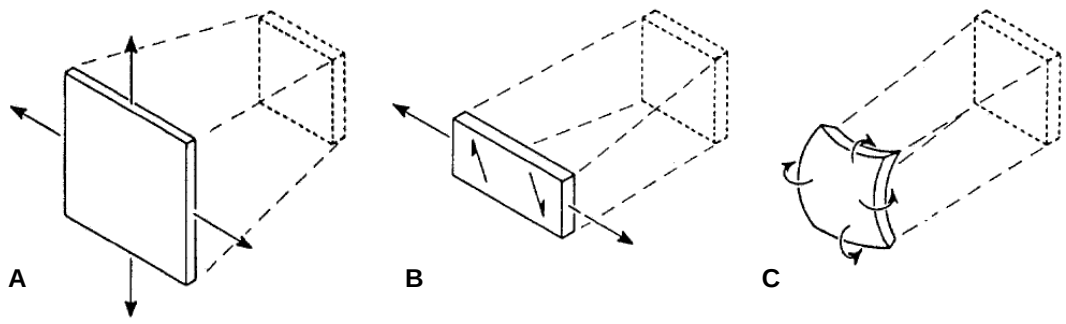

Figure 3.1: Sketch of the three independent modes of membrane deformations: A. stretching, B. shearing, C. bending. Arrows represent deformation directions. From Evans and Needham, 1987.

3.1.1 Stretching

Stretching is a deformation which modifies the area A of a membrane by either extending or compressing it (Fig.3.1.A.). The stretching energy per unit area of a membrane undergoing a relative change in area $\frac{\Delta A}{A}$ is:

$$E_{stretching} = \frac{1}{2}\chi(\frac{\Delta A}{A})^2$$

where χ is the compressibility modulus. To understand the stretching energy, the concept of membrane tension must be introduced. A membrane with a surface area A and a free energy F has a tension $\sigma = \frac{\partial F}{\partial A}$. The precise relationship between stretching and tension will be explained later in 3.1.5.

3.1.2 Shearing

Shearing a membrane is equivalent to applying coplanar forces in opposite directions on two points of the membrane while maintaining the surface area (Fig.3.1.B.). The shearing energy per unit area is:

$$E_{shearing} = \frac{1}{2}\mu(\lambda^2 + \lambda^{-2} - 2)$$

where μ is the shear modulus and λ the lateral extension rate: $\lambda = \frac{L+\Delta L}{L}$. In fluid lipid bilayers, shearing deformations are negligible compared to stretching and bending and will be ignored afterwards.

3.1.3 Bending

The last deformation category corresponds to bending the membrane at constant area (Fig.3.1.C.). The bending energy derives from the curvature of the membrane. At a given point of a surface, one can define two radii of curvature R_1 and R_2 (see Fig.3.2). The inverse of these radii are the two principal curvatures C_1 and C_2[1] . The sum of the principal curvatures is the mean curvature $J = C_1 + C_2$. The product of the principal curvatures is the Gaussian curvature $K = C_1.C_2$.

For instance on every point of a sphere of radius R, the mean curvature is $\frac{2}{R}$ and the Gaussian curvature is $\frac{1}{R^2}$. An infinite cylinder of radius R has a mean curvature $\frac{1}{R}$ and a null Gaussian curvature on every points of its surface. A saddle point has the particularity to have two principal curvatures of opposite sign and thus a negative Gaussian curvature (Fig.3.2 [74]). J and K are local parameters which completely describe the shape of the membrane.

To describe the propensity of a membrane to bend, we define two intrinsic parameters: the bending rigidity modulus κ and the Gaussian bending rigidity modulus κ_G. κ and κ_G represent the energetic cost to generate principal curvature (increasing J) and Gaussian curvature (increasing K) respectively. They both depend on the composition of the membrane. Some

[1] More precisely the principal curvatures at a given point are the maximum and minimum values of the curvature. They are the eigenvalues of the shape operator.

membranes spontaneously bend without any external forces. This can be due for instance to an asymmetric lipid composition between the two leaflets of the bilayer. This property is taken into account by defining another parameter intrinsic to the membrane: the spontaneous curvature c_0.

Finally the bending energy per unit area gathers the contributions from the mean curvature and the Gaussian curvature:

$$E_{bending} = \frac{1}{2}\kappa(J - c_0)^2 + \kappa_G K$$

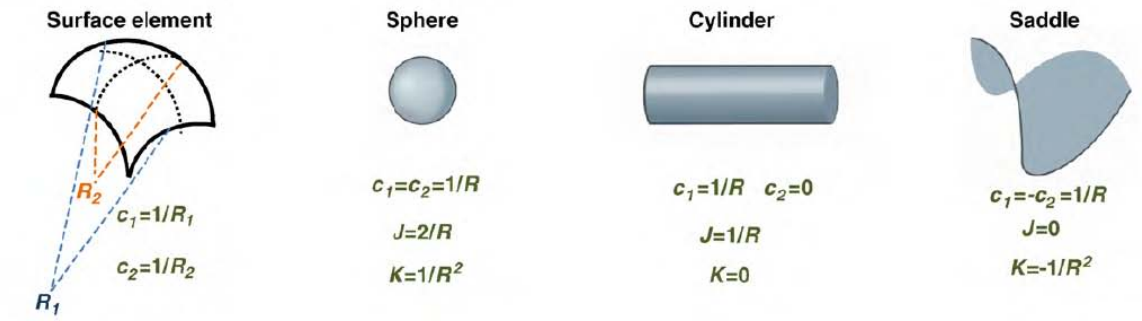

Figure 3.2: Definition of the two principal curvatures of a surface element. Examples of mean curvatures and Gaussian curvatures. From Kozlov *et al.*, Trends in Biochemical Sciences 2010.

3.1.4 Canham-Helfrich Theory

In the 1970's, Canham and Helfrich proposed a theory of membrane elasticity [16, 54]. They derived the so-called Canham-Helfrich Hamiltonian by summing, over the surface of the membrane, the contributions of the deformation energies described above:

$$H = \int_A ds\{\frac{1}{2}\kappa(J - c_0)^2 + \kappa_G K + \sigma\} \tag{3.1}$$

This formula represents the free energy of a membrane with a surface area A, a bending rigidity modulus κ, a Gaussian bending rigidity modulus κ_G and a tension σ. This formula includes the energies of the two deformations implicated in fluid membrane remodelling: stretching and bending. The Canham-Helfrich Hamiltonian embodies the idea that the energy of a membrane is linked to its shape. In particular, this theory succeeded in predicting the shapes of vesicles (stomatocytes, oblates, prolates...) and the transitions between these shapes [121].

3.1.5 Membrane Tension

Membrane tension is linked to the stretching energy of the membrane. At very low tensions, the surface of a membrane fluctuates due to thermal agitation. Stretching a fluctuating membrane

tends to flatten its surface. Once the surface is fully flattened, further stretching pulls the lipids apart increasing the tension of the membrane. These intuitive observations lead us to consider two regimes to describe the stretching deformations: first, the entropic regime at low tensions when the membrane is fluctuating and second the enthalpic regime at higher tensions when all the thermal fluctuations are unfolded.

- Entropic Regime:
  When a membrane is stretched, the resulting change in area is first due to the excess area stored in the thermal fluctuations of the membrane. The maximum amplitude of these fluctuations U_{max} can be derived from the theorem of energy equipartition and the Canham-Helfrich Hamiltonian [54, 55, 38]:

$$U_{max} \propto \sqrt{\frac{k_B T}{\sigma} ln \frac{L}{a}}$$

  where L is the macroscopic length scale of the membrane (typically 10 μm), a its microscopic length scale (typically 0.5 nm), k_B is the Boltzmann constant and T the temperature[2]. It appears clearly in this formula that membrane tension tends to reduce the amplitude of the fluctuations. More precisely the relationship between excess area and membrane tension can be calculated from fluctuations spectrum analysis:

$$\frac{\Delta A}{A} = \frac{\kappa_B T}{8\pi\kappa} ln \frac{\frac{\pi^2}{a^2} + \frac{\sigma}{\kappa}}{\pi^2 L^2 + \frac{\sigma}{\kappa}}$$

  For low tensions, when the condition $\frac{\kappa\pi^2}{L^2} \ll \sigma \ll \frac{\kappa\pi^2}{a^2}$ is satisfied, the relationship simplifies:

$$\frac{\Delta A}{A} = \frac{\kappa_B T}{8\pi\kappa} ln \frac{\pi\kappa^2}{\sigma a^2}$$

- Enthalpic Regime:
  When all the excess area stored in the fluctuations of the membrane has been unfolded, the stretching energy is then mainly due to variation in membrane tension σ. As $\Delta F = \sigma \Delta A$, the stretching energy per unit area in the enthalpic regime writes:

$$E_{stretching\ \ enthalpic} = \sigma \frac{\Delta A}{A}$$

  then we can rewrite the tension as:

$$\sigma = \frac{\partial(E_{stretching\ \ enthalpic} A)}{\partial(\Delta A)} = \frac{\partial(\frac{1}{2}\chi \frac{(\Delta A)^2}{A})}{\partial(\Delta A)} = \chi \frac{\Delta A}{A}$$

  Hence the variation in area in the enthalpic regime is linear with membrane tension:

$$\frac{\Delta A}{A} = \frac{\sigma}{\chi}$$

[2] In a system at a temperature T, each microscopic degree of freedom has a thermal energy on the order of $\frac{k_B T}{2}$, $k_B T \approx 4.10^{-21} J$ at room temperature.

Finally the relative change in area due to stretching deformations is the sum of two contributions: the entropic regime (non linear with tension) and the enthalpic regime (linear with tension)[38]:

$$\frac{\Delta A}{A} = \frac{\kappa_B T}{8\pi\kappa} ln\frac{\pi\kappa^2}{\sigma a^2} + \frac{\sigma}{\chi} \tag{3.2}$$

3.2 Experimental Studies Of Membrane Mechanics

In this section, I will describe how the theoretical description of membranes has been validated experimentally. Two techniques, which we used to study Dynamin, will be detailed: the micropipette aspiration and the nanotube extrusion. They both enable to test the Canham-Helfrich theory. To study membrane mechanics, many model membrane systems have been designed since they are less complex than living organisms' membranes (for a review see [8]). For instance the Giant Unilamellar Vesicles (GUVs) are artificial spherical lipid bilayers with typical radii of a few tens of micrometers. GUVs are good templates to study membrane mechanics. They can be observed by light microscopy. GUVs can be prepared easily by electroformation [7, 89]. This technique also allows to make multicomponent membranes, for instance GUVs containing PIP2 [17], which were widely used during this thesis.

3.2.1 Control Of Membrane Tension With A Micropipette

The micropipette technique was introduced in 1979 to study the elastic properties of red blood cell membranes [150] and was later used on GUVs [77]. This technique enables to study the stretching of membranes. It consists in aspirating a GUV with a glass capillary pipette of a few micrometers internal diameter (see Fig3.3.A). The aspiration pressure is controlled by connecting the pipette to a water reservoir. When the reservoir is at the same level as the pipette, the pressure inside the pipette is equal to the pressure outside the pipette. If the reservoir is above (respectively below) the level of the pipette, there is an overpressure (respectively a depression) in the pipette. Thus the vertical displacement Δz of the water reservoir translates into a difference of hydrostatic pressure ΔP in the pipette: $\Delta P = \rho_{water} g \Delta z$ where $\rho_{water} = 10^3\ kg.m^{-3}$ is the density of water and $g = 9.80\ m.s^{-2}$ the standard gravity. GUV aspiration stretches the membrane: the GUV remains spherical and the excess area due to stretching unfolds in the pipette. This "tongue", the GUV's portion unfolded in the pipette, is a cylinder (with a radius equal to the inner radius of the pipette $R_{pipette}$) ended by a semi-sphere (with a radius $R_{pipette}$). The tension of the membrane, set by aspirating the GUV, can be deduced from the radius of the GUV ($R_{vesicle}$), the radius of the pipette ($R_{pipette}$) and the aspiration pressure (ΔP)using the Laplace's law[3]:

$$\sigma = \frac{R_{pipette}\Delta P}{2(1 - \frac{R_{pipette}}{R_{vesicle}})} \tag{3.3}$$

[3]The Laplace's law gives the relationship between the tension of a surface σ, its mean curvature J and the difference of pressure ΔP between the two fluids on each side of the surface: $\Delta P = 2\sigma J$.

The micropipette technique was used to test experimentally the relationship between the change in area due to stretching and the membrane tension. When the aspiration pressure is modified (by vertically displacing the water reservoir), it results in a modification of the tongue length ΔL (see Fig.3.3A). Thus the experimental change in area $(\frac{\Delta A}{A})_{exp}$ can be deduced from the change in the GUV's shape [77]:

$$(\frac{\Delta A}{A})_{exp} = \frac{(\frac{R_{pipette}}{R_{vesicle}})^2 - (\frac{R_{pipette}}{R_{vesicle}})^3}{2R_{pipette}} \Delta L \tag{3.4}$$

We mentioned above (formula 3.2) a theoretical prediction for the relationship between the change in area $(\frac{\Delta A}{A})_{theory}$ and the membrane tension σ. The experimental change in area $(\frac{\Delta A}{A})_{exp}$ does not take into account all the fluctuations so that:

$$(\frac{\Delta A}{A})_{exp} = (\frac{\Delta A}{A})_{theory\ 0} - (\frac{\Delta A}{A})_{theory_{pipette}} \tag{3.5}$$

where $(\frac{\Delta A}{A})_{theory\ 0}$ is the total excess area stored in the fluctuations of the GUV before aspiration when the tension is σ_0 and $(\frac{\Delta A}{A})_{theory_{pipette}}$ is the total excess area when the GUV is aspirated in a pipette with a tension σ. Combining 3.5 with 3.2, we obtain:

$$(\frac{\Delta A}{A})_{exp} = \frac{\kappa_B T}{8\pi\kappa} ln\frac{\sigma}{\sigma_0} + \frac{\sigma}{\chi} \tag{3.6}$$

Evans' group performed experiments to verify the relationship 3.6. They did observe two regimes [38, 108]. For lower deformations, tension depends logarithmically with the change in area as predicted by the entropic regime and for higher deformations, tension increases linearly in good agreement with the enthalpic regime (Fig.3.3.B and C.). These results validate the Canham-Helfrich theory. These experiments also allow to measure the elastic parameters of membranes such as the bending rigidity modulus κ and the compressibility modulus χ and how these parameters depend on membrane composition [38, 108, 95, 88, 109]. These experimental measurements of elastic parameters are summarized in the table 3.4.

3.2.2 Nanotube Extrusion

General Concept Of Nanotube Extrusion

Nanotube extrusion is another way to probe the membrane mechanics. When a point force is exerted on a membrane, a lipid nanotube is formed. This deformation is very typical of fluid bilayers. By comparison, if a pulling force is exerted locally on a solid elastic surface, such as a rubber balloon, the whole object deforms into a conical shape. For fluid membranes, as stretching increases tension, the energy of the system is minimized by reducing the surface of the deformation. The minimal surface would be a straight line perpendicular to the plane of the membrane. However deforming a membrane into a line, which has an infinite curvature,

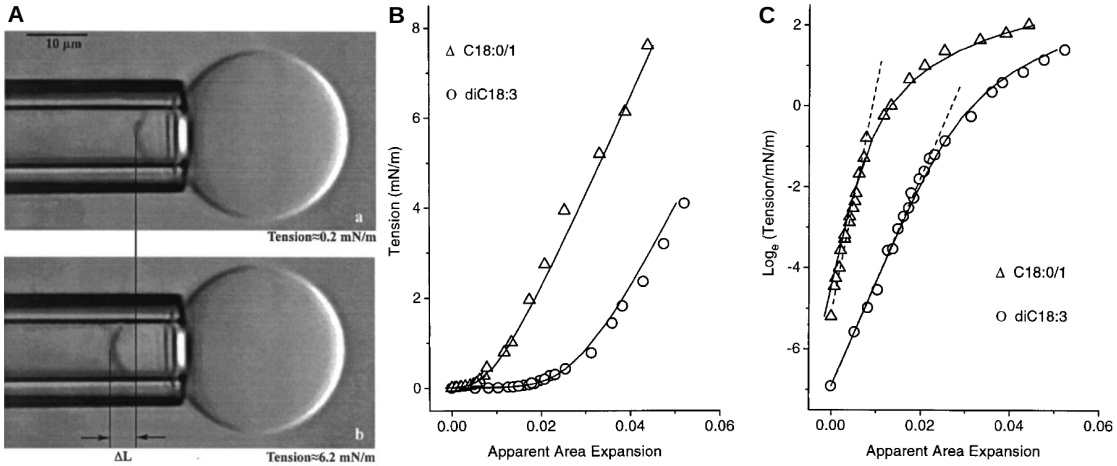

Figure 3.3: Micropipette experiments with GUVs to test the relationship linking the excess area to the tension. A. Pictures taken from video microscopy of a GUV hold in a micropipette. From a to b, the aspiration pressure is increased and results in an increase in both the length of the tongue and the tension. B. C. Linear (B.) and semi-logarithmic (C.) representations of tension vs. excess area. Tension increases first logarithmically then linearly with the excess area. The two curves in each panel correspond to two different lipid compositions. From Rawicz *et al.*, Biophysical Journal 2000.

Parameter	Value	Unit
Compressibility modulus χ	250	$mN.m^{-1}$
Membrane Tension σ	from 10^{-7} to 10^{-3}	$N.m^{-1}$
Bending Rigidity Modulus κ	from 10 to 100	k_BT
Gaussian Bending Rigidity Modulus κ_G	$\approx -0.8\kappa$	k_BT

Figure 3.4: Typical values of elastic parameters. These parameters depend on membrane composition and temperature. All these values have been measured experimentally except κ_G which is estimated from phase behaviour of DOPE/DOPC mixtures [126]. χ is measured for fluid PC bilayers [108]. The values for σ and κ are typical values for fluid bilayers obtained with micropipette and nanotube extrusion techniques. k_B is the Boltzmann constant and T the temperature. $k_BT \approx 4.10^{-21}$ J at room temperature.

would require a huge bending energy. So lipid nanotube formation results from the competition between stretching (change in area) and bending (change in curvature).

Nanotube extrusion has been studied theoretically [136, 33, 101]. We consider a membrane nanotube with a length L_{tube} and a radius R_{tube} and f is the magnitude of the force applied to extrude the nanotube (see Fig.3.5.). Then using the Canham-Helfrich Halmitonian 3.1, the free energy of the system is:

$$F = \{\frac{\kappa}{2R_{tube}^2} + \sigma\}2\pi R_{tube}L_{tube} - fL_{tube} \tag{3.7}$$

By minimizing this energy versus the radius of the tube R_{tube}, we obtain the radius of the tube

at equilibrium R_0:

$$R_0 = \sqrt{\frac{\kappa}{2\sigma}} \tag{3.8}$$

This formula illustrates the simple explanation of nanotube extrusion we gave above. The radius of the nanotube is set by the competition between the tension σ and its ability to deform, thus its bending rigidity modulus κ.
By minimizing the energy 3.7 versus the length of the tube L_{tube}, we obtain the force f_0 necessary to maintain the tube at equilibrium:

$$f_0 = 2\pi\sqrt{2\kappa\sigma} \tag{3.9}$$

We can notice that the equilibrium force does not depend on the length of the tube when the tension is fixed.

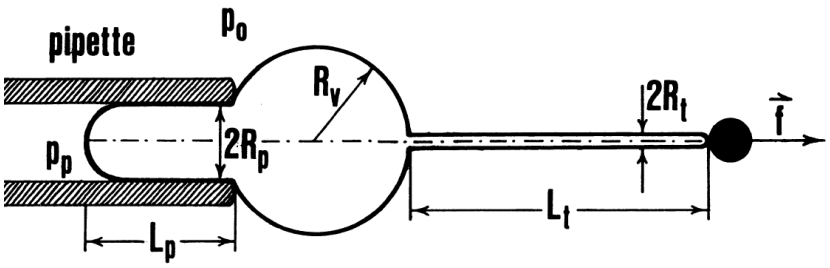

Figure 3.5: Sketch of a lipid nanotube extruded from a GUV hold in a pipette. From Svetina *et al.*, European biophysics journal 1998.

These predicted formulas for the radius R_0 3.8 and the force f_0 3.9 were experimentally tested by Heinrich and Waugh in 1996 [53]. The good agreement between predictions and measurements validates the Canham-Helfrich theory. Nanotubes have been studied using different methods of extrusion: by applying a shear flow on a GUV [151], by gravity [13], by using kinesin walking on microtubule [113, 73], or by using a bead trapped in optical tweezers in addition to the micropipette technique [28]. This last method, that I used during my thesis, presents the advantage to monitor the force via the optical trap while maintaining the tension via the micropipette (see Fig.3.5). Thus knowing the force and the tension, the radius can be calculated by combining 3.8 and 3.9:

$$R_0 = \frac{f_0}{4\pi\sigma} \tag{3.10}$$

Typical radii obtained experimentally range from 10 to 100 nm which covers the range of curvatures of *in vivo* membrane carriers.

Beyond the Canham-Helfrich theory: applications Of Nanotube Extrusion

The nanotube extrusion technique has been combined to fluorescent microscopy to study lipid sorting [130, 142]. Fluorescent probes incorporated in GUVs allow to visualize precisely lipid nanotubes with confocal microscopy (see Fig.3.6.C and D.). Some probes, such as BodipyFL-GM1, mix homogeneously in the membrane (see Fig.3.6.B). Other probes, such as TexasRed-DHPE, are sensitive to the order of the membrane (see Fig.3.6.A). The order of the membrane represents its organization state: the more ordered a membrane is, the more well packed are the lipids in the bilayer. This order depends on external parameters, like temperature, and on internal parameters, like membrane composition. Liquid-ordered (lo) and liquid-disordered (ld) phases are two examples of fluid phases. In lo-phases, the distance between lipids is on average smaller than in ld-phases. Lo-phase membranes are also thicker and stiffer [109]. As lo-phases are more organized than ld-phases, lipid diffusion is usually slower in lo-phases[67]. It is possible to observe coexisting phases *in vitro*. For example, a ternary lipid mixture of sphingomyelin, phosphatidylcholine and cholesterol can segregate in two phases (lo and ld) depending on the proportions of each component. The diagram of phase separation for this ternary mixture is well-known [32, 8]. The different phases can be observed with phase-sensitive fluorescent dyes such as TexasRed-DHPE which segregates preferentially in ld phase. Sorre *et al.* extruded nanotubes from GUV prepared from this ternary mixture complemented with TexasRed-DHPE and BodipyFL-GM1. It is important to mention that they use compositions giving homogenous fluid membranes as it is a requirement to measure tension and radius by nanotube extrusion. They quantified the ratio of fluorescence of the two probes along the nanotube relatively to the same ratio in the GUV. They observed that for compositions close to phase separation, the thinner the tube, the more enriched in TexasRed-DHPE (see Fi.3.6.D). This indicates that membrane curvature can induce lipid sorting when the lipid composition is close to phase separation. Lipid sorting is a good example showing the limitations of the Canham-Helfrich theory. Indeed the force formula 3.9 is valid only for homogeneous membranes, as soon as sorting occurs a deviation in the force curve is observed. Thus the Canham-Helfrich Hamiltonian must be corrected with a Flory-Huggins mixing free energy to describe properly lipid sorting [130].

Nanotube extrusion via optical tweezers has also been useful for studying:

- lipid and protein lateral diffusion in bilayers and its dependency on curvature [35];
  Quantum dots were attached to lipids or voltage-gated channels (KvAP) reconstituted in GUVs [2]. Diffusion coefficients were measured by following individual fluorescent particles along nanotubes with controlled radii. This study validated the Saffman and Delbrück theory [117] predicting that the diffusion coefficient depends logarithmically on the inverse of the protein size and on the nanotube radius.

- protein-membrane interactions;
  The membrane-interacting properties of certain proteins have been shown to depend on curvature. For instance ArfGAP1 proteins, implicated in COPI trafficking, bind specifically to nanotubes and not to the flat membrane of GUVs. ArfGAP1 binding is reduced for tubes with radii thinner than 35 nm [5]. Dynamin polymerization around lipid nanotubes is also curvature-dependent [115] as we will explain in the next chapter. Recent work on Amphiphysin [131] showed that the protein density on the nanotube is a critical parameter to precisely distinguish two binding regimes: curvature-sensing and curvature-generator. At low density of Amphiphysin, the properties of the protein-bound membrane

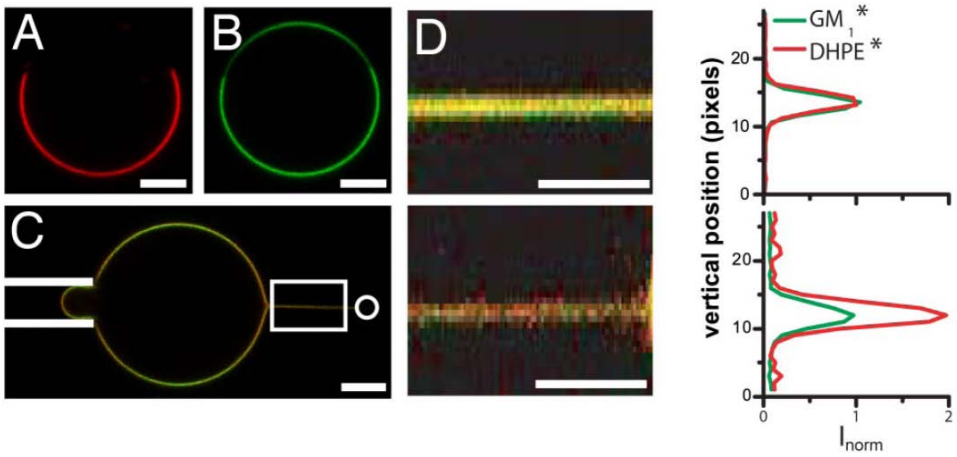

Figure 3.6: A. and B. confocal pictures of a phase-separated GUV containing sphingomyelin, DOPC, cholesterol TexasRed-DHPE (red) and BodipyFL-GM1 (green). In A. partitioning of TexasRed-DHPE in ld phase. In B. BodipyFL-GM1 present in both phases. C. Confocal pictures of a nanotube extruded from a homogeneous GUV with the same components as in A. and B. (but in different proportions to avoid phase separation). D. Left: confocal pictures of a tube. Top: radius is 70 *nm*. Bottom: radius is 20 *nm*. Right: fluorescence intensity profile of TexasRed-DHPE and BodipyFL-GM1 from the tubes shown at left. TexasRed-DHPE is enriched in the thinner tube. From Sorre *et al.*, PNAS 2009

differ slightly from the ones of a pure lipid membrane so that the tube radius and the force still depend on tension and rigidity. Whereas at high density, the radius is independent of the tension because Amphiphysin forms a scaffold around the nanotube. These studies constitute a second example showing the limitations of the Canham-Helfrich theory. When proteins bind to the nanotube, the radius formula 3.10 is no more satisfied.

- membrane tension variation in live cells;
  The Canham-Helfrich theory is not valid *a priori* in live systems as they are out of equilibrium. Nevertheless, nanotube extrusion from live cells enables to monitor in real time the variation of the plasma membrane tension. Probing membrane tension in live cells is challenging as biological membranes are submitted to many external processes: interactions with the cytoskeleton, endocytosis, exocytosis... When nanotubes are extruded from live cells, the force remains constant as the tube length increases until a certain length threshold. Above this length, the force necessary to maintain the tube becomes too high which triggers the tube retraction [107]. This indicates that the plasma membrane contains a reservoir. It has been recently demonstrated that a part of this membrane reservoir is constituted by caveolae [128].

3.3 Physics Of Membrane Fission

As we have seen in Chapter 2, vesicular traffic involves membrane deformations that have been modelled by physicists. The formation of a vesicle requires also a final step: membrane fission which separates the vesicle from the donor membrane. More generally fission is the process by which one initially closed surface split into two closed surfaces. This process modifies the

topology of the membrane and thus is strongly unfavourable energetically due to the membrane's self-sealing properties.

3.3.1 Role Of Bending Energy In Fission

To better understand the implications of fission for the energy of the membrane, let us do a simple calculation. We consider a flat membrane with a surface area A in the initial state and the final state resulting from fission: a vesicle of radius R and a flat membrane of surface area $A - 4\pi R^2$. We can estimate the energy of these two states using the Canham-Helfrich Hamiltonian 3.1. As flat surfaces have null curvatures ($J = 0$, $K = 0$), the initial state has an energy equal to $\int_A ds\{\sigma\} = \sigma A$. The final state's energy is the sum of the vesicle energy and the flat membrane energy:

$$\int_{vesicle} ds\{\frac{1}{2}\kappa(\frac{1}{2R})^2 + \frac{\kappa_G}{R^2} + \sigma_{vesicle}\} + \int_{flat\ \ membrane} ds\{\sigma_{flat}\}$$

$$= 4\pi(\frac{\kappa}{8} + \kappa_G) + \sigma_{vesicle}4\pi R^2 + \sigma_{flat}(A - 4\pi R^2)$$

If we consider that tension remains constant during the process: $\sigma_{vesicle} = \sigma_{flat} = \sigma$, the difference of energy between the two states, which is the minimal bending energy required to form a vesicle, is $4\pi(\frac{\kappa}{8} + \kappa_G)$ [4] . Note that this energy is independent of the vesicle radius and depends only on the bending rigidity modulus κ and the Gaussian bending rigidity modulus κ_G highlighting that membrane elastic properties must play an important role in the fission mechanism. It is interesting to note that the energetic term depending on κ_G in the Canham-Helfrich Hamiltonian stays constant during the whole deformation of membrane and varies only when topological changes occur. This comes from the Gauss-Bonnet theorem which stipulates that the integral of the the Gaussian curvature depends only on the topology of the surface: $\int_S dsK = 4\pi(1 - g)$ where g is called the genus of the surface and intuitively represents the number of "holes", for instance $g = 0$ for a sphere, $g = 1$ for a torus. Thus the energy of Gaussian curvature due to fission is $4\pi\kappa_G$ regardless of the vesicle shape. This draws attention to the Gaussian bending rigidity modulus κ_G which might be an interesting parameter for the fission mechanism. Gaussian bending rigidity modulus has never been direclty measured and is estimated to be negative with its absolute value similar to κ [127]. The significant role of this parameter has already been underlined in the study of fusion [126], the reverse topological change.

The energy barrier of fission is certainly much higher than the difference of energy between the final and initial states. Membrane deformations involved in the fission process lead supposedly to the generation an intermediate state named hemifission state similar to the hemifusion state in fusion: two bilayers interconnected via a local structural defect (see Fig3.7). This state is highly unstable energetically as it requires to rearrange the leaflets by packing and tilting the hydrophobic chains of lipids. An underestimate value of the energy of this state has been

[4] For $\kappa = -0.8\kappa_G$, this term is negative, meaning that the final state has a lower energy than the initial state.

calculated around 78 $k_B T$ using the Canham-Helfrich Hamiltonian [76]. However as fission occurs very locally, the membrane cannot be modelled as a thin surface and the elastic energy derived from The Canham-Helfrich Hamiltonian might not be valid. So far very few results have been established about the energy landscape of fission.

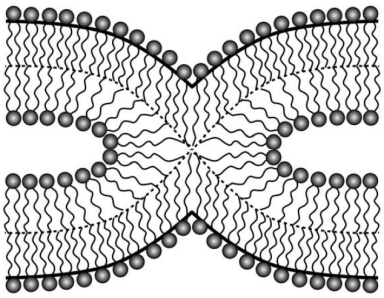

Figure 3.7: Sketch of the hemifission intermediate. Adapted from Chernomordik and Kozlov, Cell 2005

3.3.2 Fission Induced By Lipid Phase-Separation

As we have seen above, phase separation can occur in lipid mix (section 3.2.2). More precisely, in multicomponent membranes there is a competition between two phenomena: entropy favours homogeneous mixing whereas interactions between repulsive components triggers segregation. Phase separation occurs when repulsive forces overcome entropic forces.
Fission was observed in phase-separated membranes [34, 10, 114, 4]. Ternary GUVs made of sphingomyelin, phosphatidylcholine and cholesterol were prepared in proportions resulting in a single homogeneous phase close to a demixing point. Phase separation was triggered by light-induced oxidation of cholesterol (see Fig3.8.A and B.). After several seconds, fission occurs at the interface between the two phases (see Fig3.8.C.). This precise localisation of fission leads to the hypothesis that line tension triggers fission [86]. Indeed numerical calculations of the membrane shape at the interface predict that line tension and the difference in elastic parameters between the two phases (tension σ, membrane rigidity modulus κ and Gaussian membrane rigidity modulus κ_G) favours fission at the phase boundary [4]. The line tension represents the energetic cost of the boundary between the two phases. Fission occurs when reducing the line tension (by reducing the length of the boundary between the two phases) overcomes the bending energy required to pinch the membrane.

These *in vitro* study can be very useful to understand fission in a biological context. Especially it would be interesting to look at the rupture localization for other types of fission or to test how membrane elasticity is involved in fission. We chose to study fission mediated by Dynamin as this protein is involved in the well-studied Clathrin-mediated endocytic pathway.

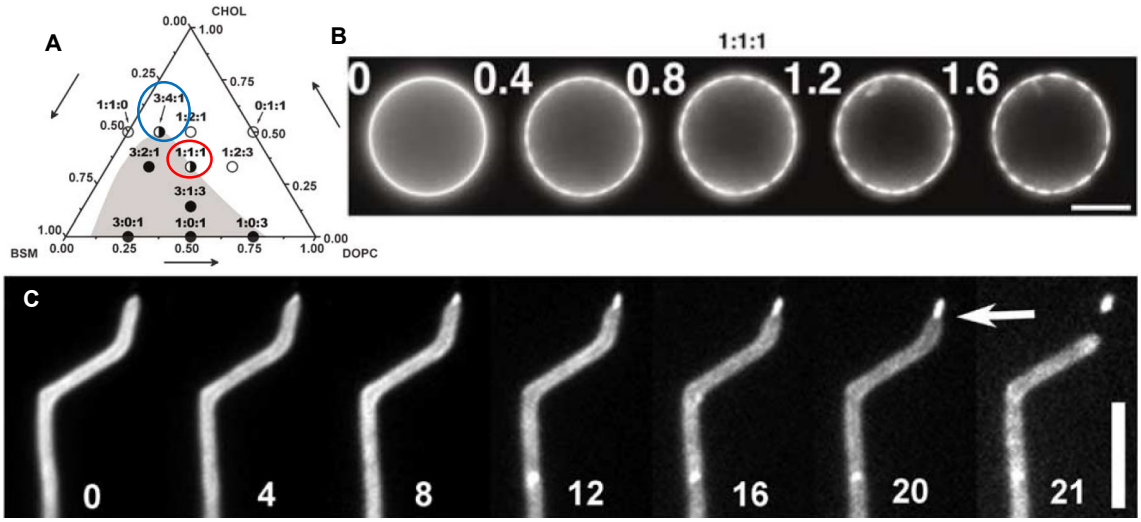

Figure 3.8: Membrane fission induced by phase separation. A. Phase diagram of the ternary mix: Brain Spingomyelin/DOPC/Cholesterol at 22°C. For composition in the white area, membrane is homogeneous. Phase separation occurs spontaneously for compositions in the grey area. Circles correspond to experiments on GUV. Open circles: no phase separation was observed. Filled circles: phase separation was observed. Half-filled circles: phase separation was observed only upon activation. Red circle: composition used in A. Blue circle: composition used in C. B. An initially homogeneous GUV (red circle in A.) undergoes phase separation upon exposure to light. Scale bars: 10 μm. C. An initially homogeneous lipid tube (blue circle in A) undergoes phase separation upon light activation followed by fission at the boundary between the two phases (white arrows). Scale bars: 10 μm. Adapted from Roux *et al.*, The EMBO Journal 2005.

Chapter 4

The Dynamin Protein

This chapter gives a review on Dynamin. Discovered during Tubulin purification, Dynamin was then identified as a mechanochemical enzyme involved in membrane fission. This protein has two major features: it hydrolyses GTP and polymerizes into a helix. The properties of this polymer will be described, especially the conformational changes observed upon GTP hydrolysis. The interplay between polymerization and GTPase activity gives rise to several models of fission that will be detailed.

4.1 Discovery Of A Membrane-Remodelling GTPase

4.1.1 Discovery

Dynamin was identified in 1989 as a protein copurified with Tubulin [124]. Like Dynein and Kinesin, this protein exhibited a nucleotide hydrolysis activity stimulated by microtubules [125]. Thus Dynamin was first considered as a microtubule-associated molecular motor. It was hypothesized that Dynamin would bundle microtubules and make them slide along one another upon nucleotide hydrolysis.
However in 1991, Dynamin was associated to vesicular traffic when sequencing showed that Drosophila Shibire gene encodes for a protein homologous to rat Dynamin [146]. The Shibire mutant was well known among neurobiologists as a thermosensitive mutant: at 19°C Shibire flies presented a normal phenotype whereas at 29°C they became reversibly paralyzed. This paralysis was due to a defect in synaptic vesicles recycling [71]. Electron microscopy on Shibire mutant synapses showed a depletion of synaptic vesicles and invaginations in the plasma membrane with an electron-dense collar at their neck (see Fig.4.1). Immunogold-labelling later confirmed that this collar indeed contained Dynamin proteins [30].

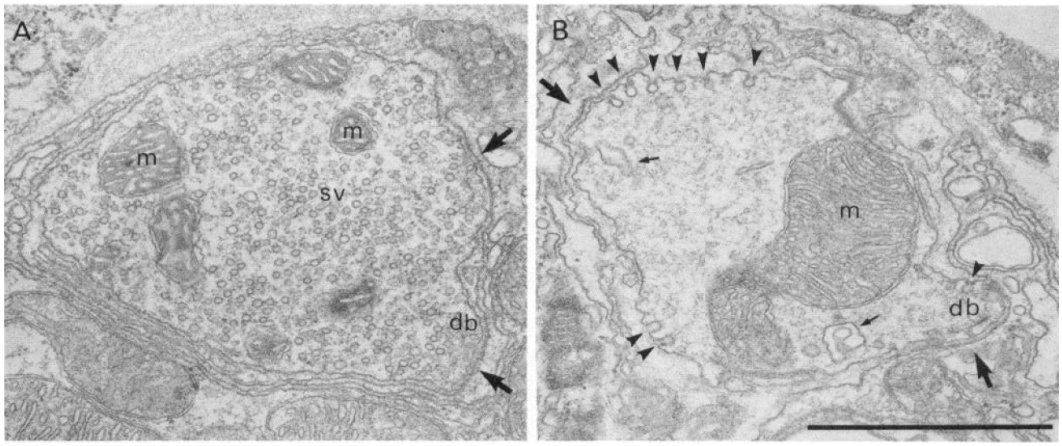

Figure 4.1: Electron micrographs of Shibire mutant synapses at 19 $^{\circ}C$ in A. and after 8 min at 29 $^{\circ}C$ in B. In A, many synaptic vesicles (sv) are present in the presynaptic neuron. In B, there are no synaptic vesicles but some plasma membrane invaginations (arrowheads). Thin arrows indicate large invaginations with their neck out of the sectioning plane. In A. and B.: m means mitochondria, db presynaptic dense body. Thick arrows indicate site of neurotransmitter release. Scale bar: 1 μm. From Koenig and Ikeda, Journal of Neuroscience 1989.

4.1.2 Role In Clathrin-Mediated Endocytosis

Since then the role of Dynamin in vesicular traffic was further investigated. Clathrin-mediated endocytosis (CME) was shown to be blocked in cells overexpressing a mutant defective in GTPase activity [30]. Live-cell imaging showed that Dynamin colocalizes transiently with Clathrin-coated pits [93] (see Fig.4.2). Precise study of endocytic protein recruitment at the plasma membrane by dual color total internal reflection fluorescence (TIRF) microscopy has revealed that Dynamin is present at low levels at early stages of Clathrin-coated pit maturation then a burst of Dynamin appears 2 to 4 s before vesicle scission [139] [1]. Experiments on genome-edited mammalians cells, where fluorescent Dynamin is expressed at endogenous level, have confirmed this transient recruitment [36]. These assays demonstrated that Dynamin is massively recruited to Clathrin-coated structures just before fission.

To further understand the role of Dynamin in CME, knockout mice have been generated. In Mammals, there are three isoforms of Dynamin: Dynamin 1 is expressed at high levels in neuronal tissue specifically, Dynamin 2 is ubiquitous and Dynamin 3 is enriched in testis, lung and neurons (but at a lower level than Dynamin 1). Dynamin 2 knockout is lethal during the early embryonic development. Dynamin 1 knockout mice are normal at birth but fail to thrive and die within two weeks [40]. Dynamin 3 mice have no obvious phenotype. However Dynamin 1 and 3 double knockout leads to a more severe phenotype than Dynamin 1 knockout [105].
In this thesis, we will focus on the Dynamin 1 isoform, one of the most abundant protein in neurons. According to knockout experiments, this isoform is not essential to prenatal development nor to synaptic vesicle recycling at basal neuronal activity since synaptic transmission is reduced but not suppressed in this case. A Dynamin-independent endocytic pathway is thought

[1] In this study, vesicle scission was detected by imposing cycles of extracellular pH and by following a pH-sensitive fluorescent probe attached to an endocytic cargo. When fission occurs, the cargo is no more accessible by extracellular medium so that the pH-sensitive probe is not affected by the pulses of pH.

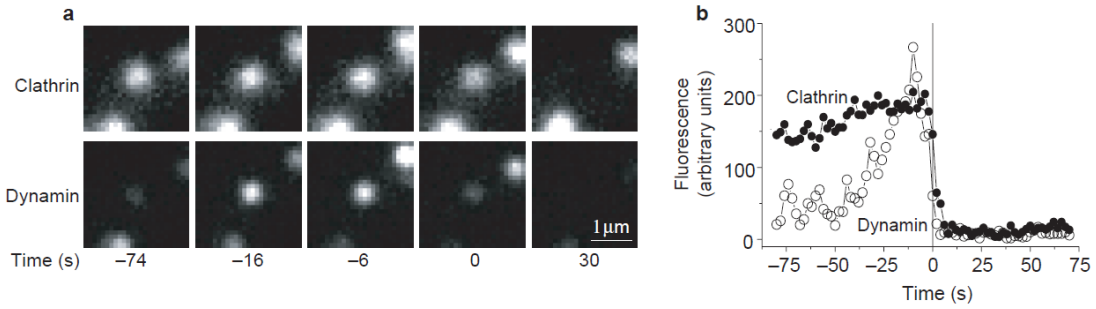

Figure 4.2: Transient colocalisation of Dynamin and Clathrin in live cells. a: Dual color total internal reflection videomicroscopy pictures of a Clathrin-coated structure in a 3T3 cell stably expressing Clathrin-light-chain-a-DsRed and transfected with Dynamin1-EGFP. Top pictures correspond to red channel (Clathrin) and bottom channel to green (Dynamin). b. Fluorescence intensities of Dynamin1-EGFP (open circles) and Clathrin-DsRed (filled circles) corresponding to the observation shown in a. Dynamin fluorescence bursts few seconds before Clathrin structure moves away from the surface. From Merrifield *et al.*, Nature Cell Biology 2002.

to rescue Dynamin 1 knockout phenotype in non-stimulated neurons. Nevertheless Dynamin 1 is required for efficient synaptic vesicle recycling at high level of activity: when neurons are stimulated in knockout mice, synaptic vesicle recycling is severly impaired. Electron tomography on stimulated neurons of Dynamin 1 knockout mice reveals branched structures in the plasma membrane of presynaptic neurons [52] (see Fig.4.3). Clathrin-coated pits are formed properly but fail to detach from the plasma membrane. These studies put in evidence the primordial role of Dynamin in synaptic vesicle recycling at the fission step.

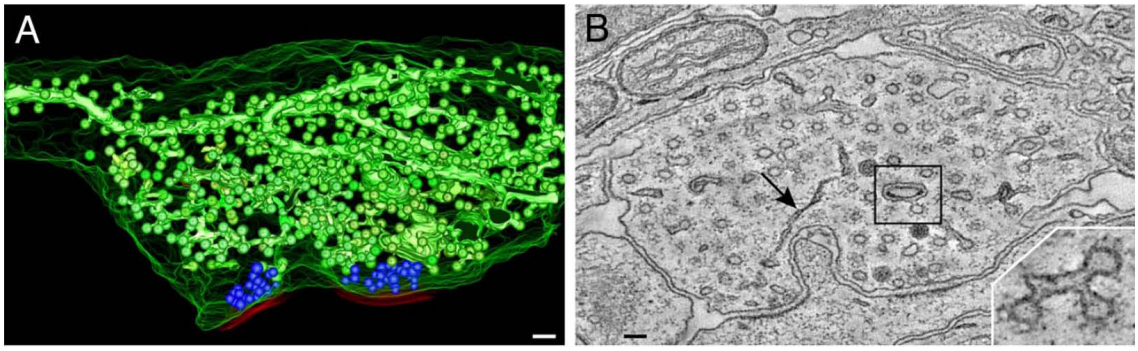

Figure 4.3: A. 3D reconstruction from 432 tomographic slices of a Dynamin 1 KO synapse. Large tubulo-vesicular structures connected to the plasma membrane are coloured in green. Synaptic vesicles are indicated in blue, the plasma membrane in green curves, post-synaptic membranes in red. B. Slice no 245 from the tomogram showed in A. Scale bars: 100 *nm*. From Hayashi *et al.*, PNAS 2008.

4.1.3 Dynamin Is Implicated In Several Membrane-Remodelling Processes

In addition to CME, it has been shown that Dynamin is involved in other endocytic pathways like in caveolae [56] and in phagocytosis [48] but also in other biological functions (see classical Dynamin in Fig4.4). For instance, Dynamin 2 has been implicated in cytokinesis where it allows membrane traffic at the cleavage furow [141, 72, 24]. Several studies argues for direct and indirect interactions between Dynamin and Actin [80, 64, 49]. However there is no consensus about the relationship between Dynamin and the cytoskeleton dynamics. More recently, Dynamin has been linked to fusion [6]: Dynamin GTPase activity regulates the dynamics of fusion pore expansion. Although Dynamin mechanism(s) is(are) still not understood for these diverse biological functions, they all require membrane deformations. Thus Dynamin is a membrane-remodelling protein.

4.1.4 Dynamin-Related Proteins

Some proteins share a similar sequence with Dynamin. These proteins are named Dynamin-Related Proteins (DRP). DRPs are involved in diverse biological functions (see Fig.4.4, [102]). For instance, Dynamin-related protein 1(Drp1) mediates fission of mitochondriae in mammalian cells [134]. The reverse process, the fusion of mitochondria, also involves DRPs: Optic atrophy 1 (Opa 1) [94] and Mitofusin 1 [26]. Chloroplast division in plant cells requires ARC5 [45]. Vacuolar protein sorting 1 (Vps 1) participates to intracelluar traffic at the Golgi apparatus in yeast [154]. Mx proteins are DRPs with an antiviral activity [51]. Although DRPs cover a broad range of functions, they do share some functional similarities. They are GTPases involved in membrane remodelling, they are also structurally similar and they self-assemble. Indeed oligomerization, that is described in the following section, is a key property of Dynamin.

4.2 Dynamin Structure: From Monomer to Helix

4.2.1 Monomer

Dynamin is a 100 kDa multidomain protein. Its five domains, from the amino- to the carboxyl-terminal, are: GTPase, Middle, PH, GED, PRD (see Fig.4.5.a and [60, 102, 41]). The GTPase domain binds and hydrolyses guanosine triphosphate (GTP). The middle domain is involved in Dynamin self-assembly. The Pleckstrin Homology (PH) domain binds non specifically to negatively charged lipids (like PS membranes) and interacts specifically with PIP_2. The GTPase Effector Domain (GED) is involved in Dynamin self-assembly and stimulates GTPase activity. The Prolin Rich Domain (PRD) is a coil-coiled region interacting with proteins containing a SH3 domain, such as Amphiphysin, Endophilin, Cortactin, Profilin.
The structure of the Dynamin monomer has been recently solved (see Fig.4.5.b and [39, 42]). The Middle and GED domains form together a stalk linking the GTPase domain to the PH domain. A Bundle Signalling Element (BSE) split in three parts (in the GTPase, the Middle and the GED domains) forms a domain which modulates the activity of self-assembled Dynamin [20].

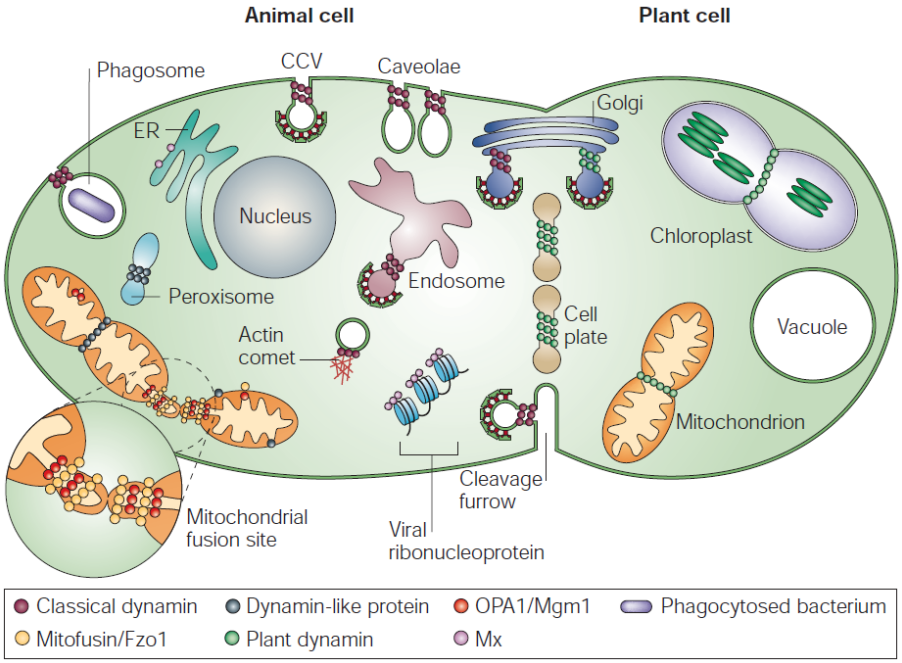

Figure 4.4: Sketch giving an overview of the main Dynamin-related proteins in the animal and plant cells. From Praefcke and McMahon, Nature reviews. Molecular Cell Biology 2004.

4.2.2 The Helix

The structue of Dynamin polymer has been established by electron microscopy. Under low ionic strength conditions and in absence of any templates (microtubules or lipid substrates), Dynamin spontaneously assembles into stacks of rings [61]. Electron micrographs reveal that the outer Diameter of those rings is $50 \pm 10nm$, compatible with the collar structure observed in Shibire. Stacks of rings are longer for higher concentrations of Dynamin. Polymerization is also observed when Dynamin is incubated with negatively charged liposomes made of PS (see Fig.4.6.A and [137, 31]) or with "nanorods" which are rigid preformed lipid nanotubes made of PC, non-hydroxylated fatty acid galactoceramide (NFA-GalCer) , PIP2 and cholesterol (see Fig.4.6.B and [132]). Under these more physiological conditions, the helical structure of the Dynamin polymer is clearly visible: lipid nanotubes are regularly striated (see Fig.4.6). The outer radius of the helix is 50 *nm* and the helical pitch (distance between two helical turns) is 13 *nm*. 3D-reconstruction shows that the subunit of this helix is a dimer of Dynamin [157]. Dimerization occurs via interactions in the stalk domain. Dynamin polymerizes around lipid nanotubes in a way that PH domains face the membrane and GTPase and PRD domains remain accessible for interactions with GTP and protein partners in the outer part of the helix (see Fig.4.6.C.).

The Dynamics of Dynamin polymerization has been investigated using the nanotube extrusion technique described in the previous chapter 3.2.2 [115]. Dynamin is injected close to preformed nanotubes made of PC and PIP_2. Dynamin first nucleates into several seeds along the tube then polymers expand from each seed (see Fig.4.7.A.). It is established that Dynamin polymerization depends on both Dynamin concentration and membrane curvature. For Dynamin concentrations between 280 nM and 12.6 μM, there is a tube radius threshold above which Dynamin does

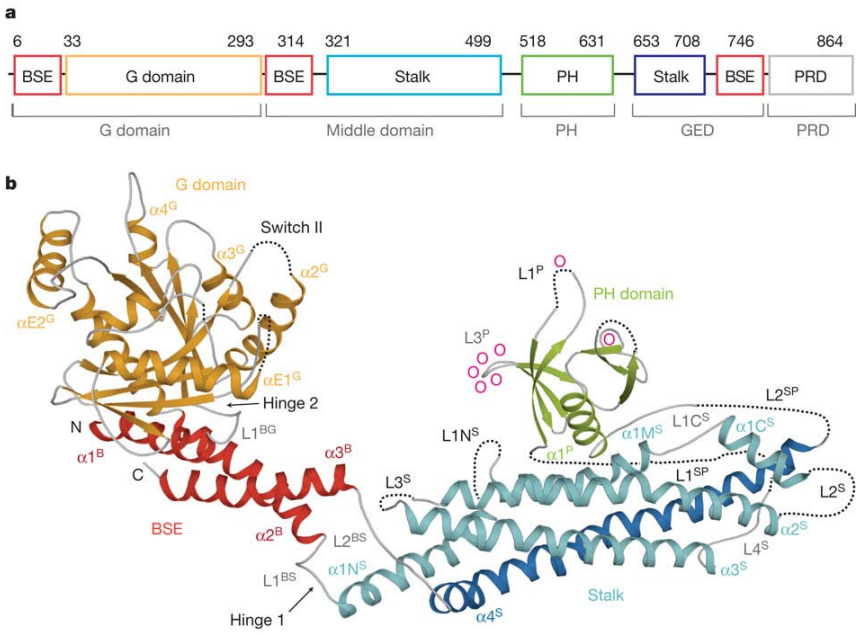

Figure 4.5: a. Domains of Dynamin. In grey the 5 classical domains of Dynamin explained in section 4.2.1. In colors, Dynamin domains including the stalk region and the bundle signalling element (BSE). b. Ribbon type representation of the structure of nucleotide-free human Dynamin 1 without the PRD. Dotted lines indicate regions not resolved in the crystal. Pink circles indicate lipid-binding residues. The same color code was used in a. and b. From Faelber *et al.*, Nature 2011.

not polymerize (see Fig4.7.B.). Below 280 nM of Dynamin, Dynamin does not polymerize at all. Above 12.6 μM Dynamin is not curvature sensitive and polymerizes for all radii.

4.3 Interplay Between GTPase Activity And Polymerization

4.3.1 Dynamin Is An Atypical GTPase

Dynamin is a GTPase: one monomer binds and hydrolyses one molecule of GTP. It is interesting to compare Dynamin to the classical family of GTPases: the small G proteins. These proteins, like the Ras family, are molecular switch: they are inactive when bound to GDP and active when bound to GTP. Small G proteins have a high affinity for nucleotide (for Ras proteins, dissociation constant: $Kd = 0.1\mu M$ [1]) but a very low basal GTP hydrolysis activity (for Ras proteins, GTP hydrolysis rate: 3.4 $10^{-4}s^{-1}$ [1]). To switch from one state to another, small G proteins require the help of other proteins: a guanine nucleotide exchange factor (GEF) catalizes GDP dissociation and a GTPase-activating protein (GAP) catalizes GTP hydrolysis. Compared to G proteins, Dynamin has a higher basal GTPase activity (GTP hydrolysis rate: 8-30 $10^{-3}s^{-1}$) and a lower affinity for nucleotide (dissociation constant: $Kd = 2.5\mu M$) (see [143, 11] and Fig.4.8). These biochemical features (low nucleotide affinity and high hydrolysis rate) are reminiscent of molecular motors which converts the chemical energy of nucleotide

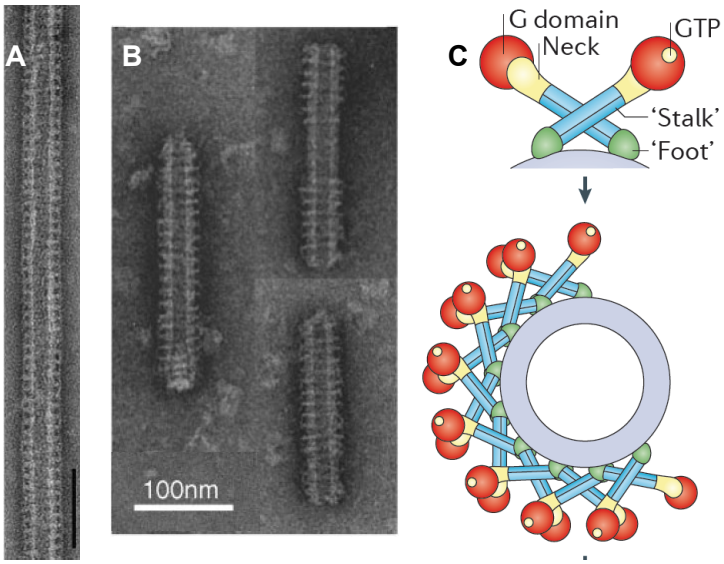

Figure 4.6: A. and B. Electron micrographs of Dynamin-coated lipid nanotubes. Horizontal striations along tubes correspond to Dynamin polymerization. A. Purified Dynamin was added to PS liposomes. Scale bar: 100 *nm* From Sweitzer and Hinshaw, Cell 1998. B. Purified Dynamin was added to nanorods made of PC, PIP2, cholesterol and non-hydroxy fatty acid galactocerebroside. From Stowell *et al* Nature Cell Biology 1999. C Top: sketch of a Dynamin dimer. Bottom: sketch of the dimer arrangement in the helix of Dynamin. From Ferguson and De Camilli, Nature Reviews Molecular Cell Biology 2012.

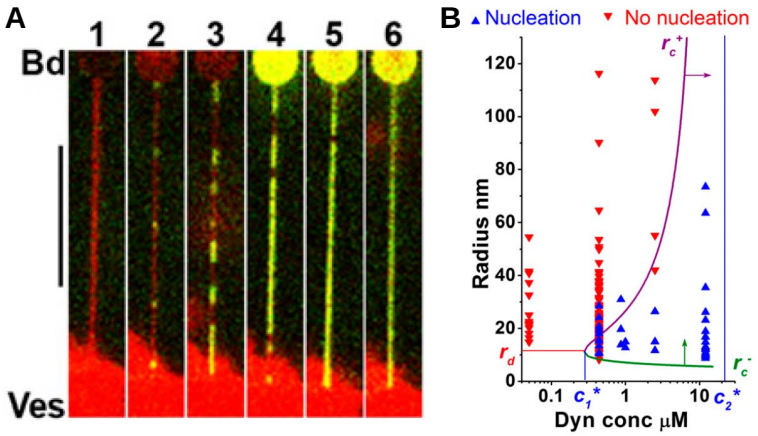

Figure 4.7: A. confocal microscopy pictures of a lipid nanotube labelled with BodipyTMR-PIP2 (in red) extruded from a GUV (1). Alexa488-labelled Dynamin (in green) is injected close to the tube. Dynamin starts nucleating along the tube in 2. then nucleation seeds expand until the full tube is covered in 6. B. Dynamin nucleation diagram as a function of nanotube radius and Dynamin concentration. Purple and green lines: theoretical predictions for nucleation threshold. Triangles represent experimental data points. Red triangles: no nucleation observed. Blue triangles: nucleation was observed. From Roux *et al* PNAS 2010.

hydrolysis into mechanical work. Thus Dynamin does not behave like a molecular switch but rather like a mechanochemical enzyme.

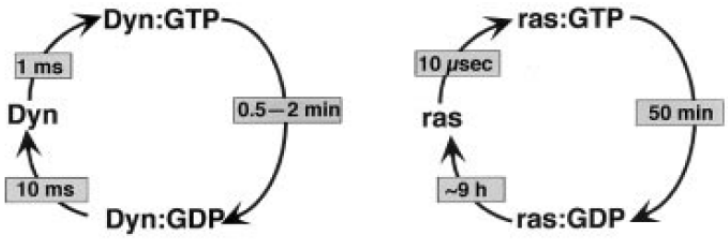

Figure 4.8: Sketches of GTPase cycles foe Dynamin (left) and Ras (right). Times indicated on arrows are half-times for the corresponding step at a basal level (in absence of cofactors). From Sever *et al.*, Traffic 2000.

4.3.2 Polymerization Stimulates GTPase Activity

Dynamin polymerization stimulates GTPase activity [143, 149]. GTPase rate increases up to 10-fold in conditions favoring spontaneous self-assembly: low ionic strength and high concentration of dynamin [149]. When Dynamin polymerizes on a lipid templates, the GTPase rate even increases up to 100-fold [84]. Structurally the BSE is thought to enhance the GTPase rate by inducing conformational changes upon dimerization [19]. However the precise mechanism by which polymerization stimulates GTPase activity is still not understood.

4.3.3 GTPase Activity Modifies The Helical Structure

GTP is not required for self-assembly. Indeed Dynamin mutant K44A, which has a very low GTPase activity, self-assembles like wild type [61] and Dynamin polymerization was observed in absence of nucleotide in nanotube extrusion experiments [115]. However GTPase activity modifies Dynamin helical structure. Electron microscopy experiments have revealed two types of structural modifications:

- increase of the helical pitch at constant radius;
  When dynamin polymerizes on nanorods, the helical pitch increases from 11 ± 2 to 20 ± 3 *nm* upon nucleotide treatment while the radius remains constant (40 ± 2.5 *nm*) (see Fig.4.9.A and [132, 87]).

- decrease of both pitch and radius;
  For Dynamin polymers prepared on negatively charged liposomes made of pure PS, upon nucleotide treatment it was observed that the outer radius decreases from 50 to 40 nm, the helical pitch decreases from 13 to 9 nm and the number of dimers by helical turn goes from 14 to 13 (see Fig.4.9.B and [137, 31, 23]).

It is likely that these different observations of helical structures result from different lipid templates for Dynamin polymerization. Indeed membrane properties, for instance the bending rigidity modulus κ, could influence Dynamin GTPase activity; exactly like membrane curvature influences Dynamin polymerization. It is also interesting to note that fission never occurs in

the case of nanorods whereas it does for pure PS liposomes under certain conditions discussed later in section 4.4.2.

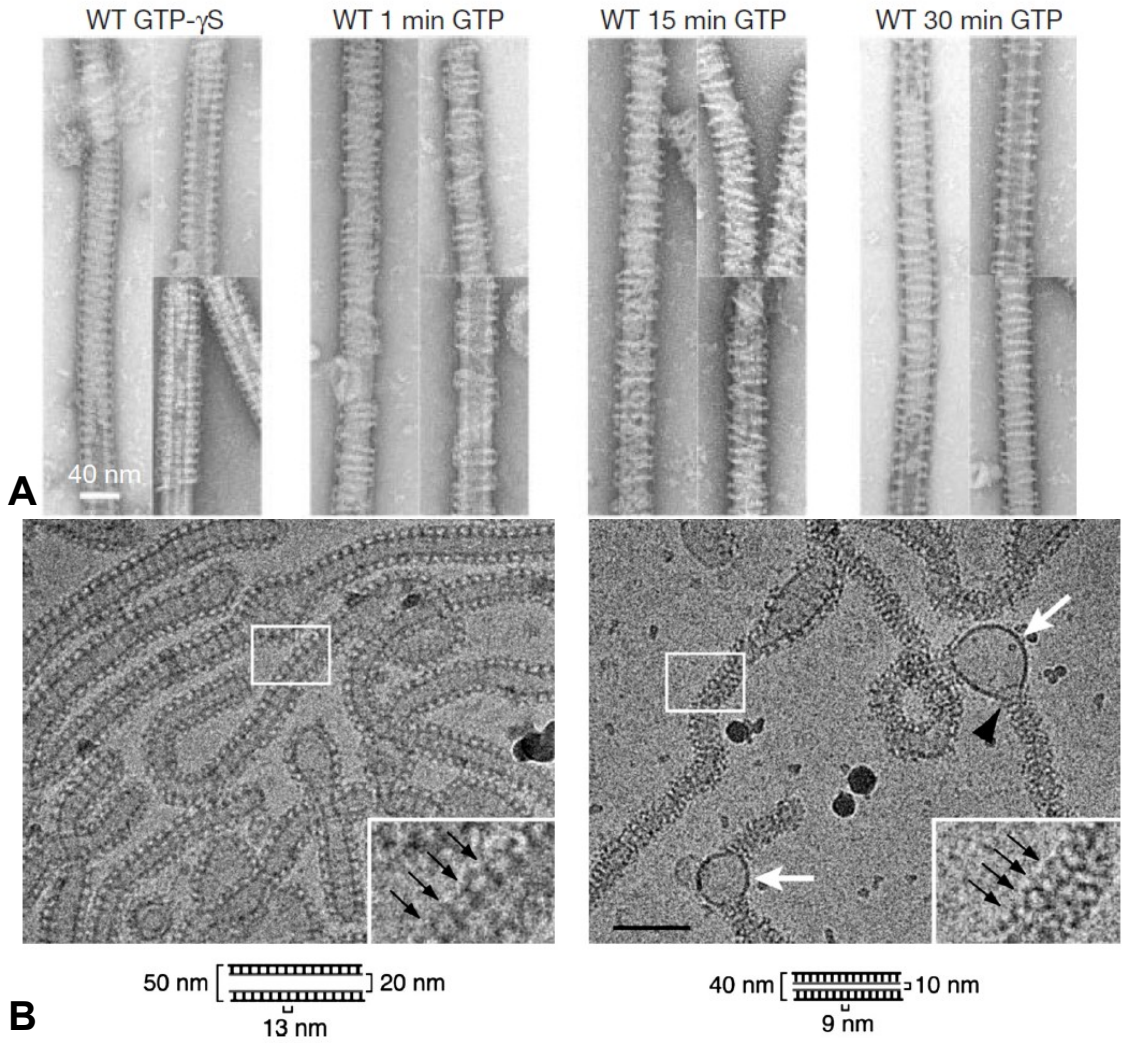

Figure 4.9: A. Electron micrographs of Dynamin-coated nanorods under different nucleotides treatment. Purified Dynamin was added to nanorods in the presence of 100 μM $GTP\gamma S$ or during the hydrolysis of 500 μM GTP. From Marks *et al.* Nature 2001 B. CryoEM-pictures of Dynamin-coated lipid nanotubes. Purified Dynamin was added to liposomes made of PS only. Left: no GTP. Right: after 5 *s* of GTP treatment. White arrows point at undecorated membrane bulge. Scale bar: 100 *nm*. From Danino *et al.*, Journal of structural biology 2004.

4.4 Fission Mechanism(s)

Fission of Clathrin-coated pits is defective in Dynamin mutants but the maturation of the pits remains normal [146, 40, 52]. More precisely Dynamin GTPase activity is required to trigger fission as GTPγS (a non-hydrolizable analogue of GTP) treatment in neurons leads to an impairement in vesicle recycling and to the formation of long Dynamin-coated tubules [138]. Moreover K142A strongly inhibits endocytosis. K142A is a Dynamin mutant with an almost normal GTPase activity but for which no conformational change is observed [87]. This indicates that fission is triggered by the GTP-dependent conformational changes of Dynamin helix. However inconsistencies emerge from *in vitro* experiments and give rise to several models.

4.4.1 Spring Or Garrote?

The first models of fission were deduced from structural data. As two types of structural changes were observed, it led to two models of fission: Dynamin would act like a "spring" or like a "garrote" [122].

- Spring model:
  this model was inferred from the observation of an increased pitch at a constant radius upon GTP hydrolysis (nanorods templates). The Dynamin helix would push away the vesicle from the plasma membrane in a "spring-like" mechanism (see Fig.4.10.A).
- Garrote model:
  a decrease in both radius and pitch, the other structural change observed (PS liposomes templates), led to the garrote model. In this case, the helix tightens upon GTP hydrolysis. This strongly suggests a mechanism where the Dynamin helix constricts the tube until fission occurs (see Fig.4.10.B).

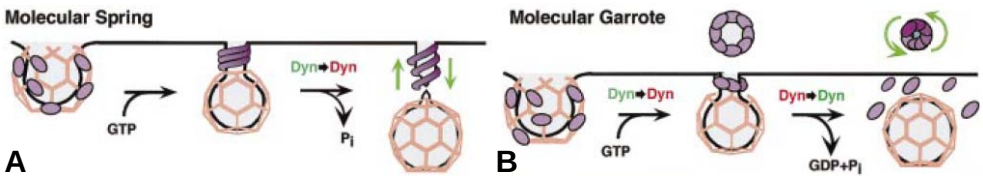

Figure 4.10: Two models of Dynamin-mediated membrane fission deduced from structural observations. A: spring model. B. garrote model. Adapted from Sever *et al.*, Traffic 2000.

A theoretical model manages to reconcile these apparently contradictory structural data. This coarse-grain model calculates membrane deformations resulting from Dynamin conformational changes. If we consider Dynamin mechanochemical action as equivalent to applying a torque and a force on the tube, then the different helical structures observed experimentally can be explained by the difference in membrane rigidities [83]. Indeed nanorods are rigid structures due to the presence of cholesterol and NFA-GalCer whereas PS liposomes are soft membranes easier to deform. Thus the same conformational changes occur at the Dynamin monomer level but result in two different helices because of membrane rigidity. This demonstrates that membrane elastic properties play an important role in Dynamin-mediated fission.

4.4.2 Is Constriction Leading to Fission?

The cryo-electron microscopy pictures shown in Figure 4.9.B. clearly suggest that constriction occurs during GTP hydrolysis. However constriction does not lead to fission in all cases. When GTP is added after fixation of Dynamin-coated tubes on the EM grid, small vesicles, remainings of tubes' fragmentation, are observed. In contrast if GTP is added in solution before fixation, unbroken constricted tubes are observed [31]. This implies that fission occurs *in vitro* only when nanotubes are attached on a surface. Indeed 3D reconstructions combining cryoEM and crystallography data highlight that the lipid nanotube is still intact underneath the constricted Dynamin helix (see Fig.4.11 and [157, 21]). The internal diameter of this lipid tube is 7 nm. This diameter is not small enough to trigger fission since hemifission[2] is predicted to happen at a diameter around 4 nm [76]. These reconstructions are based on the structure of GMPPCP-bound Dynamin. So one could argue that more constriction could come from GTP hydrolysis *in vivo*. But unbroken constricted nanotubes with GTP-bound Dynamin have also been observed by cryoEM ([31]). Reconstructions also lack the PRD domain but this domain is predicted to be on the outer part of the helix, and would not affect dramatically the conformational changes on its own. It could nevertheless recruit Dynamin cofactors which could facilitate fission.
From all these results, it appears that constriction is not enough to lead to fission. Which mechanism could be involved?

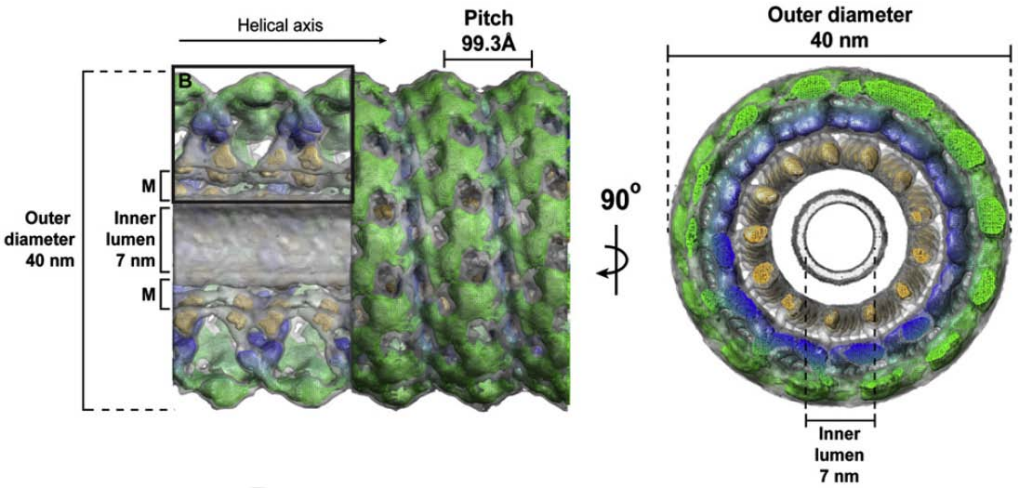

Figure 4.11: 12.2 Å reconstruction of GMPPCP-bound ΔPRD-Dynamin. In Green: GTPase domains. In Blue: stalk region. In yellow: PH domains. M means membrane bilayer. From Chappie *et al* Cell 2011

4.4.3 Does Dynamin Depolymerize Before Fission?

Dynamin depolymerization has been proposed to be the mechamism leading to fission. Sedimentation experiments show that, after polymerization, Dynamin detaches gradually from lipids upon GTP treatment: after a few minutes, around 70% of Dynamin is detached from liposomes [31]. More recently cycles of Dynamin assembly and disassembly have been detected in two

[2] hemifission is the intermediate state where the inner leaflet of the tube self-fuses while the outer leaflet remains intact

types of experiments.

- SUPER templates:
  SUPER templates are SUPported bilayers with Excess membrane Reservoir. They are made by incubating silica beads with liposomes [104]. Membrane budding is observed when Dynamin and GTP are injected on these SUPER templates. A patch of Dynamin can be detected by fluorescence at the neck of membrane buds. Fluorescence fluctuations in this patch have been measured (see Fig.4.12.A. and B. and [103]). These fluctuations are interpreted as cycles of polymerization and depolymerization.

- patch clamp:
  Patch clamp experiments on supported bilayers have been designed to measure the radius of a lipid nanotube by conductance measurement (see Fig.4.12.C.). After injection of Dynamin and GTP, fluctuations in the conductance were monitored followed by an abrupt drop corresponding to the tube break. These fluctuations are interpreted as fluctuations of the tube radius corresponding to cycles of Dynamin assembly and disassembly (see Fig.4.12.D. and [9]).

A challenging model has arisen from these results: Dynamin polymerization would stabilize the lipid tube in a state close to hemifusion, GTP hydrolysis would trigger Dynamin disassembly which would destabilize the lipid tube leading to fission. This model raises the issue of fission kinetic. To trigger fission, depolymerization should occur rapidly so that the tube does not have time to equilibrate and collapse into hemifusion. Considering the membrane viscosity, the typical tube radius and the membrane rigidity modulus, a typical timescale for membrane equilibration is 1 s[3]. *In vitro* Dynamin depolymerization takes more than 10 s. Some other proteins might facilitate Dynamin depolymerization *in vivo*. But as Dynamin and GTP are sufficent to generate fission *in vitro* [116, 103] there must exist a mechanism which does not require the help of other proteins.

4.4.4 How Does Membrane Elasticity Influence Dynamin-Mediated Fission?

We mentioned that membrane elasticity influences Dynamin polymerization (section 4.2.2) and the GTP-dependent conformational changes (section 4.4.1). Thus it seems logical that membrane properties would also affect fission.
In elctron microscopy experiments, fission occurs only when lipid nanotubes are attached on a substrate. When GTP is added on tubes freely diffusing in buffer, long unbroken constricted tubes are visible [31]. This observation suggests that maintaining the tube under tension is required for fission. This hypothesis was confirmed by Differential Interference Contrast (DIC) microscopy experiments. Dynamin was first injected on membrane sheets[4] where it spontaneously tubulates the membrane. GTP was then injected on the Dynamin-coated tubes. Fission was observed only for tubes mechanically attached at both ends (see Fig4.13.A). Free

[3] $t = \eta \frac{R}{\kappa}$ where η is the viscosity, R the radius and κ the bending rigidity modulus.

[4] Membrane sheets constitute a way to obtain easily planar lamellar sheets of membrane. Lipids are dried on a glass coverslide in a vacuum oven for at least one hour and then rehydrated with the appropriate buffer. This assay has been used to test the activity of membrane binding and/or remodelling proteins such as BAR and F-BAR proteins [64], and dynamin [116].

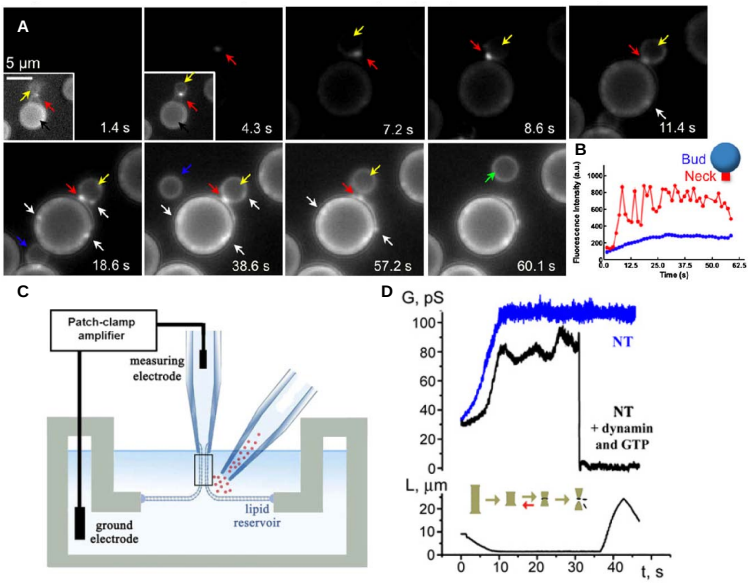

Figure 4.12: Evidence for cycles of Dynamin assembly and disassembly. A. Fluroescence microscopy images of lipid SUPER templates treated with fluorescent Dynamin and GTP. Yellow arrows indicate the bud attached to the bead, red arrows the patch of dynamin at the neck of the bud, black arrows the bead, white arrows regions with a strong Dynamin signal, green arrow the detached vesicle. B. Fluorescence intensity profiles of Dynamin at the bud (blue) and at the neck (red). From Pucadyil *et al.*, Cell 2008. C. Sketch of the patch clamp experiment. A lipid nanotube is extruded from supported bilayers with a pipette. Conductance is determined by measuring the current resulting from application of a constant potential between measuring and ground electrodes. A second pipette is used to inject Dynamin. D. Conductance curves. In balck: Dynamin and GTP are injected on a tube, there are oscillations in the conductance signal. In blue: nothing is injected, the conductance curve remains stable. From Bashkirov *et al.*, Cell 2008

tubes did not break but retracted (see Fig4.13.B). Other experiments show that fission still occurs at very low tensions [103]. Fluctuating (signature of a low tension) lipid nanotubes break after treatment with Dynamin and GTP (see Fig4.13.C). In this case, fission occurs after 20s, which is longer than the fission time measured for tubes under tension (1 s). Low membrane tension might delay fission. These results raises the question of the role of membrane tension in fission mechanism.

Conclusion

Regarding all the studies on Dynamin, the mechanism of membrane fission is still poorly understood. Does GTP hydrolysis trigger constriction and/or depolymerization? Which mechanism drives fission? What is the precise role of membrane tension and rigidity? What is the energy of fission? These are the questions addressed in this thesis.

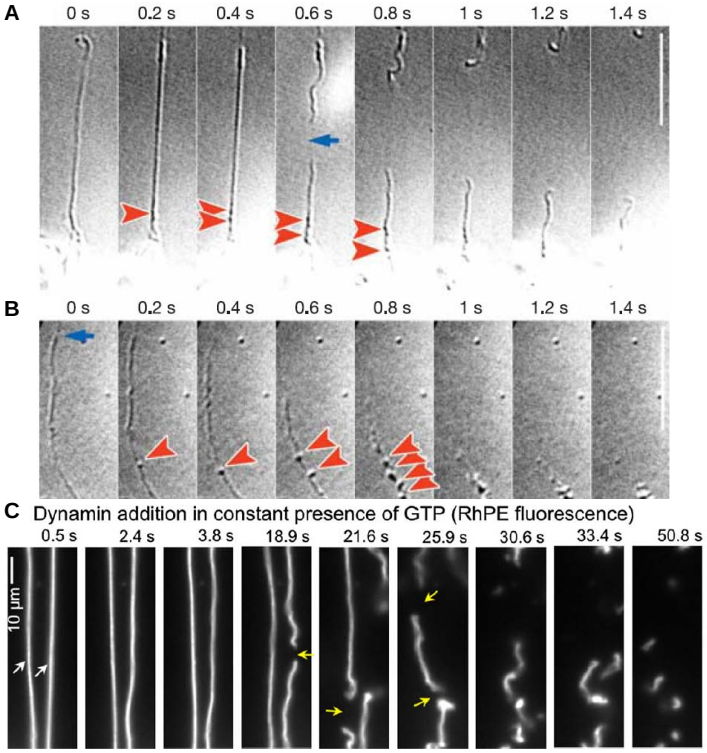

Figure 4.13: Role of tension in Dynamin-mediated fission. A. and B. DIC videomicroscopy images of Dynamin-coated lipid tubes treated with 1 *mM* GTP. In A. the tube is anchored at both ends and breaks only once (blue arrow). In B. the tube is free at one end (blue arrow) and does not break but retract toward the fixed end. Red arrows point to denser regions of the tube due to retraction, supposedly supercoils. Scale bars: 10 μm. From Roux *et al.*, Nature 2006. C. Fluorescence videomicroscopy images of two fluorescent lipid tubes treated with Dynamin and GTP simultaneously. Fission occurs several time successively on the same tube (yellow arrows). From Pucadyil *et al.*, Cell 2008

FEBS Letters 583 (2009) 3839–3846

FEBS Letters

journal homepage: www.FEBSLetters.org

Review

Mechanical requirements for membrane fission: Common facts from various examples

Martin Lenz [a], Sandrine Morlot [a,b], Aurélien Roux [a,*]

[a] Institut Curie, Centre de Recherche, CNRS, UMR 168, Physico-Chimie Curie, Université Pierre et Marie Curie/Paris 6, F-75248 Paris, France
[b] Université Denis Diderot/Paris 7, F-75013 Paris, France

ARTICLE INFO

Article history:
Received 1 September 2009
Revised 3 November 2009
Accepted 5 November 2009
Available online 11 November 2009

Edited by Daniela Corda

Keywords:
Membrane fission
Dynamin
Dynamin-like protein
ESCRT-III
Membrane tension
Lipid phase separation
Caveolae
COP
Organelle division

ABSTRACT

Membrane fission is the last step of membrane carrier formation. As fusion, it is a very common process in eukaryotic cells, and participates in the integrity and specificity of organelles. Although many proteins have been isolated to participate in the various membrane fission reactions, we are far from understanding how membrane fission is mechanically triggered. Here we aim at reviewing the well-described examples of dynamin and lipid phase separation, and try to extract the essential requirements for fission. Then, we survey the recent knowledge obtained on other fission reactions, analyzing the similarities and differences with previous examples.

1. Introduction

The early hypothesis of membrane traffic, as it was conceived just after the discovery that proteins could be transported between organelles [1], involved the formation of small vesicles that were separated from the donor membrane by a process called *membrane fission*. As a consequence, the compartimentalization of eukaryotic cells ensuring the specialization and function of each organelle was regarded as strictly dependent on this process: without membrane fission, all the organelles would end up being connected, mixing their contents and losing their function/specialization.

One of the first proteins found to be implicated in fission was dynamin. It was genetically shown to be involved in the release of synaptic vesicle from the plasma membrane [2], and the helical polymer it forms in vitro [3] and in vivo at the neck of endocytic buds [4] immediately suggested that it could trigger fission by constricting the neck of buds. In this paper, we first review 15 years of work on dynamin in order to understand how well this hypothesis is verified. The fact that dynamin-like proteins only work in a subset of fission reactions then prompts us to ask what the common features and/or functions of proteins/lipids involved in membrane fission are, and which other proteins are involved in other reactions.

2. Constriction versus shearing: what really triggers membrane fission?

As often in cell biology, morphological analysis at the ultrastructural level trigger hypothesis on molecular mechanisms. This is best exemplified by seminal work on dynamin: dynamin could constrict and fuse the two sides of the neck. In this picture, fission would be similar to fusion, as it would involve the same metastable intermediates [5]. This view was supported by studies showing that dynamin has all the features to actually drive fission by constriction/fusion: GTP is needed for fission [4], and, as shown in a milestone paper [6] by the Jenny Hinshaw group, dynamin alone can deform membranes into tubules circled by the dynamin helix. It was moreover shown in this work that upon GTP treatment such tubules constrict and break into very small vesicles. Therefore, it seemed at this point that a large-scale dynamin conformational change could provide enough work to constrict the tubule and fuse it locally, which would result in membrane breaking.

* Corresponding author. Address: 26 rue d'Ulm, 75248 Paris Cedex 05, France. Fax: +33 140510636.
E-mail address: aurelien.roux@curie.fr (A. Roux).

0014-5793/$36.00 © 2009 Published by Elsevier B.V. on behalf of the Federation of European Biochemical Societies.
doi:10.1016/j.febslet.2009.11.012

2.1. Dynamin: the paradigm of constriction

Several questions were brought about by the work of Hinshaw and co-workers: where does the constriction come from? Does the conformational change of the helical polymer induce torsion, similar to the wringing of linen fiber? Or does each individual monomer constrict, causing the helix to shrink in size, without really changing shape?

Early evidence of a linen-like conformational change came from a careful study of the biochemical interactions between different dynamin domains [7]. The strongest interactions were observed between hetero-domains and proposed to be in the continuity of the helical turn. They remained unchanged when the nucleotide load was modified, whereas the interactions between homo-domains were weaker in the presence of GTP and proposed to be between contiguous helical turns. This suggested that during the hydrolytic cycle of GTP, dynamin oligomers could undergo a cycle of binding/unbinding between adjacent helical rings. The authors of this study thus favored a mechanism by which sliding of adjacent helical turns would cause constriction.

The 3D structures [8] obtained by cryo-EM before and after constriction yielded a more detailed picture of this complex situation: as the dynamin polymer went from its non-constricted to its constricted state upon incubation with GMP–PCP, the number of dimers per turn went from 14 to 13, while constriction and bending of each dimer was also observed. This is a direct proof that some of the constriction actually occurs by torsion. The huge inward bending of each dimer however also has a dramatic influence on the membrane, and constricts it even more.

At the structural level, it thus seems that dynamin constriction comes from the combination of a global (torsion of the helical polymer) and a local (compaction of the monomers) conformational change. On the functional level, the structural studies of the Hinshaw group [8] have a remarkable feature: they show that long, continuous constricted tubules can be isolated, which is not at all expected in a situation where constriction alone induces tubule breaking. Pointing this out, the Hinshaw group also showed a striking difference between dynamin-coated tubules treated by GTP when observed by negative stain or by cryo-EM. When performing negative stain [6], which involves attaching the tubules to a substrate before GTP treatment, they observed a large amount of fission. On the other hand, when cryo-EM was used, which implies treating dynamin-coated tubules with GTP in bulk, no obvious fission occurred [9]. As a matter of fact, in the 3D constricted structure of Ref. [8], whole membrane tubules (as opposed to hemi-fission intermediates) are seen. It should however be noted that the tubules in this last reference were not treated with GTP, but with GMP–PCP, and that the comparison might therefore not stand as fission is observed with GTP only.

In a nutshell, there is compelling data supporting the early hypothesis that in addition to being required for fission, dynamin constricts membrane tubules upon GTP hydrolysis. Still, the essential question of whether this constriction is sufficient to induce membrane fission on its own was still open at this point.

2.2. What triggers membrane fission?

Recent studies have used live imaging and sensitive measurements to directly visualize dynamin-mediated membrane fission, and try to isolate the minimal requirements for dynamin-mediated membrane fission [10–12]. As membrane fission is a very transient event, the strength of these studies was the ability to follow a membrane template in real time while it is being broken by dynamin. Using dynamin-coated tubules grown from planar membrane sheets, a first study showed that rapid twisting of the dynamin helix occurred upon GTP treatment [10]. This twisting activity was further evidenced by the formation of supercoils, which also caused the long dynamin-coated tubules to retract. Surprisingly, tubules anchored only at one end never broke, while tubules anchored at both extremities ruptured after experiencing longitudinal tension, probably generated by the torsional activity of dynamin through the formation of supercoils. On top of confirming that part of the constriction comes from torsion, this study stresses the role of mechanical forces in dynamin-mediated membrane breaking. Such mechanical forces could be provided by the actin cytoskeleton, which would account for its known involvement in this process [13,14].

The fact that torsion occurs very rapidly led to the hypothesis that dynamin could break membranes by shearing/tearing (Bruno Antonny, private communication). Indeed, although a membrane sheared on long time scales will tend to flow, applying a torque very quickly to the membrane tubule could tear the membrane (see Fig. 1). An interesting feature of this mechanism is that its efficiency is crucially dependent on the velocity associated with torsion. If torsion is slower than membrane's viscoelastic time (defined as its viscosity over its stretching modulus and thus of order 10^{-8} s), dynamin will just crawl on the liquid membrane, which will be drained out by the squeezing action of the helix. If it is faster, shearing-induced breakage could occur. On those short time scales, the tube is expected to behave like a piece of rubber, and thus to collapse on itself under shear (see Fig. 1C). This collapse should occur in the early stages of the shearing (i.e. prior to tearing), meaning that membrane breakage will immediately be followed be self-sealing of the two resulting pieces into two separate tubules. Membrane breakage through shearing/tearing should thus be a non-leaky process. A recent theoretical description of dynamin's helical torsion/constriction [15] showed that the propagation of the helix' strain along the axis of very long helical polymers should follow a diffusive dynamics. It also predicts that on experimentally observable time scales, the rate of this

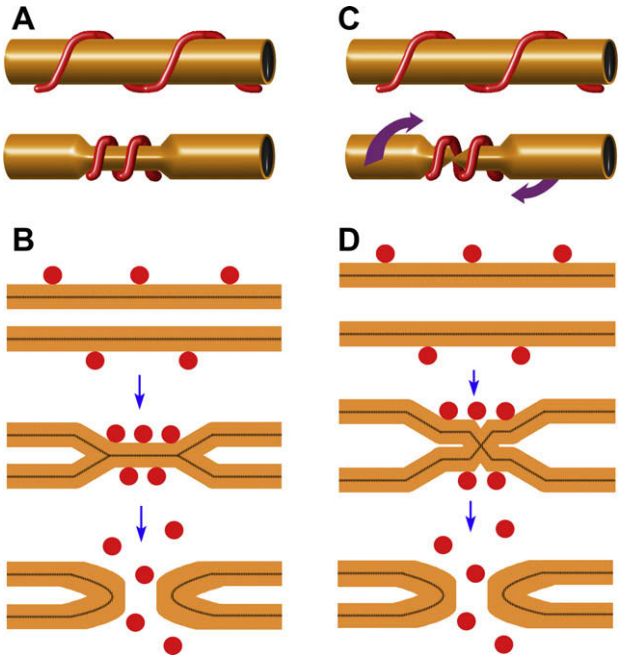

Fig. 1. Membrane tube fission by dynamin. (A and B) Dynamin breaks tubules by constriction. The conformational change (A) of the helix constricts the tubule until it hemi-fission is reached (B), and full fission is obtained when dynamin depolymerizes. (C and D) Dynamin breaks tubules by shearing. The conformational change (C) generates enough torsion to shear the membrane and either tear it (not shown) or fuse it. (D) Fission leads to dynamin depolymerization by removal of the membrane.

propagation and thus the torsion activity of dynamin are imposed by a friction of the helix onto the membrane. Strikingly, the longer the helix, the more difficult the membrane drainage and thus the slower the shearing of the membrane. Therefore, this study predicts that if dynamin breaks membrane by shearing, long dynamin helices break the membrane less efficiently than short ones.

This length-dependent efficiency of dynamin is indeed one of the important conclusions of a recent study [12]. Using supported bilayers on micron-size beads, Pucadyil and Schmid studied the fission efficiency when preformed dynamin-coated tubules were treated with GTP, or when a dynamin/GTP mix was directly applied to membranes. They showed that dynamin combined with GTP could create small vesicles out of the supported membranes. Using preformed dynamin-membrane tubes, they found that when dynamin was allowed to polymerize for a longer time on its own, less fission occured upon GTP addition. They concluded that fission was more efficient when dynamin formed short helices, a situation similar to the one encountered in vivo.

Another conclusion of this paper is that fission is concomitant with the depolymerization of the dynamin coat. This is also the main conclusion of a study by Bashkirov and coworkers [11]. By using membrane tubules extracted with a patch-clamp micropipette from a black lipid membrane, Bashkirov and coworkers monitored the conductance through the tubule while dynamin interacts with it, with or without GTP. When dynamin is added to the tubule in the presence of GTP, the conductance abruptly fell to zero after a random time lag, which is a signature of fission. Conversely, when dynamin was added onto the tubule in the absence of GTP, a gradual decrease of the tubule's conductance was seen, stabilizing at very low values compatible with squeezing of the tubule by dynamin polymerization. When GTP was added to these tubules, a gradual increase of the conductance was first observed, which showed a release of dynamin squeezing by depolymerization. Then, after a time lag, a sudden decrease to zero was observed, which indicated fission. Based on their quantitative evaluation of the tubule radius when dynamin is polymerized, the authors propose that polymerization itself would drive sufficient constriction to bring the membrane into a metastable state. Then, hemi-fission and fission would spontaneously occur when dynamin comes off the membrane, as the dynamin coat maintains the continuity of the membrane until it is released through GTP-dependent depolymerization. It has been argued [16] that the radius measured (5–6 nm, including membrane) for dynamin-coated tubules in the absence of GTP is surprising in view of other studies [4,6,8,9], and might reflect a technical underestimation of the real radius. A tubule of 5 nm radius is certainly in a highly constrained state that makes it metastable, but 10 nm is compatible with stability.

The merit of these two studies is to put the focus on what really triggers membrane fission. Bashkirov et al. [11] clearly showed that fission occurs by hemi-fission, since no leakage is observed. These studies lead us to ask when sufficient constriction is reached to drive hemi-fission, and what triggers full fission. Clearly, these two papers agree on the fact that fission is triggered by dynamin depolymerization. But when is hemi-fission generated?

Putting all this data together, a two-step model for dynamin-mediated membrane fission can be proposed (see Fig. 1). After polymerization of a dynamin helix, full constriction is obtained by GTP-dependent constriction/twisting. This constriction could lead to hemi-fission of the membrane, and fission would occur subsequently to the depolymerization of the coat. This depolymerization could be induced either by conformational stresses appearing upon torsion, or directly from GTP hydrolysis that would weaken the polymer bonds. Alternatively, constriction/twisting could shear the membrane, leading to full membrane fission, promoting depolymerization by removing the substrate for dynamin continuity.

3. Role of membrane properties

In this section, we temporarily turn away from the role of proteins in membrane fission, and consider how the properties of the membrane itself might assist, or even drive its own fission. Lipid membranes are auto-sealable objects, a property that makes them very difficult to break. However, this is mostly true for membranes that are composed of one single lipid, as the non-miscibility of lipids makes lipid bilayers more fragile, and here we first review membrane fission driven by lipid separation. Consistent with our observation that mechanics is relevant for the action of dynamin, we then turn to two important mechanical properties of the membrane, namely its the bending rigidity and tension, which could affect the action of fission machineries, including dynamin.

3.1. Membrane fission by lipid phase separation

The first pieces of evidence for phase separation in lipid bilayers date back to the 70s [17,18]. The formation of domains with a certain lipid composition, floating in an ocean of a different composition, led to the "raft" hypothesis in the late 80s, revealing how membrane properties could affect membrane traffic.

Phase separation is usually associated with an energy cost proportional to the size of the interface. In a three-dimensional system, e.g. oil and water, interfaces are surfaces. The energy cost is thus proportional to the *surface area* of the interface between the two fluids, through a coefficient known as the interface's "surface tension". For two-dimensional lipid domains, interfaces are lines, and the energy cost is proportional to the *length* of the interface, thus defining a "line tension". Both surface and line tension measure how badly the different components want to separate. The requirement that the interfacial energy be minimal implies that fluid membrane domains have a circular shape, which minimized the interfacial length at constant domain surface area. For high line tensions, it was theoretically proposed [19] that another way of reducing the length of the interface would be to bud the domain out of the plane of the membrane, the connecting neck where the interface sits being narrower than the domain (see Fig. 2A). In this case, an extra energetic cost must however be paid to bend the membrane into a curved vesicle. In extreme cases where the

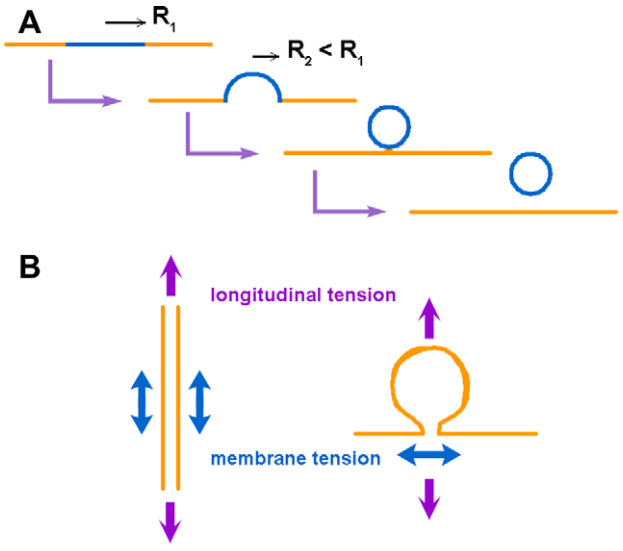

Fig. 2. (A) A lipid domain (blue) is budding and fissioning from the donor membrane (yellow) while line tension is increasing. (B) Combined effects of longitudinal tension and membrane tension depending on the geometry of the membrane (tubule vs. sphere).

line tension is high enough to override this bending cost [20], it was proposed that the constriction generated by phase separation at the neck of these buds would be sufficient to break the membrane. Deformation of membranes by lipid phase separation has been studied experimentally quite recently [21], and led to the first direct measurement of line tension between lipid domains, close to 1 piconewton (pN). In some case, the authors of this work observed the complete disappearance of the neck, suggesting fission, which was confirmed by other studies (see for example [22]). Similarly, lipid phase separation induced along membrane tubules formed by kinesins in vitro leads to fission [23] at the boundary between domains.

3.2. Role of membrane tension

In the instances of phase separation-driven membrane breaking, the membrane geometry and tension play an important role in crossing the energy barrier for fission. For instance, highly tense membrane tubules formed by kinesins (tension larger than 5×10^{-5} N/m) break less than 1s after induction of phase separation, whereas tubules formed at a low tension (smaller than 10^{-6} N/m) take up to 20 s to break ([24] and unpublished data). The role of membrane tension in facilitating tubule fission is twofold: first, as the radius of the tubule is dependent on membrane tension ($radius = \sqrt{\frac{\kappa}{2\sigma}}$, where κ is the membrane bending rigidity and σ is the membrane tension [25]), an increase in membrane tension drives the radius down, which takes the membrane closer to a fissioned state; second, *surface* tension (expressed in N/m) is concomitant with the tubule's *longitudinal* tension (in N), which is defined as the externally applied force required to prevent the tubule from retracting. This longitudinal tension could help fission by maintaining the structure during the operation of the fission machinery. As discussed previously, longitudinal tension facilitates dynamin-mediated fission. This is analogous to the case of a rubber band that needs to be slightly extended in order to be cut by scissors.

To further clarify the relationship between surface tension and longitudinal tension, we note that they may either act in the same direction or have antagonistic effects depending on geometry. As mentioned above, tubules are an example of a synergetic effect between membrane tension and longitudinal tension, as both are coaxial with the tubule (see Fig. 2B). In the case of a spherical bud, on the other hand, longitudinal tension (pulling on the bud) favors fission by facilitating the detachment of the bud, whereas membrane tension has an opposite effect (see Fig. 2B): it tends to flatten the membrane, and therefore to the collapse the bud into a flat membrane. By counteracting constriction, membrane tension could therefore hinder fission. In vivo, it was actually shown that an increased membrane tension can block endocytosis [26], whereas a decreased membrane tension tends to increase the endocytosis rate [27].

3.3. Conclusion

Dynamin and lipid phase separation are two examples of how tubular membrane structures can be broken. Beyond the specifics of these two examples, we are interested in extracting some basic principles of how membrane fission is mediated, which could help understand other fission machineries. In the case of lipid phase separation, fission occurs by constriction, as the domains are fluid and no torsion occurs [23,24]. Membrane parameters can crucially up- or down-regulate the energy barrier to be crossed for fission to occur. A theoretical model [28] shows how the combined actions of actin pulling on an endocytic bud and constriction generated by lipid phase separation could promote fission in systems lacking the active role of dynamin. The main lessons from studies on pure lipid membranes are: (1) fission by a pure constriction mechanism can occur; (2) membrane tension, depending on the geometry of the membrane (a neck between two vesicles or a tubule) can either reduce or enhance the energy barrier to fission and (3) applying external stresses on the constriction neck can help overcome the energy barrier.

However, it is not clear yet how small the radius has to be made in order to lead to fission. The structure of the dynamin helix provides some information about this threshold constriction radius. Dynamin does drive constriction on two occasions: (1) when it polymerizes, and (2) when it undergoes a conformational change while hydrolyzing GTP. Most probably, polymerization does not provide enough constriction to reach fission, as the internal radius is larger than 10 nm after polymerization, a tubule size compatible with membrane stability, as tubules of this size are experimentally observed. After GTP hydrolysis, internal radius was measured to be in the range of 4–5 nm by cryo-EM [9]. This is larger than the thickness of a bilayer (3 nm). However, it is smaller than the thickness of a bilayer plus the threshold radius (3 nm) that was proposed to spontaneously lead to membrane hemi-fission intermediates [29]. It is thus difficult to conclude on the state of the membrane inside the coat after GTP treatment. These data however indicate that the threshold radius for fission must be smaller than 5 nm.

4. Other examples in the light of these principles

As far as we know, most of the fission events happening within a cell are dynamin-independent. Although the fission mechanisms underlying most of these events are still largely unknown, the insight gained from the examples of dynamin and lipid phase separation may help understand the mechanisms at work in other systems involving fission.

In this section, we consider other fission machineries in the light of the systems described above. This discussion is not intended as an exhaustive review, but rather as an attempt to extract similarities and divergences between various biological solutions to the membrane fission problem.

4.1. Other dynamin-like proteins

Many homologues of dynamin have been identified and most of them are involved in membrane remodeling [30]. Several examples come from the fission machinery of mitochondria and chloroplasts. The protein Dnm1/Drp1 (yeast and mammalian, respectively) is the most characterized member of the dynamin superfamily, other than dynamin [31]. It is the main player of mitochondria division, which is mediated by a single fission machinery to break the two mitochondrial membranes in a single event. In chloroplast division, ARC5, another dynamin-like protein, forms the ring necessary for constriction. ARC5 is a cytosolic protein that binds to the outer membrane of the plast, and ARC6 is involved in the alignment of this ring with the matricial collar of FtsZ [32]. Chloroplasts have kept the prokaryotic division machinery through evolution (the FtsZ ring) and its positioning system (the Min proteins). ARC5 was shown to participate in a GTP-dependent constriction of purified chloroplast rings [33], and the amazing supercoiling of these rings could be reminiscent of a twisting activity as described for dynamin constriction [10].

Dnm1 forms helices much wider than those formed by dynamin (55 nm compared to 25 nm, outer radii) that fit the thickness of a double membrane [34]. By analogy, one could expect that ARC5 is structurally similar to Dnm1, and that Dnm1 is able to mediate constriction in a similar GTP-dependent way than ARC5. They also both bind to the outer membrane of the organelle through binding to trans-membrane proteins (PDV1 for ARC5 and Fis1 for Dnm1 through a cytosolic linker called Mdv1, [31,35]).

All these similarities suggest that the mitochondrial and plastid fission machineries work in a very similar way to dynamin itself. However, as we discussed above, if dynamin fission occurs by constriction only, it requires a very tight constriction (radius < 5 nm). Although two membranes are present in mitochondria, Dnm1 has to reach the same final constriction to break the last membrane. Thus, the larger size of these rings that fits the fission intermediates observed in vivo is required for assembly on a larger structure, but would need to constrict to the same radius to complete fission. Increasing the starting size of the helix requires a bigger conformational change to complete fission: dynamin outer radius goes from 25 nm to 20 nm during constriction, an already considerable conformational change. For a similar constriction mechanism to occur in the case of Dnm1/drp1, the radius of the tubules it forms would need to go from 55 nm to 20 nm, and to break two membranes: this would be a formidable constriction, and would probably cause breaks in the polymer. Disruption of the Dnm1 spiral was actually seen when treated with GTP [34]. If dynamin-mediated fission is conducted through a shearing mechanism, the break in the membrane does not depend on the final radius of the tube, but rather on how fast the torsion is applied. Thus, shearing can in principle break thick membrane necks, but probably with leaks. The larger size of Dnm1/drp1 spirals may be the indirect indication that membrane is broken by shearing. Another explanation could account for this larger size. Indeed, the large radius of Dnm1/drp1 might just be required to accommodate the cytosolic domain of the transmembrane receptor (Fis1 for Dnm1) and the cytosolic linker (Mdv1). In this case, after assembly of the three components, the space left in the helical coat for the membrane must be much smaller than when Dnm1/drp1 is alone. In other words, the thickness of the coat containing Dnm1/drp1, the cytosolic linker and the transmembrane receptor would be much bigger than for Dnm1/drp1 alone. Thus, the membrane would already be more constricted by assembled coats and thus a smaller conformational constriction would be required to complete fission. Indeed, a recent study showed that Mdv1 enhances the ability of Dnm1 to self-assemble on liposomes in the presence of nucleotides [36]. The thickness of the coat is enhanced in the presence of Mdv1, even though the size of the helix is unchanged. However, the human equivalent of Dnm1, Dlp1, induces the formation of tubules both in vitro and in vivo [37], but their size is very similar to that of classical dynamin-coated tubules.

Surprisingly, almost all other dynamin-like proteins have been implicated in fusion instead of fission, and have either a transmembrane domain or a highly hydrophobic region that suggest a deep insertion in the membrane: whether there is a connection between these properties, which diverge from the classical dynamins, is still unknown.

A recent study of Atlastin, a GTPase located at the ER, shows that it is critical for homotypic fusion of the ER, maintaining a dense, highly connected network [38]. Atlastin, besides having sequence and structural homology with dynamin [30], was recently shown to form tubules in vitro [39]. Also, the fusion of mitochondria is a two-steps mechanism as it involves two membrane fusions and therefore two fusion machineries, one for each membrane. Both of these machineries have dynamin-like proteins, the mitofusins 1 and 2 and Fzo1 for the outer membrane, and Mgm1/OPA1 for the inner membrane.

The fact that dynamin-like proteins (DLPs) are involved in fusion reactions supports the idea that fission is mediated through a fusion-like mechanism. In this interpretation, fusion would be mediated by the generation of high curvature, as in the case of synaptotagmin [40]. The tip of DLP-coated tubules would be a highly fusogenic point if sufficient curvature is reached. Even though nothing is known about oligomers formed by these specific proteins, one can expect that highly curved tubules and destabilization of the bilayer due to the deep insertion of their hydrophobic parts in the lipids would drive fusion. A consistent biochemical fact with this fusion activity is that they share low GTP hydrolysis rates compared to DLPs involved in fission [41]. It means that fusogenic DLPs would live longer in a GTP bound state, more favorable for polymerization and tubule formation. Long-life tubules would be then more favorable for fusion, having time to connect and fuse with the acceptor membrane.

Based on this assumption, one would predict that the recently described Epsin-Homology Domain (EHD) family of proteins [42] would belong to the fusogenic class of dynamin-like proteins. Proteins of this family are able to polymerize and form tubules coated by a helix. They hydrolyze ATP instead of GTP, but are otherwise both structurally and functionally very similar to other dynamin-like proteins. These proteins are implicated in membrane remodeling, but have no clear fission activity, at least in in vitro assays used for dynamin. They might thus just constitute another type of fusogenic dynamin-like protein.

4.2. Caveolae fission

Caveolae were shown to fission the plasma membrane by a dynamin-mediated process [43]. However, the lipid composition enriched in sphingolipids and cholesterol of caveolae led to the hypothesis that caveolin, the main component of caveolae, could drive lipid phase separation by locally increasing the cholesterol concentration in the membrane [44], as it binds cholesterol. This lipid phase separation could help/drive both the budding and the fission reaction of caveolae. A theoretical study [45] also proposed that not only the lipid phase separation, but the specific ordering of chiral and tilted lipids in the caveolin-coated phase could drive budding, fission and the formation of the surprising proteic patterns observed in vivo [46]. This lipid chirality-induced phenomenon was first proposed to explain the formation of endocytic tubular carriers driven by the binding of a toxin cargo to specific lipids [47].

It thus seems that caveolae are an endocytic route where all the known factors to drive fission are present, but nevertheless their time lapse at the plasma membrane is very long, arguing for a low fission rate. Experimental evidence suggests that caveolae could be endocytic structures blocked at the fission step [48]. It has been proposed that caveolin actually stabilizes raft endocytosis, probably by blocking fission [49]. One can speculate that the role of caveolin, if inhibiting fission, would be to reduce line tension at the boundary between caveolae and the plasma membrane, thus preventing their fission. This function is analogous to that of detergents, which can stabilize oil/water emulsions (i.e. very small droplets of oil in water) by reducing the surface tension of the oil–water interface. This would ensure good sorting of lipids and proteins by lipid phase separation without promoting fission. Fission would still be tightly regulated by the recruitment of dynamin, or by direct removal of the caveolin coat, which would enhance line tension and thus drive fission.

4.3. Golgi COPs

COPs I and II are coat proteins forming spherical carriers involved in trafficking between the ER and the Golgi. It is one of the most studied systems in membrane trafficking, and their sorting, assembly process and regulation are very well characterized. There is however only little knowledge about the fission reaction in these trafficking pathways. It has been proposed that the polymerization of the coat could drive fission by closing on itself as a sphere. This hypothesis is however in conflict with the fact that non-fissioned buds can be isolated in semi-reconstituted systems [50], and with the one that no obvious fission is seen in an assay

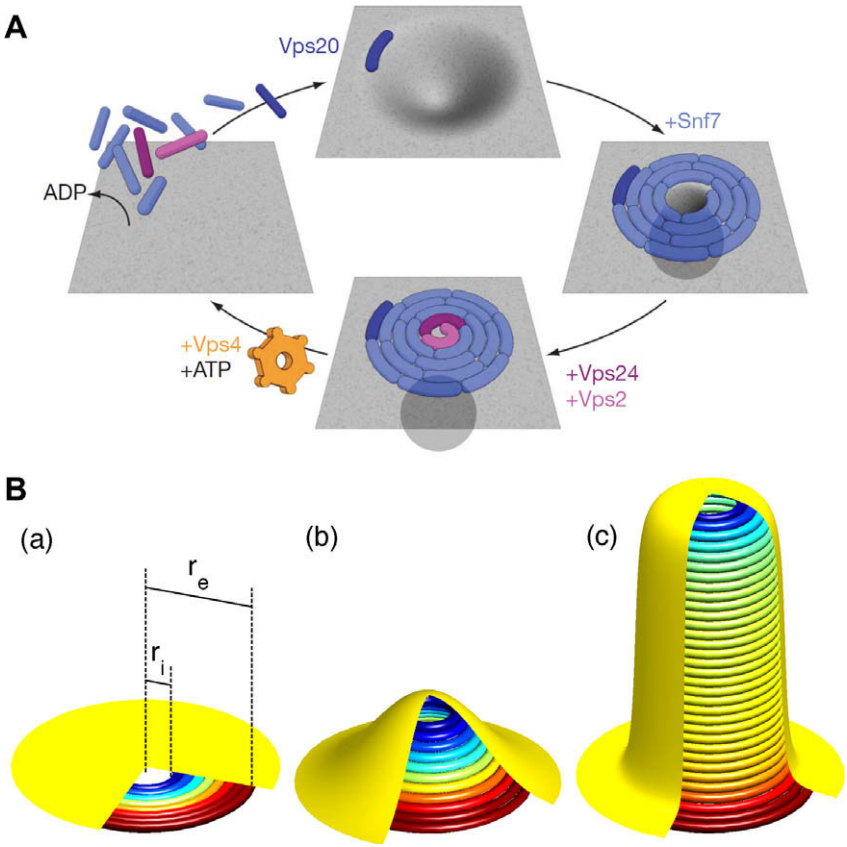

Fig. 3. (A) Budding and fission of membrane generated by the ESCRT-III complex. Polymerization of Snf7 into a spiral drive the deformation into a sphere, and then Vps24 stops the polymerization and finalizes the fission of the bud. Adapted from Ref. [59]. (B) Membrane buckling induced by Snf7 polymerization. As Snf7 polymerizes into rings (a), the smaller (blue) and the larger (red) rings accumulate potential energy as they are not at their preferred radius (yellow). A relaxation can occur by buckling the membrane (b), most of the rings being able to adjust to their preferred radius (c). Adapted from Ref. [58].

reconstituting purified COP I coats on Giant Liposomes [51]. In the COP I system, it was discovered early that Palmitoyl-CoA, a lipid intermediate in acyl chains metabolism, is necessary for the fission of buds [50]. Acyl-CoAs are strong detergents as they associate acyl chains with a large hydrophilic group (the Coenzyme A) which is required for their interactions with enzymes. This may drive fission per se, by destabilizing membranes, and by stabilizing pores and fusion intermediates. However, it is important to notice that non-hydrolysable analogs of Palmitoyl-CoA can block the fission reaction of these buds [50]. This strongly favors a role of Acyl-CoA in the acylation of fission proteins rather than a direct role in membrane fission.

Recent progress has been made on the fission reaction of COP II buds: Sar1p, the small GTPase controlling the recruitment of the coat to the membrane, was shown to participate both in the generation of curvature and in the fission reaction. It was shown that the amphipathic helix used by Sar1p to bind to the membrane could create curvature by insertion, thus tubulating membranes [52]. The same mechanism would help the squeezing of the necks of COP II buds. This could allow for direct fission [52] or fission upon release of Sar1p from the membrane (which itself occurs upon GTP hydrolysis) and the subsequent membrane destabilization [53]. Unexpectedly, the COP coat itself came back in the play recently. A mutation causing Cranio-lenticulo-sutural dysplasia was isolated in SEC23A, a component of the first block of COP II (Sec23/24), recruited to the membrane by Sar1p. Surprisingly, this mutation led to a defect of COP II traffic, where buds and pearled tubules accumulate in vivo [54]. Also, they showed evidences for a defect in recruiting the second level of COP II (Sec13/31 complex), and a synergy with Sar1p, as the Sar1A isoform partially compensate the SEC23A mutant phenotype, as the Sar1B does not. This is probably due to the higher affinity of Sar1A for Sec23/24, recruiting more Sec23/24 to the membrane. Taken together, these observations show that a defect of polymerization is associated with a defect of fission. All other steps of budding (membrane deformation, sorting) seemed unaffected. Thus, it suggests that closing of the bud by polymerization of the coat may cause fission. In other words, the forces needed to break the membrane by constriction could be in part provided by polymerization of the COP II coat. Nevertheless, as expected from previous studies, the coat alone is not able to perform fission and is probably assisted by co-factors, Sar1p in the case of COP II. The role of these co-factors is probably to reduce the energy barrier for fission by facilitating membrane bending, reducing the cost of constriction. However, it is still difficult to picture exactly how mechanically membrane fission occurs in the COPs systems, and hopefully future work will reveal interesting mechanical properties involved in this specific reaction.

4.4. ESCRT-III: deforming and severing the membrane from the inside

ESCRT complexes (Endosomal Sorting Complex Required for Transport) were first identified for their role in endosomal traffic [55]. Among the four known ESCRT complexes, ESCRT-III is the only one involved in the generation of intralumenal vesicles during the maturation of late endosomes to Multi-Vesicular Bodies (MVBs). These membrane-remodeling properties have recently been linked to two importants molecular features. First, one of the proteins of the ESCRT-III complex called Snf7 (CHMP4A,B in mammals) was shown to polymerize once nucleated by Vps20 (CHMP6), another protein of the complex. More precisely, when

overexpressed in cells, Snf7/CHMP4 binds at the plasma membrane, polymerizing into spirals that can form elongated tubules pointing out of the cell [56]. Two different explanations have been proposed for this membrane deforming activity: It was first proposed that the oligomerization of Snf7/CHMP4 would form a lasso-like structure, and that its depolymerization would cause the loop of the lasso to shrink in size, forcing the membrane enclosed by the polymer to curve in order to adjust the reducing size of the loop [57]. Based on morphological images obtained in Snf7/CHMP4 overexpressing cells, a recent theoretical study [58] proposed another, more intuitive explanation: it assumes that Snf7/CHMP4 filaments have a preferred radius of curvature and bind to each other as well as to the membrane, which accounts for the formation of tubular structures. Also, Snf7/CHMP4 has a strong affinity for the membrane. Therefore, in the presence of a membrane, the protein forms planar spirals covering the membrane, as observed experimentally [56]. In this configuration, the spiral rings smaller than the preferred radius of polymerization (the radius of helical polymers in the absence of membrane) are compressed, and spiral rings larger than the preferred radius are extended (see Fig. 3). This frustration of the polymer can be released by buckling the membrane in the center of the spiral, forming a tubule that allows most of the rings to adjust to their desired radius, as well as the binding of a larger number of filaments (see Fig. 3). This buckling mechanism resembles the spiral spring of a watch that pushes the frame out when overloaded.

Further discussions are required to understand how fission is mediated in this system. In order to tackle this question, we first note that the vesicles in the MVBs are budding inside the endosome, and that proteins or lipids involved in fission are *inside* the neck of the bud, which is the exact opposite of dynamin-mediated fission. This geometry seems incompatible with external forces applied to the membrane to squeeze it as in the case of dynamin. Thus, it was proposed that fission could be caused by depolymerization of Snf7/CHMP4, as it required ATP and Vps4 for completion. In the "lasso" hypothesis, fission would be triggered when the loop closes on itself. However, a recent study [59] showed that fission occurs when polymerization is stopped by Vps24. Vps4 and ATP, which are required for the disassembly of the complex, are actually required to resolubilize the proteins and to allow for several cycles of membrane deformation/fission, but not for fission itself. The authors of this last reference propose that the Snf7 spirals could curve the membrane in a similar way than in the "lasso" hypothesis, but with the difference that the reduction of the radius enclosed by the first ring of Snf7 is made by polymerization inside the first ring, forming a spiral (see Fig. 3). At the end, the spiral is closed by addition of Vps24, which completes fission.

Surprisingly, in this case, fission occurs without the need of an energy source. ATP and Vps4 are only required for depolymerizing both Snf7/CHMP4 and Vps24, Vps2 (CHMP3 and CHMP3 resp.) polymers. This means that the energy needed for fission comes from another source. Clearly, ESCRT-III generates membrane deformation and fission in a coupled manner. Vps24, which is the protein completing fission, when combined to its partner Vps2 is able to deform membranes into tubules and make a special dome-like structure that could participate in this fission event [60]. It also participates in the recruitment of Vps4 and Vps2 to the ESCRT-III complex and could be localized at the inner tip of the spirals generated by Snf7/CHMP4. One can speculate that the constriction needed for fission may arise from the tight association of the membrane on this dome-like structure. Then, depolymerization of ESCRT-III structures could occur at the tip/dome-like structure after fission has occurred. Because it challenges our views on membrane fission, ESCRT-III is obviously a system of choice to study membrane fission.

5. General conclusion

Membrane fission is an important topological change in the organization of cellular membranes. Here we have briefly described general principles of membrane fission mediated by lipid phase separation and by dynamin. The common principle of these two fission reactions seems to be a mechanism by which constriction brings the two sides of the membrane into close contact until they fuse, which is an energetically costly step. The differences in the origin of this energy in the examples presented here illustrates the diversity and richness of the field of membrane fission: at one end of the spectrum, the energy required for lipid phase separation originates in the physical interactions between different lipids, which manifest themselves as a line tension; on the other, dynamin-mediated fission is protein-driven and draws its energy from an active mechanism: nucleotide hydrolysis. Although the molecular ingredients involved in membrane fission are very diverse, emerging quantitative approaches taking into account physical parameters might provide a unified framework to study it. A first step in that direction could be a more precise determination of the energies it requires.

References

[1] Palade, G. (1975) Intracellular aspects of the process of protein synthesis. Science 189, 347–358.
[2] Koenig, J.H. and Ikeda, K. (1989) Disappearance and reformation of synaptic vesicle membrane upon transmitter release observed under reversible blockage of membrane retrieval. J. Neurosci. 9, 3844–3860.
[3] Hinshaw, J.E. and Schmid, S.L. (1995) Dynamin self-assembles into rings suggesting a mechanism for coated vesicle budding. Nature 374, 190–192.
[4] Takei, K., McPherson, P.S., Schmid, S.L. and De Camilli, P. (1995) Tubular membrane invaginations coated by dynamin rings are induced by GTP-gamma S in nerve terminals. Nature 374, 186–190.
[5] Kozlov, M.M. and Chernomordik, L.V. (2002) The protein coat in membrane fusion: lessons from fission. Traffic 3, 256–267.
[6] Sweitzer, S.M. and Hinshaw, J.E. (1998) Dynamin undergoes a GTP-dependent conformational change causing vesiculation. Cell 93, 1021–1029.
[7] Smirnova, E., Shurland, D.L., Newman-Smith, E.D., Pishvaee, B. and van der Bliek, A.M. (1999) A model for dynamin self-assembly based on binding between three different protein domains. J. Biol. Chem. 274, 14942–14947.
[8] Chen, Y., Zhang, P., Egelman, E. and Hinshaw, J.E. (2004) The stalk region of dynamin drives the constriction of dynamin tubes. Nat. Struct. Mol. Biol. v11, 574–575.
[9] Danino, D., Moon, K.H. and Hinshaw, J.E. (2004) Rapid constriction of lipid bilayers by the mechanochemical enzyme dynamin. J. Struct. Biol. 147, 259–267.
[10] Roux, A., Uyhazi, K., Frost, A. and De Camilli, P. (2006) GTP-dependent twisting of dynamin implicates constriction and tension in membrane fission. Nature 441, 528–531.
[11] Bashkirov, P.V., Akimov, S.A., Evseev, A.I., Schmid, S.L., Zimmerberg, J. and Frolov, V.A. (2008) GTPase cycle of dynamin is coupled to membrane squeeze and release, leading to spontaneous fission. Cell 135, 1276–1286.
[12] Pucadyil, T.J. and Schmid, S.L. (2008) Real-time visualization of dynamin-catalyzed membrane fission and vesicle release. Cell 135, 1263–1275.
[13] Itoh, T., Erdmann, K.S., Roux, A., Habermann, B., Werner, H. and De Camilli, P. (2005) Dynamin and the actin cytoskeleton cooperatively regulate plasma membrane invagination by BAR and F-BAR proteins. Dev. Cell 9, 791–804.
[14] Merrifield, C.J., Perrais, D. and Zenisek, D. (2005) Coupling between clathrin-coated-pit invagination, cortactin recruitment, and membrane scission observed in live cells. Cell 121, 593–606.
[15] Lenz, M., Prost, J. and Joanny, J.F. (2008) Mechanochemical action of the dynamin protein. Phys. Rev. E Stat. Nonlinear Soft Mat. Phys. 78, 011911.
[16] Roux, A. and Antonny, B. (2008) The long and short of membrane fission. Cell 135, 1163–1165.
[17] Jain, M.K. and White 3rd, H.B. (1977) Long-range order in biomembranes. Adv. Lipid Res. 15, 1–60.
[18] Klausner, R.D., Kleinfeld, A.M., Hoover, R.L. and Karnovsky, M.J. (1980) Lipid domains in membranes. Evidence derived from structural perturbations induced by free fatty acids and lifetime heterogeneity analysis. J. Biol. Chem. 255, 1286–1295.
[19] Jülicher, F. and Lipowsky, R. (1993) Domain-induced budding of vesicles. Phys. Rev. Lett. 70, 2964–2967.
[20] Jülicher, F. and Lipowsky, R. (1996) Shape transformations of vesicles with intramembrane domains. Phys. Rev. E Stat. Phys. Plasmas Fluids Rel. Interdisciplin. Top. 53, 2670–2683.
[21] Baumgart, T., Hess, S.T. and Webb, W.W. (2003) Imaging coexisting fluid domains in biomembrane models coupling curvature and line tension. Nature 425, 821–824.

[22] Bacia, K., Schwille, P. and Kurzchalia, T. (2005) Sterol structure determines the separation of phases and the curvature of the liquid-ordered phase in model membranes. Proc. Natl. Acad. Sci. USA 102, 3272–3277.
[23] Roux, A., Cuvelier, D., Nassoy, P., Prost, J., Bassereau, P. and Goud, B. (2005) Role of curvature and phase transition in lipid sorting and fission of membrane tubules. EMBO J. 24, 1537–1545.
[24] Allain, J.M., Storm, C., Roux, A., Ben Amar, M. and Joanny, J.F. (2004) Fission of a multiphase membrane tube. Phys. Rev. Lett. 93, 158104.
[25] Derényi, I., Jülicher, F. and Prost, J. (2002) Formation and interaction of membrane tubes. Phys. Rev. Lett. 88, 238101.
[26] Dai, J., Ting-Beall, H.P. and Sheetz, M.P. (1997) The secretion-coupled endocytosis correlates with membrane tension changes in RBL 2H3 cells. J. Gen. Physiol. 110, 1–10.
[27] Raucher, D. and Sheetz, M.P. (1999) Membrane expansion increases endocytosis rate during mitosis. J. Cell Biol. 144, 497–506.
[28] Liu, J., Kaksonen, M., Drubin, D. and Oster, G. (2006) Endocytic vesicle scission by lipid phase boundary forces. Proc. Natl. Acad. Sci. USA 103, 10277–10282.
[29] Kozlovsky, Y. and Kozlov, M.M. (2003) Membrane fission: model for intermediate structures. Biophys. J. 85, 85–96.
[30] Praefcke, G. and Mcmahon, H. (2004) The dynamin superfamily: universal membrane tubulation and fission molecules? Nat. Rev. Mol. Cell. Biol. 5, 133–147.
[31] Hoppins, S., Lackner, L. and Nunnari, J. (2007) The machines that divide and fuse mitochondria. Annu. Rev. Biochem. 76, 751–780.
[32] Glynn, J.M., Miyagishima, S.Y., Yoder, D.W., Osteryoung, K.W. and Vitha, S. (2007) Chloroplast division. Traffic 8, 451–461.
[33] Yoshida, Y. et al. (2006) Isolated chloroplast division machinery can actively constrict after stretching. Science 313, 1435–1438.
[34] Ingerman, E. (2005) Dnm1 forms spirals that are structurally tailored to fit mitochondria. J. Cell Biol. 170, 1021–1027.
[35] Osteryoung, K.W. and Nunnari, J. (2003) The division of endosymbiotic organelles. Science 302, 1698–1704.
[36] Lackner, L.L., Horner, J.S. and Nunnari, J. (2009) Mechanistic analysis of a dynamin effector. Science 325, 874–877.
[37] Yoon, Y., Pitts, K.R. and McNiven, M.A. (2001) Mammalian dynamin-like protein DLP1 tubulates membranes. Mol. Biol. Cell 12, 2894–2905.
[38] Orso, G. et al. (2009) Homotypic fusion of ER membranes requires the dynamin-like GTPase Atlastin. Nature 460, 978–983.
[39] Muriel, M.P., Dauphin, A., Namekawa, M., Gervais, A., Brice, A. and Ruberg, M. (2009) Atlastin-1, the dynamin-like GTPase responsible for spastic paraplegia SPG3A, remodels lipid membranes and may form tubules and vesicles in the endoplasmic reticulum. J. Neurochem. 110, 1607–1616.
[40] Martens, S., Kozlov, M.M. and McMahon, H.T. (2007) How synaptotagmin promotes membrane fusion. Science 316, 1205–1208.
[41] Hoppins, S. and Nunnari, J. (2009) The molecular mechanism of mitochondrial fusion. Biochim. Biophys. Acta 1793, 20–26.
[42] Daumke, O., Lundmark, R., Vallis, Y., Martens, S., Butler, P. and Mcmahon, H. (2007) Architectural and mechanistic insights into an EHD ATPase involved in membrane remodelling. Nature 449, 923–927.
[43] Oh, P., McIntosh, D.P. and Schnitzer, J.E. (1998) Dynamin at the neck of caveolae mediates their budding to form transport vesicles by GTP-driven fission from the plasma membrane of endothelium. J. Cell Biol. 141, 101–114.
[44] Anderson, R.G. and Jacobson, K. (2002) A role for lipid shells in targeting proteins to caveolae, rafts, and other lipid domains. Science 296, 1821–1825.
[45] Sarasij, R., Mayor, S. and Rao, M. (2007) Chirality-induced budding: a raft-mediated mechanism for endocytosis and morphology of caveolae? Biophys. J. 92, 3140–3158.
[46] Rothberg, K.G., Heuser, J.E., Donzell, W.C., Ying, Y.S., Glenney, J.R. and Anderson, R.G. (1992) Caveolin, a protein component of caveolae membrane coats. Cell 68, 673–682.
[47] Römer, W. et al. (2007) Shiga toxin induces tubular membrane invaginations for its uptake into cells. Nature 450, 670–675.
[48] Hommelgaard, A., Roepstorff, K., Vilhardt, F., Torgersen, M., Sandvig, K. and Van Deurs, B. (2005) Caveolae: stable membrane domains with a potential for internalization. Traffic 6, 720–724.
[49] Nabi, I. (2003) Caveolae/raft-dependent endocytosis. J. Cell Biol. 161, 673–677.
[50] Pfanner, N., Orci, L., Glick, B.S., Amherdt, M., Arden, S.R., Malhotra, V. and Rothman, J.E. (1989) Fatty acyl-coenzyme A is required for budding of transport vesicles from Golgi cisternae. Cell 59, 95–102.
[51] Manneville, J.B. et al. (2008) COPI coat assembly occurs on liquid-disordered domains and the associated membrane deformations are limited by membrane tension. Proc. Natl. Acad. Sci. USA 105, 16946–16951.
[52] Lee, M.C., Orci, L., Hamamoto, S., Futai, E., Ravazzola, M. and Schekman, R. (2005) Sar1p N-terminal helix initiates membrane curvature and completes the fission of a COPII vesicle. Cell 122, 605–617.
[53] Antonny, B. (2006) Membrane deformation by protein coats. Curr. Opin. Cell Biol. 18, 386–394.
[54] Fromme, J.C. et al. (2007) The genetic basis of a craniofacial disease provides insight into COPII coat assembly. Dev. Cell 13, 623–634.
[55] Hurley, J.H. (2008) ESCRT complexes and the biogenesis of multivesicular bodies. Curr. Opin. Cell Biol. 20, 4–11.
[56] Hanson, P.I., Roth, R., Lin, Y. and Heuser, J.E. (2008) Plasma membrane deformation by circular arrays of ESCRT-III protein filaments. J. Cell Biol. 180, 389–402.
[57] Saksena, S., Wahlman, J., Teis, D., Johnson, A.E. and Emr, S.D. (2009) Functional reconstitution of ESCRT-III assembly and disassembly. Cell 136, 97–109.
[58] Lenz, M., Crow, D.J. and Joanny, J.F. (2009) Membrane buckling induced by curved filaments. Phys. Rev. Lett. 103, 038101.
[59] Wollert, T., Wunder, C., Lippincott-Schwartz, J. and Hurley, J.H. (2009) Membrane scission by the ESCRT-III complex. Nature 458, 172–177.
[60] Lata, S., Schoehn, G., Jain, A., Pires, R., Piehler, J., Gottlinger, H.G. and Weissenhorn, W. (2008) Helical structures of ESCRT-III are disassembled by VPS4. Science 321, 1354–1357.

Chapter 5

Dynamin Constriction Is Concerted And Damped by Membrane Friction

5.1 Introduction To Article 1

Electron microscopy experiments show that the Dynamin helix constricts upon nucleotide treatment [31] but little is known about the dynamics of this constriction. It is particularly interesting to study this dynamics as constriction does not systematically lead to fission. By attaching microbeads to Dynamin-coated lipid nanotubes, it is possible to follow in real time the conformational changes of dynamin helices. These nanotubes were formed by injecting a mix of non-labelled Dynamin, biotinilatied Dynamin and Strepatvidin-coated beads on membrane sheets. Dynamin at high concentration ($10\mu M$) tubulates spontaneously the membrane forming long tubes coated with Dynamin and microbeads. After injection of GTP, these beads start rotating around the tube (see Fig5.1 and [116]). It has been observed that the rotation speed decreases with time (see Fig5.1). This decay suggest a damping phenomenon that could hinder the fission mechanism.

The dynamics of Dynamin constriction has been described theoretically [83]. The hydrodynamic formalism used in this study relies on two assumptions: only the long time scales and the large length scales are taken into account and the system is weakly out of equilibrium. In this coarse-grain model, a long Dynamin-coated tube is considered as a system of two bidimensional fluids with a helical geometry (see Fig.5.2). The conservation laws (mass and energy are conserved) and the relationship between fluxes and forces supplemented with a free energy source representing the hydrolysis of GTP allow to conclude to the existence of three successive diffusive hydrodynamic modes. The two fastest modes are not detectable experimentally ($t < 10ms$). On this time scale, there is no relative flow between the helix and the membrane. Thus the dissipation of energy is dominated by the friction against the surrounding water. On time scales corresponding to the third mode, the only one observable ($t > 1s$), the membrane is drained out of the helix and the friction between the membrane and the helix is the main dissipative mechanism. This implies that the dynamics of Dynamin constriction should follow

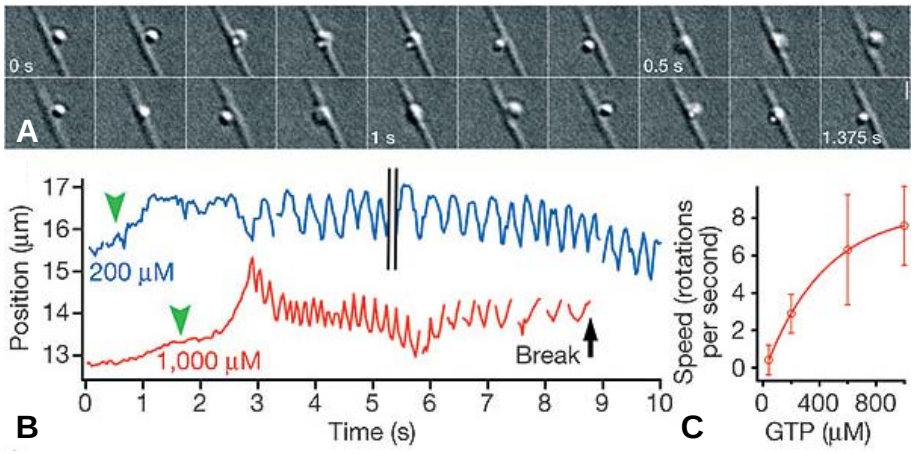

Figure 5.1: Direct evidence of Dynamin constriction upon GTP hydrolysis. A: DIC videomicroscopy pictures of a Dynamin-coated lipid nanotube with a microbead attached on it after injection of 200 μM GTP. The bead turns twice around the lipid tube. Scale bar: 1 μm B: Trajectories of two beads at different GTP concentrations. Trajectories were measured as the displacement perpendicular to the tube axis. Green arrowheads indicate GTP injection. C: Average rotation speed (and standard deviation) as a function of GTP concentration. From Roux *et al.*, Nature 2006.

a diffusive behaviour.

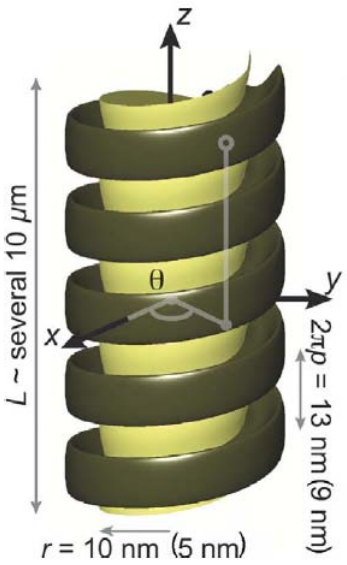

Figure 5.2: Sketch representing the geometry of the two fluids modelling a Dynamin-coated tube. The Dynamin helix is depicted in brown and the membrane in yellow. The system follows a helical symmetry. From Lenz *et al.*, PRE 2008.

This theoretical model has been tested using the rotating bead assay described above. The results are detailed in the article below 5.2: Deformation of Dynamin Helices Damped by Membrane Friction. A short summary is presented afterwrads in section 5.3

5.2 Article 1: Deformation of Dynamin Helices Damped by Membrane Friction.

Article published on December 1, 2010 in Biophysical Journal, Volume 99, Issue 11, pages 3580-3588.

Authors: Sandrine Morlot, Martin Lenz, Jacques Prost, Jean-Francois Joanny and Aurélien Roux.

Deformation of Dynamin Helices Damped by Membrane Friction

Sandrine Morlot,[†‡§¶‖△] Martin Lenz,[†‡§△*] Jacques Prost,[†‡**] Jean-François Joanny,[†‡§] and Aurélien Roux[†‡§‖]

[†]Laboratoire Physico-Chimie Curie, Institut Curie, Centre de Recherche, Paris, France; [‡]Centre National de Recherche Scientifique, UMR 168, Paris, France; [§]Université Pierre et Marie Curie Paris 6, Paris, France; [¶]Université Paris Diderot Paris 7, Paris, France; [‖]Department of Biochemistry, University of Geneva, Geneva, Switzerland; and **École Supérieure de Physique et de Chimie Industrielles—ParisTech, Paris, France

ABSTRACT Dynamin and other proteins of the dynamin superfamily are widely used by cells to sever lipid bilayers. During this process, a short helical dynamin polymer (one to three helical turns) assembles around a membrane tubule and reduces its radius and pitch upon guanosine triphosphate hydrolysis. This deformation is thought to be crucial for dynamin's severing action and results in an observable twisting of the helix. Here, we quantitatively characterize the dynamics of this deformation by studying long dynamin helices (many helical turns). We perform in vitro experiments where we attach small beads to the dynamin helix and track their rotation in real time, thus collecting information about the space and time dependence of the deformation. We develop a theoretical formalism to predict the dynamics of a mechanically continuous helix deforming on long timescales. Longer helices deform more slowly, as predicted by theory. This could account for the previously reported observation that they are less fission-competent. Comparison between experiments and our model indicates that the deformation dynamics is dominated by the draining of the membrane out of the helix, allowing quantification of helix-membrane interactions.

INTRODUCTION

Living cells are open systems, which continuously exchange matter with their surroundings. A major route for these exchanges is membrane traffic, during which lipid membranes are shaped, fissioned, and fused. The dynamin protein is a tool used by eukaryotic cells to break membranes apart (1). This happens during clathrin-coated endocytosis, for example. Toward the end of this endocytosis process, a roughly spherical membrane bud is attached to the cell membrane by a thin membrane neck. Dynamin polymerizes into a helix of internal radius $r = 10$ nm and pitch $2\pi p = 13$ nm around this neck and severs it upon guanosine triphosphate (GTP) hydrolysis (2).

In vitro, long (several tens of micrometers) helical dynamin-covered membrane tubules (henceforth referred to as tubes) form in the absence of GTP when dynamin is added to a negatively charged membrane template (3). Addition of GTP induces a deformation of the tubes, and their radius and pitch become $r + \Delta r = 5$ nm and $2\pi(p + \Delta p) = 9$ nm, respectively, while the dynamin helix as a whole undergoes a right-handed twist (Δr and Δp are negative). At the structural level, this deformation is related to a conformational change of dynamin: in the constricted state, dynamin dimers are more condensed toward the inside of the tube, and each helical turn comprises 13 dimers, compared to 14 in the relaxed state (4). GTP hydrolysis by dynamin is required for tube breaking (3), suggesting a relationship between this conformational change and fission.

The precise biochemical and biomechanical processes underlying tube fission are still a matter of debate. It was demonstrated by Danino et al. (5) that breaking requires that the tubes adhere to a solid substrate (6–8). We moreover observed (6) that longitudinal tension increases in tubes rigidly attached at both ends after treatment with GTP. Rupture then occurs within a few seconds, similar to the situation of tubes adhered to a solid substrate. This suggests that force build-up within the dynamin helix is an important condition for fission. Another indication of stress build-up is that tubes treated with GTP tend to form supercoils, which indicates the presence of torque within the helix. However, it was recently observed that helix depolymerization can occur before breakage in tubes treated with GTP (7,8). These studies hypothesize that the main effect of GTP hydrolysis is not to generate stresses, but to break molecular bonds within the dynamin polymer and with the membrane. This would then release the highly constricted membrane, and could lead to spontaneous membrane fission. In this model, breakage would thus be due to depolymerization rather than to deformation and stresses. This raises questions regarding the ability of the dynamin helix to withstand such stresses—i.e., its mechanical continuity—which is required for a deformation-based fission mechanism but would be compromised by a large-scale disassembly of the dynamin polymer.

Another interesting finding, by Pucadyil and Schmid (7), is that tube rupture is less likely in long tubes than in short ones. This observation yields interesting insights into the dynamics of dynamin deformation, the typical timescale

Submitted June 11, 2010, and accepted for publication October 13, 2010.

[△]Sandrine Morlot and Martin Lenz contributed equally to this work.

*Correspondence: martinlenz@uchicago.edu

Martin Lenz's present address is James Franck Institute, University of Chicago, 929 E. 57th Street, Chicago, IL 60637.

Editor: Michael Edidin.

0006-3495/10/12/3580/9 $2.00

doi: 10.1016/j.bpj.2010.10.015

of which, it has been suggested (9), is imposed by the damping of tube constriction, torsion, and contraction by friction against the surrounding medium and the membrane. As such effects are more pronounced in longer tubes, they could lead to a slower tube deformation there and therefore hinder fission, as hypothesized previously (10).

In this article, we tackle these issues through a quantitative study of the dynamics of the GTP-induced deformation of dynamin. A good understanding of this phenomenon on the timescales over which fission occurs is an important step toward the characterization of the dynamin severing action and the role of deformation therein. Using a joint experimental and theoretical approach, we clarify the physics of this process.

We first present experiments in which the space-dependent twisting of long tubes is monitored by tracking small polystyrene beads attached to the dynamin coat. This methodology allows us to record the tube rotation velocity and number of turns in several locations as a function of time. A theoretical analysis of the deformation is then proposed, which yields detailed predictions regarding this bead motion. We then combine the results of the two approaches, and show that upon GTP hydrolysis, long dynamin coats are able to withhold stresses as a consequence of their continuity or through viscous coupling over small gaps separating essentially continuous adjacent helices. On observable timescales, which coincide with the timescales implicated in dynamin-mediated fission (6), the rate-limiting step for the dynamics of this deformation is the drainage of the membrane out of the helix. We also gain some geometrical insight into the successive steps involved in the deformation. Finally, we discuss the implications of our findings for dynamin's membrane-severing action, and their potential impact on previously proposed models of dynamin-mediated membrane fission.

MATERIALS AND METHODS

Lipids

All lipids were purchased from Avanti Polar Lipids (Alabaster, AL). We use a synthetic lipid mixture composed of 30% brain phosphatidylethanolamine (PE), 5% liver phosphoinositides (PIs), 30% palmitoyl-oleoyl phosphatidylserine (POPS), and 35% palmitoyl-oleoyl phosphatidylcholine (POPC) and supplement it with 15% (m/m) cholesterol and 5% (m/m) final phosphatidylinositol-4,5-bisphosphate (PtdIns(4,5)P_2). This composition mimics a commercial porcine brain polar lipid extract (141101, Avanti) without the 30% unknown lipids. Nucleotides are obtained from Roche Biosciences (Palo Alto, CA).

Dynamin purification and labeling

Dynamin is purified from six rat brains using the GST-tagged SH3 domain of rat amphiphysin 2 as an affinity ligand (6). After elution with low pH and salt, the two fractions most enriched in dynamin are pooled (2 ml total), dialyzed against storage buffer (20 mM HEPES, pH 7.4, 100 mM NaCl, 50% v/v glycerol—final volume ~0.5 ml, typical concentration ~2 mg/ml), flash-frozen in liquid nitrogen, and stored at −80°C. For conjugation to biotin, DSB-X biotin C2-iodoacetamide (D-30753, Invitrogen, Carlsbad, CA) is dissolved into dimethyl sulfoxide (DMSO) at a 10 mg/ml stock. Dynamin is labeled for a few minutes by adding a 10× molar excess of DSB-X. Labeled dynamin is dialyzed against storage buffer, aliquoted, flash-frozen, and stored at −80°C. Thiol-reactive biotin DSB-X ensures good functionality of dynamin after labeling.

Formation of membrane sheets

Glass coverslips 22 × 40 mm in size are cleaned by sonication (5 min) in 1% Decon 90 (Modec, Houston , TX) in distilled water, followed by thorough washing and sonication (5 min) in distilled water to remove any trace of detergent and a final wash with 100% ethanol before storage in ethanol. Coverslips are dried under a N_2 flux, and 1-μl droplets of lipid solution (10 mg/ml in pure chloroform) are deposited and allowed to dry on the coverslip. Typically, two drops are deposited at different sites on the same coverslip. The use of pure chloroform is essential to allow lipid droplet drying in a way that is optimal for the subsequent formation of membrane sheets upon hydration. Coverslips are then dried again under vacuum (0.2 millitorr) for at least 1 h and kept up to several days under vacuum.

Tube preparation

Before use, coverslips are placed for 20–30 min in a wet incubator (37°C, 100% humidity) to allow partial hydration of the lipids. Next, a small chamber (~15-μl volume) is built by placing the coverslip onto a glass slide with lipids facing the glass slide, using a double-sided Scotch (3M, St. Paul, MN) tape as a spacer. The lipids are fully rehydrated by applying to the side of the chamber 15–20 μl of GTPase buffer (20 mM HEPES, pH 7.4, 100 mM NaCl, 1 mM $MgCl_2$), which is taken up into the chamber by capillarity. Lipid deposits then transform into membrane sheets. The glass slide is placed on the stage of an Axiovert 150 microscope (Zeiss, Oberkochen, Germany) for observation with a JAI Pulnix (San Jose, CA) TMR-1405L camera and Streampix software for video acquisition (Norpix, Montreal, Quebec, Canada). A dynamin-containing solution (5 μl) is applied to one side of the chamber and the deformation of membrane sheets produced by its diffusion into the chamber is recorded at normal video rate (30 fps) with high resolution (1300 × 1024) imaging under differential interference contrast (DIC) settings. Nucleotide-containing GTPase buffer (5 μl) is added after formation of the tubes.

Bead labeling and observation

In experiments involving streptavidin-coated polystyrene beads (190-nm diameter, Bangs Labs, Fishers, IN), biotinylated dynamin is used, and the dynamin solution also contains beads at an ~500- to 1000-fold dilution relative to the commercial stock solution. For the experiments, only tubes adherent to the glass surface at their ends but not throughout their length are selected for observation.

Movie processing and compression

Uncompressed DIC movies (AVI files) are resized, contrasted, and accelerated using the VirtualDub freeware (www.virtualdub.org). Raw movies are compressed using the DivX codec (San Diego, CA) to ensure good quality compression for data storage. For the analysis of bead movement, movies are contrasted using VirtualDub, and transformed to 8-bit grayscale stack (.stk) files using the ImageJ (National Institutes of Health, Bethesda, MD) freeware. The spinning beads are tracked using the optional Tracking function of the Metamorph software (Molecular Devices, Silicon Valley, CA), which detects the beads on each frame by pixel thresholding and returns the center of mass of the selected pixels. The bead trajectories are then

analyzed with the pick peaks tool in the Origin Pro software (OriginLab, Northampton, MA), yielding the number of turns as a function of time for each bead. We finally obtain the rotation velocity as a function of both time and position along the dynamin helix.

REAL-TIME OBSERVATION OF THE DEFORMATION

We follow the rotation of beads attached to dynamin-coated membrane tubules during GTP hydrolysis in vitro. Our setup is similar to one used in a previous study (6), with minor modifications. We first prepare membrane sheets by drying a mixture of pure lipids with 5% phosphatidylinositol-4,5-bisphosphate on a coverslip (this mixture comprises the main components of a plasma membrane in similar proportions—see Materials and Methods). Brain purified dynamin, including 1/5 biotinylated dynamin, and streptavidin-coated polystyrene beads (diameter 190 nm), are then injected into the lipids after rehydration with buffer. As a result, the membrane is deformed into tubules, each coated by a dynamin helix to which beads are anchored through streptavidin-biotin bonds. Tubes are typically several tens of micrometers long, with many beads attached (Fig. 1, *a* and *b*). This is in contrast to the procedure in our previous study (6), where only single beads were monitored. To best observe the dynamics along the whole helix, we focus only on tubes that lie more or less parallel to and mostly away from the glass surface forming the bottom of our experimental chamber, which enables free rotation of the beads (Fig. S1). The membrane tubules forming the core of those tubes usually adhere non-specifically to the glass at one of their ends and are connected at the other end to the thick (50 μm) lipid deposit, which acts as a membrane reservoir. Whether the dynamin helix itself is firmly anchored to the glass or is free to rotate cannot be determined before GTP addition. We next inject 100 μM GTP into the chamber and monitor the rotation of the beads around the tubes (Movie S1). This relatively low GTP concentration leads to a relatively slow bead dynamics (6), which allows for reliable tracking of the beads. Movies are acquired in DIC microscopy at 30 frames/s. We track the displacement of a bead perpendicular to the tube (Fig. 1 *c*). The beads appear to move right and left of the tube, and each quasiperiod of this motion corresponds to a full rotation of the bead around the tube. We can thus calculate the bead rotation velocity as a function of both time and position along the dynamin helix (Fig. 1 *d*). Treatment with 100 μM GTP induces no bead detachment but causes the tubes to shrink longitudinally, which occasionally leads to their breakage (6). During this contraction, beads move closer to each other in a homogeneous and well-coordinated manner, suggesting that the coat does not break apart and behaves as a single continuous unit.

More detailed information about the coat continuity is obtained by analyzing the bead rotation. The rotation velocity

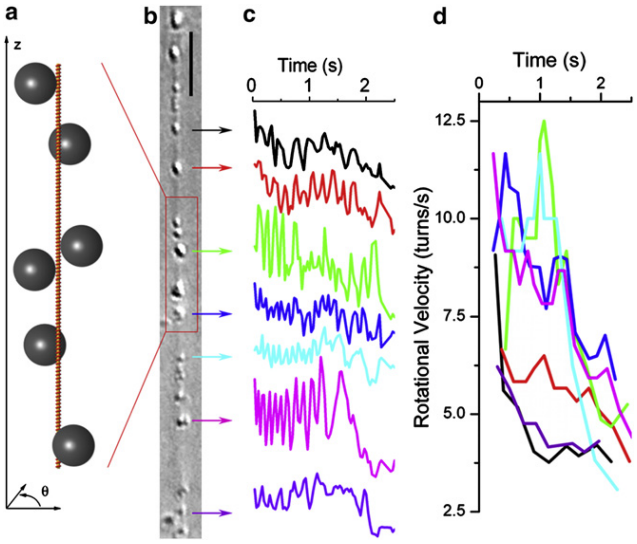

FIGURE 1 Direct observation of the bead motion. (*a*) Cartoon of a dynamin-coated membrane tubule with beads attached. (*b*) DIC image of a tube with several beads. Scale bar, 5 μm. (*c*) Tracking of seven beads perpendicular to the tube axis. The different amplitudes of oscillation are due to variation in bead size. (*d*) Rotation velocities as a function of time, calculated from the traces of *c* and with the same color-coding. The rotation velocity of each bead decreases with time, and neighboring beads have similar rotation velocities. The beads toward the center of the tube rotate the fastest.

of each bead usually increases very rapidly after GTP addition, reaches a short plateau phase after three to five turns, then decreases (6) (Fig. 1 *d*). Some tubes undergo fission at this stage, but for most tubes, the motion smoothly slows down to a halt within a few seconds. It is important to note that the beads all start rotating at the same time and that neighboring beads have a similar rotation velocity (Fig. 1 *d* and Movie S1). The bead velocity profile indicates the boundary conditions on the dynamin polymer: an increase of the velocity near one end indicates that the helix is free to rotate, whereas a decrease to zero implies that it is blocked (see Fig. S2). The coordinated bead rotation, just like the coordinated longitudinal motion, again suggests that the dynamin coat remains mechanically continuous throughout GTP hydrolysis. This is confirmed by the fact that no obvious discontinuities in the dynamin coat are observed upon GTP treatment in fluorescence microscopy (Fig. S3). Note that discontinuities smaller than the optical resolution might still be present. However, if they are few and $<$100 nm, they allow the transmission of stresses through viscous coupling and therefore have little influence on the tube dynamics (see Supporting Material).

THEORETICAL ANALYSIS

Here, we describe the long-time dynamics of a long tube ($L \gg r$) during GTP hydrolysis. We show that beads bound

to a mechanically continuous deforming helix display distinctive patterns of motion, among which the coordination of neighboring beads discussed above. Even when tube fission occurs, we only consider deformations that precede it (and possibly lead up to it) and thus describe the tube as continuous. We find that on observable timescales it has a diffusive dynamics dominated by an effective helix-membrane friction. These predictions are tested against experimental data in the next section.

We do not describe the local relaxation of the tube but focus on the propagation of the deformation along the tube axis. We are interested in the timescales on which these modes of deformation propagate over distances of order L. It is fairly intuitive that propagation over a longer tube should take a longer time. Therefore, we expect the relaxation timescales of interest to diverge in the so-called hydrodynamic limit $L/r \to +\infty$. The systematic study of relaxation phenomena obeying this criterion is known as generalized hydrodynamics, and it can be shown that the complete hydrodynamic behavior of a system can be captured by focusing on its conserved quantities (e.g., mass, momentum, etc.) and broken symmetry variables (describing periodic order in the system) (11). We collectively refer to these as the hydrodynamic variables of the system. Even systems as complex as the dynamin-membrane tube have only a few hydrodynamic relaxation processes, and we are able to give a simple, yet complete mathematical description of its dynamics on those so-called hydrodynamic timescales. This simplicity stems from the fact that generalized hydrodynamics allows us to systematically enclose the unknown microscopic details of the tube in a few phenomenological coefficients. For clarity in this section, we further restrict our discussion to experimentally observable timescales, but a more comprehensive presentation of our formalism is given in Lenz et al. (9).

We follow the standard hydrodynamic approach, which starts by writing conservation equations for the hydrodynamic variables. These equations express, e.g., the time derivative of the mass as a function of a mass current, and we supplement them with a discussion of the timescales involved. For a system close to equilibrium, this current (or flux) is generically proportional to some thermodynamic forces (including, e.g., chemical potential gradients), which characterize how far from equilibrium the system is. These forces are then related to the hydrodynamic variables, which results in a closed set of equations describing the system studied.

Mass conservation and helical structure

We now present the rather minimal set of assumptions required by our formalism: the conservation of dynamin and membrane mass, and a seamless helical structure of the tube. Our approach implies coarse-graining the tube over a lengthscale of $\approx r$. We thus treat it as a one-dimensional system with spatial coordinate z (Fig. 1 *a*).

We assume that exchanges of dynamin or membrane between the tube and the surrounding solution are negligible over seconds, and thus the helix and membrane densities, $\rho_h(z,t)$ and $\rho_m(z,t)$ (i.e., masses of helix and membrane per unit length), are conserved quantities. Equivalently, we can consider the local tube mass density, $\rho(z,t) = \rho_h + \rho_m$, and mass fraction of dynamin, $\Phi(z,t) = \rho_h/\rho$, as conserved quantities, which implies the conservation law

$$\rho \partial_t \Phi = -\partial_z J, \tag{1}$$

where a nonlinear advection term was dropped, as we assume that the tube is weakly displaced from its reference state (defined as its state in the absence of GTP and of externally applied force and torque). Here, $J(z,t)$ is the mass flow of helix in the local center-of-mass reference frame.

We furthermore hypothesize that the helix does not break, and thus retains a solid-like periodic structure throughout. We define $\theta(z,t)$ as the angle at which the helix intersects the horizontal plane located at altitude z (Fig. 1 *a*). As the helix rotates or translates, the intersection point between the static plane and the moving helix is displaced, and thus, $\theta(z,t)$ varies. We further define the torsional strain $u_{z\theta}(z,t) = \partial_z \theta(z,t)$. Because of the helix continuity, this strain component is a broken-symmetry variable, i.e., plays a similar role to a conserved quantity. Indeed, just like a depletion of tube mass (a conserved quantity) can only occur through mass flow to neighboring regions, a local extension (decrease in strain) of the solid-like helix requires that the neighboring regions be compressed (increase in strain).

On hydrodynamic timescales, all dynamical processes that occur within the tube are slaved to the hydrodynamic variables $\delta\rho$, $\delta u_{z\theta}$, and $\delta\Phi$ (here, δ denotes the deviation from the reference state). Thus, we may describe the tube state only by these three degrees of freedom.

Comparison of typical timescales

The fact that the tube has three hydrodynamic variables implies that it has three relaxation modes (11). Because its dynamics is overdamped, all three modes are diffusive. The relaxation of these modes toward the new steady state imposed by GTP hydrolysis is driven by the tube elasticity, which is characterized by its persistence length, $\ell_p = 37 \pm 4\ \mu$m (12). Energy dissipation during this process occurs through two different phenomena: hydrodynamic drag against the surrounding water (characterized by the water viscosity, $\eta \simeq 10^{-3}$ Pa·s) and relative helix-membrane motion, which involves intra-membrane dissipative phenomena (characterized by an inter-monolayer friction coefficient $\beta \approx 10^8\ \mathrm{Pa}/(\mathrm{m}\cdot\mathrm{s}^{-1})$ (13)). The two phenomena happen on widely different timescales, as seen when comparing the associated characteristic diffusion coefficients:

$$D_w \approx \frac{k_B T \ell_p}{\eta r^2} \approx 10^6\,\mu\mathrm{m}^2\cdot\mathrm{s}^{-1} \gg D_m \approx \frac{k_B T \ell_p}{\beta r^3} \approx 10^3\,\mu\mathrm{m}^2\cdot\mathrm{s}^{-1}. \tag{2}$$

Since we are concerned with describing experimental systems with lengths of order 10 μm over timescales of order 1 s, we are only interested in phenomena characterized by diffusion coefficients of order 10^2 $\mu m^2 \cdot s^{-1}$, i.e., only in those involving helix-membrane friction. The hydrodynamic drag of water is thus neglected in the following analysis, so that no external forces are applied to the tube except at its ends. Using $\sigma(z,t)$ and $\tau(z,t)$ to denote the local internal longitudinal tension of the tube and its local internal torque, respectively, this implies that σ and τ are independent of z. They are thus equal to the force and torque imposed at the ends of the tube, which we assume to be constant.

Internal forces governing tube relaxation

The relaxation of the tube is driven by the reactive forces conjugate to its hydrodynamic variables: the longitudinal pressure, $\delta\mathfrak{p}(z,t)$ (which has units of force in a one-dimensional system); the elastic torque, $\delta h(z,t)$; and the helix-membrane exchange chemical potential, $\delta\mu_e(z,t)$. All of these vanish in the reference state. They are defined in terms of derivatives of the tube free energy per unit length, $f(z,t)$, and for small deviations from the reference state they are linearly related to the hydrodynamic variables:

$$\begin{pmatrix} \delta\mathfrak{p} \\ \delta h \\ \delta\mu_e \end{pmatrix} = \begin{pmatrix} \rho^2 \partial_\rho (f/\rho)|_{u_{z\theta},\Phi} \\ \partial_{u_{z\theta}} f|_{\rho,\Phi} \\ \rho^{-1} \partial_\Phi f|_{\rho,u_{z\theta}} \end{pmatrix} = \chi \begin{pmatrix} \delta\rho \\ \delta u_{z\theta} \\ \delta\Phi \end{pmatrix}, \quad (3)$$

where the 3×3 susceptibility matrix χ expresses this linear relation. This matrix characterizes the tube elasticity. The derivatives in Eq. 3 are taken in the tube reference state.

Dissipative processes, including GTP hydrolysis

Whereas the conservative (reactive) part of the tube dynamics close to equilibrium is captured by Eq. 3, dissipative phenomena are described by the flux-force relations in an isothermal tube:

$$\sigma - \delta\mathfrak{p} - \delta h/p = \tilde{\xi}_z \Delta\mu \quad (4a)$$

$$\tau + \delta h = \tilde{\xi}_\theta \Delta\mu \quad (4b)$$

$$J = -\tilde{\lambda}\partial_z \delta\mu_e - \tilde{a}\partial_z \delta h. \quad (4c)$$

The left-hand sides of Eqs. 4a, 4b, and 4c are equal to the dissipative fluxes of linear momentum (dissipative force), angular momentum (dissipative torque), and helix mass (diffusion flux), respectively. Those fluxes are linearly related to thermodynamic forces $\Delta\mu$ (representing the free energy liberated by GTP hydrolysis), $\partial_z \delta\mu_e$, and $\partial_z \delta h$ through the phenomenological transport coefficients $\tilde{\xi}_z$, $\tilde{\xi}_\theta$, $\tilde{\lambda}$, and $\tilde{a}$.

Although the values of these coefficients are a priori unknown, only certain couplings are allowed by symmetries. In agreement with structural data (4,14,15), we assume that the tube is nonpolar, i.e., invariant under up-down symmetry. As a consequence, Eqs. 4a and 4b (where the fluxes are even under this transformation), but not Eq. 4c (where the fluxes are odd), involve the chemical potential difference, $\Delta\mu$, between GTP and its hydrolysis products (which is even). Therefore, GTP hydrolysis plays the same role in the tube dynamics as an externally applied force and torque, as seen in Eq. 4. Note that viscous terms are omitted from Eqs. 4a and 4b, as they are subdominant compared to $\tilde{\xi}_z \Delta\mu$ and $\tilde{\xi}_\theta \Delta\mu$ in the hydrodynamic limit.

The coefficient $\tilde{\lambda}$ relates the amount of helix-membrane motion (characterized by J) to the force, $\delta\mu_e$, that drives this motion. It is therefore essentially a helix-membrane friction coefficient. Here, we consider that helix-membrane friction stems from intra-membrane dissipative phenomena, and thus involves the membrane viscosity. To be able to quantitatively test this hypothesis, we consider the simplistic model described in our previous article (9), where the helix is rigidly attached to the membrane's outer monolayer, which itself drags against the inner monolayer. This model yields the estimate $\tilde{\lambda} = \frac{\Phi^2(1-\Phi)}{2\pi}\frac{\rho^2}{r\beta} \simeq 10^{-26}$ kg·m^{-1}·s, which is compared to experimental measurements in the next section. Note that in this formula $\tilde{\lambda}$ is related to β and thus characterizes the dominant form of dissipation discussed above (see Eq. 2).

Tube behavior on observable timescales

Combining Eqs. 1, 3, and 4, and using the fact that σ and τ are constants, we find that the hydrodynamic behavior on observable timescales is given by the diffusion equation

$$\partial_t \delta u_{z\theta} = D_m \partial_z^2 \delta u_{z\theta}, \text{ where } D_m = \frac{\tilde{\lambda}}{\rho} \frac{\det\chi}{\chi_{1,1}\chi_{2,2} - \chi_{1,2}\chi_{2,1}}. \quad (5)$$

The associated relaxation timescale is set by the friction of the helix against the membrane. In a previous article (9), we computed χ using an elastic model of the tube (see also Fig. 3) and predicted $D_m \simeq 2.2 \times 10^2$ $\mu m^2 \cdot s^{-1}$.

TUBE DYNAMICS CONTROLLED BY MEMBRANE FRICTION

The previous section characterizes the dynamics of long ($L \gg r$) unbroken dynamin helices. In this section, we compare its predictions to data from the experiments described in Real-Time Observation of the Deformation. We find that they are indeed compatible, and argue that this can only be accounted for by the fact that helices in our experiments are mostly unbroken. We then discuss the physics underlying the relaxation.

We find that the longest relaxation timescale of the tube apparently diverges with its length, which indicates a hydrodynamic relaxation process. According to our theoretical reasoning, only two types of relaxation processes are compatible with this behavior: 1) friction against water, and 2) friction between the helix and the membrane. According to the estimate of Eq. 2, the timescales involved in 1), are of the order of $D_w L^2 \approx 100\ \mu$s. The longest relaxation time of the tube is observed to be of the order of 1 s (Fig. 1 *d*), i.e., much longer than this. This allows us to rule out friction against water as a major influence in the relaxation process on observable timescales. On the other hand, we show below that the relaxation timescale involved in 2), and predicted using our estimate of the friction coefficient $\tilde{\lambda}$ is indeed compatible with the experiments. This supports our hypothesis that helix-membrane friction is mostly due to effects related to the membrane viscosity.

Final state of the tube

Let us consider an unbroken helix stuck to the glass at $z = 0$ (thus imposing $\theta(0, t) = 0$) and free to rotate at its other end, $z = L$, and discuss the motion of a bead located at altitude z. As a consequence of the helix continuity, the piece of helix between 0 and z cannot rotate without dragging along the piece between z and L in its rotation. Each turn of helix eventually undergoes an identical twisting deformation and thus rotates the portion of the helix above it by a fixed quantity. As these elementary rotations add up, the total number of rotations of a bead increases linearly with increasing z. This reads $\Delta\theta(z) = \Delta u_{z\theta} z$, where $\Delta u_{z\theta}$ is a constant. More specifically, this is due to the up-down symmetry of the tube, which imposes that GTP hydrolysis acts as a force and torque and thus imposes a constant strain on the helix.

In Fig. 2 *a*, we present two experiments where the tubes do not break after addition of 100 μM GTP, which allows us to count the total number of turns of each bead between GTP injection and the end of the deformation. As expected, these data display a linear relationship between bead position z and the total amount of rotation, $\Delta\theta$, with $\Delta u_{z\theta} = 2.8\ \text{rad}\cdot\mu\text{m}^{-1}$ (*open circles*) and $1.5\ \text{rad}\cdot\mu\text{m}^{-1}$ (*solid circles*). This is to be compared with the structural data of Zhang and colleagues (14,15), where it is stated that the helix goes from 14.2 to 13.2 dimers/helical turn, which corresponds to $\Delta u_{z\theta} = 7.9\ \text{rad}\cdot\mu\text{m}^{-1}$. Although these numbers are in order-of-magnitude agreement, our measurements yield noticeably smaller values, meaning that tubes submitted to 100 μM GTP (as opposed to the nucleotide concentration of 1 mM used in Zhang and Hinshaw (14)) only reach a partially constricted state.

These observations are consistent with structural evidence of the up-down symmetry of the helix (14,15). More important, they constitute strong evidence of its mechanical continuity, meaning that if gaps in the helix are present, they are few and significantly smaller than 100 nm. Indeed, larger gaps would spoil the linear relationship observed here (see discussion above and the Supporting Material). Note that large, optically resolvable gaps are observed when multiple dynamin polymers nucleate on a preformed membrane tubule (16), but not when tubes are grown from a flat membrane, as is the case here. The data presented in Fig. 2 *a* also show that bead rotation in our experiments is not due to the unbraiding of two tubes, as was suggested previously (7) (see Supporting Material).

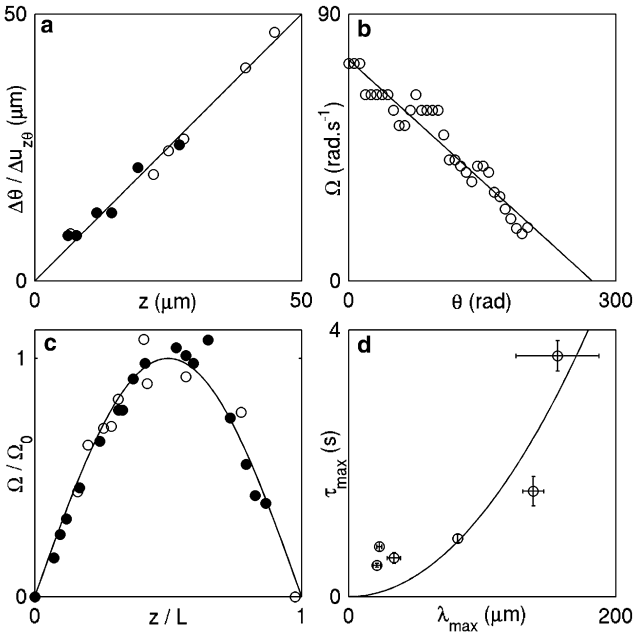

FIGURE 2 Experimental data validate the predictions from our hydrodynamic formalism, implying that dynamin deforms as a mechanically continuous entity and that this process is damped by an internal friction. (*a*) Linear relationship between $\Delta\theta(z)$ and z, where $\Delta\theta(z)$ is determined by counting the final number of rotations in a trace similar to those presented in Fig. 1 *c* for the bead located in z. Open and solid circles represent data from two independent experiments. For each of these, the $\Delta\theta$ values are divided by the value of $\Delta u_{z\theta}$ indicated in the main text to collapse the data onto a line. (*b*) Exponential relaxation of bead rotation on long timescales. As the rotation velocity $\Omega = \partial_t\theta$ (measured as in Fig. 1 *d*) decreases, tracking becomes increasingly difficult and no data are collected for $\theta \gtrsim 200$ rad. (*c*) Velocity profiles for two independent experiments, each involving a single tube. The Ω values of the experiment represented by open circles and solid circles were divided by $\Omega_0 = 5.2\ \text{rad}\cdot s^{-1}$ and $\Omega_0 = 9.2\ \text{rad}\cdot\text{s}^{-1}$, respectively, and the bead positions, z, were scaled by the independently measured $L = 31\ \mu$m and $L = 47\mu$m, respectively, to collapse the data onto a sinusoidal master curve. (*d*) Dependence of the largest relaxation time (fit procedure described in Fig. S4) on the largest wavelength compatible with the tube boundary conditions. Horizontal error bars represent the estimated uncertainty regarding the length of each tube, and vertical error bars stand for the fit uncertainty as calculated by the Origin software.

Bead rotation dynamics

The diffusive dynamics of Eq. 5 predicts the long-time relaxation of bead rotation as a function of space and

time. At long times, the strain $\delta u_{z\theta}$ is dominated by its longest-lived Fourier mode, i.e., the one with the largest wavelength $\lambda_{\max}$ compatible with the boundary conditions. This yields

$$\theta(z,t=+\infty)-\theta(z,t)\underset{t\to+\infty}{\propto}e^{-t/\tau_{\max}}\sin\left(\frac{2\pi z}{\lambda_{\max}}\right). \quad (6)$$

In this paragraph, we focus our attention on the time dependence of this relaxation, which decays exponentially with time constant

$$\tau_{\max}=\frac{\lambda_{\max}^2}{4\pi^2 D_m}. \quad (7)$$

This can be equivalently expressed as

$$\Omega(z,t)=\partial_t\theta(z,t)=-\tau_{\max}^{-1}[\theta(z,t)-\theta(z,t=+\infty)]. \quad (8)$$

In Fig. 2 *b*, we test this linear relationship between θ and the rotation velocity, Ω, in an experiment where a 1 mM GTP concentration is used, which allows for the observation of many turns of the bead and therefore provides a stringent test of Eq. 8. The agreement is very good, and the slope of the linear fit yields $\tau_{\max}=3.7$ s. In this experiment, we evaluate the length of the tube to be $L\simeq 100\ \mu\text{m}\approx\lambda_{\max}/2$, which yields $D_m\simeq 3.0\times10^2\ \mu\text{m}^2\cdot\text{s}^{-1}$. This is in good order-of-magnitude agreement with our theoretical prediction.

Long-time bead velocity profile

Now turning to the spatial profile described in Eq. 6, we expect Ω to have a sinusoidal dependence in the coordinate z. In Fig. 2 *c*, we plot the value of the velocities of beads attached to two different tubes as a function of their scaled positions and after addition of 100 μM GTP. The motion of neighboring beads is clearly coordinated, as expected from our continuous helix model.

Relation between length and relaxation time

Using sinusoidal fits similar to those seen in Fig. 2 *c*, we establish that $\lambda_{\max}=4L$ for tubes attached at only one end, whereas $\lambda_{\max}=2L$ for tubes attached at both ends (see Fig. S2; the possibility for a tube attached at both ends to rotate is discussed in the Supporting Material). Therefore, Eq. 7 predicts that long tubes have a slower long-time dynamics than short ones. We test this by measuring $\tau_{\max}$ for several tubes with either one or two ends attached (fit procedure described in Fig. S4). These data are plotted against $\lambda_{\max}$ in Fig. 2 *d*.

A quadratic fit corresponding to Eq. 7 is represented by a line in Fig. 2 *d* and yields $D_m=2.0\times10^2\ \mu\text{m}^2\cdot\text{s}^{-1}$, in agreement with our prediction. Note that the experimental relaxation times are larger than predicted by theory for short tubes ($\lambda_{\max}\lesssim 40\ \mu$m). This is likely due to the injection of GTP into the experimental chamber, which takes a few tenths of a second and could interfere with the relaxation of the tube on this timescale: as the amount of available GTP increases with time over this period, the bead rotation tends to accelerate, and the predicted slowing down is not observed until after the end of GTP injection. This leads to an experimental overestimation of $\tau_{\max}$ that is most apparent in short tubes. Another possible cause for this delay is the inherent timescale associated with GTP hydrolysis by dynamin, which is also of the order of a few hundreds of milliseconds (14). These timescales are negligible in the hydrodynamic limit $L/r\to+\infty$, where our formalism is valid. Indeed, Fig. 2 *d* clearly shows that the longest relaxation time of the tubes is an increasing function of their length, which retrospectively justifies our focusing on hydrodynamic timescales. This is further evidence of the mechanical continuity of the tubes used in our experiments, as we would expect a broken long tube to behave similarly to a collection of small tubes (e.g., have the same relaxation time as short tubes), which is not observed here. Finally, the reasonable agreement between the values of D_m inferred from Fig. 2 *b* (where [GTP] = 1 mM) and the value fitted in Fig. 2 *d* ([GTP] = 100 μM) confirms our prediction that the tube relaxation timescale does not depend on GTP concentration (see Eq. 5).

Full predictions for the deformation dynamics

The good agreement of our theoretical analysis with experimental results suggests that it may also give a reasonable description of dynamin-coated membrane tubes on shorter length- and timescales. In Fig. 3, we present predictions from a detailed analysis of our hydrodynamic formalism (9) (see also Supporting Material) in the case where the tube reaches its full deformation, as when treated with 1 mM GTP (5).

This analysis is based on the changes of pitch and radius of the helix observed by Danino et al. (5), which allow us to infer the active force and torque $\tilde{\xi}_z\Delta\mu$ and $\tilde{\xi}_\theta\Delta\mu$ describing GTP hydrolysis. We also assume that the helix elastic properties are similar to those of a spring with persistence length $\ell_p=37\pm4\ \mu$m (12). This somewhat coarse assumption implies that the details of the deformation described in Fig. 3 are speculative to some extent, although plausible and thermodynamically consistent. A more refined characterization of the matrix χ could be obtained through additional mechanical measurements (e.g., of the compressional elasticity of the helix). We allow membrane bending and stretching and assume that the corresponding moduli have the typical values 10 k_BT and 0.25 $\text{N}\cdot\text{m}^{-1}$ (9). This allows us to evaluate the elastic susceptibility matrix χ. As discussed previously, the tube dynamics can be decomposed into three chronologically well-separated diffusive modes, and we evaluate the associated diffusion

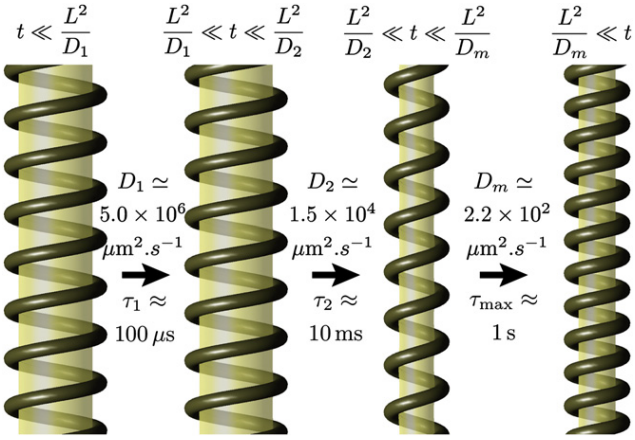

FIGURE 3 Illustration of the time-dependent deformation as predicted by the full hydrodynamic formalism of Lenz et al. (9). (See the Supporting Material for a proper description of the membrane reservoir.) The images in this figure represent the tube state during the lag phases between the relaxation of the three well-separated diffusive relaxation modes of the tube. See Movie S2 for an animated version. Note that our model allows for both stretching and bending of the membrane, but in practice, the membrane area per polar head varies by <1.5% and the inhomogeneities in membrane radius due to bending are always <7%—they are thus hardly discernible in this figure.

coefficients, $D_1 \approx D_w \gg D_2 \approx D_w \gg D_m$, as well as the amplitude of the deformations, as pictured in Fig. 3.

On short (although hydrodynamic) timescales ($\tau_1 \approx L^2/D_1 \approx 100\ \mu s$), the tube undergoes an almost imperceptible retraction in the vertical direction, without rotation or relative helix-membrane motion—longitudinal friction on the surrounding medium is the dominant dissipative mechanism. On intermediate timescales $\tau_2 \approx L^2/D_2 \approx 10$ ms, the tube radius decreases. Both longitudinal friction and the dissipation associated with the flux of water inside the tube are negligible (9). Rotational friction against water is the dominant dissipative mechanism, and no relative helix-membrane flux occurs (helix and membrane extend longitudinally at the same rate). Only on timescales of order $\tau_{max} \approx L^2/D_m \approx 1$ s is membrane expelled from the helix to the membrane reservoirs at its boundaries. Fig. 3 shows that this process involves a decrease in tube pitch, which is consistent with the notion that membrane is being squeezed out of the helix.

DISCUSSION

This article describes the deformation dynamics of long dynamin-coated membrane tubules upon GTP hydrolysis as essentially governed by dynamin flow, membrane flow, and the winding of the dynamin helix. Combining experimental data and theoretical analysis, we show that on observable timescales this dynamics essentially consists in the drainage of the membrane out of the mechanically continuous helix by nucleotide-induced effective force and torque. The numerical value of the relevant friction coefficient suggests that dissipation occurs mostly within the lipid bilayer, possibly as strongly dynamin-bound lipids move relative to and exert friction against the surrounding nonbound lipids. As a consequence, short tubes deform more slowly than long ones.

Although our study focuses on long tubes, our results reveal the stability of the dynamin helix throughout GTP hydrolysis, as well as the nature of the out-of-equilibrium interactions between dynamin and membrane. These findings can readily be transposed to short helices such as those encountered in vivo, and are therefore of interest for the study of dynamin in a biological context. Note, however, that the separation of timescales between microscopic and hydrodynamic relaxation processes does not hold in such short helices; for instance, Fig. 2 *d* shows that dynamin-membrane friction dominates the dynamics only in tubes longer than a few microns. It is therefore likely that other relaxation phenomena also have an influence on the dynamics of short tubes, and it is thus not obvious what mechanisms set the timescale for their breaking.

Our approach also allows us to use macroscopic information from in vitro experiments to predict the shape and dynamics of the helix on small (≈10 nm) lengthscales without need of further structural studies (Fig. 3). This provides a qualitative picture of the microscopic dynamics of the tube.

Our results have implications for the mechanism of dynamin-mediated membrane fission and shed new light on several previous models. A first possibility is that dynamin drives fission purely by constricting the membrane. As indicated in Fig. 3, we expect this type of deformation to take place on timescales of the order of 10 ms after GTP injection. After having been brought into close proximity by constriction, the two sides of the membrane would presumably fuse together to complete fission. This step implicates an energy barrier of several k_BT, and may thus take a long time to complete. In our in vitro experiments and in a previous article (6), fission typically occurs a few seconds after GTP injection, and another study (7) reports fission times of several tens of seconds. Since we predict that the radius of the tube shrinks on a much shorter timescale (Fig. 3), we may interpret these fission times as dominated by the barrier crossing step, which could provide insight into the energetics of the membrane fusion process. However, the observation made in other studies (5,6) that anchoring of the tube to the substrate is required for breaking is not accounted for by this mechanism. Pure constriction might thus not be able to account for the dynamin-mediated fission observed in those experiments.

Another proposal is that helix constriction plays a negligible role in membrane fission, whereas an increase in the helix pitch would drive a dramatic thinning of the membrane tubule on short timescales. This would fuse the opposite sides of the tubule (18), leading to breakage. Our

predictions of the tube dynamics on timescales ranging from a few hundreds of microseconds (17) to seconds (Fig. 3) suggest that neither this nor dramatic membrane stretching occur on hydrodynamic length- and timescales. If correct, this scenario is therefore likely to apply only to short dynamin helices, such as those observed in vivo.

Our results also allow a discussion of results from more recent studies (7,8), where it is reported that dynamin disassembles from the membrane during GTP hydrolysis. The authors suggest that long dynamin coats are quickly released from the membrane upon GTP addition and are promptly replaced by smaller, more fission-competent coats. This would imply that helix depolymerization is the central event of dynamin-mediated membrane fission, and therefore that dynamin deformation is secondary, if not irrelevant, to its severing action. Our results concerning the mechanical continuity of the dynamin helix upon GTP hydrolysis do not support this picture and indeed suggest that in our experimental system, the mechanochemical action of dynamin is central to its severing action.

Lenz et al. (19) propose that deformation on a timescale shorter than the membrane viscoelastic timescale might lead to a tear in the membrane, possibly through shearing, which could initiate tube fission. We estimate this viscoelastic timescale, τ_{ve}, as the ratio of a typical lipid surface viscosity, $\approx 5 \times 10^{-9}$ kg·s^{-1} (20), to a typical membrane stretching modulus, ≈ 0.25 N·m^{-1} (21), yielding $\tau_{ve} \approx 10^{-8}$ s. Here, we report that the tube dynamics is slower for longer tubes, which could imply a less efficient tearing action for tubes where $\tau_{max} \gg \tau_{ve}$, i.e., in tubes longer than $\sqrt{D_m \tau_{ve}}$, which is a few nanometers. This is compatible with the observation made by Pucadyil and Schmid (7) that long dynamin-covered membrane tubules are less likely to break than short ones. More broadly, this model puts forward the interesting notion that the strong helix-membrane interactions characterized in this article may participate in the destabilization of the bilayer during fission. Such interactions have indeed been shown to be essential for the membrane fission activity of dynamin (22). This finding and our new theoretical insight into dynamin deformation pave the way for further quantitative studies of dynamin-mediated fission.

SUPPORTING MATERIAL

Supporting theoretical text, four figures, and two movies are available at http://www.biophysj.org/biophysj/supplemental/S0006-3495(10)01265-8.

We thank Timo Betz, Pierre Nassoy, and Gilman Toombes for inspiring discussions and critical reading of this manuscript, and Patricia Bassereau for her support and scientific interest in this project.

This work was supported by the Centre National de la Recherche Scientifique ("Interface Physique Chimie Biologie: soutien à la prise de risque") (A.R.), the Agence Nationale de la Recherche (Young Investigator Program, No. JC08_317536) (A.R.), and the Human Frontier Science Program Career Development Award (No. 0061/2008 to A.R.).

REFERENCES

1. Praefcke, G. J. K., and H. T. McMahon. 2004. The dynamin superfamily: universal membrane tubulation and fission molecules? *Nat. Rev. Mol. Cell Biol.* 5:133–147.
2. Takei, K., P. S. McPherson, …, P. De Camilli. 1995. Tubular membrane invaginations coated by dynamin rings are induced by GTP-γ S in nerve terminals. *Nature.* 374:186–190.
3. Sweitzer, S. M., and J. E. Hinshaw. 1998. Dynamin undergoes a GTP-dependent conformational change causing vesiculation. *Cell.* 93:1021–1029.
4. Mears, J. A., P. Ray, and J. E. Hinshaw. 2007. A corkscrew model for dynamin constriction. *Structure.* 15:1190–1202.
5. Danino, D., K.-H. Moon, and J. E. Hinshaw. 2004. Rapid constriction of lipid bilayers by the mechanochemical enzyme dynamin. *J. Struct. Biol.* 147:259–267.
6. Roux, A., K. Uyhazi, …, P. De Camilli. 2006. GTP-dependent twisting of dynamin implicates constriction and tension in membrane fission. *Nature.* 441:528–531.
7. Pucadyil, T. J., and S. L. Schmid. 2008. Real-time visualization of dynamin-catalyzed membrane fission and vesicle release. *Cell.* 135:1263–1275.
8. Bashkirov, P. V., S. A. Akimov, …, V. A. Frolov. 2008. GTPase cycle of dynamin is coupled to membrane squeeze and release, leading to spontaneous fission. *Cell.* 135:1276–1286.
9. Lenz, M., J. Prost, and J.-F. Joanny. 2008. Mechanochemical action of the dynamin protein. *Phys. Rev. E Stat. Nonlin. Soft Matter Phys.* 78:011911.
10. Roux, A., and B. Antonny. 2008. The long and short of membrane fission. *Cell.* 135:1163–1165.
11. Chaikin, P. M., and T. C. Lubensky. 1995. Principles of Condensed Matter Physics. Cambridge University Press, Cambridge.
12. Frost, A., R. Perera, …, V. M. Unger. 2008. Structural basis of membrane invagination by F-BAR domains. *Cell.* 132:807–817.
13. Evans, E., and A. Yeung. 1994. Hidden dynamics in rapid changes of bilayer shape. *Chem. Phys. Lipids.* 73:39–56.
14. Zhang, P., and J. E. Hinshaw. 2001. Three-dimensional reconstruction of dynamin in the constricted state. *Nat. Cell Biol.* 3:922–926.
15. Chen, Y.-J., P. Zhang, …, J. E. Hinshaw. 2004. The stalk region of dynamin drives the constriction of dynamin tubes. *Nat. Struct. Mol. Biol.* 11:574–575.
16. Roux, A., G. Koster, …, P. Bassereau. 2010. Membrane curvature controls dynamin polymerization. *Proc. Natl. Acad. Sci. USA.* 107:4141–4146.
17. Stowell, M. H. B., B. Marks, …, H. T. McMahon. 1999. Nucleotide-dependent conformational changes in dynamin: evidence for a mechanochemical molecular spring. *Nat. Cell Biol.* 1:27–32.
18. Kozlov, M. M. 1999. Dynamin: possible mechanism of "Pinchase" action. *Biophys. J.* 77:604–616.
19. Lenz, M., S. Morlot, and A. Roux. 2009. Mechanical requirements for membrane fission: common facts from various examples. *FEBS Lett.* 583:3839–3846.
20. Dimova, R., B. Pouligny, and C. Dietrich. 2000. Pretransitional effects in dimyristoylphosphatidylcholine vesicle membranes: optical dynamometry study. *Biophys. J.* 79:340–356.
21. Rawicz, W., K. C. Olbrich, …, E. Evans. 2000. Effect of chain length and unsaturation on elasticity of lipid bilayers. *Biophys. J.* 79:328–339.
22. Ramachandran, R., T. J. Pucadyil, …, S. L. Schmid. 2009. Membrane insertion of the pleckstrin homology domain variable loop 1 is critical for dynamin-catalyzed vesicle scission. *Mol. Biol. Cell.* 20:4630–4639.

Deformation of dynamin helices damped by membrane friction
Supporting Material

S1 Supporting theoretical analysis

S1.1 Screening of rotation by bare membrane sections

Here we discuss the consequences of the presence of a hypothetical break in the helix. If the break is very short, the resulting bare membrane region is still able to transmit torques thanks to its membrane viscosity, and therefore the break is not evident in the measurements presented in Fig. 2 of the main text. Longer breaks, however, result in a mechanical discontinuity of the tube and would therefore have noticeable consequences on bead rotation.

Let us consider a tube with a dynamin coat disassembled between two altitudes z_1 and z_2. In that case, it is difficult for the piece of helix between 0 and z_1 to drag the piece between z_2 and L along, as the mechanical connection between the two is only realized through a section of bare membrane tubule. In order to assess the range of this mechanical connection, we consider an infinite membrane tubule covered by dynamin only up to the altitude z_1. We denoting by $\Omega(z)$ the rotation velocity of the membrane tubule and the water it encloses at altitude $z \in [z_1, +\infty]$. It is easily shown that the upward flux of angular momentum transmitted through the water within the tubule at altitude z is equal to $\frac{\pi}{2}\eta r^4 \partial_z \Omega$. The angular momentum transmitted by the membrane is $2\pi r^3 \eta_m \partial_z \Omega$, where $\eta_m \simeq 10^{-9}\mathrm{kg.m}^{-1}.\mathrm{s}^{-1}$ is a typical membrane viscosity (1). Meanwhile, the surrounding fluid exerts a friction on the tubule. It thus acts as a momentum drain and sucks an amount $2\pi\eta r^2\Omega$ of angular momentum per unit length per unit time (this expression assumes that the length scale ℓ over which Ω varies is much larger than r). Writing the conservation of angular momentum along the membrane tubule, we conclude that its rotational velocity decays as $\Omega(z) = \Omega(z_1)\exp\left[-(z-z_1)/\ell\right]$, where $\ell = \frac{r}{2}\sqrt{1+4\frac{\eta_m}{\eta r}} \simeq \sqrt{\frac{r\eta_m}{\eta}} \simeq 100\,\mathrm{nm} \gg r$. Therefore, friction of the membrane with the surrounding fluid screens the tube's rotation over length scales of order ℓ. This means that disassembling the helix over a patch of size $\approx 100\,\mathrm{nm}$ would be enough to spoil the linear relationship observed in Fig. 2(a), as well as the sinusoidal profile of Fig. 2(c). From this we deduce that if any helix discontinuities are present in our experiments, they must be few and much smaller than 100 nm.

S1.2 Bead rotation is not due to unbraiding

It has been suggested in Ref. (2) that bead rotation in experiments similar to ours (3) is due to the unwinding of a braid formed by two tubes attached at $z = 0$ and $z = L$ respectively—here we refer to those as tubes 1 and 2. Within this hypothesis, a bead attached to tube 1 in the vicinity of $z = 0$ should rotate by only a modest amount, as it is close to the tube attachment point. Statistically, about half of the beads in this region should be bound to tube 2. These are expected to rotate by a large amount, comparable to those located in $z = L$ in Fig. 2(a) of the main text. That no such dispersion is observed in our data is proof that we monitor the rotation of a single tube.

S1.3 Thermodynamic description of the membrane reservoir

In order to predict the dynamics of a tube as in Fig. 3 of the main text, the diffusion equation Eq. (5) of the main text [or more generally Eq. (21) of Ref. (4)] must be supplemented with boundary conditions. Ref. (4) proposes the boundary condition $\delta\mu_e(z=0)=\delta\mu_e(z=L)=0$, where $z=0$ and $z=L$ correspond to the extremities of the tube. This is meant to describe contact of the tube with two reservoir: one of membrane and one of helix. Although the former is perfectly legitimate in our experimental setting, interpreting the latter is somewhat more difficult. Moreover, using this boundary condition leads to very strongly bent and stretched membrane profiles [Eq. (45) and Fig. 3 of Ref. (4)]. These profiles suggest that the membrane should break much sooner than is actually observed (5), and are somewhat at odds with the physical intuition that the membrane should relax to a weakly bent, low-energy configuration at long times.

In this section we propose a more satisfactory set of boundary conditions by properly describing the contact of the tube with membrane-only reservoirs in $z=0$ and $z=L$. Denoting by

$$\delta\mu = \left.\frac{\partial f}{\partial \rho}\right|_{u_{z\theta},\Phi} \tag{S1}$$

the tube total chemical potential, the Gibbs-Duhem relation reads

$$\mathrm{d}(\delta\mu) = \frac{\mathrm{d}(\delta\mathfrak{p})}{\rho} + \delta\mu_e \mathrm{d}(\delta\Phi) + \frac{\delta h}{\rho}\mathrm{d}(\delta u_{z\theta}). \tag{S2}$$

As the two last terms in the right-hand side are of second order in δ (defined in the main text), we neglect them in the following. The chemical potential is defined up to a constant, which we choose such that $\delta\mu=0$ in the reference state (hence the δ in $\delta\mu$). Contact with a membrane reservoir fixes the membrane chemical potential, which is defined as

$$\mu_m = \left.\frac{\partial f}{\partial \rho_m}\right|_{\rho_h,u_{z\theta}}, \tag{S3}$$

where $\rho_h=\rho\Phi$ and $\rho_m=\rho(1-\Phi)$ are the mass densities of helix and membrane, respectively. Eqs. **S1**, **S3** and the definition of $\delta\mu_e$ [see Eq. (3) of the main text] imply that $\mu_m=\delta\mu-\Phi\delta\mu_e$. Because of the convention chosen above, $\delta\mu$ vanishes in the reference state. According to its definition, so does $\delta\mu_e$. Therefore $\delta\mu=\delta\mu_e=0$ in contact with the reservoir. Since the definition of the reference state assumes that the tube is in equilibrium with the reservoir, we deduce from this that equilibrium with the membrane reservoir is expressed by the condition $\mu_m=0$, and we can thus write $\mu_m=\delta\mu_m$.

Integrating Eq. (S2) to first order in δ yields $\delta\mu=\delta\mathfrak{p}/\rho$, and so $\delta\mu_m=0=\delta\mathfrak{p}/\rho-\Phi\delta\mu_e$. Combining this with Eqs. **4a** and **4b**[1], the boundary conditions are expressed by the fact that the reactive forces $\delta\mathfrak{p}(z=0 \text{ or } z=L,t)$, $\delta h(z=0 \text{ or } z=L,t)$ and $\delta\mu_e(z=0 \text{ or } z=L,t)$ in contact with the membrane reservoirs are respectively equal to

$$\delta\mathfrak{p}^r = \sigma_{\mathrm{ext}} + \frac{\tau_{\mathrm{ext}}}{p} - \left(\tilde{\xi}_z\Delta\mu + \frac{\tilde{\xi}_\theta\Delta\mu}{p}\right) \tag{S4a}$$

$$\delta h^r = -\tau_{\mathrm{ext}} + \tilde{\xi}_\theta\Delta\mu \tag{S4b}$$

$$\delta\mu_e^r = \frac{\sigma_{\mathrm{ext}}}{\rho\Phi} + \frac{\tau_{\mathrm{ext}}}{\rho\Phi p} - \left(\frac{\tilde{\xi}_z\Delta\mu}{\rho\Phi} + \frac{\tilde{\xi}_\theta\Delta\mu}{\rho\Phi p}\right), \tag{S4c}$$

[1] In the more general case where the two first modes of the tube are not ignored, this equation should be combined with Eqs. (19a) and (19b) of Ref. (4). Noting that the terms with z-derivatives in these equations are vanishingly small in the hydrodynamic limit, this yields the same result as the one presented here.

where we use the fact that the tube's tension and torque at its endpoints are equal to the externally applied force and torque $\sigma_{\rm ext}$ and $\tau_{\rm ext}$. Combining Eq. (21) of Ref. (4) and Eqs. **S4** with the initial condition $(\delta\rho, \delta u_{z\theta}, \delta\Phi)(z, t = 0) = (0, 0, 0)$, we compute the tube's full relaxation dynamics in the case $\sigma_{\rm ext} = 0$, $\tau_{\rm ext} = 0$, which yields the results presented in Fig. 3 of the main text. As in Ref. (4), the values of the active terms are chosen to reproduce the changes of pitch and radius observed in electron microscopy (6), which reads

$$\tilde{\xi}_z \Delta\mu \simeq -3.5 \times 10^{-11}\,\mathrm{N} \quad \text{and} \quad \tilde{\xi}_\theta \Delta\mu \simeq 2.6 \times 10^{-17}\,\mathrm{N.m.} \tag{S5}$$

Note that this new description yields a negative $\tilde{\xi}_z \Delta\mu$, as opposed to the positive $\tilde{\xi}_z \Delta\mu$ calculated in Ref. (4). This means that we now predict that the tube tends to contract upon GTP hydrolysis, whereas a positive $\tilde{\xi}_z \Delta\mu$ implies an extension. Our new description, unlike that of Ref. (4), is therefore in agreement with the experimental observations of Ref. (3) and the main text.

S1.4 Long-time dynamics of a tube attached at both ends

In this paragraph we discuss the possibility for a continuous tube attached to the glass in two points (and therefore prevented from rotating) to induce bead rotation. Assuming a continuous helix whose axis is a straight line throughout the dynamics, no such motion seems possible, and indeed none is expected from our formalism. In order to show this we consider a tube whose initial state is described by $\delta u_{z\theta}(z, t = 0) = 0$. As discussed in the main text and the previous section, the final state has a uniform tension σ and torque τ, as well as a uniform membrane chemical potential, which implies $\delta u_{z\theta}(z, t = +\infty) = \text{constant}$. Moreover, the fact that the helix is held in $z = 0$ and $z = L$ implies

$$[\theta(L, +\infty) - \theta(L, 0)] - [\theta(0, +\infty) - \theta(0, 0)] = \delta u_{z\theta}(z, +\infty) L = 0, \tag{S6}$$

hence $\delta u_{z\theta}(z, +\infty) = 0$ and the tube does not undergo any rotation.

Rotation of a tube bound at its two ends is however observed in Fig. 2(c), and is found to yield a sinusoidal velocity profile. Here we propose a possible explanation for this observation. Because of the propensity of the helix to rotate, torques build up in the tube following GTP injection, and have been observed to lead to supercoiling of the tube (3, 6). The formation of a supercoil from a stressed rod is a local phenomenon, which does not require an overall rotation of the rod or flow of membrane. Consequently, we expect supercoils to form quickly (on non-hydrodynamic time scales) following the GTP-induced build-up of torque. To simplify, let us assume that the formation of these supercoils is irreversible—once formed they are thus "frozen" for the rest of the dynamics. Supercoil formation leads to a local relaxation of the tube, and therefore we expect that the helix in the vicinity of the supercoils will change its pitch and radius to some extent. This creates an inhomogeneous initial condition for the tube's hydrodynamic relaxation. As a consequence, and unlike in the case considered above, $\delta u_{z\theta}(z, t = 0)$ is not equal to zero everywhere. The precise structure of this initial condition depends on the details of the supercoiling mechanism, and is beyond the scope of this study. Assuming however that no additional supercoiling occurs on hydrodynamic time scales, we predict that this initial condition relaxes according to the diffusion equation Eq. (5). Since the now complicated function $\delta u_{z\theta}(z, t = 0)$ generically has a non-vanishing projection onto the slowest mode of the diffusion equation, we expect that the long-time dynamics of the tube is dominated by the sinusoidal profile observed in Fig. **2**(c).

Note that the mechanism presented here might not be the only possible explanation for this phenomenon, and is only meant as an illustration of the fact that rotation in a tube bound at its two ends is not logically forbidden. Moreover, it illustrates the general feature that if the paradox

proposed here is indeed resolved through local, microscopic relaxation processes, then the form of long-time relaxation of the tube is not affected and we expect our hydrodynamic predictions to hold.

References

1. Dimova, R., B. Pouligny, and C. Dietrich, 2000. Pretransitional effects in dimyristoylphosphatidylcholine vesicle membranes: optical dynamometry study. *Biophys. J.* 79:340–356.

2. Pucadyil, T. J., and S. L. Schmid, 2008. Real-time visualization of dynamin-catalyzed membrane fission and vesicle release. *Cell* 135:1263–1275.

3. Roux, A., K. Uyhazi, A. Frost, and P. De Camilli, 2006. GTP-dependent twisting of dynamin implicates constriction and tension in membrane fission. *Nature (London)* 441:528–531.

4. Lenz, M., J. Prost, and J.-F. Joanny, 2008. Mechanochemical action of the dynamin protein. *Phys. Rev. E* 78:011911.

5. Kozlov, M. M., 1999. Dynamin: Possible mechanism of "pinchase" action. *Biophys. J.* 77:604–616.

6. Danino, D., K.-H. Moon, and J. E. Hinshaw, 2004. Rapid constriction of lipid bilayers by the mechanochemical enzyme dynamin. *J. Struct. Biol.* 147:259–267.

S2 Supporting movies—legends

S2.1 Supporting movie 1

Experimental movie corresponding to Fig. 1(b). See main text for legend.

S2.2 Supporting movie 2

Illustration of the dynamics presented in Fig. 3 of the main text. Only a few helical turns are shown, and in this small region the deformation looks spatially homogeneous—it however has a more complicated spatial structure on larger length scales, as discussed in the main text and in Ref. (4). The movie displays the asymptotically exponential relaxation of the helix's three hydrodynamic modes. The relaxation times involved in a real system are well separated and range from hundreds of microseconds to seconds (see Fig. 3). Here these time scales are modified for easier visualization. Each of the three modes therefore appears to have a relaxation time equal to 0.4 s. Note that the amplitude of the first mode is very small compared to the next two and might therefore escape the reader's attention on first viewing. Finally, the model used allows for both bending and stretching of the membrane (4). Although its amplitude is small, the former induces some bulging of the membrane visible in this movie. The membrane is represented as a semi-transparent surface, and its transparency is proportional to its stretching ratio.

S3 Supporting figures

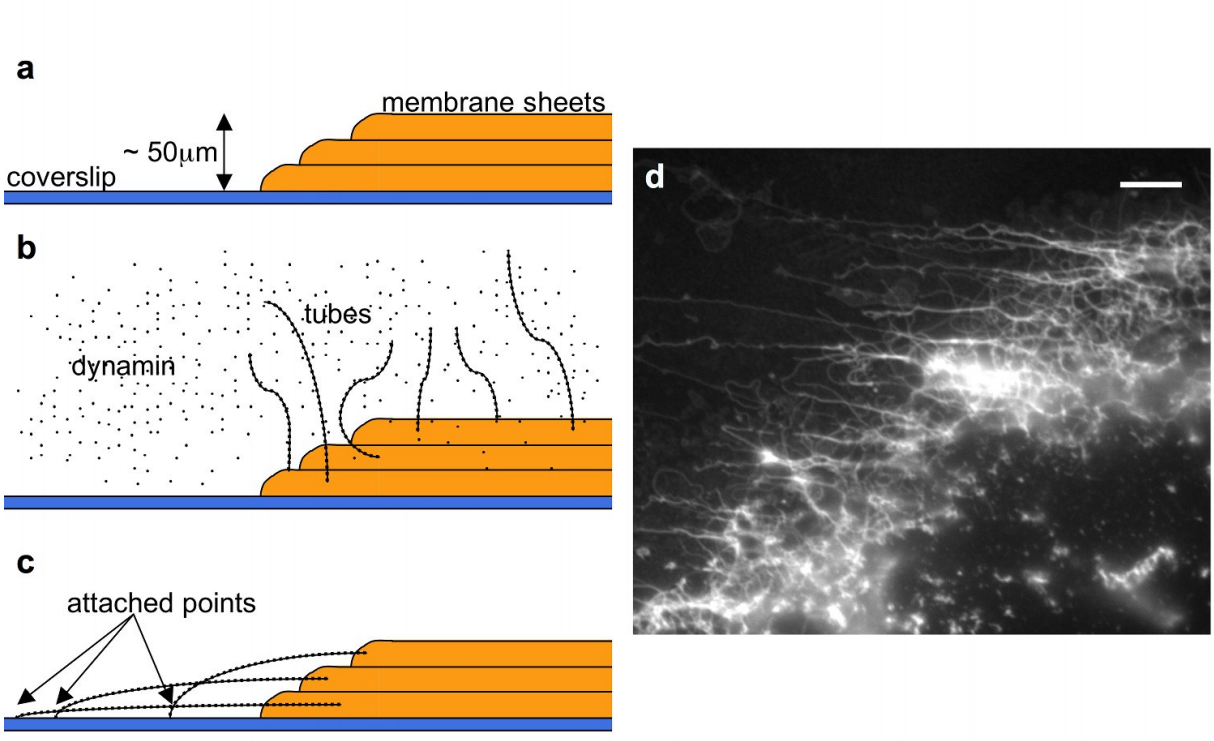

Figure S1: Geometry of the membrane sheets assay. (a-c) Side-view schematics representing (a) the membrane sheets after rehydration and before dynamin injection, (b) the appearance of dynamin-coated tubes on membrane sheets after dynamin injection, and (c) tubes bound to the coverslip following dynamin injection. Note that the tubes represented here are essentially parallel to the coverslip, enabling us to monitor their dynamics, but are some distance away from it, thus allowing the beads to rotate freely. (d) Top-view fluorescence microscopy image of a membrane sheet at the stage represented in (c) (dynamin is fluorescently labeled). Scale bar, 5 μm.

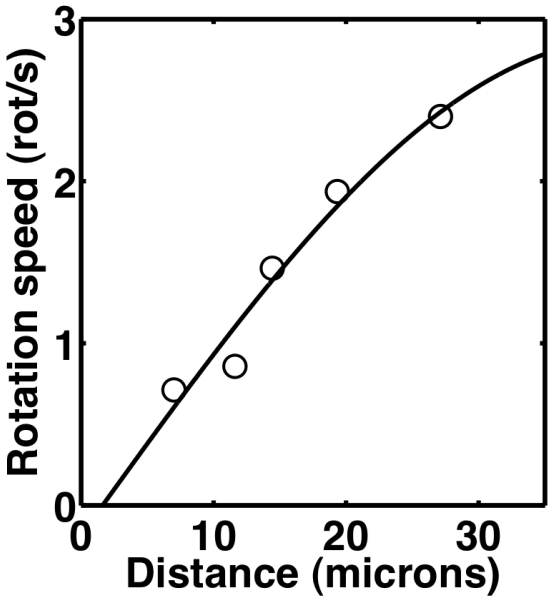

Figure S2: Experimental determination of the boundary conditions for a tube bound at one end only. In order to calculate the maximum wavelength $\lambda_{\max}$ compatible with the boundary conditions of a given tube, we assume that tubes visibly bound to the glass at both ends obey the boundary conditions $\delta\theta(z = 0, t) = \delta\theta(z = L, t) = 0$, which yields $\lambda_{\max} = 2L$. Fig. 2(c) of the main text demonstrates the validity of this description, as it shows that the best sinusoidal fit to the bead velocity data coincides with the boundary conditions directly assessed from video microscopy data. For tubes bound in $z = 0$ and free to rotate in $z = L$, we assume $\delta\theta(z = 0, t) = 0$ and $\partial_z\delta\theta(z = L, t) = 0$, where the latter condition corresponds to a zero torque being applied to the tube in $z = L$. This implies $\lambda_{\max} = 4L$. In this figure we present experimental data (circles) similar to that of Fig. 2(c) for such a tube, as well as the best sinusoidal fit of the form $\Omega = \Omega_0 \sin[2\pi(z - z_0)/\lambda_{\max}]$ for this data (line), where Ω_0, z_0 and $\lambda_{\max}$ are adjustable parameters. The sinusoidal fit yields $\lambda_{\max} \simeq 160\,\mu$m, consistent with the direct measurement $L \simeq 45\,\mu$m. Note that no beads are attached to the vicinity of the end of this tube, and therefore no data was collected in the region $z > 30\,\mu$m. Moreover, the fit places the tube's origin within $2\,\mu$m of the directly observed attachment point ($z_0 = 1.6\,\mu$m). This shows that a sinusoid with $\lambda_{\max} = 4L$ is a good description of a tube bound at one end only, and validates the use of this condition in constructing Fig. 2(d).

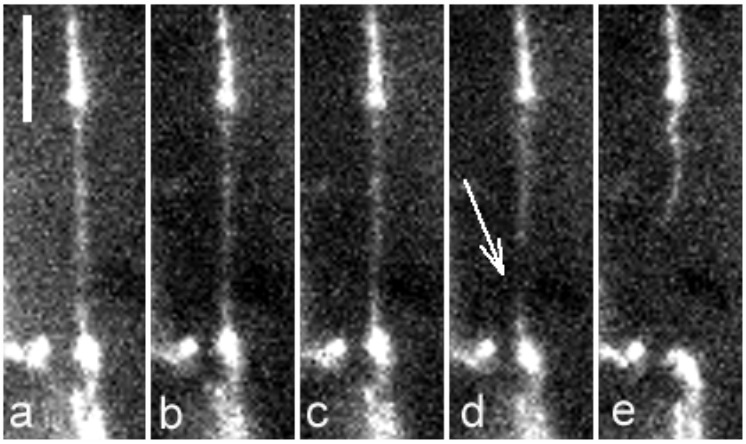

Figure S3: Direct epifluorescence observation of an Alexa-488–dynamin polymer [prepared as in Ref. (3)] during GTP hydrolysis using an EMCCD Andor camera. (a) tube anchored at both ends after injection of 6.3 μM fluorescently labeled dynamin on membrane sheets and before GTP injection. (b) 12.74 s after injection of 100 μM GTP. (c) 13.33 s after GTP injection. (d) Fission occurs (white arrow) 13.93 s after GTP injection. (e) 15.11 s after GTP injection and 1.18 s after tube fission. As mentioned in the main text, no significant discontinuity of the dynamin helix is observed during this experiment apart from the main breaking event. This is evidence that the dynamin coat remains continuous up until tube breaking. Scale bar: 5 μm.

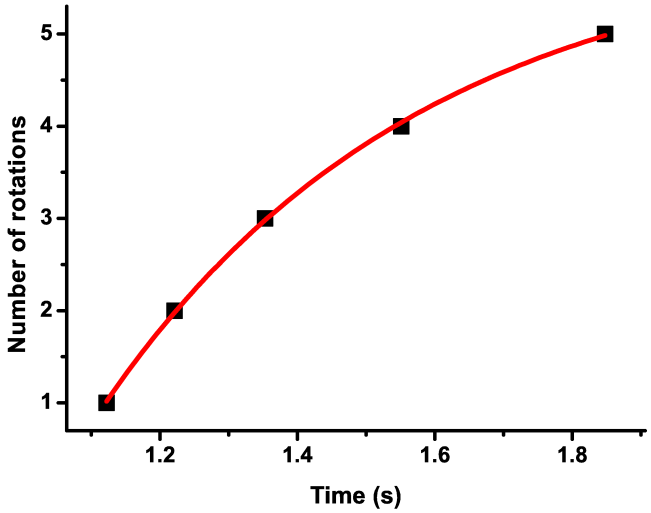

Figure S4: Fit procedure for the relaxation times presented in Fig. 2(d) of the main text. Relaxation times are deduced from the data points representing the number of turns $\theta/2\pi$ of a specific bead as a function of time t (black squares). Ignoring the initial phase where GTP injection and short wavelength modes interfere with the tube relaxation, these curves are fitted with the function $\theta/2\pi = a\exp(-t/\tau) + b$ in the Origin 8.1 software (red line), where a, b and τ are adjustable parameters. The optimal value for τ is the relaxation time plotted in Fig. 2(d).

5.3 Summary of Article 1

The goal of this study is to quantify spatially and temporally Dynamin constriction to test a theoretical model predicting the diffusing behaviour of long Dynamin-coated tubes upon GTP treatment. We follow simultaneously several beads attached to a single Dynamin-coated tube. After injection of 100 μM GTP, the beads start rotating at the same time. The rotations of each bead are tracked as functions of time and of their position on the tube. Four observations are made:

1. The total number of rotations measured at several positions z along a single tube is linear with the position z on the tube (Fig.2.a). The strain is around $2 rad.\mu m^{-1}$, in agreement with previous structural data.
2. The rotation speed of a bead decays exponentially (Fig.2.b). The typical time of decay is 3.7 s.
3. The rotation speed profile along a tube is sinusoidal (Fig.2.c).
4. The decay time increases with the square root of the tube length (Fig.2.d). This relationship yields a diffusion coefficient $D_m = 2\ 10^2\ \mu m^2.s^{-1}$

These experimental quantifications are then confronted to theory. The first observation confirms that Dynamin is a non polar polymer and shows that the helix remains continuous during constriction. The three other observations show that the propagation of constriction is diffusive. These results validate the hydrodynamic model. This study demonstrates that Dynamin conformational change is highly concerted and that the relaxation of the helix constriction is driven by the internal friction between Dynamin and membrane.

Confronting experiments and theory allows to make a full prediction of the dynamics of membrane deformations induced by Dynamin. Constriction occurs within 100 ms. However fission happens on the time scale of seconds. This means that Dynamin-mediated constriction is not enough to trigger fission. Thus it would be interesting to study the kinetics of the fission process.

Chapter 6

Fission is Regulated by Membrane Shape

6.1 Introduction to Article 2

In chapter 6, I conclude that constriction is not enough to trigger fission. So what mechanism controls fission? To better understand fission, it would be useful to follow the dynamics of the full fission process not only constriction. It was highlighted in chapter 4 that tension and rigidity could play a crucial role in membrane fission. So It would also be interesting to control the elastic parameters of membrane while monitoring fission events. Thus the nanotube extrusion technique seems well adapted to study Dynamin polymerization and fission.

6.2 Article 2: Membrane Shape at the Edge of the Dynamin Helix Sets Location and Duration of Fission

Article submitted

Authors: Sandrine Morlot, Valentina Galli, Marius Klein, John Manzi, Frédéric Humbert, Luis Dinis, Martin Lenz, Giovanni Cappello and Aurélien Roux.

Membrane shape at the edge of the Dynamin helix sets location and duration of the fission reaction.

Sandrine MORLOT[1,3], Valentina GALLI[1], Marius KLEIN[3], John MANZI[3], Frédéric HUMBERT[1], Luìs DINIS[4], Martin LENZ[5], Giovanni CAPPELLO[3], Aurélien ROUX[1,2].

[1]Biochemistry Department, University of Geneva, CH-1211 Geneva, Switzerland.

[2]Swiss National Centre for Competence in Research Programme Chemical Biology, CH-1211 Geneva, Switzerland.

[3]Institut Curie, Centre de Recherche; CNRS, UMR 168, Physico-Chimie Curie; Université Pierre et Marie Curie, F-75248 Paris, France.

[4]Departamento de Fìsica Atòmica, Molecular y Nuclear, Facultad de Ciencas Fìsicas, Universidad Complutense de Madrid, ES-28040, Madrid, Spain.

[5]James Franck Institute, University of Chicago, IL-60637 Chicago, U.S.A.

SUMMARY

The GTPase Dynamin polymerizes into a helical coat that constricts membrane necks of Clathrin-coated pits to promote their fission. However minimal requirements for fission are still debated as Dynamin constriction is necessary but not sufficient for fission. Here we show that fission occurs at the interface between the Dynamin coat and the uncoated membrane. At this location, the considerable change in membrane curvature increases locally membrane elastic energy, reducing the energy barrier for fission. Fission kinetics depends on tension, bending rigidity and the Dynamin constriction torque. Indeed, we experimentally find that the time it takes for fission depends on membrane tension *in vitro* and during Clathrin-mediated endocytosis *in vivo*. By i) estimating the energy barrier from the increased elastic energy at the edge of the Dynamin coat, and ii) measuring the Dynamin torque, we show that the mechanical energy

spent in Dynamin constriction can reduce sufficiently the energy barrier for fission to promote spontaneous fission.

INTRODUCTION

Membrane fission is an essential step in membrane traffic as it separates membrane cargoes from donor compartments. It is the inverse reaction to fusion. In many of the various fusion events in cells, a single type of machinery, the SNAREs, mediate the collapse of membranes. The general principle of the SNAREs mechanism is that the energy spent in the assembly of the SNARE complex overcomes the energy barrier to fusion by generating a hemi-fusion intermediate, also called the "stalk intermediate" (Kozlovsky and Kozlov, 2008b). The stalk intermediate is a structure where the cytosolic leaflets of the two membrane compartments are fused into one, whereas the lumenal leaflets are still separated. In the case of fission, different machineries mediate the separation of two compartments depending on the cellular context: Dynamin during endocytosis, Endosomal Sorting Complex in Retrograde Transport-III (ESCRT-III) in multivesicular body biogenesis, cytokinesis and viral budding. Small GTPases (Sar1, Arf1) involved in the initiation of the COat Proteins (COPs) dependent Golgi trafficking, have also been recently implicated in the fission reaction of the COPs. However in all these fission reactions, it is not known whether the different machineries mediate fission on the basis on the same principle, mostly because physical understanding of how fission is mediated is lacking. By analogy to fusion, it has been however suggested that they operate through a similar stalk intermediate (Kozlovsky and Kozlov, 2008a). Here, we focused on the physics of membrane fission taking the Dynamin system as a model in which the biochemistry is arguably better characterized than in other systems.

Dynamin has been biochemically and genetically implicated in fission of endocytic vesicles (Ferguson and De Camilli, 2012). It is a GTPase that polymerizes into helical collars at the neck of Clathrin-coated pits (CCPs). The helical structure of Dynamin immediately suggested that fission could be driven by a constriction of the helix.

When assembled in absence of GTP, the non-constricted Dynamin helix surrounds a membrane tube with radius R_u = 10 nm (Chen et al., 2004; Danino et al., 2004). Upon GTP hydrolysis, a conformational change of Dynamin at the dimer and the polymer levels (Chappie et al., 2011; Faelber et al., 2011; Ford et al., 2011), constricts the membrane (Danino et al., 2004; Sweitzer and Hinshaw, 1998). Constriction correlates with a reduction of the helix radius, itself reflected by a reduction of the number of dimers per helix turn from 14 to 13 (Chappie et al., 2011) and torsion. This torsion of the entire helical polymer can be monitored by live imaging (Roux et al., 2006). Early models (Hinshaw and Schmid, 1995; Takei et al., 1995) proposed that constriction was sufficient to break the neck, as constriction would proceed until fission is fully completed. More recent data has modified our understanding of the possible role of constriction in Dynamin-mediated membrane fission: i)- Dynamin cryo-electron microscopy images and 3D reconstruction showed that the polymer can constrict down to a constriction radius R_c of 4-5nm (Danino et al., 2004), filled with a tubular membrane (2nm thick) which surrounds a water lumen (2-3nm) (Chappie et al., 2011). These structural data support the idea that Dynamin does not reach the hemi-fission state by constriction. ii)-GTP-mediated constriction (Danino et al., 2004) and torsion (Roux et al., 2006) do not lead to fission unless the tube is both attached to the substrate (Danino et al., 2004) and subjected to longitudinal tension (Roux et al., 2006). These results showed that membrane constriction is not sufficient for fission, and also suggested that

mechanical parameters of the membrane (tension, bending rigidity) could play role in controlling fission.

Theory of membrane mechanics links the elastic energy E_{el} of the membrane to its shape via the Canham-Helfrich equation (Helfrich, 1973) : $E_{el} = \sigma\Delta A + \int_A \frac{\kappa}{2} J^2 \, dA$.

The first term of this equation (σΔA) is the energy associated with membrane stretching, with depends on the membrane tension σ and the change in its surface area ΔA. The second term is the energetic cost associated with membrane bending, a function of the local curvature J (which characterizes the local shape of the membrane) multiplied by the membrane bending rigidity κ integrated over the whole membrane area A. This rigidity depends on the lipid composition of the membrane. The Canham-Helfrich equation allows to calculating shapes and energies of lipid membranes in practically any conditions by measuring both membrane tension and rigidity.

As the Dynamin helix constricts, it imposes a strong curvature on the membrane tube that it covers. This strong curvature has a high energetic cost. We thus reasoned that Dynamin constriction could be significantly impeded by membrane elasticity, leading us to study how membrane mechanics influences the Dynamin-mediated fission reaction.

In this study we show that membrane fission is occurring at the frontier between the constricted Dynamin coat and the bare membrane, a place where the important change in membrane curvature increases locally the elastic energy of the membrane. We further show that the energy barrier to fission is reduced by this local increase of membrane elastic energy, making fission spontaneously occurring at the edge of Dynamin. By calculating the elastic energy difference between the unconstricted state of Dynamin and the hemi-fission intermediate, we estimate the energy barrier to fission to be of the order of 30-60 k_BT. By measuring the constriction strength, the torque of Dynamin, we show that it is in the order of 700-1000 pN.nm, about 10 times larger than torques

measured for other proteins. The huge value of the torque is however required to constrict the membrane to such extent. Moreover, we show the mechanical energy spent by Dynamin in constriction is sufficient to reduce the energy barrier to fission by the same amount evaluated from the elastic energy of the membrane. Our results support a mechanism by which Dynamin constricts fast, within a few hundreds of milliseconds, forcing the membrane to reach a high elastic energy state at the edge of the Dynamin coat. The increased elastic energy of the membrane then triggers spontaneous fission at the edge of Dynamin, which takes a few seconds.

RESULTS

Fission occurs at the edge of the Dynamin coat

We adapted an *in vitro* assay (see Fig. 1A) developed for the study of curvature-dependent lipid sorting (Sorre et al., 2009) and protein binding (Roux et al., 2010; Sorre et al., 2012). The assay is based on the generation of a membrane nanotube pulled out of a Giant Unilamellar Vesicle (GUV) by means of optical tweezers. The membrane tension σ was set through aspiration of the GUV in a micropipette, allowing control over the Dynamin-free tube radius $r = \sqrt{\kappa/2\sigma}$. Using a second micropipette, we injected a mix of fluorescent Alexa-488 Dynamin 1/non-fluorescent Dynamin 1 in the vicinity of these nanotubes (see Experimental Procedures). In absence of GTP, nucleation of Dynamin seeds onto the nanotube, but no fission, was observed ((Roux et al., 2010) and data not shown). When GTP was added along with Dynamin, small Dynamin seeds formed along the tube and membrane fission subsequently occurred (see Fig. 1B and Movie S1). As previously described (Roux et al., 2006), the tube retracted rapidly following the first break and no further break was observed. Using fast dual-color confocal imaging (see Extended Experimental Procedures), we observed that fission occurred at the edge of

Dynamin domain in 90% (N=10) of the events (see Fig. 1C, Movie S2 and Fig. S1). Indeed, after fission, one extremity of the broken tube was covered with Dynamin whereas the other one was not (Figs. 1C and S1 and Movie S2). No fission was observed in the uncoated regions of the tube.

We hypothesized that the considerable change of curvature from the highly constricted Dynamin-coated part to the less curved bare tube could favor fission. We were thus prompted to look at the efficiency of fission at the connection between the tube and the GUV, where the change in curvature is even more dramatic. Indeed, most of the fission events occurred at the boundary between the tube and the GUV (38%) or at the boundary between the tube and the bead (36%) (N=44, Figs. 1D-E and Movie S3). It is worth noting that shapes of the membrane at both connections are similar as the membrane-bead adhesion patch is much larger (several hundreds of nm) than the size of the tube in this assay (Koster et al., 2005). Dynamin nucleation was homogeneous along the tube axis (Fig. 1D blue curve), indicating that this higher probability of fission was not due to preferential nucleation of Dynamin at the bead, at the GUV or on the parts of the nanotube adjacent to them, but consistent with an influence of the local membrane shape (Fig. 1F).

The membrane shape at the Dynamin-membrane edge facilitates fission

We then calculated the shape of the membrane at the edge of the constricted Dynamin tube (called "Dynamin-membrane edge" in the following). By setting the constriction radius R_c, σ and κ (see Extended Experimental Procedures) and numerically minimizing the elastic energy of the membrane, we can calculate the shape of the Dynamin-membrane edge (Figs. 1F and 1G). The funnel shape of the Dynamin-membrane edge is associated with a local increase in elastic energy that can be estimated numerically (Fig.

2B and (Shlomovitz et al., 2011)). This elastic energy depends on the ratio $\alpha=R_m/R_c$, where R_m is the radius of the bare tube, which is set by membrane tension and bending rigidity. Thus, the smaller R_c is (the more Dynamin constricts), the higher the elastic energy of the Dynamin-membrane edge is.

We reasoned that the local increase of elastic energy of the membrane edge could favor fission by reducing its energy barrier. Fission was proposed to occur wherever the membrane reaches a hemi-fission state, when the membrane radius shrinks below a threshold $R_i \sim 3nm$ (Kozlovsky and Kozlov, 2003), comparable to the membrane thickness (see fission intermediate in Fig. 2A). The existence of such hemi-fission intermediate is supported by the experimental fact that fission is non-leaky (Bashkirov et al., 2008). Reaching an intermediate state with such a strongly curved membrane is a rare event, and must thus be the rate-limiting step of membrane fission. We propose that by constriction of Dynamin, the elastic energy of the membrane increases most at the edge of the Dynamin coat, thereby reaching the constricted state (Fig. 2A). Then thermal fluctuations of the membrane edge would allow spontaneous fusion of the inner layer of the tube, reaching the hemi-fission state. Since the energy of the intermediate state E_i and of the unconstricted state E_u corresponds to the elastic energy of the membrane at the edge of Dynamin, the full energy barrier is $\Delta E_{tot} = E_i - E_u$ (see Fig. 2A).

We numerically estimated the magnitude of the energy barrier ΔE_{tot} in two cases: (i) for the membrane edge connected to the bead or GUV and (ii) for the membrane edge connected to the bare tube. For (i), ΔE_{tot} = 20 - 65 k_BT, and for (ii), 35 - 70 k_BT (Fig. 2C, k_BT is the thermal energy). These values are close to previous theoretical estimations for the fission energy barrier (Kozlovsky and Kozlov, 2003). The actual value of the barrier depends on membrane tension (see Fig. 2C) and rigidity (data not shown). Also, as

shown in Figure 2C, we predict that the energy barrier is smaller close to the bead or vesicle, thus accounting for a higher fission probability there (Fig. 1D). We further estimated the probability to break close to the bead or GUV from the difference of these energy barriers (see Extended Experimental Procedures). Considering the range of tensions we have in our experiments (10^{-6} N/m – 10^{-4} N/m), we found this probability to be between 70% and 95%, consistent with the above experimental value of 38+36=74%.

To further test the role of membrane elasticity in Dynamin-mediated fission, we used our model to estimate the expected dependence of the average fission time $\langle t_f \rangle$ with membrane tension and bending rigidity. According to the model (see Fig. 2A), after constriction, fission at the Dynamin-membrane edge is spontaneous and the residual energy barrier after constriction $\Delta E_{res} = E_i - E_c$ is, this way, small enough to be overcome by thermal fluctuations of the membrane (see Fig. 2A). If after constriction, fission is thermally activated, $\langle t_f \rangle$ should satisfy a simple Arrhenius equation $\langle t_f \rangle = \tau e^{\Delta E_{res}/k_B T}$, where $\tau \sim 1$ns is the typical time scale of the membrane tube thermal fluctuations. By taking a linear approximation for the elastic energy of the edge with the curvature of the constricted Dynamin-tube ($1/R_c$), we find (see Extended Experimental Procedures):

$$\langle t_f \rangle \simeq \tau e^{\frac{b\kappa^{3/2}}{\sqrt{\sigma}}/k_B T} \qquad \text{Eq. 1}$$

where b is a constant that depends on R_i and R_c, σ membrane tension and κ membrane rigidity.

We experimentally validated Eq.1 by studying how long it takes for Dynamin to break membrane tubes. As Dynamin and GTP are co-injected, we defined the fission time t_f as the time elapsed between nucleation of Dynamin seeds and fission (see kymograph in Fig. 3A). At 150 μM GTP, a physiological concentration of GTP (Otero, 1990), the average fission time $\langle t_f \rangle$ was 10.3±2.0s, similar to the *in vivo* values (Taylor et al., 2011). The fission time decreased with the GTP concentration, with $\langle t_f \rangle$ at 1μM GTP equals to 85.3±8.7s and $\langle t_f \rangle$ at 10mM GTP equals to 6.2±0.8s (see Table 1). As a first test of our model, we verified that the fission times were exponentially distributed (Fig. 3B; see also Table 1), as expected for a thermally activated, single-step process obeying Poisson statistics.

We next tested the dependence of the fission time with membrane tension and rigidity (see Eq. 1). In our *in vitro* assay, membrane tension can be tuned by changing the aspiration pressure in the micropipette, and rigidity by changing the lipid composition (see Table S1 and Extended Experimental Procedures). As expected, the fission time increased with membrane rigidity (Fig. 3C), following exp $(constant \times \kappa^{3/2})$ (see Eq. 1). Dependence of the fission time with membrane tension compatible with the predicted relation in exp $(constant/\sqrt{\sigma})$ was also observed (Fig. 3D). The observed dependences of the fission time with tension and rigidity are in good agreement with our model, but our model also states that they should be the dominant membrane parameters controlling the fission time. Following this statement, we expect the logarithm of $\langle t_f \rangle$ to have a linear dependence with $\frac{\kappa^{3/2}}{\sqrt{\sigma}}$ (Eq.1), which is experimentally verified (Fig. 3E). We concluded that the dependences of the fission time with membrane tension and rigidity further show that the mechanical determinants of the membrane shape control the kinetics of the Dynamin fission reaction.

The Dynamin torque is sufficient for constriction

The mechanism proposed above for Dynamin-mediated fission reaction is strongly dependent on the ability of Dynamin to constrict. We thus wondered if the constriction strength of Dynamin was sufficient to constrict such membrane necks. As Dynamin undergoes torsion during constriction, it generates a torque (see Figs. S2C, 4A and Movie S4). Thus, the constriction torque of Dynamin must be strong enough to counteract membrane bending elasticity that widens the tube. In order to verify this, we measured the torque Γ exerted by Dynamin during constriction by monitoring the position of beads of radius r attached to the Dynamin coat. The beads rotated following GTP addition, allowing us to track the torsion of the Dynamin coat (Morlot et al., 2010; Roux et al., 2006). Because of this fast motion, the beads incurred a viscous drag, which counteracted the torque generated by Dynamin, which limits the maximal angular speed. The viscous drag acting on a bead of radius r spinning around a linear axis is: $\Gamma_{visc} = 14\pi\eta r^3\omega$, where ω is the angular velocity of the bead and η the viscosity of water. We used beads of 675 nm radius, and measured an average angular speed ω=15.8±5 rad/s at 2 mM GTP (Fig. 4B), corresponding to an average torque of 214±74 pN.nm. These beads are significantly slower than beads of 95-180nm radii used in previous studies (approx. 55 rad/s, see (Morlot et al., 2010; Roux et al., 2006)) indicating that the viscous torque acting on the 675nm beads is of the same order of the Dynamin torque. Because the beads are rotating, the torque of Dynamin is larger than the measured viscous torque. The highest value of the viscous torque (730 pN.nm, see Fig. 4C) obtained for the fastest bead is thus a closer underestimate of the Dynamin torque. Γ =730 pN.nm is 20 times larger than the torque developed by proteins twisting

DNA (10-20 pN.nm such as the recombinase RecA (Lipfert et al., 2010)) or the rotational motor F1 ATPase, which usually generate torques of 40 pN.nm (Yasuda et al., 1998).

We measured the maximum torque of Dynamin (stall torque Γ_s) by attaching magnetic beads to Dynamin-coated tubules, and blocking their rotation with a magnetic field. After calibration of the set-up (see Extended Experimental Procedures and Figs. S2A, B and D), magnetic fields were translated into the magnetic torque experienced by the bead in the magnetic field. We found that beads stopped to rotate when magnetic torques exceeded 1300 pN.nm at 1mM GTP. Rotational movement started again upon switching off the magnetic field (Fig. S2E and Movie S5), confirming that abrupt stop was due to magnetic field. We observed that the angular velocity of the bead decreased linearly with increasing intensities of the magnetic field (Figs. 4D and 4E). Linear fits (Fig. 4E) gave an average value of the stall torque of Dynamin of 1100±340 pN.nm.

From the free energy of a Dynamin constricted tube (see Extended Experimental Procedures), we calculated that R_c is related to the Dynamin torque by $R_c = R_u/\left(1+\frac{\Gamma R_u}{2\pi\kappa h}\right)$, where h=13nm is the Dynamin pitch. According to this relation, constriction from R_u=10nm to R_c=5nm radius would require a torque of approx. 500 pN.nm. We concluded that the large value of the Dynamin torque measured above was necessary and sufficient for constriction of membrane necks.

Dynamin mechanical work reduces the energy barrier to fission

The mechanical work of Dynamin is partially spent in reducing the energy barrier to fission. If our model is valid, this fraction of the mechanical work is still required to reduce significantly the energy barrier. The residual barrier ΔE_{res} should be in the range of a few k_BT. Thus we expect the Dynamin work to be of the same order of the full barrier ΔE_{tot} estimated from the elastic energy of the membrane (see above).

Theoretically, the fraction of the Dynamin work can be subtracted from the energy barrier (see Extended Experimental Procedures), with $\Delta E_{res} = \Delta E_{tot} - c\Gamma\theta$, where $\Gamma\theta$ is the Dynamin work (Fig. S2C, and below). The fission time expression is then:

$$\langle t_f \rangle \simeq \tau e^{(\Delta E_{tot} - c\Gamma\theta)/k_B T} \qquad \text{Eq.2}$$

where c is a constant and θ is the angle by which the helix rotates for each GTP it hydrolyses (Fig. S2C). According to this definition, we can identify $\Gamma\theta$ as the work performed by the helix per hydrolysed GTP. According to Eq. 2, for each amount $\Gamma\theta$ of mechanical work performed per GTP, ΔE_{tot} is lowered by an amount $c\Gamma\theta$. Thus c characterizes the efficiency with which mechanical work is used to lower the fission barrier. The work performed by Dynamin upon the hydrolysis of one GTP is proportional to the difference in chemical potential between GTP and its hydrolysis products. Thus for experimental concentrations of GTP, we expect:

$$\Gamma\theta = \xi k_B T ln([GTP]) + constant \qquad \text{Eq. 3}$$

where the dimensionless number ξ is the yield of the conversion of chemical energy into work. As a consequence, the product cξ characterizes the efficiency with which Dynamin uses chemical energy to lower the barrier to fission. Inserting Eq. 3 into Eq. 2, we finally find:

$$ln(\langle t_f \rangle) = c\xi ln([GTP]) + constant \qquad \text{Eq. 4}$$

To validate this extended mechano-chemical framework experimentally, we sought to verify the predicted GTP-dependences and to characterize the efficiency cξ. We first showed (Fig. 4B) that the torque Γ depended linearly on $ln([GTP])$, as expected from Eq. 3. The slope allows us to estimate ξ/θ=18.5. Knowing the full constriction angle θ_{full} from structural data ((Mears et al., 2007), 1/14 of a turn leads to $\theta_{full} = 2\pi/14 \approx 0.45$

rad), and assuming that ξ = 1, we can calculate the minimal number of GTP hydrolysed to reach full constriction $N = \frac{\theta_{full}}{\theta} = 18.5 \times 0.45 \approx 8$. We then measured the dependence of the fission time on GTP concentration, yielding very good agreement with Eq. 4 (Fig. 4F) for values of GTP concentration lower than 10mM. The experimental verification of Eq. 4 validates our picture of the role of GTP hydrolysis in lowering the energy barrier to fission through a modification of the membrane shape. Interestingly, the slope of this curve gives cξ= 0.37±0.07, meaning that over a large range of GTP concentrations, the reduction of the fission energy barrier represents 37% of the energy available from GTP hydrolysis. Knowing the minimal number *N* of GTP required for a full constriction of Dynamin, we estimated the minimal energy E_{min} spent by Dynamin in reducing the energy barrier to fission: one GTP delivers approximately 20 k_BT, thus $E_{min} = 37\% \times 8 \times 20\ k_BT \approx 59\ k_BT$. It is of the same order than the energy barrier ΔE_{tot} values (35-70 k_BT) estimated from the change in shape of the Dynamin-membrane edge mediated by Dynamin constriction. This simple calculation shows that Dynamin through its constriction transfers enough energy to the membrane to significantly reduce the energy barrier to fission so that it becomes spontaneous at the Dynamin-membrane edge.

Dynamin reaction kinetics is controlled by membrane tension *in vivo*.

We next studied if shape of the Dynamin-membrane edge could control the kinetics of Dynamin fission *in vivo*. We aimed at reducing membrane tension, and track the effect on the dynamics of Clathrin-coated pits (CCPs) formation. We exchanged quickly the culture medium of Cos7 cells to medium containing 0.45 M sucrose (Heuser and Anderson, 1989), and followed the dynamics of Clathrin-GFP by confocal imaging. As previously described (Heuser and Anderson, 1989), the rapid turn-over of Clathrin-GFP

dots at the plasma membrane in Cos7 cells stopped within seconds after the shock (Fig. 5A and Movie S6). The number of Clathrin-GFP dots increased after the shock. These Clathrin-GFP structures seemed to stay attached to the plasma membrane, suggesting a block of the Clathrin-coated pits at the fission level. Consistently, Dynamin-GFP followed the same behavior: more dots were seen after the shock (Fig. 5B and Movie S6), without turnover (see kymograph). Moreover, the Clathrin-RFP structures perfectly colocalized with Dynamin-GFP dots after the shock (approx. 85%, see Fig. 5C), showing that Clathrin structures were blocked at the stage of Dynamin ring formation. As the dynamics of Clathrin bud are altered by overexpression of endocytic proteins, we tested the effect of hypertonic shock on genome-edited SKML-2 cells, where Clathrin-RFP and Dynamin-GFP are expressed at the same level than endogenous proteins (Doyon et al., 2011). When hypertonic medium was applied to these cells, the number of Clathrin/Dynamin dots increased and their dynamic exchange was blocked (data not shown). As in Cos7 cells, clathrin-RFP dots colocalized with Dynamin-GFP dots (see Fig. S3).

We next verified that the Clathrin dots blocked at the fission step were fully assembled CCPs. They indeed partially colocalized with transferrin, showing that cargo were present in these structures (see Fig 5D). As well, the plasma membrane lipophilic dye MASK (Invitrogen Inc.) showed a slightly increased signal in Clathrin structures, reflecting the curved membrane of the bud (see Fig 5E). Taken together, these results strongly support the idea that many of the Clathrin coated dots frozen at the plasma membrane are fully assembled CCPs, blocked at the assembled Dynamin stage, unable to break the membrane. These *in vivo* results are consistent with our *in vitro* results: they show that a membrane tension decrease blocks Dynamin-dependent endocytosis at the fission step, in a similar way than reduced membrane tension strongly delayed fission *in vitro*. Moreover, as previously reported (Boulant et al., 2011), we find that hypo-osmotic

shock delays CCPs formation, but does not alter Dynamin dynamics in the first few minutes after the shock (data not shown).

DISCUSSION

In this study, we first showed that Dynamin-mediated fission occurs at the edge of the Dynamin coat. Consistently, in mitochondrial fission, breakage was often observed at the boundary between the DNM1 ring and the rest of the mitochondria (Bleazard et al., 1999). We then showed that fission was facilitated at the Dynamin-membrane edge because of the local membrane elastic energy increase due to considerable change in curvature. We next showed that not only the location, but also the kinetics of the reaction is set by the shape of the membrane connecting the constricted tube to the bare part of the membrane. The constriction torque of Dynamin and membrane elasticity parameters such as tension and bending rigidity that control the membrane edge shape thus act directly on the kinetics of Dynamin-mediated membrane fission. Moreover, we showed in this study that the calculation of the energy barrier estimated either from the shape of the membrane (from which we can estimate the elastic energy of the membrane) or from the mechanical work generated by Dynamin during constriction gave similar values (in the range of 50-70 k_BT). Importantly, the contributions of the Dynamin work, tension and rigidity to the kinetics of the fission reaction are different: - measured GTPase rate of Dynamin in the assembled form (Praefcke and Mcmahon, 2004)) suggests that the minimal amount of GTP required for full constriction is hydrolysed within hundreds of milliseconds. Our previous study of the dynamics of Dynamin constriction (Morlot et al., 2010) consistently showed that constriction should also happen within a few hundreds of milliseconds. As for non-limiting GTP concentrations, fission takes a few seconds at least, our results are compatible with i)

first, a fast constriction of Dynamin, and ii) then, a long delay to spontaneous fission of the constricted neck. Thus, at non-limiting GTP concentrations (closer to *in vivo* situation), the kinetics of Dynamin-membrane fission are expected to be primarily regulated by the elasticity of the membrane. Indeed, we showed that, *in vivo*, Clathrin-mediated endocytosis is blocked by reducing membrane tension, consistently with our *in vitro* results. Also, *in vivo* and *in vitro* typical fission times (a few seconds) are similar. These observations strengthen the idea that fission kinetics is controlled by elasticity of the membrane *in vivo*.

Recent studies (Bashkirov et al., 2008; Pucadyil and Schmid, 2008) have been taken to suggest that Dynamin-mediated fission could be triggered by GTP-induced depolymerization instead of constriction. Our result showing that fission occurs at the edge of the Dynamin coat indicate that it requires partial coating of the membrane, which can be achieved either by partial polymerization of a bare membrane, or partial depolymerization of a fully coated membrane. However, in our experiments, we never observed depolymerization of the Dynamin coat prior (see Fig. 3A) or after (see Fig. 1C, t=2.5s) fission. As in our experiments the optical resolution limit is above the size of a Dynamin turn, we cannot exclude depolymerization restricted to a few turns. In the hypothesis that fission is mediated through depolymerization, it was predicted that long coats would have a reduced fission efficiency (Pucadyil and Schmid, 2008), as they would require more time to be fully depolymerized. In our experiments, we saw no dependence of the fission time with length of single Dynamin seeds, from 150 nm to 10 microns (see Fig. S1B). Also, GTP energy was proposed to be spent in depolymerization rather than constriction (Bashkirov et al., 2008). The good agreement between energetics of membrane constriction and Dynamin torque work favors the hypothesis that GTP energy is primarily spent in constriction, rather than in depolymerization.

In a broader perspective, the model presented here to explain the mechanism by which Dynamin performs fission may be valid for all fission reactions mediated by the constriction of a narrow membrane neck, as it is proposed for ESCRT-III mediated fission (Fabrikant et al., 2009), and as it is the case in lipid phase separation (Roux et al., 2005).

EXPERIMENTAL PROCEDURES

A full description of the methods is in the Extended Experimental Procedures.

Nanotube Pulling From GUV

Giant Unilamellar Vesicles (GUVs) were made by a modified protocol of the electroformation technique (Angelova et al., 1992; Roux et al., 2010). The aspiration of a GUV of radius R_{GUV} within a micropipette of radius $R_{pipette}$ allowed to set membrane tension: $\sigma = \frac{1}{2}\frac{R_{pipette}\Delta P}{1-\frac{R_{pipette}}{R_{GUV}}}$ (Evans and Rawicz, 1990). A lipid nanotube was extruded from a micropipette-aspirated GUV containing 0.03% mol/mol of a biotinylated lipid (DSPE-PEG2000-Biotin, Avanti Polar Lipids, Alabaster, Alabama, USA) by moving away the pipette from an optically trapped, 3 microns diameter Streptavidin-coated bead (Spherotec, Lake Forest, Illinois, USA) attached to the GUV prior to pulling. The fixed optical trap was custom-made and calibrated (see extended experimental procedures, stiffness $k=360 pN.\mu m^{-1}.W^{-1}$). A mix of baculovirus purified human Dynamin 1 (see extended experimental procedures for purification details) and Guanosine Tri-Phosphate (GTP, Roche Applied Science, Indianapolis, IN, USA) was injected in the vicinity of the lipid tube via a second micropipette. 2 color time-lapse acquisitions were

performed with either a confocal microscopy (Eclipse C1 Nikon, Tokyo, Japan) or a spinning disk confocal (Intelligent Imaging Innovations, Denver, Colorado, USA).

Torque Measurement by Viscous Drag and Magnetic Field

Streptavidin beads (1.35 µm diameter Streptavidin-coated, polystyrene beads, Spherotec, Lake Forest, Illinois, USA) are grafted onto biotinylated Dynamin tubules formed from membrane sheets (see extended experimental procedures and (Morlot et al., 2010; Roux et al., 2006)). The beads rotate following GTP addition and resulting constriction of the Dynamin coat (Morlot et al., 2010; Roux et al., 2006), experiencing a viscous torque $\Gamma_v = 14\pi\eta(R + r)^3\,\omega = \xi\omega$ (Happel J. and Brenner H. 1983), where η is the viscosity of the surrounding fluid, R the radius of the bead, r the radius of the tubule and ω is the angular spinning velocity. Differential Interference Contrast (DIC) and computer-based live recording of the rotating beads with a GUPPY camera (Allied Vision Technologies, Stadtroda, Germany) allowed direct measure of the angular spinning velocity and estimation the viscous torque from the formula above.

The stall torque Γ_S was measured by using magnetic beads (1.31 µm diameter Streptavidin-coated, paramagnetic beads, Spherotec, Lake Forest, Illinois, USA), to which is applied an external torque via a variable electro-magnetic field. This magnetic field was calibrated by two independent methods detailed in the extended experimental procedures.

Cell transfections, plasma membrane staining, Transferrin uptake and hypertonic shock

COS-7 cells were transfected using FuGENE-6 (Roche Applied Science, Indianapolis, Indiana, USA) with Dynamin 2 fused to Green Fluorescent Protein (GFP) (kindly provided by P. De Camilli; HHMI, Yale University) or mouse Clathrin-Light-Chain fused to mCherry or GFP (kindly provided by C. Merrifield, Cambridge and by P. De Camilli, HHMI, Yale University). Cells were imaged 18 to 24 hours post transfection in Leibovitz medium (Gibco, Life Technologies Ltd, Paisley, UK). While imaging, the medium was changed with a hypertonic solution of 0.25M sucrose in Leibovitz medium. Cell membrane staining was achieved by incubating cells for 5' at 37°C with deep red Cell Mask (Molecular Probes, Life Technologies Ltd, Paisley, UK) before imaging. For Transferrin uptake assays, cells were starved in serum deprived DMEM-F12 medium for 30' on ice, then incubated with 5 μg/ml Alexa-fluor 594 Transferrin (Invitrogen, Grand Island, NY, USA) in hypertonic medium (0.25M sucrose Leibovitz medium) for 3' at RT. Cells were washed with hypertonic buffer before imaging.

SUPPLEMENTAL INFORMATION

Supplemental Information includes Extended Experimental Procedures, three figures and six movies.

ACKNOWLEDGMENTS

We thank Marcos Gonzalez-Gaitàn, for inspiring discussions and critical reading of this manuscript. We thank Pietro De Camilli, Jacques Prost and Jean-François Joanny for thoughtful comments on this study.

This work was supported by the Agence Nationale de la Recherche (France, Young Investigator Program, N° JC08_317536 to A.R. and G.C.), the Human Frontier Science

Program Career Development Award (N° 0061/2008 to A.R.), and Young Investigator Research Grant (N° RGY0076/2009-C to A.R.), the Swiss National Fund for Research grant (N° 31003A_130520/1 to A.R.), the Société Académique de Genève, and the Swiss National Centre for Competence in Research Programme Chemical Biology.

REFERENCES:

Angelova, M.I., Soléau, S., Méléard, P., Faucon, J.F., and Bothorel, P. (1992). Preparation of giant vesicles by external AC electric fields. Kinetics and applications. Prog Colloid Polym Sci *89*, 127-131.

Bashkirov, P.V., Akimov, S.A., Evseev, A.I., Schmid, S.L., Zimmerberg, J., and Frolov, V.A. (2008). GTPase Cycle of Dynamin Is Coupled to Membrane Squeeze and Release, Leading to Spontaneous Fission. Cell *135*, 1276-1286.

Bleazard, W., McCaffery, J.M., King, E.J., Bale, S., Mozdy, A., Tieu, Q., Nunnari, J., and Shaw, J.M. (1999). The dynamin-related GTPase Dnm1 regulates mitochondrial fission in yeast. Nat Cell Biol *1*, 298-304.

Boulant, S., Kural, C., Zeeh, J.-C., Ubelmann, F., and Kirchhausen, T. (2011). Actin dynamics counteract membrane tension during clathrin-mediated endocytosis. Nature cell biology *13*, 1-10.

Chappie, J.S., Mears, J.A., Fang, S., Leonard, M., Schmid, S.L., Milligan, R.A., Hinshaw, J.E., and Dyda, F. (2011). A pseudoatomic model of the dynamin polymer identifies a hydrolysis-dependent powerstroke. Cell *147*, 209-222.

Chen, Y., Zhang, P., Egelman, E., and Hinshaw, J.E. (2004). The stalk region of dynamin drives the constriction of dynamin tubes. Nat Struct Mol Biol *v11*, 574-575.

Danino, D., Moon, K.H., and Hinshaw, J.E. (2004). Rapid constriction of lipid bilayers by the mechanochemical enzyme dynamin. J Struct Biol *147*, 259-267.

Doyon, J.B., Zeitler, B., Cheng, J., Cheng, A.T., Cherone, J.M., Santiago, Y., Lee, A.H., Vo, T.D., Doyon, Y., Miller, J.C.*, et al.* (2011). Rapid and efficient clathrin-mediated endocytosis revealed in genome-edited mammalian cells. Nature cell biology *13*, 331-337.

Evans, E., and Rawicz, W. (1990). Entropy-driven tension and bending elasticity in condensed-fluid membranes. Phys Rev Lett *64*, 2094.

Fabrikant, G., Lata, S., Riches, J., Briggs, J., Weissenhorn, W., and Kozlov, M. (2009). Computational model of membrane fission catalyzed by ESCRT-III. PLoS Comput Biol *5*.

Faelber, K., Posor, Y., Gao, S., Held, M., Roske, Y., Schulze, D., Haucke, V., Noe, F., and Daumke, O. (2011). Crystal structure of nucleotide-free dynamin. Nature *477*, 556-560.

Ferguson, S.M., and De Camilli, P. (2012). Dynamin, a membrane-remodelling GTPase. Nature reviews Molecular cell biology.

Ford, M.G., Jenni, S., and Nunnari, J. (2011). The crystal structure of dynamin. Nature *477*, 561-566.

Helfrich, W. (1973). Elastic properties of lipid bilayers : theory and possible experiments. Zur Naturforschung *28c*, 693-703.

Heuser, J.E., and Anderson, R.G. (1989). Hypertonic media inhibit receptor-mediated endocytosis by blocking clathrin-coated pit formation. The Journal of cell biology *108*, 389-400.

Hinshaw, J.E., and Schmid, S.L. (1995). Dynamin self-assembles into rings suggesting a mechanism for coated vesicle budding. Nature *374*, 190-192.

Koster, G., Cacciuto, A., Derenyi, I., Frenkel, D., and Dogterom, M. (2005). Force barriers for membrane tube formation. Phys Rev Lett *94*, 068101.

Kozlovsky, Y., and Kozlov, M.M. (2003). Membrane fission: model for intermediate structures. Biophys J *85*, 85-96.

Kozlovsky, Y., and Kozlov, M.M. (2008a). Membrane Fission: Model for Intermediate Structures. Biophysical Journal *85*, 85-96.

Kozlovsky, Y., and Kozlov, M.M. (2008b). Stalk Model of Membrane Fusion: Solution of Energy Crisis. Biophysical Journal *82*, 882-895.

Lipfert, J., Kerssemakers, J.W., Jager, T., and Dekker, N.H. (2010). Magnetic torque tweezers: measuring torsional stiffness in DNA and RecA-DNA filaments. Nat Methods *7*, 977-980.
Mears, J.A., Ray, P., and Hinshaw, J.E. (2007). A corkscrew model for dynamin constriction. Structure *15*, 1190-1202.
Morlot, S., Lenz, M., Prost, J., Joanny, J.F., and Roux, A. (2010). Deformation of dynamin helices damped by membrane friction. Biophys J *99*, 3580-3588.
Otero, A.D. (1990). Transphosphorylation and G protein activation. Biochem Pharmacol *39*, 1399-1404.
Praefcke, G., and Mcmahon, H. (2004). The dynamin superfamily: universal membrane tubulation and fission molecules? Nat Rev Mol Cell Biol *5*, 133-147.
Pucadyil, T.J., and Schmid, S.L. (2008). Real-time visualization of dynamin-catalyzed membrane fission and vesicle release. Cell *135*, 1263-1275.
Roux, A., Cuvelier, D., Nassoy, P., Prost, J., Bassereau, P., and Goud, B. (2005). Role of curvature and phase transition in lipid sorting and fission of membrane tubules. EMBO J *24*, 1537-1545.
Roux, A., Koster, G., Lenz, M., Sorre, B., Manneville, J.-B., Nassoy, P., and Bassereau, P. (2010). Membrane curvature controls dynamin polymerization. Proc Natl Acad Sci USA *107*, 4141-4146.
Roux, A., Uyhazi, K., Frost, A., and De Camilli, P. (2006). GTP-dependent twisting of dynamin implicates constriction and tension in membrane fission. Nature *441*, 528-531.
Shlomovitz, R., Gov, N., and Roux, A. (2011). membrane-mediated interactions and the dynamics of dynamin oligomers on membrane tubes. New Journal of Physics *13*, 065008.
Sorre, B., Callan-Jones, A., Manneville, J.B., Nassoy, P., Joanny, J.F., Prost, J., Goud, B., and Bassereau, P. (2009). Curvature-driven lipid sorting needs proximity to a demixing point and is aided by proteins. Proc Natl Acad Sci U S A *106*, 5622-5626.
Sorre, B., Callan-Jones, A., Manzi, J., Goud, B., Prost, J., Bassereau, P., and Roux, A. (2012). Nature of curvature coupling of amphiphysin with membranes depends on its bound density. Proceedings of the National Academy of Sciences of the United States of America *109*, 173-178.
Sweitzer, S.M., and Hinshaw, J.E. (1998). Dynamin undergoes a GTP-dependent conformational change causing vesiculation. Cell *93*, 1021-1029.
Takei, K., McPherson, P.S., Schmid, S.L., and De Camilli, P. (1995). Tubular membrane invaginations coated by dynamin rings are induced by GTP-gamma S in nerve terminals. Nature *374*, 186-190.
Taylor, M.J., Perrais, D., and Merrifield, C.J. (2011). A high precision survey of the molecular dynamics of Mammalian clathrin-mediated endocytosis. PLoS biology *9*, e1000604.
Yasuda, R., Noji, H., Kinosita, K., and Yoshida, M. (1998). F1-ATPase is a highly efficient molecular motor that rotates with discrete 120 degree steps. Cell *93*, 1117-1124.

FIGURES:

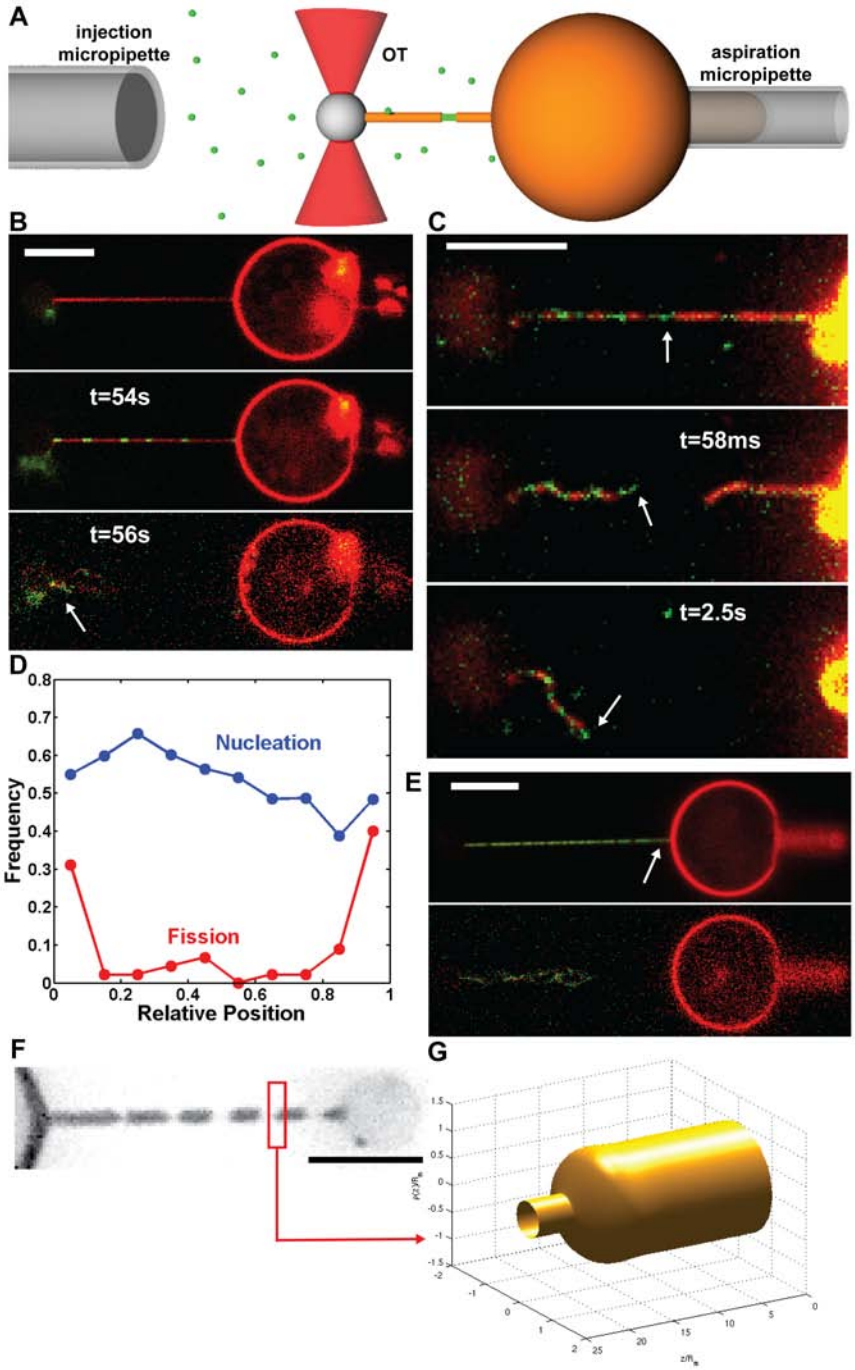

Fig. 1. Localisation of fission events at Dynamin-membrane edges. A- Schematic drawing of the experimental setup. A micropipette (right) set the GUV's tension. A membrane nanotube is extracted from the GUV via a microbead trapped in optical tweezers (red cones). A second micropipette (left) injects locally Dynamin and GTP. **B-** Confocal pictures of a GUV labeled with BodipyTMR-PI(4,5)P2 (red channel) and Dynamin labeled with Alexa 488 (green channel), see also Movie S1. Top: membrane nanotube before injection of Dynamin+GTP. Middle: nanotube partially coated with Dynamin after injection of Dynamin+GTP. Bottom: fission 56s after start of polymerisation. Remaining tube is still attached to the bead (white arrow). **C-**Images from dual-color spinning disk confocal microscopy. Top: tube before fission. Middle:

same tube 58ms after fission. Bottom: same tube 2.5s after fission. After fission, extremity of the left stump is covered with green Dynamin, whereas the right stump is uncoated, showing that fission occured at the edge between a seed of Dynamin (white arrows) and the Dynamin-free membrane nanotube (see also Figure S1). **D-** Frequency of Dynamin-nucleation (blue) and fission (red) along the nanotube. Position is normalized so that 0 and 1 are respectively the bead boundary and the connection between the tube and the GUV. N=44 tubes. **E-** Confocal pictures of a GUV and a Dynamin-coated nanotube as shown in B (see also Movie S2). No remaining of the tube is seen on the GUV, showing that fission occurred at the connection between the tube and the GUV (white arrow). **F-** Fluorescence image of a membrane tube constricted by Dynamin in presence of GTP (TMR-PE). **G-**Calculated shape a single Dynamin-membrane edge by simulations. Scale bars. (B) (C) (E) and (F) 5 μm.

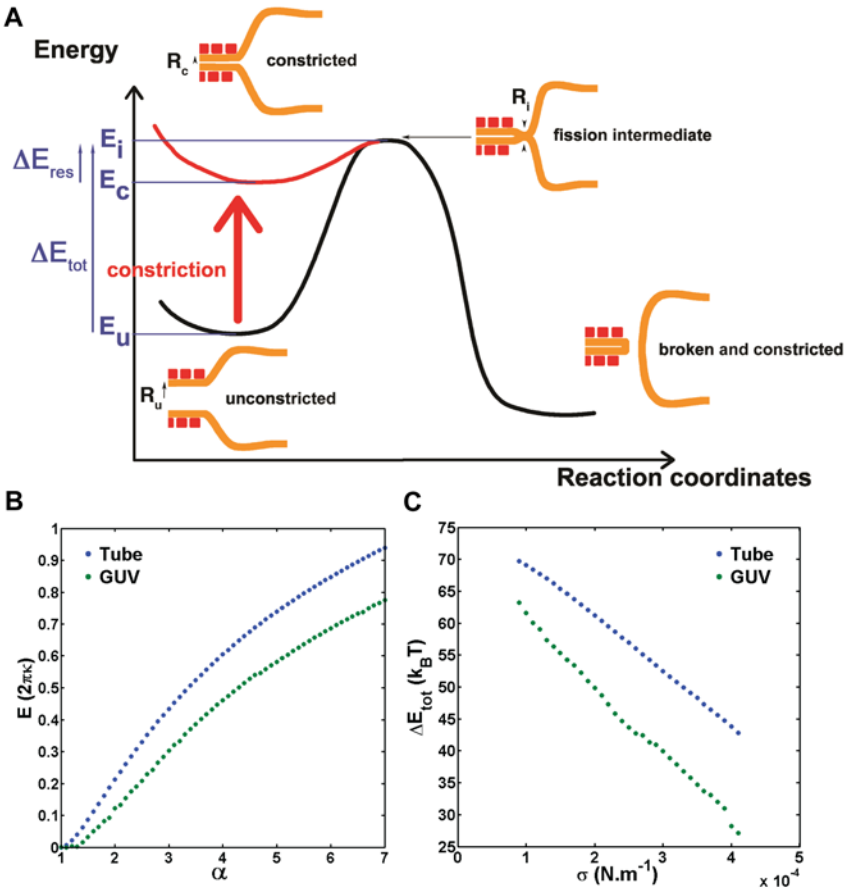

Fig. 2. Energy landscape of Dynamin-mediated fission. A- Mechanism and associated energy landscape for Dynamin-mediated fission reaction. **B-** Energy of the neck joining the bare membrane tube with the Dynamin-coated tube (blue) and energy of the neck joining a GUV or bead to a Dynamin-coated tube (green) as a function of $\alpha=R_m/R_c$ with R_m the radius of the Dynamin free tube and R_c the radius of the constricted Dynamin-coated tube. **C-** Energy barrier for fission within the lipid tube (blue) or in the GUV-Dynamin or bead-Dynamin edge (green) as a function of tension for $\kappa = 16k_bT$ and R_i = 3nm, R_d = 10nm.

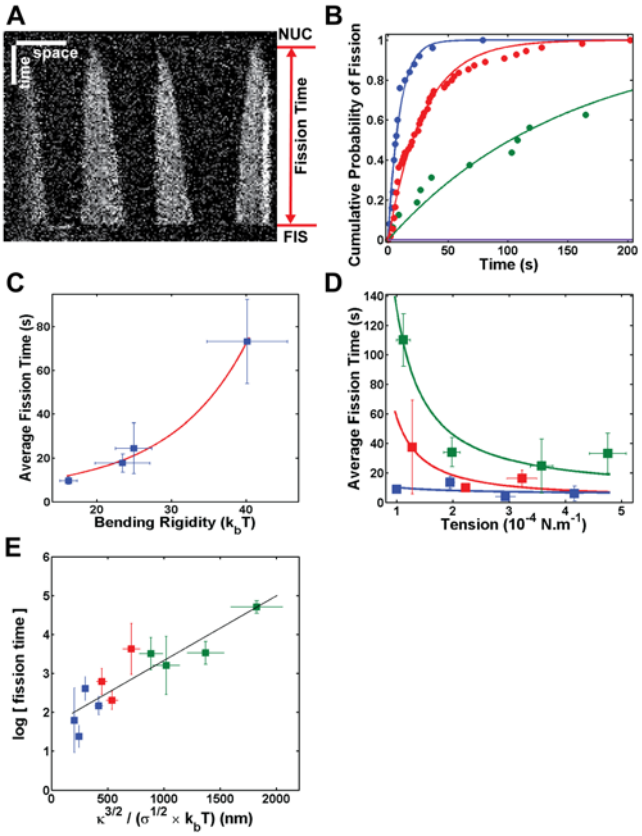

Fig. 3. Kinetics of Dynamin fission. A- Kymograph. Fluorescence of Alexa488-Dynamin along a membrane tube as a function of time. Dynamin polymerizes from four initial nucleation seeds until fission occurs. Fission time is measured as the time elapsed between start of polymerization (NUC) and fission (FIS). Here t_f=168s. **B-** Cumulative probability of fission at four different conditions: [GTP]=500µM (blue), [GTP]=5µM (red), [GTP]=375µM + [GTPγS]=125µM (green), [GTP]=250µM + [GTPγS]=250µM (purple). Circles: experimental points. Line: exponential fit 1-exp(-t/τ). The fitted parameters τ for different GTP concentrations are listed in Table 1. **C-** Bending rigidity dependence of fission time. Blue squares and bars: experimental points, average+SEM. Red line: $y=a*\exp(b*x^{3/2})$. Different lipid compositions are used to obtain different bending rigidities, see Table S1. **D-** Tension dependence of fission time. Blue κ=16.2±1.2kT (EggPC+PI(4,5)P_2). Red: 25.0±2.4kT (EggPC+Cholesterol+PI(4,5)P_2). Green: κ=44.8±5.1kT (Sphingomyelin+PI(4,5)P2). Squares and bars: experimental points, average+SEM. Lines: $y=a*\exp(b/x^{0.5})$. **E-** Relationship between the log of fission time and $\kappa^{3/2}/\sigma^{1/2}$. As predicted by our model, we observe a linear dependence (black line), linear fit: Y=a*X+b, a=1.17±0.42 10^6, b=0.59±0.27, R^2=0.82. Scale bars: (B) Horizontal: 5µm. Vertical: 30s.

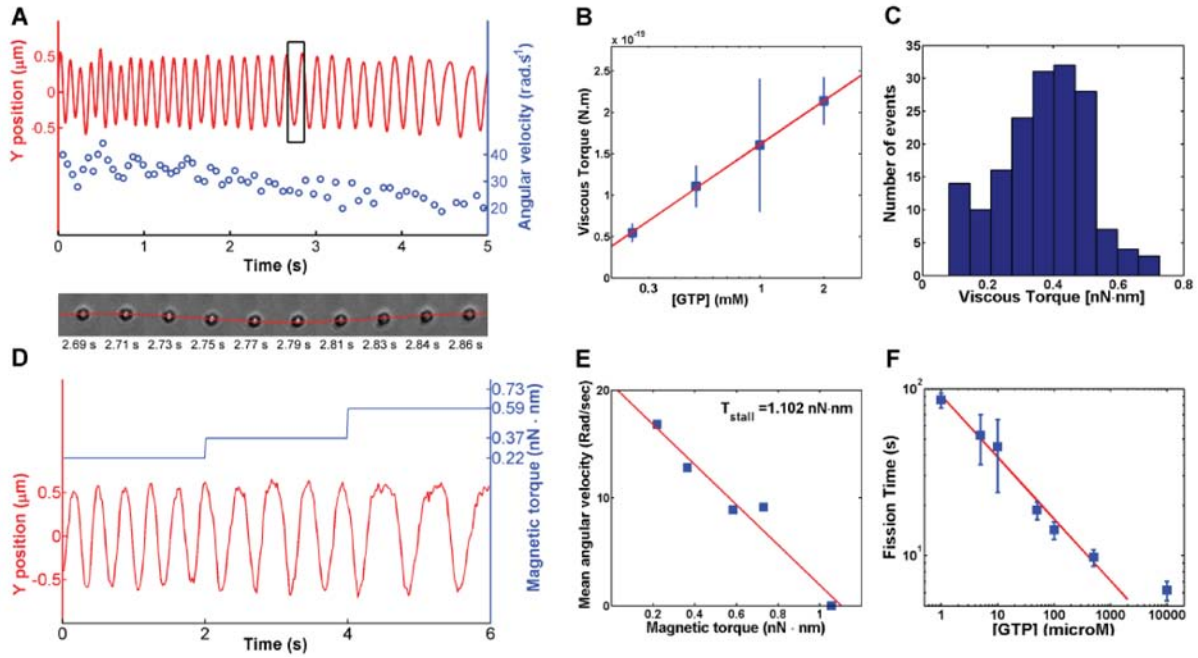

Figure 4 : Torque measurements : A-Top: Y-position trace (red) and corresponding angular velocity values (blue) of a bead rotating around a membrane tube induced through Dynamin twisting upon GTP hydrolysis. Bottom: sequence of ten frames of the bead performing exactly one rotation corresponding to the black rectangle. **B-** Linear dependence of the viscous torque with the log of the GTP concentration. Red line: linear fit, y=a*x+b, a=1.43±1.00 10^{-19}, b=9.80±3.70 10^{-20}, R^2=0.95. **C-** Histogram of viscous torques measured from the fastest bead as shown in movie S4. **D-** Position relative to the axis of the tube of a magnetic, 695nm radius Streptavidin bead rotating after addition of 1mM GTP, and under the magnetic torque (blue, see text for explanations) generated by a magnetic field. The bead slows down as magnetic torque increases, see also Figure S2. **E-** velocity of a rotating bead as the function of the magnetic torque. Bead stops at 1.1 nN.nm. **F-** [GTP]-dependence of fission time. Blue squares and bars: experimental points, average + SEM. Red line: linear fit, y=a*x+b, a=-0.37±0.07, b=4.51±0.27, R^2=0.9805.

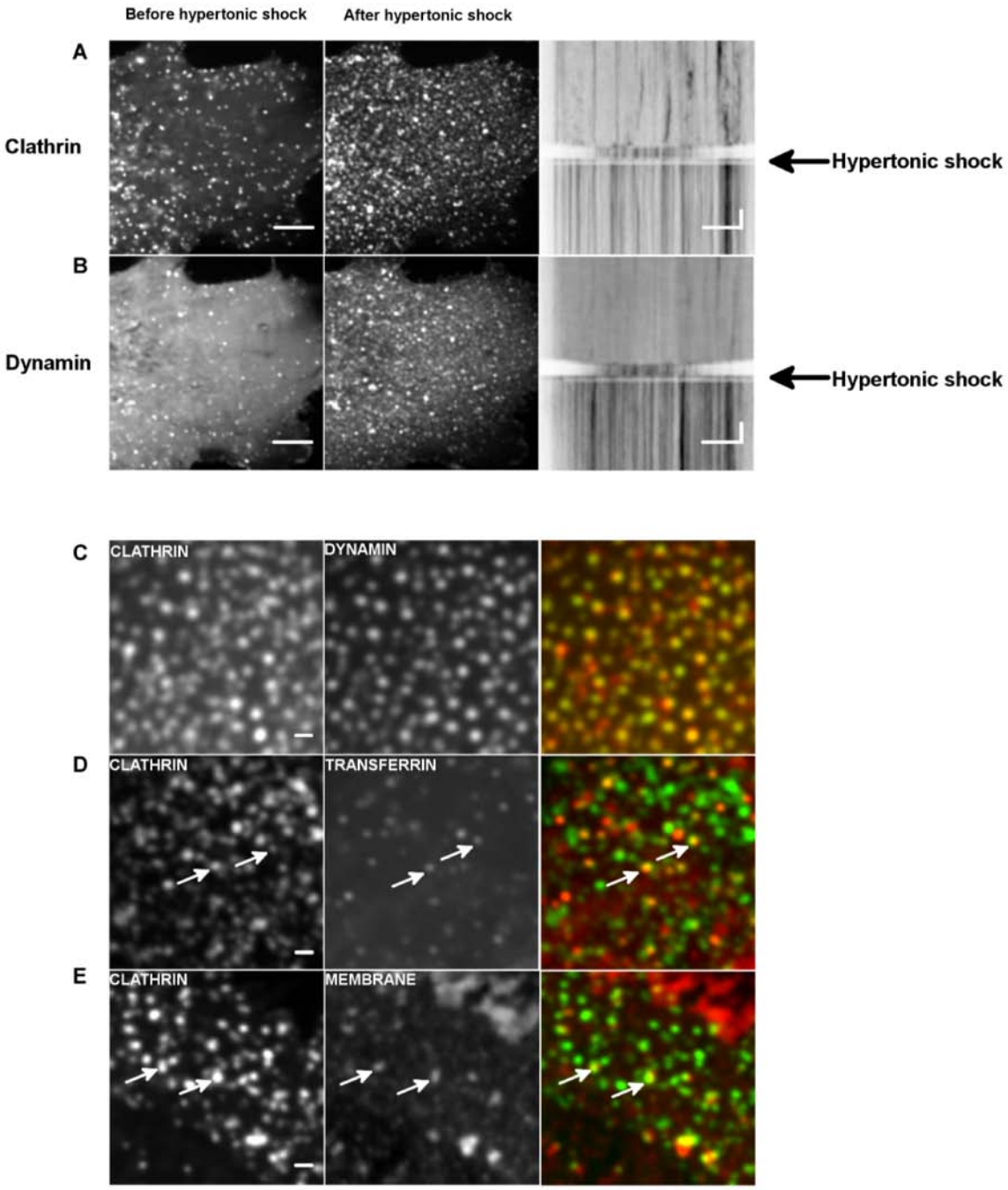

Fig. 5: Block of fission of Clathrin-coated pits by hypertonic shock. A- COS-7 cells transfected with mCTLA-mCherry before and after hypertonic shock; resulting kymograph that follows the time course before and after hypertonic shock. **B-** COS-7 cells transfected with DNM2-GFP before and after hypertonic shock; resulting kymograph that follows the time course before and after hypertonic shock (scale bar: 5 µm; timescale 5 sec.). **C-** Co-localization of mCTLA-mCherry (red) and DNM2-GFP (green) in COS-7 cells after hypertonic shock. **D-** Colocalization of mCTLA-GFP (green) and transferrin (red) in COS-7 cells after hypertonic shock. **E-** Colocalization of mCTLA-GFP (green) and plasma membrane (red) in COS-7 cells after hypertonic shock (scale bar: 1 µm).

TABLE

Table 1: Fission times follow an exponential distribution.

GTP concentration (μM)	Average Fission Time (s)	Fitted time parameter τ (s)
10000	6.2±0.8	6.22 (3.78, 8.65)
500	9.8±1.1	9.56 (8.50, 10.62)
100	14.2±1.7	19.62 (14.87, 24.37)
50	18.7±.3	27.73 (25.47, 30)
10	44.8±20.8	31.47 (22.66, 40.29)
5	52.6±17.4	48.41 (41.72, 55.1)
1	85.3±8.7	89.75 (60.45, 119.2)

Fission times were measured for several tubes at different concentrations of GTP. The average fission time (center column) is similar to the parameter τ given by an exponential fit of the fission time distribution (right column) (see Figure 3B).

SUPPLEMENTAL DATA

SUPPLEMENTAL FIGURES

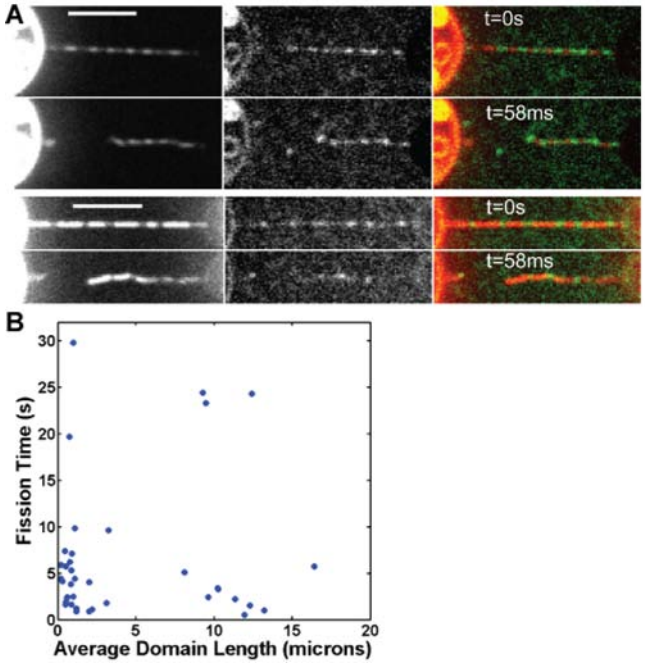

Figure S1: Fission occurs at the edge of Dynamin coat and fission time does not depend on the polymer length, Related to Figure 1.

(A) Other examples of fission at the edge of Dynamin-coated tubes equivalent to Figure 1C. Green is Dynamin (center column). Red is membrane (left column). Bars are 5 microns.

(B) Fission times depending on Dynamin domain length. For each experiment, Dynamin was injected alone on the tube to generate separated domains. Size of the domains was controlled by controlling polymerization time through injection time. Once polymerization done, GTP was injected, and in this case, fission time was defined as time between GTP injection and break. For each data point, domain size is the average size of domains for one tube.

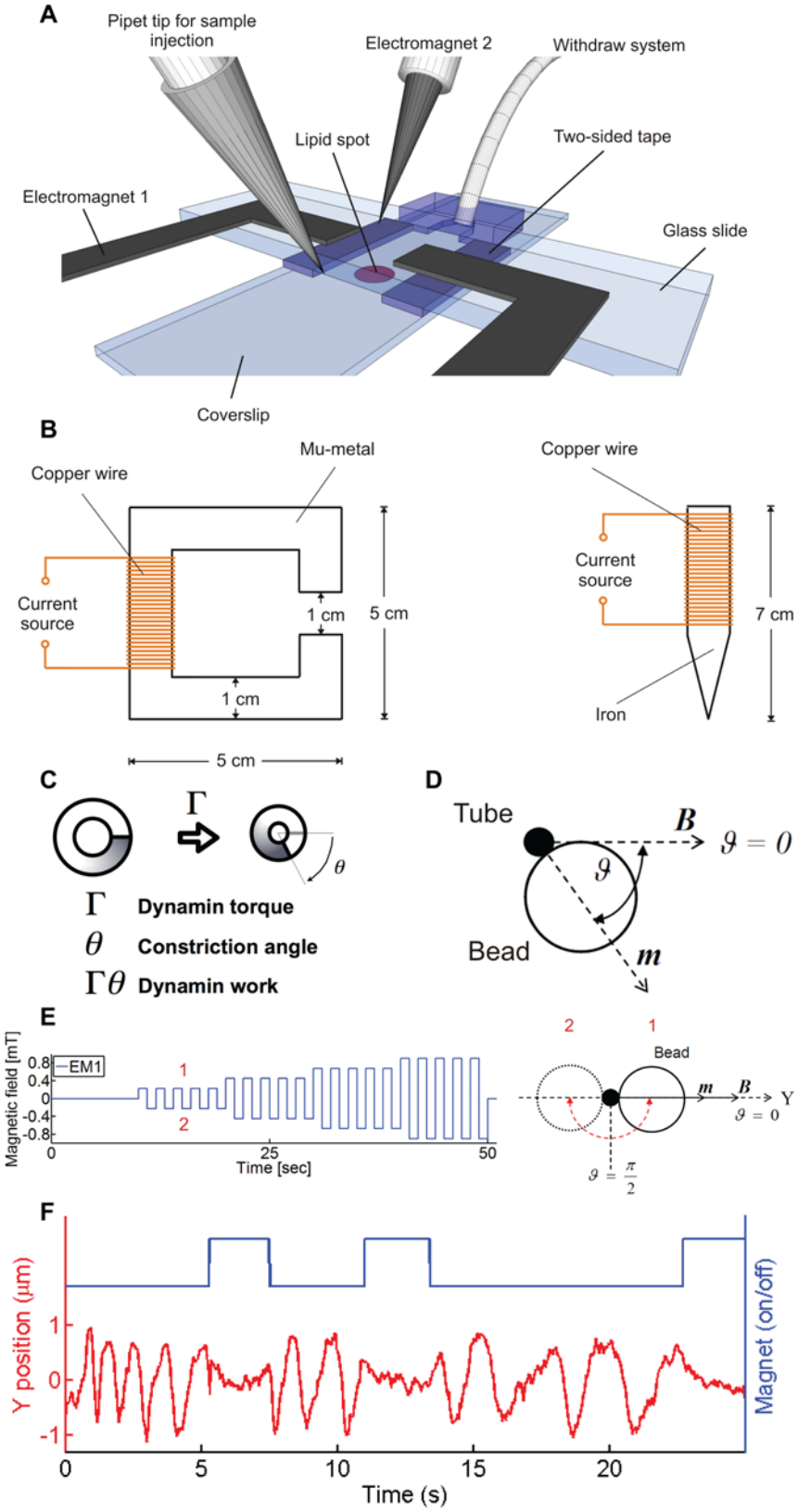

Figure S2: Dynamin torque counteracted by an external torque generated by a magnetic field, Related to Figure 4.

(A) Schematic view of the observation chamber made of a coverslip, a glass slide and two-sided tape as a spacer. Lipids are spotted on the coverslip. The fluids are placed

on one side with a pipette and withdrawn using a syringe pump from the other side of the chamber. The observation chamber is surrounded by two electromagnets EM 1 and EM 2 (dark gray) to impose a controlled magnetic field.

(B) Left: EM 1 is about 1 mm thick and consists of a coil of insulated copper wire wrapped around a mu-metal core. Right: EM 2 consists of a coil of insulated copper wire wrapped around an iron tube (1 cm diameter) with a tip to focus the magnetic field.

(C) Sketch representing Dynamin torque and constriction angle.

(D) Sketch of the magnetic bead bound to the tube.

(E) Right – a schematic view of the magnetic bead bound to the membrane tube (in black). When the magnets polarity is switched, the bead passes from one side of the tube to the other. The maximum angular speed of the bead is proportional to the maximum value of the applied torque. Left – typical magnetic field profile used for torque calibration.

(F) Y-position trace (red curve) of a magnetic bead attached to a Dynamin-coated tube (see Movie S5) upon GTP hydrolysis manipulated with magnetic tweezers illustrated by the blue rectangular function where the lower line marks the state of zero field (“off”) and the upper line the state of an applied constant field of 4 mT (“on”).

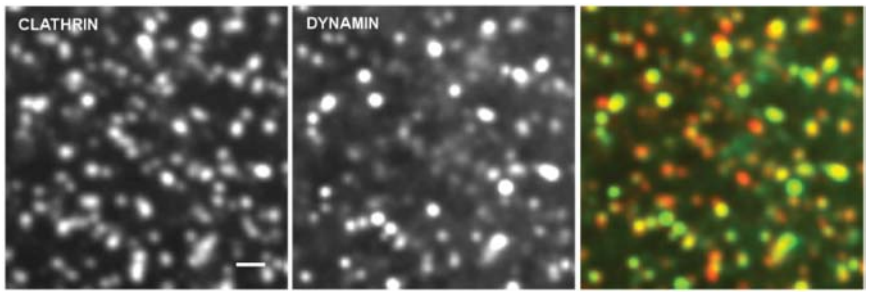

Figure S3: Dynamin and Clathrin colocalize in live cells, Related to Figure 5.

Colocalization of Clathrin –RFP and Dynamin-GFP in genome edited SKML-2 cells. Scale bar: 1 micron.

SUPPLEMENTAL TABLE

Table S1: Cholesterol and Sphingomyelin rigidify membranes, Related to Figure 3.

Lipid Composition	Bending Rigidity (k_BT)
80% EggPC + 20% PI(4,5)P_2	16.2 ± 1.2
70% EggPC + 10%BSM + 20 %PI(4,5)P_2, 40% Cholesterol	23.5 ± 3.7
80% EggPC + 20% PI(4,5)P_2, 50% Cholesterol	25 ± 2.4
80% BSM + 20% PI(4,5)P_2, 50% Cholesterol	40.2 ± 5.4

Average bending rigidity and SEM for different lipid compositions. The bending rigidity of a GUV was calculated from the relationship between force and tension. The proportions of PIP_2 is the same for all compositions. These four lipid compositions were used to test the dependence of fission time on bending rigidity (see Figure3C).

LEGENDS OF SUPPLEMENTAL MOVIES

Movie S1: Real-time observation of Dynamin-mediated membrane fission, Related to Figure 1.

Observation of Dynamin polymerization and fission by dual-color confocal videomicroscopy. Same field as Figure 1B. Accelerated 24 times, real frame rate: 1fps. Green channel corresponds to Alexa488-Dynamin signal, red channel to BodipyTMR-PIP_2.

Movie S2: Fission at the edge between Dynamin free and Dynamin-coated membranes, Related to Figure 1.

Observation of fission at the edge of Dynamin coat by dual-color spinning disk confocal videomicroscopy. Same field as Figure 1C. 17 fps, real acquisition time . Green channel corresponds to Alexa488-Dynamin signal, red channel to BodipyTMR-PIP_2.

Movie S3: Fission at the edge between the GUV and the Dynamin-coated tube, Related to Figure 1.

Observation of fission at the edge between the GUV and Dynamin-coated tube by dual-color confocal videomicroscopy. Same field as Figure 1E. Accelerated 24 times, real frame rate: 1fps. Green channel corresponds to Alexa488-Dynamin signal, red channel to BodipyTMR-PIP_2.

Movie S4: Rotations of a microbead attached to a Dynamin-coated tube after injection of GTP, Related to Figure 4.

Observation of a rotating microbead attached to a Dynamin-coated tube by DIC videomicroscopy. Non-labelled Dynamin, biotinylated Dynamin and streptavidin beads were injected on membrane sheets. The beads measure 1.31 µm diameter. After injection of 250 µM GTP, the bead starts rotating around the nanotube due to Dynamin conformational changes. Measuring the rotation speed of these beads allows to calculate the viscous torque encountered by the beads as it is represented in Fig4B.

Movie S5: Dynamin torque counteracted by magnetic torque, Related to Figure 4.

Observation of rotating magnetic microbeads attached to Dynamin-coated tubes by videomicroscopy like in Movie S4. Beads rotations were blocked by switching on a magnetic field (red arrowhead). Rotations resume when magnetic field is switched off. This experiment and the calibration of the magnetic field allow to estimate the stall torque of Dynamin as it is shown in Fig4E.

Movie S6: Hypertonic shock slows down the dynamics of Clathrin and Dynamin structures in live cells, Related to Figure 5.

Observation of COS-7 cells cotransfected with mCLAT-mCherry (red) and DNM2-GFP (green) by dual-color spinning disk confocal videomicroscopy. A hyperosmotic shock is made at frame 105. Same Field as in Fig5A and Fig5B. Accelereted 10X. Real frame rate: 1.8 fps.

EXTENDED EXPERIMENTAL PROCEDURES

Materials

Egg L-α-phosphatidylcholine (EPC), brain sphingomyelin (BSM), L-α-phosphatidylinositol-4,5-bisphosphate (PIP_2), di-stearoyl phosphatidyl ethanolamine-PEG(2000)-Biotin (DSPE-PEG2000-Biotin) and cholesterol were purchased from Avanti Polar Lipids, Alabaster, Alabama, USA. BodipyTMR-PIP_2 ($RedPIP_2$) was purchased from Echelon Bioscience, Salt Lake City, Utah, USA, and Guanosine Triphosphate (GTP) from Roche Applied Science, Indianapolis, Indiana, USA. Four lipid preparations were used (molar percentage): 80% EPC + 19%PIP_2 + 1%$RedPIP_2$; 70% EPC + 10% BSM + 19%PIP_2 + 1%$RedPIP_2$ supplemented with 40% cholesterol; 80% EPC + 19%PIP_2 + 1%$RedPIP_2$ supplemented with 50% cholesterol; 80% BSM + 19%PIP_2 + 1%$RedPIP_2$ supplemented with 50% cholesterol. These four mixtures also contained 0.03% DSPE-PEG2000-Biotin.

Protein purification

Recombinant human Dynamin 1 was purified from Sf9 cells infected with recombinant baculovirus using the BD baculogold expressing system (BD Biosciences, Franklin Lakes, NJ USA). Dynamin was purified from cell lysate with the GST-tagged SH3 domain of rat Amphiphysin 1 as an affinity ligand as previously described (Stowell et al., 1999). Briefly, cells from twenty 150cm^2 flasks were resuspended in 20 mL of Buffer A (20 mM Hepes pH 7.4, 100 mM NaCl, 1mM EGTA, 1 mM DTT, 1% Triton-X100) supplemented with the protease inhibitor cocktail (cOmplete ULTRA Tablets, Roche Applied Science, Indianapolis, Indiana, USA) and homogenized with a 60 ml dounce. The lysate was centrifuged at 40krpm on a Ti70 rotor (Beckman-Coulter inc., Brea, CA USA), and the supernatant was incubated for 2 hours with glutathione beads to which 3-5 mg of purified GST-SH3 domain of rat Amphiphysin 1 were attached. Next, the beads were batch-washed with 150 ml of Buffer A without Triton-X100. Elution was done with high salt (20 mM Hepes, pH 7.4, 1.2 M NaCl, 1 mM $MgCl_2$). Unlabeled Dynamin was dialyzed against storage buffer (20mM Hepes, pH 7.4, 100mM NaCl, 1 mM $MgCl_2$), concentrated using Amicon (50kDa CO), aliquoted, flash-frozen in liquid N_2 and stored at -80ºC.

To fluorescently label Dynamin, we dialyzed Dynamin against PBS 50% glycerol. The labeling reaction was conducted using standard procedures (Alexa-488 protein labeling kit from Invitrogen, cat# A-10235). In some case, Dynamin 1 was labeled with Alexa Fluor 488 C5 maleimide (Molecular Probes, Life Technologies Ltd, Paisley, UK). To attach Streptavidin-coated microbeads to Dynamin polymers, Dynamin was conjugated to DSB-X Biotin C2-iodoacetamide (Molecular Probes, Life Technologies Ltd, Paisley, UK). Labeled Dynamins were dialysed against storage buffer, aliquoted and kept at -80°C.

Nanotube pulling from GUV

Lipid mix (0.5mg/ml) was deposited on indium-tin oxide coated glass slides and dried 1h at 55°C to remove all solvents. GUVs were electroformed (1V, 10Hz) (Angelova et al., 1992; Stowell et al., 1999) for 1h at 55°C in a 200mM sucrose solution then transferred in an observation chamber pretreated with Casein solution (2mg/ml). GUVs were aspirated in a micropipette controlled with a motorized micromanipulator (MP-225, Sutter Instrument, Novato, California, USA) and a custom-made hydraulic system to control aspiration pressure ΔP and to set the tension: $\sigma = \frac{1}{2}\frac{R_{pipette}\Delta P}{1-\frac{R_{pipette}}{R_{GUV}}}$ where $R_{pipette}$ and R_{GUV} are the radii of the pipette and the GUV respectively (Evans and Rawicz, 1990). A membrane nanotube was formed by pulling away a micropipette aspirated GUV whose membrane was attached to a Streptavidin-coated bead (3.05µm diameter, Spherotec, Lake Forest, Illinois, USA) hold in a fixed optical trap. The custom-made optical trap was made by focusing an ytterbium fiber laser (IPG laser, Burbach, Germany) through a 100X 1.3 NA oil immersion objective (Nikon, Tokyo, Japan). The force F exerted on the bead was calculated from the Hooke's law: F= k*Δx where k is the stiffness of the trap (k=360pN.µm^{-1}.W^{-1}) calibrated by viscous drag method (Neuman and Block, 2004) and Δx the displacement of the bead from its equilibrium position in the optical trap. Video-rate movies and displacement measurements were done via a C-MOS Camera (Pixelink, Ottawa, Canada) with a user-made video recorder and bead tracking software under Matlab.

Dynamin and GTP were injected closed to the nanotube with a second micropipette of typical radius 10µm controlled with a hydraulic micromanipulator (Narishige Inc., Tokyo, Japan). Nanotubes were observed simultaneously by bright field imaging and by dual-color confocal microscopy (λ1=488nm and λ2=543nm) on a Nikon eclipse Ti inverted microscope (Nikon, Tokyo, Japan). For fast 2-colors confocal experiments, a spinning disk (Intelligent Imaging Innovations, Denver, Colorado, U.S.A.) and a two-channel simultaneous-imaging system (Dual-View, Photometrics, Tucson, Arizona, USA) were used instead of standard confocal microscopy (Eclipse C1 Confocal, Nikon, Tokyo, Japan).

Membrane sheets and Dynamin tubules formation

To form membrane sheets, 22x40 mm glass coverslips were first cleaned by sonication (5 min) in 1% Decon 90, Modec Inc., USA, in distilled water. After thorough washing and sonication (5 min) in distilled water to remove any trace of detergent, coverslips were finally washed with 100% ethanol prior to storage in ethanol. Coverslip were dried under a N_2 flux, and 1µl droplets of lipid solution (10 mg/ml in pure chloroform) were deposited and allowed to dry on the coverslip. Typically, two drops were deposited at different sites on a same coverslips. The use of pure chloroform was essential to allow lipid droplet drying in a way that was optimal for the subsequent formation of

membrane sheets upon hydration. Coverslips were then dried again under vacuum (0.2 milli-torr) for at least one hour, and kept up to several days under vacuum.

Before use, coverslips were placed for 20-30 min in a wet incubator (37°C, 100% humidity) to allow partial hydration of the lipids. Next, a small chamber (approximately 15 µl volume) was built by placing the coverslip onto a glass slide, with the lipids facing the glass slide, using a double-sided Scotch (3M) tape as a spacer. The lipids were fully rehydrated by applying to the side of the chamber 15-20 µl of GTPase buffer (20 mM HEPES pH 7.4, 100 mM NaCl, 1 mM $MgCl_2$) containing 0.1 mg/ml casein (C7078, Sigma, USA)(casein buffer) which were taken up into the chamber by capillarity. Lipid deposits then transformed into membrane sheets. Dynamin solution, typically 0.5-1 mg/ml was then added to the side of the chamber, and transferred into the chamber by capillarity. Membrane sheets were then deformed into Dynamin-coated tubules visible by DIC (Morlot et al., 2010; Roux et al., 2006).

Torque measurement by viscous drag

Streptavidin beads (1.35 µm diameter Streptavidin-coated, polystyrene beads, Spherotec, Lake Forest, Illinois, USA) were grafted onto biotinylated Dynamin tubules formed from membrane sheets (Morlot et al., 2010; Roux et al., 2006) by adding them to the chamber after tubule growth. The beads rotate following GTP addition and resulting constriction of the Dynamin coat (Morlot et al., 2010; Roux et al., 2006), experiencing a viscous torque $\Gamma_v = 14\pi\eta(R + r)^3\ \omega = \xi\omega$ (Happel J. and Brenner H. 1983), where η is the viscosity of the surrounding fluid, R the radius of the bead, r the radius of the tubule and ω is the angular spinning velocity. Differential Interference Contrast (DIC) and computer-based live recording of the rotating beads with a GUPPY camera (Allied Vision Technologies, Stadtroda, Germany) allowed direct measure of the angular spinning velocity and estimation of the viscous torque from the formula above.

Stall torque measurement by magnetic field

To measure the stall torque Γ_S that arrests the constriction of the membrane tube, we use a magnetic bead, to which an external torque via a variable magnetic field. The observation chamber (Figure S2A) is placed on the stage of an Axiovert 100 microscope (Zeiss, Oberkochen, Germany) equipped with a differential interference contrast (DIC), a fluorescence lamp and a UI-2220SE charge-coupled-device (CCD camera - IDS, Obersulm, Germany). The magnetic field to manipulate the magnetic beads is generated by two homemade electromagnets (see FigureS2B). Both the electromagnets are controlled using a NI USB-6211 multifunction data acquisition card (National Instruments, Austin, Texas, USA) and a homemade power supply. Magnets are calibrated using a DC magnetometer (AlphaLab, West Salt Lake City, Utah, USA). The bead motion is recorded and tracked using user-developed procedure under MATLAB.

To calibrate the torque induced by the magnetic field, the bead is attached to a Dynamin-lipid nanotube and oriented with a magnetic field parallel to the coverslip (position ‘1’ in

the schema shown in FigureS2C - Top). When the magnets polarity is switched, the bead rotates around the nanotube to follow the magnetic field and goes from position '1' to position '2'. According to Langevin's equation, the angular speed $\omega(\theta)$ of the bead is proportional to the magnetic torque $\Gamma(\theta)$

$$\varepsilon\omega(\theta) = \Gamma(\theta) + \mu(t) = \Gamma_{\max} sin(\theta) + \mu(t),$$

Where ε is the viscous drag of the bead, $\mu(t)$ is a thermal noise and $\Gamma_{\max}$ is the torque exerted when the magnetic moment of the bead is perpendicular to the field ($\theta = \pi/2$). As the thermal noise is negligible compared to the magnetic torque, the maximal angular speed $\omega(\theta = \pi/2) = \varepsilon\Gamma_{\max}$, where $\varepsilon = 14\ \pi\ \eta(R+r)^3$ (see above, [Happel 1983]). In our measurements η is the viscosity of the water (1 mPa·s), R is the radius of the bead (655nm) and r is the radius of the Dynamin-coated tube (25nm). For each bead $\Gamma_{\max}$ is evaluated for different magnetic fields (FigureS2C – Bottom).

Alternatively, the torque is calibrated with respect to the applied magnetic field through the thermal fluctuations of the beads. According to the equipartition theorem, the mean square amplitude of angular fluctuations is:

$$\langle \Delta\vartheta^2 \rangle = \frac{k_B T}{\kappa_\Gamma},$$

Where k_B is the Boltzmann constant, T is the temperature and $\kappa_\Gamma = -\partial\Gamma/\partial\vartheta|_{\Gamma=0}$ is the curvature of the magnetic potential around its minimum. The magnetic dipole moment is evaluated for different magnetic field B to obtain the calibration curve $\Gamma(B,\theta)$.

Cell Transfection, treatment and imaging

COS-7 cells were transfected using FuGENE-6 (Roche Applied Science, Indianapolis, Indiana, USA) with Dynamin 2 fused to Green Fluorescent Protein (GFP) (kindly provided by P. De Camilli; HHMI, Yale University) or mouse Clathrin-Light-Chain fused to mCherry or GFP (kindly provided by C. Merrifield, Cambridge and by P. De Camilli, HHMI, Yale University). Cells were imaged 18 to 24 hours post transfection in Leibovitz medium (Gibco, Life Technologies Ltd, Paisley, UK). While imaging, the medium was changed with a hypertonic solution of 0.25M sucrose in Leibovitz medium. Cell membrane staining was achieved by incubating cells for 5' at 37°C with deep red Cell Mask (Molecular Probes, Life Technologies Ltd, Paisley, UK) before imaging. Genome edited SK-MEL-2 cells expressing Dynamin2-GFP and Clathrin Light Chain-RFP were provided by D.G. Drubin (University of California Berkeley, USA).

Transferrin labeling

cells were starved in serum deprived DMEM-F12 medium for 30' on ice, then incubated with 5 µg/ml Alexa-fluor 594 Transferrin (Invitrogen Inc., U.S.A.) in hypertonic medium (0.25M sucrose Leibovitz medium) for 3' at RT. Cells were washed with hypertonic buffer before imaging.

Image analysis

Images were analyzed and processed with ImageJ. Kymographs were made with Multiple Kymograph plugin (J. Rietdorf; A. Seitz). Fits were made with the curve fitting toolbox in Matlab.

Membrane shape computation

In this section we first derive the equilibrium equation for the shape of the membrane from Canham-Helfrich Hamiltonian and express the shape computation as a boundary value problem suitable for solution with Matlab's bvp4c.

Canham-Helfrich Hamiltonian gives the energy of the membrane as a function of its shape:

$$E = \sigma \int dA + \frac{\kappa}{2} \int J^2 \, dA$$

The first term is related to the energy cost of stretching the membrane and σ is the membrane tension which can be controlled in the experiment. The second term represents the energy cost of bending which is given by the integral of membrane curvature J over the surface. The bending modulus κ depends on the composition of the membrane.

Considering the axial symmetry of the experiment we will restrict ourselves to axisymmetric shapes. For an axisymmetric surface with an axial coordinate z, and angle φ around the z-axis, and a radius $r(z)$, curvature can be expressed as:

$$J = \frac{r(z)r''(z) - r'(z)^2 - 1}{r(z)(1 + r'(z)^2)^{3/2}}$$

Writing the area element in the same coordinates $dA = r(z)\sqrt{r'(z)^2 + 1}\, dz d\varphi$, the integral in the angle φ can be directly performed and the energy can be cast in the following form:

$$E = \int (\sigma + \frac{\kappa}{2} J^2) r(z) \sqrt{r'(z)^2 + 1}\, dz d\varphi = 2\pi \int (\sigma + \frac{\kappa}{2} J^2) r(z) \sqrt{r'(z)^2 + 1}\, dz$$

It will be convenient for numerical solution of the equations to adimensionalize the Hamiltonian using the bare membrane radius $R_m = \sqrt{\frac{\kappa}{2\sigma}}$ to rescale all lengths, and $\pi\kappa$ to rescale the energy:

$$e = \int (1 + j^2) \rho(\theta) \sqrt{\dot{\rho}(\theta)^2 + 1}\, d\theta = \int \ell\big(\rho(\theta), \dot{\rho}(\theta), \ddot{\rho}(\theta)\big) d\theta$$

where

$$j = \frac{\rho(\theta)\ddot{\rho}(\theta) - \dot{\rho}(\theta) - 1}{\rho(\theta)(1+\dot{\rho}(\theta)^2)^{3/2}}, \rho(\theta) = \frac{r(z)}{R_m}, \theta = \frac{z}{R_m}, e = \frac{E}{\pi\kappa}, \ell = (1+j^2)\rho(\theta)\sqrt{\dot{\rho}(\theta)^2+1}$$

are all adimensional quantities and the dot represents differentiation with respect to θ. At equilibrium, membrane shape minimizes the energy. Thus, the equilibrium shape is given by the solution of Euler-Lagrange equation

$$\frac{d\ell}{d\theta} = \frac{d}{d\theta}\frac{\partial \ell}{\partial \dot{\rho}} - \frac{d^2}{d\theta^2}\frac{\partial \ell}{\partial \ddot{\rho}}$$

which is the non-linear fourth order differential equation:

$$\begin{aligned}\Big(&-1-6\dot{\rho}^2-10\dot{\rho}^3-9\dot{\rho}^4-10\dot{\rho}^5-4\dot{\rho}^6+\rho\ddot{\rho}(3+30\dot{\rho}-9\dot{\rho}^2-40\dot{\rho}^3-12\dot{\rho}^4)\\&+\rho^2(1+\dot{\rho}^2)(1+\dot{\rho}^4+\dot{\rho}^6+3\ddot{\rho}^2+\dot{\rho}^2(3-12\ddot{\rho}^2)+4\dot{\rho}\dddot{\rho}+4\dot{\rho}^3\ddot{\rho})\\&+\dot{\rho}^3\big(5(-1+6\dot{\rho}^2)\ddot{\rho}^3-(1+\dot{\rho}^2)\ddot{\rho}(1+2\dot{\rho}^2+\dot{\rho}^4+20\dot{\rho}\ddot{\rho})+2(1+\dot{\rho}^2)^2\,\dddot{\rho}\big)\Big)\\&=0\end{aligned}$$

This equation was solved in the domain $\theta \in [0,10]$, with two different sets of boundary conditions. For the junction between the tube and the Dynamin-coated tube, it was required that

$$\rho(0) = 1\,, \dot{\rho}(0) = 0$$

$$\rho(10\,) = r_d\,, \dot{\rho}(10) = 0$$

with $r_d = \frac{R_d}{R_m}$ the adimensional Dynamin radius, which was varied to compute the energy at different levels of constriction.

For the neck joining the vesicle or bead to the Dynamin-coated tube, boundary conditions were

$$\rho(0) = 20\,, \qquad \rho(0)\ddot{\rho}(0) - \dot{\rho}(0) - 1 = 0$$

$$\rho(10\,) = r_d\,, \dot{\rho}(10) = 0$$

The first condition ensures membrane joins the flat wall that mimics the vesicle at $\theta = 0$ with vanishing curvature. See SOI for more details on the rationale for these boundary conditions.

Boundary conditions for the vesicle geometry do not directly produce a solution with Matlab's bvp4c boundary value problem solver. A technique known as *continuation* was used to find the desired solution. The solution for a less *stringent* boundary condition (i.e. giving a less bent membrane) with $\rho(0) = 7, \rho(10) = 1$ was first computed and used as initial guess for a subsequent iteration with a slightly greater value of $\rho(0)$. This process was then repeated until the desired $\rho(0) = 20$ condition was met. Finally, the same process was used to decrease $\rho(10)$ from 1 to the desired value r_d.

Once membrane shapes were computed, we calculated the corresponding energy by numerical integration of Canham-Helfrich Hamiltonian.

Theory for reduced fission energy barrier at the Dynamin-membrane edge

We model membrane fission as a one-step rate reaction thermally activated with a single energy barrier, biased by the GTP hydrolysis driven constriction force. The constriction radius R_d, that is, the radius of the Dynamin-coated membrane, constitutes the reaction coordinate. In this analogy, the radius R_d is a brownian degree of freedom that may overcome a fission energy barrier by thermal fluctuations. GTP hydrolysis by Dynamin generates a constriction force which in our model would operate as a force on the R_d degree of freedom, tilting the energy landscape and decreasing the total energy barrier ΔE_{tot} to a smaller value ΔE_{res}, biasing the transition towards the fission state (see Figure 2A in main text).
The energy barrier originates from differences in elastic and surface energy of the membrane neck that joins the edge of the Dynamin-coated part to the bare tube with radius R_d, set by tension and bending rigidity.

After constriction, the residual barrier can be overcome by thermal fluctuations of the constricted radius, at a rate

$$r = \tau^{-1} e^{-\Delta E_{res}/k_b T}$$

where τ is a molecular characteristic time of reaction, k_b is the Boltzmann constant, T the temperature. A constant rate of reaction yields an average fission time

$$< t_f > = \tau e^{\Delta E_{res}/k_b T}$$

A process with just one constant rate of reaction r gives an exponential distribution of reaction times

$$\rho(t_f) = r e^{-r t_f}$$

and consequently a cumulative probability of reaction

$$F(t_f) = \int_0^{t_f} \rho(x) dx = 1 - e^{-r\, t_f}$$

Our experiments both present an exponential distribution of fission times (not shown) and the corresponding cumulative probability is well fit by $1 - e^{-r\, t_f}$ as shown in Figure3B in the main text.

To compute the bending and surface energy of the membrane we numerically solved the non-linear shape equation that arises from Canham-Helfrich Hamiltonian minimization (see above) for the neck joining a bare membrane tube with a Dynamin-coated one (see figure 1G in the main text). This implies boundary conditions where the radius matches the bare tube radius R_m on one side and R_d, the radius of the Dynamin-coated part, on the other. In both ends, the derivative of the radius with respect to the axial coordinate

must vanish to smoothly join either the bare or Dynamin-coated tube. The equation was numerically solved using Matlab bvp4c boundary problem solver for different values of R_d and constant R_m. From the shape, we compute the bending and surface energy energy $E(\alpha)$ as a function of dimensionless parameter $\alpha = R_m/ R_d$, as depicted in Figure 2B.

To estimate the energy barrier we assume Dynamin polymerizes and constricts the Dynamin-coated membrane very fast compared to fission times (Morlot *et al.* 2010) to a radius R_c of the order of 4-5nm in the presence of GTP (the actual R_c should depend on GTP concentration in our model as fission time decreases with increasing GTP concentration; we nevertheless disregard this dependence for the sake of simplicity by taking a fixed GTP concentration and defer the discussion on the effect of GTP concentration for a later section). The coated membrane tube is still connected to the bare membrane tube by a neck-like shape. In order for the membrane to break, it makes a transition from this configuration with $R_d=R_c$, to another with a constricted radius $R_d=R_i$ corresponding to a hemifission intermediate state with a radius R_i independent of tension and bending rigidity. A hemifission intermediate is a state where the internal monolayer of the membrane is fused while the outer monolayer keeps its integrity. Evidence for the existence of a hemifission state has already been reported in (Bashkirov *et al*. 2008). Kozlovsky and Kozlov have proven for a different but related geometry where a constricted neck also exists that once this hemifission intermediate is attained the transition to complete fission proceeds spontaneously, due to a negative free energy difference between hemifission and complete fission state (Kozlovsky and Kozlov 2003). We assume there is no barrier once the hemifission is attained and therefore the fission reaction quickly proceeds to fission.
Hence, the energy barrier is the difference between the energy of these two configurations

$$\Delta E_{res}^{tube} = E\left(\frac{R_m}{R_i}\right) - E\left(\frac{R_m}{R_c}\right) \equiv E_i^{tube} - E_c^{tube}$$

Taking R_i of the order of 3-5nm and R_c in the range 4-5nm and for the R_m used in our experiment, the ratio α ranges from 1 to 10, which allows us to approximate $E(\alpha)$ by a straight line with slope $\alpha \simeq 1/4$ and get an analytical prediction of the barrier dependence with tension and bending modulus

$$E \simeq a2\pi\kappa(\alpha - 1) \Rightarrow \Delta E_{res}^{tube} \simeq 2\pi a(\frac{1}{R_i} - \frac{1}{R_c})\frac{\kappa^{3/2}}{\sqrt{2\sigma}}$$

where we already substituted the value of the bare membrane radius $Rm = \sqrt{\frac{\kappa}{2\sigma}}$. The average fission time thus depends on membrane parameters as

$$< t_f >= \tau e^{\frac{b\kappa^{3/2}}{k_b T\sqrt{\sigma}}}$$

giving for $log<t_f>$ a dependence

$$log < t_f > = \log\tau + \frac{b\kappa^{3/2}}{k_b T\sqrt{\sigma}}$$

which fits all the experimental data for different values of κ and σ as shown in Figure 3 in the main text.

Fission at GUV-Dynamin or bead-Dynamin edge

As explained in the main text, fission occurs preferentially at the boundary between the tube and the GUV or between the tube and the bead. To analyze these cases we solved the shape equation with a modified boundary condition at GUV/bead's end. Due to the difference in size between the tube and the bead or GUV we can approximate GUV/bead by an infinite flat membrane wall perpendicular to the tube. This can be mimicked in the numeric computations by requiring that membrane radius at the wall (GUV) is much bigger than R_d and that membrane joins smoothly to a flat membrane, i.e., with vanishing curvature. At Dynamin's edge, membrane has a radius R_d and enters the Dynamin domain with vanishing slope to smoothly match the Dynamin-coated tube. The Dynamin coating is assumed to progress until a distance $10R_m$ from the flat wall. This coincides with the end of the bare tube that would form in the absence of Dynamin (Derényi *et al*. 2002) and we expect the Dynamin polymer to grow approximately until that position. Varying R_d again we can compute the energy as a function of α. The energy of the GUV-Dynamin edge has the same approximate shape as in the bare tube-Dynamin case (see Figure 2B) and therefore the above discussion remains valid, giving a similar dependence with κ and σ for fission time. Furthermore, the residual energy barrier for the vesicle or bead edge for $\kappa=16k_bT$, $R_i=3nm$ and $R_c=4.5nm$ ranges from 20 k_bT to 23 k_bT as a function of tension σ giving an expected fission time

$$< t_f > = \tau e^{\frac{\Delta E_{res}^{ves}}{k_b T}}$$

which agrees with experimentally observed times. Using hydrodynamic arguments we can estimate $\tau \simeq 10^{-9}$s giving in turn fission times in the range [1, 13]s depending on tension, in agreement with experimental fission times.

Higher probability of fission at GUV's end

Differences in energy barrier for fission at the GUV-Dynamin and at the tube-Dynamin neck translate in different rates of fission. Disregarding differences in the number of tube-Dynamin versus GUV-Dynamin edges in front of the exponential factors, the probabilities to find a break in the GUV or tube edge in an experiment would be proportional to the rates of fission. According to our model, rates are exponentially related and therefore:

$$\frac{P_{ves}}{P_{tube}} = \frac{e^{-\Delta E_{res}^{ves}/k_B T}}{e^{-\Delta E_{res}^{tube}/k_B T}} = e^{(\Delta E_{res}^{tube} - \Delta E_{res}^{tube})/k_B T}$$

with ΔE_{res}^{tube} and ΔE_{res}^{ves} the barriers for fission at the tube or vesicle respectively. Using normalization $P_{ves} + P_{tube} = 1$ we find

$$P_{ves} = \frac{1}{1 + e^{(\Delta E_{res}^{tube} - \Delta E_{res}^{tube})/k_B T}}$$

Taking R_i=3nm, R_c=4.5nm and κ=16k_bT, the numerical computation of the barriers from the surface and bending energy shows that the energy barrier at the vesicle edge is always smaller than the barrier corresponding to the tube, at least for the values of tension used in the experiment, as shown in Figure2C. For tensions used in experiments from $\sigma \simeq 1\times10^{-4}\ \mathrm{N.m^{-1}}$ to $\sigma \simeq 5\times10^{-4}\mathrm{N.m^{-1}}$, the difference in energy barriers $\Delta E_{res}^{tube} - \Delta E_{res}^{tube}$ is in the range [1, 3]×k_bT, which in turn gives probabilities of fission in the vesicle $P_{ves} = [0.75,\ 0.93]$ in accordance with 75% of the breaks occurring in the vesicle observed in experiment (see Figure1D).

Effect of GTP concentration

The presence of GTP in the system, which entails Dynamin contraction, is equivalent, at least for small deformations of the helix, to applying a homogeneous constriction force or pressure and a torque to the membrane in the Dynamin domain proportional to Δμ, the GTP hydrolysis chemical potential difference (Lenz *et al*. 2008). In our model, that would mean that a constant force is applied to the radius variable, which can be seen as a tilt in the energy landscape proportional to Δμ. Thus, the total energy barrier decreases in an amount proportional to Δμ with a constant *d* that is related to the position of the intermediate state in the reaction path:

$$\Delta E_{res} = \Delta E_{tot} - d\Delta\mu = \Delta E_{tot} - c\Gamma\theta$$

where we used the proportionality between Δμ and Dynamin induced torque upon hydrolysis Γ, which is derived assuming the energy for constriction is coming from GTP hydrolysis and thus work done by Dynamin should be $\Gamma\theta\xi\Delta\mu$ where Δμ is the variation of chemical potential in the hydrolysis and ξ can be thought of as an efficiency of Dynamin in the sense of how much energy is converted into work.
This gives for fission time

$$< t_f > = \tau e^{\frac{\Delta E_{tot}}{k_b T} - c\frac{\Gamma\theta}{k_b T}}$$

Finally, assuming an ideal dynamin solution, $\Delta\mu = \xi k_b T log[GTP]$ and therefore

$$< t_f > = \tau e^{\frac{\Delta E_{tot}}{k_b T} - c\xi log[GTP]}$$

Experiments indeed show the expected dependence: $log < t_f > = constant - c\xi \log [GTP]$ as shown in Figure 4F of the main text.

Torque and final helix radius

As the Dynamin helix hydrolyses GTP, it exerts a torque which tends to constrict the underlying membrane tubule. This torque is counteracted by the elasticity of the membrane, which favours a widening of the tubule. Here we derive a mathematical expression for the membrane's radius resulting from the balance of these two effects. We consider a cylindrical membrane constrained by a Dynamin helix and first consider the geometrical relationships between the helix' radius, pitch and length. We then use them to analyse the competition between Dynamin torque and membrane elasticity

We approximate the Dynamin helix by an inextensible ribbon wound around a cylinder of radius r and length L. No polymerization or depolymerization is assumed to take place over the time scales considered and the ribbon has an approximately constant width. Therefore, the total surface area of the ribbon is conserved:

$$2\pi rL = 2\pi R_u L_u$$

where the index u refers to the initial state of the helix, prior to the introduction of GTP, when the Dynamin helix is unconstricted. We define Θ as the total winding angle of the ribbon, expressed in radian. For instance, a helix that winds three times around the cylinder has $\Theta = 3 \times (2\pi)$. Denoting by h the helix' pitch, this angle is given by

$$\frac{\Theta}{2\pi} = \frac{L}{h}$$

expressing the fact that adding one turn to the helix increases its length by h. To the level of approximation used here, we can assume that the pitch of the helix is constant and equal to 10nm.

We denote by κ the bending modulus of the membrane and assume that the tubule is in contact with a membrane reservoir of tension σ. Due to the small radius of the tubule (much smaller than the bare membrane equilibrium radius $\sqrt{\kappa/2\sigma}$), the energetic contribution of surface tension is small compared to the bending energy, and is neglected in the following.

The bending energy of the membrane is given by the Canham-Helfrich energy presented in the main text. Its bending term is reproduced here for convenience:

$$E_{bending} = \frac{\kappa}{2}\int_A c^2 dA.$$

For a cylindrical geometry, the curvature of the tube is $c = \frac{1}{r}$ and the integral runs over a surface $A = 2\pi rL$. The bending energy thus reads $\pi\kappa L/r$, which is minimal for a flat membrane ($r \to +\infty$). In the absence of GTP hydrolysis, the membrane is confined to a finite radius R_u by the rigidity of the Dynamin helix. We represent this passive effect by an elastic equilibrium torque Γ_u implying a contribution $-\Gamma_u\Theta$ to the energy of the system.

For the purpose of determining the membrane shape, the internal, active torque induced by the Dynamin polymer upon GTP hydrolysis is equivalent to an additional external torque Γ imposed on the passive helix. Therefore, Dynamin activity can be described as a further lowering of the energy of the system by an amount equal to the work $\Gamma\Theta$ of this torque. Summing all the contributions to the energy, we find

$$E = -(\Gamma_u + \Gamma)\Theta + \pi\kappa\frac{L}{r} = -(\Gamma_u + \Gamma)\frac{L_u R_u}{hr} + \pi\kappa\frac{L_u R_u}{r^2}$$

Minimizing E with respect to r, we find that

$$r = \frac{2\pi\kappa h}{\Gamma_u + \Gamma}$$

While the passive torque Γ_u has been left unspecified until this point, it must satisfy the condition that r goes to R_u as goes to zero. This implies that $\Gamma_u = 2\pi\kappa h/R_u$, and therefore

$$r = \frac{R_u}{1 + \frac{\Gamma R_u}{2\pi\kappa h}}$$

Using $\kappa = 20\ \mathrm{kbT} = 8 \times 10 - 20$ J, we can thus compute the torque required to obtain a constricted radius r = R_c = 5 nm to be $\Gamma \simeq 500$ pN. nm. This value is compatible with the experimental measurements presented in the main text (see Figure 4), thus validating our assessment of the role of the competition between Dynamin torque and membrane bending rigidity.

SUPPLEMENTAL REFERENCES

Derényi, I., Jülicher, F. and Prost, J. (2002) Formation and Interaction of Membrane Tubes. Phys. Rev. Lett. 88, 238101

Neuman, K.C. and Block, S.M. (2004) Rev. Sci. Instrum. 75:2787-2809

Stowell, M.H., Marks, B., Wigge, P., and McMahon, H.T. (1999). Nucleotide-dependent conformational changes in dynamin: evidence for a mechanochemical molecular spring. Nat. Cell. Biol. *1*, 27-32.

6.3 Complementary Experiments

6.3.1 Constriction Radius

The radius of a constricted Dynamin-coated nanotube R_c plays an important role in the model we propose. CryoEM data have shown that upon GMPPCP treatment, the Dynamin helix constricts the lipid tube until it reaches a lumen of 7nm diameter. However GTP hydrolysis could lead to a more constricted state. We were thus prompted to measure this constricted radius with the nanotube extrusion technique.

Calibration Of Radius Fluorescence

The radius formula $R_0 = \sqrt{\frac{\kappa}{2\sigma}}$ is valid only for bare membrane tubes at equilibrium and cannot be used for measuring the radius of a Dynamin-coated tube. Thus we used the fluorescence signal of the nanotube to measure its radius. Two fluorescent lipid dyes were incorporated in GUVs: $BodipyTMR-PIP_2$ that was used in all our experiments and $BodipyFL-HPC$. We use a second lipid probe because Dynamin interacts with PIP_2. Dynamin polymerization could induce a local enrichment in PIP_2 and would bias the measurement. $BodipyFL-HPC$ is a fluorescent lipid which does not interact with Dynamin and incorporates homogeneously in GUVs. We established a calibration curve to correlate the radius of a bare membrane nanotube to its average fluorescence intensity. For different aspiration pressures, we recorded the corresponding force and took a picture of the fluorescent nanotube (see Fig.6.1.A). For each pressure step, the radius was calculated from the force and the tension values. The average fluorescence intensity along the tube was measured for both fluorescent lipids. We obtained a linear relationship between the radius and its fluorescence intensity for $BodipyFL-HPC$ and $BodipyTMR-PIP_2$ (see Fid6.1.B). This linear relationship and the fact that we observed similar slopes for the two dyes show that there is no lipid sorting: PIP_2 is not sensitive to curvature in the lipid composition we used ($PC+PIP_2$). This calibration curve was established for each nanotube individually before injection of Dynamin.

Radius Measurement Without GTP

We first measured the radius of Dynamin-coated tubes in absence of nucleotide. Non-labelled Dynamin was injected close to the tube. We could not use fluorescent Dynamin as the lipid tube was already labelled in green and red. Full coverage of the tube by Dynamin was thus noticed by a typical force drop [115]: when the tube was fully covered, the Dynamin coat "pushed" on the bead. Polymerization was also confirmed at the end of the measurements by switching off the optical tweezers, polymerized tubes did not retract whereas bare tubes retracted rapidly. From the measurement of the nanotube fluorescence intensity and the radius-fluorescence intensity calibration curve, we inferred the radius of the Dynamin-coated nanotube in absence of nucleotide: 10.3 ± 2 *nm* from the green signal and 10.2 ± 2.8 *nm* from the red signal. These results give two interesting pieces of information. First the radius values are in good agreement with structural data, which validates this technique of measurement. Second we

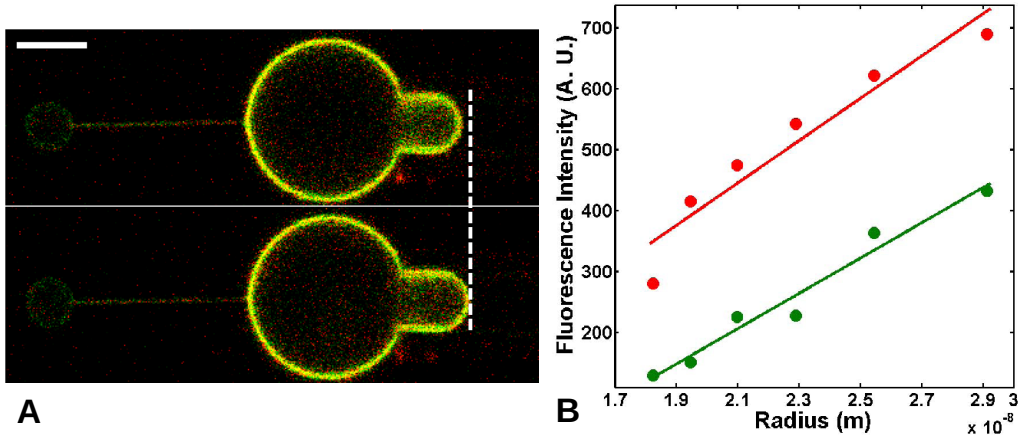

Figure 6.1: A. Confocal microscopy pictures of the same nanotube extruded from a GUV containing BodipyFL-HPC (green) and BodipyTMR-PIP2 (red) at two different aspiration pressures. From top to bottom, the aspiration pressure increases of 0.39 *Pa*, the force exerted on the bead increases from 21.8 *pN* to 27.4 *pN* thus the radius decreases from 23.2 *nm* to 19.5 *nm*. Scale bar: 5 μm B. Calibration curves to correlate the radius and its fluorescence intensity. Average fluorescence intensities of BodipyFL-HPC (green points) and BodipyTMR-PIP2 (red points) along the same nanotube at different aspiration pressures. Red line: linear fit $y = 3.5\ 10^{10}\ x - 2.910^2$, $R^2 = 0.92$. Green Line: linear fit $y = 2.9\ 10^{10}\ x - 4.010^2$, $R^2 = 0.92$

obtained the same value with $BodipyFL-HPC$ and $BodipyTMR-PIP_2$ which shows that there is no significant PIP_2 enrichmement upon Dynamin polymerization. This was not known before.

Radius Measurement With GTP

The same experiment was reproduced with injection of non-labelled Dynamin and GTP (150 μM). Fluorescence intensities were measured on the last frame before fission. We obtained an experimental estimation of the constricted radius R_c: 12.5 $\pm$ 1 *nm* for the green signal and 14.0 $\pm$1.6 *nm* for the red signal (see Fig.6.2). These values do not agree with structural data which shows a reduced radius upon GTP treatment. Our measurement could be biased by a partial polymerization of the tube. Indeed if we look at the histograms of constricted radii, we observe a peak below 10 nm. The tail beyond 10 nm could be in part due to partially-coated tubes where bulges of free membrane increase the radius value. On this histogram, we can also notice that the radii measured via $BodipyTMR-PIP_2$ have a different distribution than those measured with $BodipyFL-HPC$. There could be some sorting of PIP_2 when Dynamin constricts the tube. To solve this problem, one option could be to reproduce this experiment with sequential injections: one would first inject Dynamin, wait for the full polymerization of the lipid tube and then inject GTP.

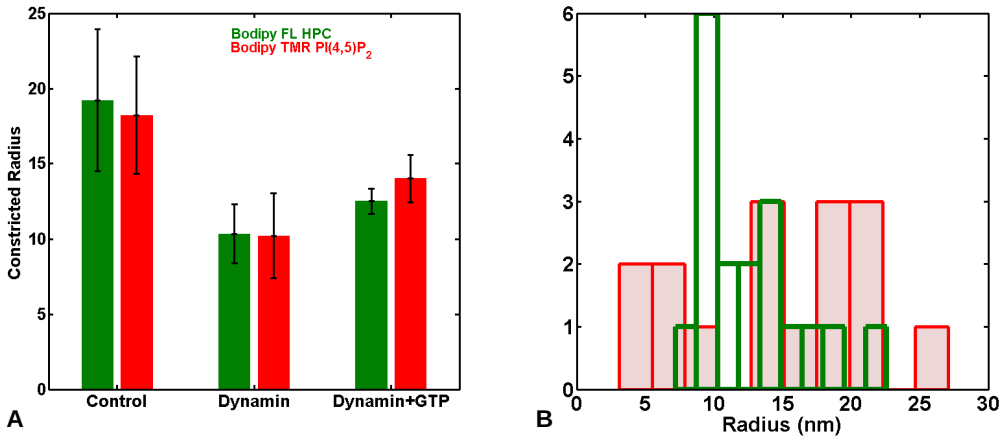

Figure 6.2: A.Radii of nanotubes after injection deduced from the calibration curves with the fluorescence intensity value. Control: no polymerization, no fission after injection. $N = 7$. Dynamin: injection of Dynamin leads to polymerization detected by a force drop. $N = 7$. Dynamin + GTP: injection of Dynamin and GTP simultaneously. Fluorescence intensity was measured on the last frame before fission. $N = 20$. Green: fluorescence of BodipyFL-HPC. Red: fluorescence of BodipyTMR-PIP2. B. Histogram of constricted radii. Green: BodipyFL-HPC. Red: BodipyTMR-PIP2.

6.3.2 Dynamin Mutant Experiments

To better understand Dynamin GTPase activity, we took advantages of two well-known mutants: K44A and K142A. They both have a single point mutation in the GTPase domain and a dominant-negative effect on endocytosis. K44A has a lower GTPase activity due to a decreased affinity for GTP[30]. K142A has an almost normal GTPase activity but is defective in changing conformation [87].

We first tested these two mutants individually. When a mix of non labelled K44A, Alexa488-labelled K44A and GTP (150 μM) was injected near lipid nanotubes, we observed polymerization followed by the fission of the tube. However fission was considerably slower and could take several minutes (see Fig6.3.B blue data points). When we injected non-labelled K142A, Alexa488-labelled K142A and GTP (1mM), the mutant polymerized around the tube but we never observed any fission event (see Fig6.3.B red line). These results are in good agreement with previous observations. We show in addition that K142A is completely inefficient for fission whereas K44A is slower.

We then decided to test hybrid polymers $\{wildtype + K142A\}$. We injected near the tube a mix of non-labelled WT, non-labelled K142A, Alexa488-labelled K142 and GTP (150 μM). We observed polymerization followed by fission for several ratios of mutants and wild type: $\{50\%wt+50\%K142A\}$, $\{20\%wt+80\%K142A\}$ and $\{90\%wt+10\%K142A\}$. These three proportions always lead to fission with a cumulative probability close the wild type's (see Fig6.3.B orange data points). The fact that we observed fluorescently homogeneous polymerization proves that K142A (the only fluorescent protein in this experiment) incorporates well within the wild type polymer. These results indicate that few functional Dynamin dimers are required within the polymer to trigger fission. Further experiments need to be performed to confirm this interesting result. In particular we should quantify precisely how well the Dynamin mutant and wild type polymerize together. There could be a segregation between the two polymers:

WT and K142A could be present as small polymers in solution and nucleate in distinct seeds on the tube. K142A could also polymerize more slowly than wild type, thus the proportion of K142A within the polymer could be overestimated. Then we could find the minimal amount of functional Dynamin required to maintain the fission phenotype.

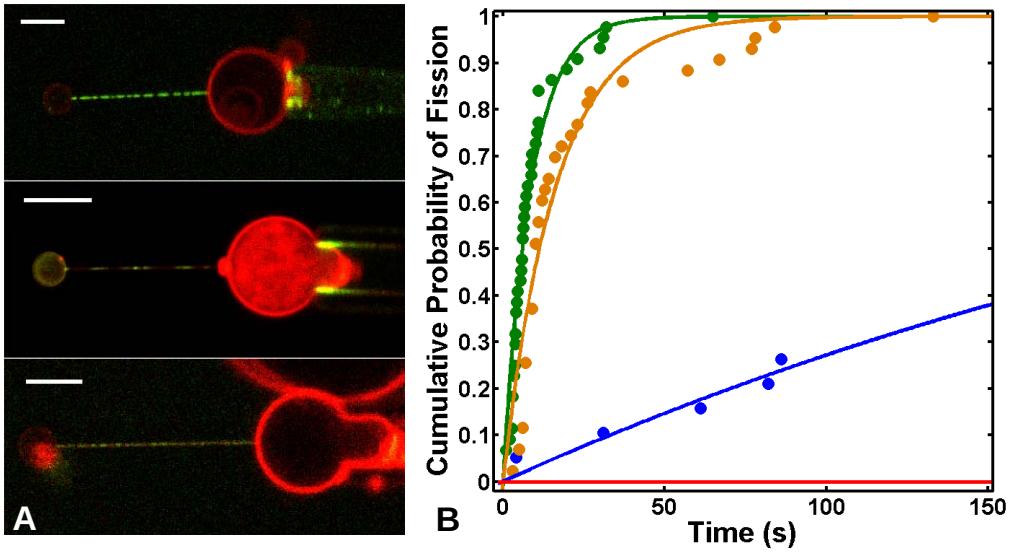

Figure 6.3: A. Confocal microscopy pictures of Dynamin mutants polymerizing on lipid tubes. Top: Dynamin K44A + Alexa488-Dynamin K44A. Middle: Dynamin K142A + Alexa488-Dynamin K142A. Bottom: Dynamin WT + Dynamin K142A + Alexa488-Dynamin K142A. Scale bars: $5 = \mu m$. B. Cumulative probability of fission. Circles: experimental points. Green: WT, N=44. Red: K142A, N=7. Blue: K44A, N=39. Orange: 10%WT + 90%K142A, N=43. Lines: Green $\tau = 8.5 \pm 0.6\ s$, $R^2 = 0.95$. Blue: $\tau = 315 \pm 70\ s$, $R^2 = 0.89$. Orange: $\tau = 16.2 \pm 2.2\ s$, $R^2 = 0.92$. Red: Polymerization and no fission N=7.

6.3.3 Dynamin Depolymerization

Dynamin depolymerization has been observed upon GTP hydrolysis [149, 103, 9] and has been proposed to trigger fission. However depolymerization has never been observed in our fluorescence microscopy experiments. Indeed Dynamin fluorescence is sill visible on broken tubes. Fission time does not depend on the length of the Dynamin polymer (see Fig.6.4) so total depolymerization is not required for fission. If polymerization occurs prior to fission, it must be very rapid and/or partial (few dimers depolymerize) so that we do not detect it. To test the hypothesis of depolymerization, we try to trigger Dynamin disassembly without GTP to test if fission would happen. Our strategy was to use a phosphatase to hydrolyse PIP_2. Decreasing PIP_2 levels at the edge of the Dynamin coat[1] would destabilize the polymer and trigger depolymerization. We choose to use SigD, a bacterial phosphatase. During Salmonella invasion SigD rapidly hydrolyses PIP_2 in the host plasma membrane, it was proposed that this depletion would facilitate membrane invaginations and fission in the host cell [140]. We first let Dynamin starts polymerizing around the nanotube then we injected SigD on the polymerizing nanotube. Injection of SigD on preformed helices did not affect polymerization. We then

[1] within the Dynamin coat, it is hardly possible that a phosphatase could access to the underlying lipids.

injected simultaneously Dynamin and SigD. We observed either normal polymerization or no polymerization at all. We did not manage to trigger Dynamin depolymerization even at high concentration of SigD ($50\mu M$) (see Table 6.5). Dynamin-coated tubes are very stable.

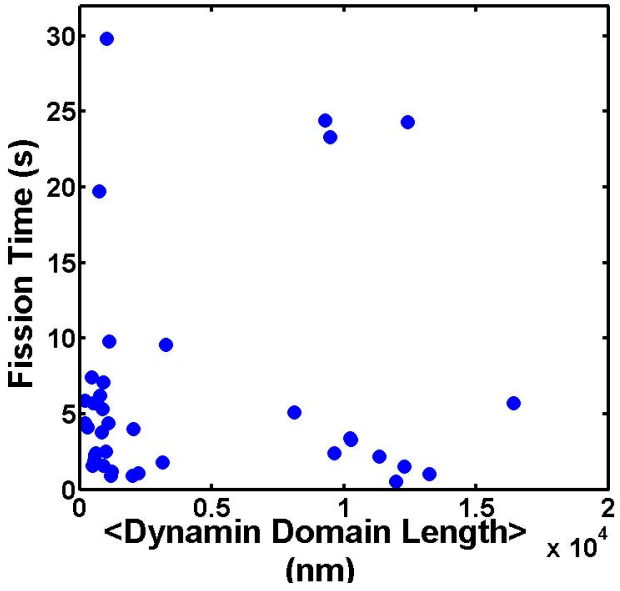

Figure 6.4: Fission times depending on Dynamin domain length. For each experiment, Dynamin was injected alone on the tube to generate separated domains. Size of the domains was controlled by controlling polymerization time through injection time. Once polymerization done, GTP was injected, and in this case, fission time was defined as time between GTP injection and break. For each data point, domain size is the average size of all detectable domains for one tube.

[*Dynamin*] (μM)	[*SigD*] (μM)	injection	polymerization	fission	depolymerization
1.2	50	sequential	$+++$	$-$	$-$
1.2	25	simultaneous	$-$	$-$	$-$
3	25	simultaneous	$+$	$-$	$-$

Figure 6.5: Results of Dynamin and phosphatase experiments. Three conditions were tested. Sequential injection means that Dynamin was injected first then SigD. Simultaneous injection means that Dynamin and SigD were injected concomitantly on the lipid tube. Nor fission neither depolymerization has been detected.

6.4 Summary of Article 2

The objective of the article is to probe the localization and the kinetics of Dynamin-mediated membrane fission. Dynamin polymerization and tube breaking are observed with the nanotube extrusion technique. Whereas Dynamin polymerization does not require the presence of any nucleotide, fission is observed only with GTP. Dynamin-mediated fission takes 10 s at 150 μM of GTP consistently with *in vivo* data. It is observed that fission takes place preferentially at the curved regions of the membrane such as the neck linking an extruded nanotube to a GUV. More precisely, by combining the nanotube extrusion technique to spinning disk confocal microscopy, fission events are precisely localized at the edge of the Dynamin polymer. At these boundaries, the membrane is stressed by the mismatching curvatures imposed by Dynamin on one side and by the membrane elasticity on the other side. The energetic cost of this stress is proposed to trigger fission. This hypothesis leads to formulate a model of the fission reaction with a single energy barrier. The histogram of fission times follows an exponential distribution in good agreement with a rate-limiting single energy barrier. Moreover the proposed model gives predictions for the fission time dependence on membrane tension and rigidity. These predictions have been validated experimentally: the average fission time increases with increasing bending rigidities and decreasing tensions. Furthermore the single energy barrier model takes into account the torque exerted by Dynamin during constriction. It is predicted that the mechanical work due to the torque exerted by Dynamin is proportional to the energy released during GTP hydrolysis. The stall torque is measured by counteracting Dynamin torque with magnetic beads attached to the helix and trapped by magnetic tweezers. An underestimate of Dynamin torque is calculated from the viscous drag exerted on these magnetic beads during GTP-driven rotations. Thus the torque exerted by Dynamin is estimated to be in the range of 730 - 1100 pN.nm. The viscous torque inferred from the rotating magnetic beads is measured at different GTP concentrations and the prediction from the model is validated. The efficiency of Dynamin to convert chemical energy into a reduction of energy barrier is estimated at 37%. Finally the relevance of these *in vitro* experiments is tested. Plasma membrane tension is modified through osmotic shocks. Dynamin activity is blocked when tension is decreased (hyperosmotic shocks) which is consistent with the model. In conclusion, this article presents a model of the fission reaction which is tested experimentally both *in vitro* and *in vivo*. It demonstrates that the kinetics and location of membrane fission is regulated mainly through membrane elasticity.
Complementary experiments attempt to measure the radius of constriction and the minimal amount of functional Dynamin dimers required for fission. The hypothesis of depolymerization was tested but no clear conclusion can be stated.

Chapter 7

Discussion

In this chapter, I will discuss the results detailed in Chapters 5 and 6 under four perspectives. First I will comment in section 7.1 the mechanochemical properties of Dynamin in analogy with the classical molecular motors. In section 7.2, some general features of the fission mechanism will be extrapolated from the particular case of Dynamin and applied to other fission machineries. Fission will be then compared in section 7.3 to its reverse reaction: fusion. Finally *in vivo* and *in vitro* data will confronted in section 7.4.

7.1 Dynamin: a Molecular Motor

Dynamin is a mechanochemical enzyme with a nucleotide hydrolysis activity reminiscent of a molecular motor's activity as we underlined in Chapter 4.3.1. To decipher the mechanochemical coupling of Dynamin, I performed experiments which took inspiration from molecular motor studies.
For instance *in vitro* experiments have unravelled the mechanism of Kinesin, a molecular motor which hydrolyses ATP to transport cargo along microtubules. Optically-trapped microbeads attached to Kinesins are tracked during the motor displacement along microtubules (see Fig.7.1.A) and a stepping behaviour is observed. The statistical analysis of the dwell time between Kinesin steps gives an exponential distribution. In the case of Dynamin, histograms of fission times also show an exponential distribution. These results indicate that both mechanisms are stochastic and can be treated as rate-limited thermally-activated barriers. By limiting the amount of ATP, the elementary step of kinesin was resolved: one Kinesin makes a step of 8 nm by hydrolysing one ATP [120]. Similarly I quantified Dynamin activity as a function of GTP concentration. I obtained that Dynamin-mediated fission rate depends on GTP concentration as a power low, with an exponent equal to 0.37. This exponent is interpreted as the mechanochemical efficiency of Dynamin. However there are strong differences between Kinesin and Dynamin studies. Kinesin was investigated in single molecule conditions but not Dynamin since its fission activity relies on polymerization. Thus I could not directly measure how much GTP is consumed per Dynamin monomer during fission. Another interesting difference between the two motors is that Kinesin activity is more tighlty coupled to nucleotide hydrolysis than in the Dynamin case. This indicates that the energy landscapes of the two reactions are different. Indeed we estab-

lished that Dynamin-mediated fission can be treated as a single step reaction whereas Kinesin walk has at least two rate-limiting steps [148]. However this statement must be qualified as the energy landscape of Dynamin might actually be more complex if studied on a higher time resolution.

Another relevant example of molecular motor is the $F_1 - ATPase$. This complex is part of the ATP-synthase, the machinery synthesizing ATP in mitochondria. $F_1 - ATPase$ is made of three $\alpha\beta$ subunits encircling a protruding γ subunit (see Fig7.1.B). The $\alpha\beta$ subunits constitute three catalytic sites of ATP hydrolysis. By attaching an actin filament to the γ subunit, the rotation of the filament was observed upon ATP treatment (see Fig.7.1.B and [97]). This directly puts in evidence the rotatory activity of this motor. Angular steps of 120° can be observed at limiting concentration of ATP. Moreover due to the viscous drag exerted on the actin filament, the torque of $F_1 - ATPase$ has been estimated at 40 pN.nm [97, 70]. Similarly by attaching microbeads to Dynamin-coated tubes, I observed the rotation of the beads upon GTP injection due to the Dynamin conformational changes. Following the rotation of small beads of 95 nm radius allows to study the dynamics of Dynamin constriction. Dynamin helices deforms the membrane in a concerted manner, meaning that the dimers within the polymer are well coordinated during GTP hydrolysis. For bigger beads of 650 nm radius, the rotation speed is slower. This is due to the viscous drag encountered by the beads which counteracts the Dynamin torque. These experiments enable to estimate that the Dynamin torque lies between 730 and 1100 pN.nm.

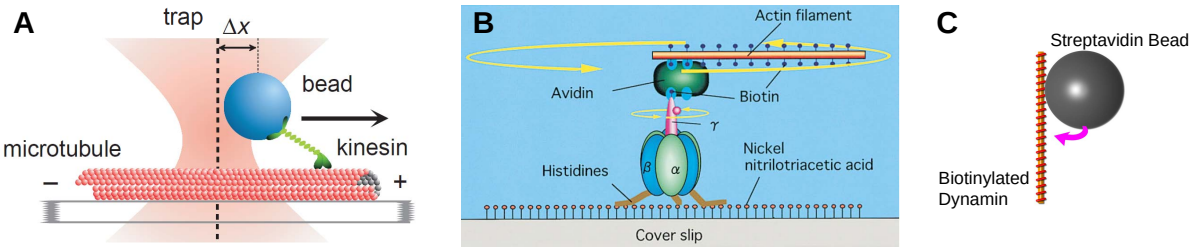

Figure 7.1: Three *in vitro* studies of molecular motors. A: Sketch of an experiment monitoring Kinesin movement along a microtubule. Microtubules are attached to a glass coverslip. Microbeads are bound to Kinesins. An optical trap with a position feedback loop follows the Kinesin displacement. From Visscher *et al* Nature 1999. B: Sketch of the experiment showing the rotation of an actin filament attached to $F_1 - ATPase$. From Kinosita *et al*. Cell 1998. C: Sketch of a Dynamin-coated membrane tube with a microbead. Varying the size of the bead enables to counteract more or less Dynamin torque.

Dynamin is a molecular motor in the sense that it converts the chemical energy released during GTP hydrolysis into mechanical work to constrict the membrane. I have shown that 37 % of the energy released during GTP hydrolysis is used by Dynamin to reduce the energy barrier of fission. However Dynamin is different from classical molecular motors. Unlike Kinesin and $F_1 - ATPase$ for which discrete steps were detected at low concentrations of nucleotide, sequential rate-limited steps were not observed in the mechanism of fission. For instance the rotation of microbeads attached to Dynamin polymers is smooth and continuous even at low concentrations of GTP and with large beads which slow down Dynamin mechanical activity. Instead of discrete steps, we measured that Dynamin constriction is concerted in time and space [96].

Motor	Step Size	Maximum Force or Torque	Efficiency
Kinesin	8 nm	5 pN	50 %
$F_1 - ATPase$	120°	40 pN.nm	100 %
Dynamin	not detected	730-1100 pN.nm	37 %

Figure 7.2: Main properties of three molecular motors. Kinesin and $F_1 - ATPase$ data come from Kinosita *et al* Cell 1998.

7.2 Different Fission Mechanisms?

Dynamin mechanochemical activity triggers membrane fission. In this section, I will explain how the particular case of Dynamin can be useful to understand the mechanism of fission in general. For this purpose, Dynamin-mediated fission will be compared to the fission induced by phase-separation. Some general features of the fission mechanism can be inferred from this comparison. These features will be then applied to less-understood mechanisms of fission: Dnm1- and ESCRT-III-mediated fissions.

7.2.1 Common Features Between Phase Separation-Induced and Dynamin-Mediated Fission

In section 3.3.2, we introduced the mechanism of fission induced by phase separation. We highlighted that fission occurs at the interface between the two phases. Interestingly, in the case of Dynamin, we found that fission also occurs at an interface: at the edge between the Dynamin-coated tube and the free membrane. In both mechanisms, fission localizes at an interface between two pre-defined domains. Phase separation generates two domains of membrane with different lipid compositions, for instance l_o and l_d phases. Dynamin activity creates also two domains: a portion of the tube is coated with Dynamin and the other one is free of protein. In both case the boundary between the two domains has an energetic cost: the line tension for phase separation and for Dynamin the elastic energy of the membrane due to the mismatching curvatures of the two domains. The energetic cost of creating a boundary helps fission. Line tension has been estimated around $\lambda \approx 1\ pN$ for ternary composition made of sphingomyelin, PC and cholesterol segregating into l_o and l_d phases [10]. For a tube of 20 nm radius, this corresponds to an energy of line tension $E_{line\ tension} \approx 120\ pN.nm \approx 30\ k_BT$. In the case of Dynamin-mediated fission, the edge energy depends on the bending rigidity modulus κ and on the ratio of the radii: $\frac{R_m}{R_c}$ where R_m is the radius of the protein-free tube portion and R_c the radius of the tube portion constricted by Dynamin [123]. For instance for a radii ratio of 5 and a rigidity $\kappa = 16 k_BT$, we calculate an elastic energy around $E_{elastic} \approx 70\ k_BT$ (see Supplementary Figure 3 Chapter 6). These "boundary" energies contribute to reduce the energy barrier of fission that we estimated to be around 80 k_BT. The boundary energy could be a common feature of all fission mechanisms.
However generating a boundary is not enough for fission. Indeed Dynamin constriction does not trigger fission in all conditions. Similarly phase separation does not lead necessary to fission as stable phase-separated domains can be observed *in vitro* [10]. In both processes, membrane elastic parameters (tension, rigidity) must help fission. Indeed we find that high tension increases fission rate and this was also observed for phase-separation fission: 1s for

tensed tubules pulled by Kinesins and 20s for tubules with lower tensions [114]. Thus a second requirement for efficient fission is to regulate membrane tension and rigidity.

7.2.2 Predictions For Other Fission Machineries

Dynamin is not the unique fission machinery in the cell. For instance, Dnm1 is a DRP involved in mitochondrial fission in yeast [12]. ESCRT-III has been implicated in membrane scission in the multivesicular body, during viral budding and in membrane abscission during cytokinesis [63, 119, 50]. In the following sections, I will propose some predictions for the fission activity of these two proteins based on the current knowledge of Dynamin.

Dynamin-Related Proteins

Dnm1 is a DRP required for the fission of mitochondrial membranes. Recent cryo-electron microscopy experiments show that Dnm1 has an helical structure and a conformational change very similar to the Dynamin ones [91]. Thus Dynamin and Dnm1 are expected to follow a similar fission mechanism. However they do differ at some points.
Dnm1 helices have a larger radius than Dynamin polymers. In the non-constricted state, Dnm1 inner lumen diameter is 89 nm (17 nm for Dynamin), its pitch is around 28.8 nm (10.6 nm for Dynamin). Upon GTP treatment, Dnm1 inner lumen diameter decreases to 25 nm (7 nm for Dynamin) while the pitch remains constant (it decreases to 9.4 nm for Dynamin) (see Fig.7.3). Like in the case of Dynamin, Dnm1-mediated fission involves a constriction mechanism. However Dnm1 constricts much more than Dynamin. Indeed the ratio of the unconstricted radius over the constricted radius is 3.6 for Dnm1 and 2.4 for Dynamin. It means that the torque generated by Dnm1 is more important than the one exerted by Dynamin. It would be interesting to measure this torque with the rotating bead technique and compare its value with Dynamin.

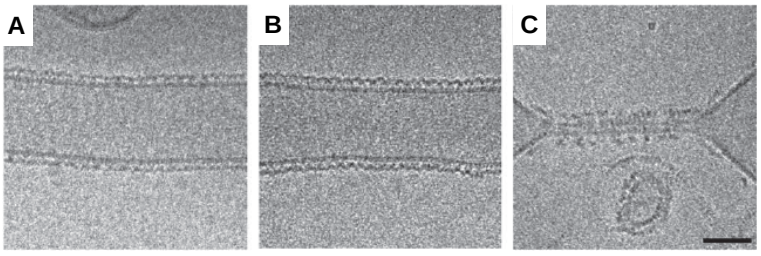

Figure 7.3: Cryo-EM pictures of Dnm1-coated lipid tubes. A: in absence of nucleotide. B: in the presence of GMP-PCP. C: after addition of 1 mM GTP. Scale bar: 50 nm. From Mears *et al* 2011.

Another striking difference between Dnm1 and Dynamin comes from the interactions between the helical polymer and the lipid bilayer. Dynamin inserts within the outer leaflet of the membrane via its PH domain [106] whereas Dnm1 helix stays apart from the lipid bilayer [91]. Dynamin constriction is damped by the friction between the helix and the membrane [96]. One would expect a different dynamics of constriction for Dnm1 resulting from its different interaction with the membrane. Dnm1 constriction might be less damped by membrane-protein

friction, which might enable to produce a higher torque. Thus it would be interesting to measure the mechanochemical efficiency of Dnm1 and compare it with Dynamin.
It is probable that the energy barrier of fission is higher in the case of mitochondrial double membranes than in the case of the plasma membrane. Measurement of fission time and torque would allow to estimate this barrier. A higher energy barrier resulting from the elastic properties of mitochondrial membranes might be the reason of the particular features of Dnm1 compared to Dynamin.

ESCRT-III

ESCRT-III is a complex of several proteins recruited sequentially at the membrane (see Fig.7.4.A). Vps20 binds first to the membrane and nucleates the polymerization of Snf7. This proteins polymerize into a spiral and might induce membrane buckling [82]. Vps24 and Vps2 end the polymerization and allow the fission of the vesicle [155]. The mechanism of ESCRT-III-mediated fission is not known. Contrary to Dynamin, ESCRT-III is located inside the membrane neck that need to be cut. Thus it is interesting to compare Dynamin and ESCRT-III as they both trigger fission but with inverted topologies.

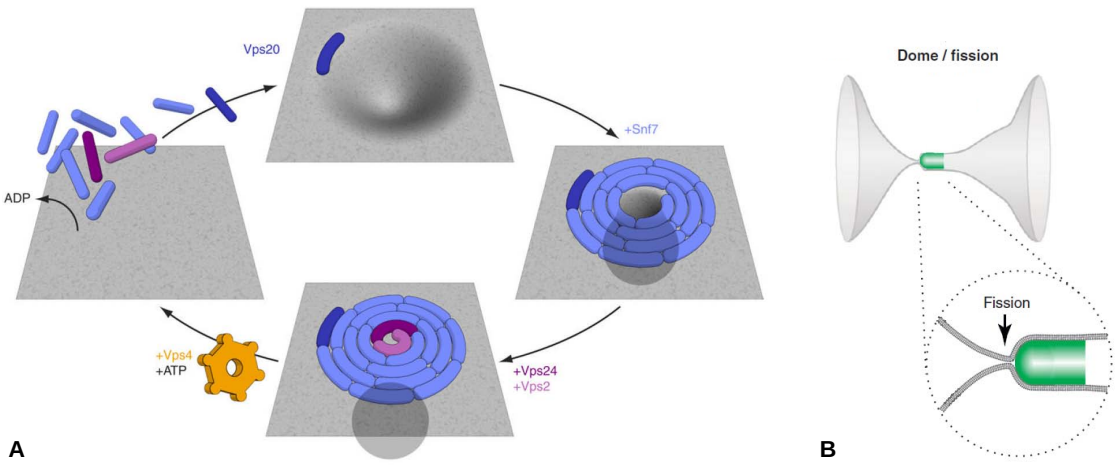

Figure 7.4: A: Sketch representing the main steps of ESCRT-III activity. From Wollert *et al* Nature 2009. B: Sketch representing a membrane neck with a hypothetical dome of ESCRT-III and the probable location of fission. Adapted from Guizetti *et al* Trends in Cell Biology 2012.

As ESCRT-III-mediated fission is independent of any nucleotide hydrolysis unlike Dynamin, one would expect a totally different energy landscape for ESCRT-III-mediated fission. However the general features of fission developed previously might apply as well to the case of ESCRT-III. The first proposed requirement for fission is to create locally a membrane stress between two domains. We can hypothesize that ESCRT-III-mediated fission would occur at the interface between the Snf7-bound-membrane and the free membrane. The membrane stress would be created by the structure of the Snf7 polymer (see Fig.7.4.B). This structure has been hypothesized to form a dome according to observations by electron microscopy in cells overexpressing Snf7 [63]. In this model, the membrane shape at the interface of a dome of ESCRT-III is similar to the one at the edge of Dynamin. Thus fission might occur through a similar mechanism in

both cases. As we noticed for Dynamin and phase separation, membrane tension and rigidity should also affect ESCRT-III-mediated fission. It would be interesting to perform *in vitro* experiments similar to the ones we did for Dynamin to investigate the fission rate mediated by ESCRT-III as a function of the membrane elastic parameters. We could compare Dynamin and ESCRT-III and find which one is more efficient under which conditions. In addition to their topological specificity, they might each have their own range of rigidities and tensions where they are the most fission-competent.

7.3 Fission Versus Fusion

Fission and fusion are two biological mechanisms where membrane deformations lead to a topological change. They are also the reverse process of each other. Fission splits one membrane into two distinct membranes, while fusion merges two separate compartments into a single one. Thus it is interesting to compare these two complementary mechanisms.

As we mentioned in section 2.2.1, SNARE proteins are involved in fusion during vesicular traffic. Two types of SNARE proteins are required for fusion: v-SNAREs and t-SNAREs. v-SNAREs are anchored in the membrane of the vesicle. t-SNAREs are bound to the target membrane. After docking of the vesicle at the target membrane via RAB proteins, the two membranes are brought closer through interactions between cognate v-SNAREs and t-SNAREs. These interactions occurs in a "zipper"-like mode leading to the formation of a four-α-helix bundle. The tight binding between v-SNARE and t-SNARE forms a complex called a SNAREpin. Fusion of the two membranes occurs upon complete "zipping" of the SNAREpin. After fusion, the remaining SNAREpin complex becomes the cis-SNARE complex which is very stable and requires the help of other proteins to disassemble (see Fig.7.5).

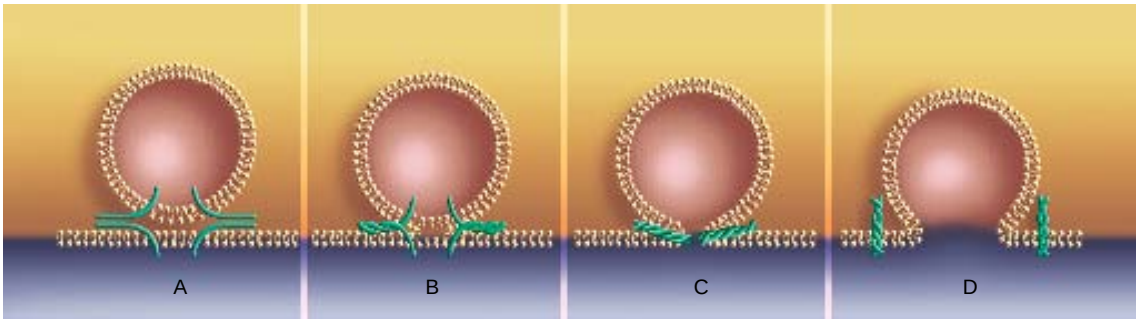

Figure 7.5: Sketch representing the main steps of SNARE-mediated fusion. A: initiation of fusion, cognate v-SNARE and t-SNARE (both represented in green) start to assemble. B: zipping of the SNAREpin brings the membranes closer to each other and facilitates the formation of the hemifusion intermediate. C: complete formation of the SNAREpin leads to fusion and generates a fusion pore. D: expansion of the fusion pore, the cis-SNARE complex remains embedded in the membrane. From Roux *et al* Pour la Science 2007.

Strikingly, although Dynamin and SNAREs are two distinct families of proteins, some DRPs are implicated in intracellular fusion processes especially for mitochondria and chloroplast. The fusion of these organelles is more complex as they are delimited by two membranes. For instance Mitofusins and OPA1, two DRPs, mediate fusion of the outer and inner mitochondrial

membranes respectively [92]. The mechanism of fusion for these DRPs is not known so far and might be different from the mechanism of Dynamin-medited fission. Dynamin has also been linked to fusion. It has been proposed that Dynamin regulates the expansion of the fusion pore [6]. The implication of Dynamins in both fission and fusion prompts us to look for the similarities and differences between the two processes.

Fission and fusion share the same intermediate state: the hemifission/hemfusion stalk. The proximal membrane leaflets merge their lipid content while the distal leaflets are still separated (see Fig.7.6). The stalk intermediate enables both non-leaky fusion and non-leaky fission which are necessary for efficient transport. This state has been detected during the fusion process by observing the mixing of two fluorescent membranes while the content of the two compartments remains separated [47]. Evidence for a non-leaky intermediate has been found also for the Dynamin-mediated fission mechanism in patch clamp experiments [9]. Interestingly both mechanisms use the same strategy to reach the stalk intermediate: to reduce the distance between bilayers. Zipping of the SNAREpin and Dynamin constriction both bring the bilayer closer to each other. Thus one would expect that the energies involved in both processes have the same order of magnitude. Indeed the energy of the stalk has been estimated in fission and fusion. For SNAREs-mediated fusion, the hemifusion energy has been calculated around 40-50 $k_B T$ [75]. For fission mediated by coat proteins, a calculation based on the Canham-Helfrich theory gives an underestimate of 78 $k_B T$ for the hemifission state energy [76]. Thus energy input is required to reach the stalk. *In vivo* this energy barrier is crossed with the help of specific protein machineries. In fusion, the energy released during the assembly of the SNAREpin complex contribute to generate hemifusion. The energy of a single SNAREpin assembly has been measured at 35 $k_B T$ [85]. Although several SNAREpin complexes per fusion site are proposed to be required for rapid fusion [68], it seems that one complex is energetically sufficient. In fission, Dynamin constriction reduces the energy barrier and facilitate fission. We estimate this constriction energy around 80 $k_B T$.

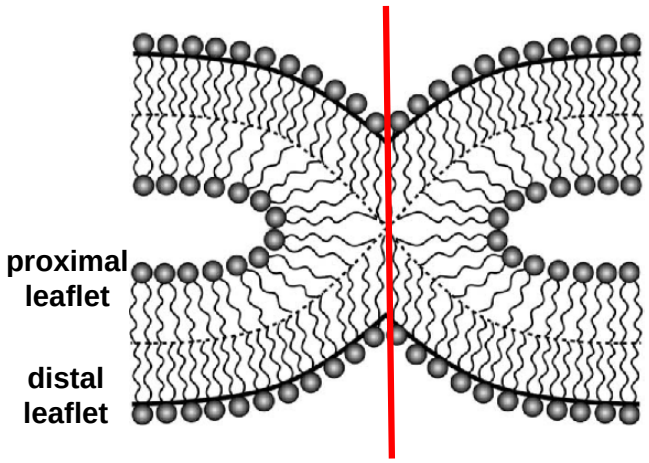

Figure 7.6: Sketch of the stalk: intermediate of fission and fusion. The proximal leaflets are merged while the distal leaflets remain separated. The red line indicates where the rupture must occur to complete the process. Adapetd from Chernomordik and Kozlov, Cell 2005.

Although fission and fusion share the same intermediate, these mechanisms have different source of energy: Dynamin-mediated fission is fuelled by nucleotide hydrolysis while SNAREs-mediated fusion relies on structural affinity[1]. This difference could be due to the fact that reaching the stalk state is more costly from the hemifission side (more than 78 $k_B T$) than from the hemifusion side (40-50 $k_B T$). Once the stalk intermediate has been reached, rupture within the structure must occur along the red line as depicted in Fig.7.6. This step is spontaneous in the case of fission [76]. For the fusion process, this step is energetically more costly as it requires at least to expand the fusion pore. Thus the energy landscape of fission and fusion should be different.

These different energetic signatures of fission and fusion translate into different membrane properties requirements. As we calculated in paragraph 3.3.1, the energy difference between the initial and the final state of fission is

$$\Delta E_{fission} = 4\pi(\frac{\kappa}{8} + \kappa_G)$$

As fusion is the reverse process, we expect:

$$\Delta E_{fusion} = -\Delta E_{fission}$$

$$\Delta E_{fusion} = -4\pi(\frac{\kappa}{8} + \kappa_G)$$

This implies that increasing the bending rigidity modulus κ and the Gaussian bending rigidity modulus κ_G should favour fusion and inhibit fission. Indeed we have found that stiffer membranes are less fission competent (see Fig.1 Chapter 5). Consistently, SNARE proteins have been shown to localize at cholesterol-rich regions where membrane is more rigid [79, 78]. These clusters are thought to enhance exocytosis by locally concentrating the fusion machinery but the rigidity of the membrane by itself could favour fusion. To test this hypothesis, it would be interesting to measure *in vitro* how the fusion rate depends on the membrane rigidity modulus.

Although membrane rigidity controls differently fission and fusion, it seems that membrane tension regulates similarly both processes. In nanotube extrusion experiments, I show that decreasing tension delays fission. Hyperosmotic shocks on live cells, which decrease membrane tension, confirm that Dynamin-mediated fission is impaired at low tensions. Concerning fusion it is showed that an increase in plasma membrane tension activates exocytosis [46]. Theoretical works also predict that increasing tension is critical for the fusion pore expansion [25]. So higher membrane tension stimulates both fission and fusion. *In vivo* the regulations of membrane tension is believed to be achieved in part by the cytoskeleton. Actin filaments might help fission by pulling on the bud [15]. Local disassembly of the cortex might facilitate the fusion pore expansion and thus favour fusion [22]. It would be interesting to further address this question *in vivo*: how is membrane tension regulated by the cytoskeleton (or by another way) to activate preferentially fission or fusion?

[1] It is interesting to note that ESCRT-III-mediated fission does not require nucleotide hydrolysis.

7.4 *In Vitro* Fission Versus *In Vivo* Fission

During my thesis, I studied Dynamin mainly through *in vitro* experiments: purified Dynamin and artificial membranes were used in order to control precisely membrane elastic parameters such as tension and rigidity. In this section, I will analyse to which extent the *in vitro* results give information about Dynamin activity *in vivo*. First the characteristics of the Dynamin helix *in vitro* will be confronted to *in vivo* observations. Then I will discuss what are the requirements for a biological membrane to ensure efficient fission *in vivo*.

7.4.1 *In Vitro* Helix Versus *In Vivo* Helix

In vivo Dynamin polymerizes into short helices (supposedly 2 or 3 helical turns) whereas most *in vitro* experiments, such as electron microscopy or nanotube extrusion experiments, study long Dynamin helices (several μm which correspond to several hundreds of helical turns). This raises questions about the physiological relevance of long Dynamin polymers [103, 9, 111]. It has been proposed that pre-assembled long Dynamin helices are kinetically non active [103]. During my thesis, I have measured that Dynamin constriction is damped by internal friction between the membrane and the helix, which could explain why long polymers are less fission competent. Moreover I have identified a precise localization of fission events: the edge of the Dynamin polymer. This could explain why fewer fission events are observed on long polymers compared to short helices. When Dynamin is pre-assembled without GTP, continuous and long polymers are generated, thus the number of edges is low, which results in a low fission rate. On the contrary, when Dynamin polymerizes in presence of GTP, its constriction activity leads to fission at an early stage and limits the length of the polymers. Thus long polymers of Dynamin are still relevant to study fission mechanism since fission is localized at the interface between the edge of the polymer and the free membrane.

In vivo Dynamin interacts with other proteins via its PRD domain. These proteins could modulate the Dynamin helix. For instance during CME, Dynamin colocalizes transiently with Amphiphysin, Endophilin and FBP17 [139]. These proteins are involved in membrane remodelling but they could also regulate Dynamin activity. Indeed it has been shown *in vitro* that Dynamin-coated tubes have a thinner radius when they are prepared in presence of FBP17 [64] or Endophilin [135]. These proteins could help Dynamin to further constrict lipid nanotubes. Thus It would be interesting to test how the fission rate is modified in presence of Dynamin partners. These proteins could also recruit Dynamin at a precise location within the neck of the bud and thus indirectly control where fission would happen. These hypothesis could be investigate *in vitro* with the nanotube extrusion technique.

It has also been proposed that fission would result from Dynamin depolymerization [103, 9]. This hypothesis remains an open question. I was not able to detect any Dynamin disassembly before fission by fluorescence microscopy. Even after fission, Dynamin was still present on the broken tubules. *In vivo* as well, it is not clear if Dynamin depolymerization precedes and triggers fission. It would require a higher temporal resolution (2s in [139]) to detect *in vivo* both Dynamin disappearance and vesicle scission. The model proposed in Chapter 6 does not require Dynamin depolymerization prior to fission but it does not exclude it neither. In particular, an uncoated part on the lipid tube is necessary for fission in our model. To test if

depolymerization of Dynamin is required for fission, one should observe if fission still occurs when depolymerization is prevented for instance by crosslinking Dynamin within the polymer.

7.4.2 Membrane Requirements For Fission *In Vivo*

The results linking Dynamin activity to membrane elasticity were obtained for homogeneous membranes at equilibrium and with simple lipid compositions. However biological membranes are more complex. Thus it is interesting to confront *in vitro* data with *in vivo* studies.

Membrane rigidity is an important parameter of the fission mechanism. *In vitro* the average fission time increases almost ten times when the bending rigidity increases from 16.2 to 35.5 $k_B T$. This could indicate a cellular mechanism controlling the timing of fission events. *In vivo* the dynamics of fission could be regulated by modifying locally the lipid composition of the membrane. Indeed PIP_2 hydrolysis by Synaptojanin has already been correlated to Dynamin-mediated fission [18]. It would be interesting to know how cholesterol and sphingolipids behave within Clathrin-coated structures as these lipids greatly contribute to the rigidity of the membrane. It would also be newsworthy to correlate membrane lipid compositions and endocytosis rates for different cellular types. It is expected that membranes undergoing a high endocytic activity are less rigid. This would test the consistency of the observation that rigidity slows down fission.

In addition to membrane rigidity, membrane tension plays a role in fission. *In vitro*, fission time is affected by membrane tension, especially for membranes containing cholesterol and sphingolipid, (lipids in which the plasma membrane is particularly enriched) (see Fig.1 in Chapter 5). For tension lower than 10^{-4} $N.m^{-1}$, fission is drastically slower. Plasma membrane tension has been estimated around 10^{-3} $N.m^{-1}$ by nanotube extrusion on blebbing cells [29]. Thus it appears that the plasma membrane tension is in a range where Dynamin-mediated fission is efficient. Moreover it has been shown that Clathrin-coated pits are blocked when lowering plasma membrane tension [58]. This correlates also with our *in vivo* data (see Fig. 4 in Chapter 5). Hyperosmotic shocks on live cells block Dynamin structures which colocalize with Clathrin-coated pits. These experiments show that the defective CME after a hyperosmotic shock is not due to the precipitation of Clathrin, as it was believed so far, but is really due to the reduced activity of Dynamin. One would expect an enhanced fission rate after hypoosmotic shocks. But hypoosmotic shocks delays the formation of clathrin-coated pits making it difficult to probe Dynamin activity. However long tubules of Dynamin are observed to polymerize at the plasma membrane after hypoosmotic shocks, which indicates that Dynamin is still active. Membrane tension regulates Dynamin-mediated fission. But what controls membrane tension *in vivo*? The cytoskeleton is a good candidate for membrane tension regulation. Some studies show an interplay between actin, membrane elastic properties and endocytosis. On one hand, plasma membrane tubulation is facilitated by cytoskeleton disruption [64]. On the other hand, actin cytoskeleton is required for proper endocytosis at location of high membrane tensions [15]. The precise mechanism coordinating membrane elasticity, cytoskeleton dynamics and fission is still not understood.

An interesting membrane parameter which was not tested during this thesis is the asymmetry in the lipid bilayer. The plasma membrane is especially intriguing as the exoplasmic leaflet is enriched in sphingomyelin while the cytoplasmic leaflet contains a higher level of PS. During

endocytosis, in the stalk structure, the proximal leaflet is enriched in SM, and is thus less deformable than the distal leaflet. Asymmetric leaflets generate spontaneous curvature which could influence the fission mechanism. This hypothesis could be investigated *in vitro*. For instance, fission rate could be measured with asymmetric bilayers prepared with the inverted emulsion technique [98]. These *in vitro* experiments might help to understand how the asymmetry of biological membranes influence fission during endocytosis.

Chapter 8

Conclusion

During this thesis, a model of Dynamin-mediated membrane fission has been proposed based on the observation that fission occurs at Dynamin edges. It leads to the formulation of the energy barrier of fission:

$$\Delta E \simeq a(\frac{1}{R_i} - \frac{1}{R_u})\frac{\kappa^{3/2}}{\sqrt{\sigma}} = a(\frac{1}{R_i} - \frac{1}{R_c})\frac{\kappa^{3/2}}{\sqrt{\sigma}} + c\Gamma\theta$$

where R_i is the tube radius of the intermediate state, R_c the radius of the constricted Dynamin-coated tube, R_u the radius of the unconstricted Dynamin-coated tube, κ the bending rigidity modulus of the membrane, σ the membrane tension, Γ the torque delivered during constriction, θ the angle by which the helix rotates per hydrolysed GTP, a and c are two constants. The barrier is estimated from 30 to 70 k_BT depending on membrane tension and rigidity. *In vitro* and *in vivo* experiments allow to test this model. We calculate theoretically and validate experimentally how the fission time depends on membrane rigidity, membrane tension and Dynamin torque. Statistical analysis shows that fission time follows an exponential distribution in agreement with a single energy barrier reaction. Torque measurements demonstrate that the energy delivered by Dynamin torque is proportional to the energy released during GTP hydrolysis and reduces the energy barrier of fission. From these experiments, the efficiency of Dynamin is estimated at 37%.
The validations of our model gives a quantitative analysis of the energy landscape of fission. Although constriction is not enough to proceed to fission, it supplies energy to reduce the energy barrier. This barrier can be crossed by thermal fluctuations when the membrane satisfies specific conditions of tension and rigidity.

In vivo the energy barrier of Dynamin-mediated fission is probably modified by other proteins, like Endophilin or Amphiphysin. Membrane tensions and rigidities are certainly actively regulated. Thus it would be interesting to perform further experiments to complete the energy landscape depicted in Fig. 8.1 and integrate it into to the full mechanism of endocytosis.

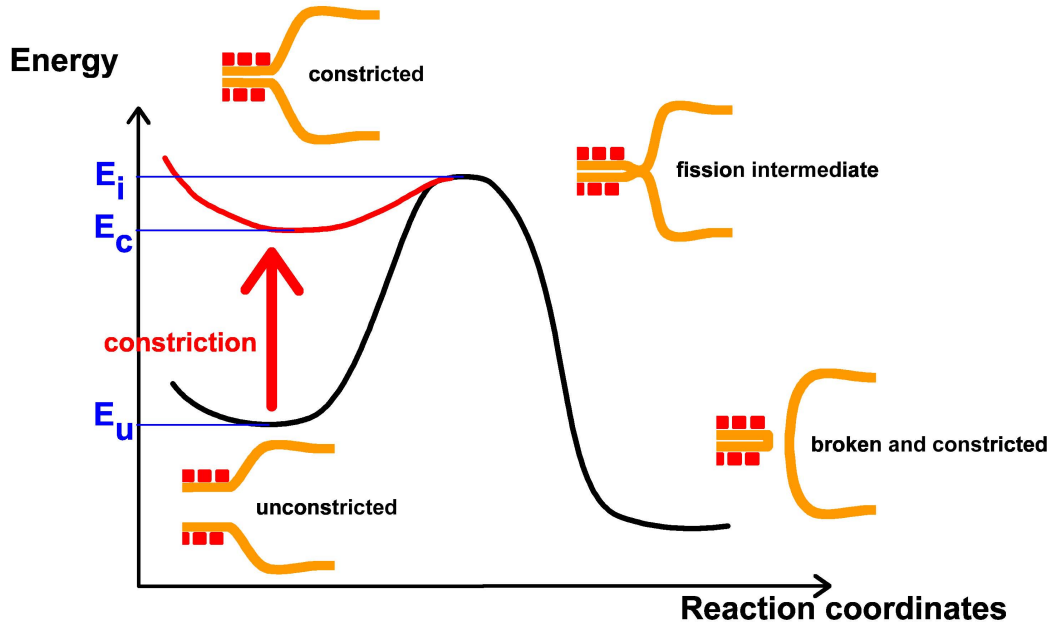

Figure 8.1: Sketch of the energy landscape of the fission reaction. Dynamin constriction reduces the height of the energy barrier of fission to a level where the barrier can be crossed by thermal fluctuations.

Bibliography

[1] M. R. Ahmadian, U. Hoffmann, R. S. Goody, and A. Wittinghofer. Individual rate constants for the interaction of ras proteins with gtpase-activating proteins determined by fluorescence spectroscopy. *Biochemistry*, 36:4535–4541, 1997. 30

[2] S. Aimon, J. Manzi, D. Schmidt, J. A. Poveda Larrosa, P. Bassereau, and G. E. S. Toombes. Functional reconstitution of a voltage-gated potassium channel in giant unilamellar vesicles. *PLoS One*, 6(10):e25529, 2011. 19

[3] Bruce Alberts, Dennis Bray, Alexander Johnson, Julian Lewis, Martin Raff, Keith Roberts, and Peter Walter. *Essential Cell Biology*. Garland Publishing Inc., New-York, London, 1998. 3, 4

[4] J.-M. Allain, C. Storm, A. Roux, M. Ben Amar, and J.-F. Joanny. Fission of a multiphase membrane tube. *Physical Review Letters*, 93(15):1–4, 2004. 22

[5] E. Ambroggio, B. Sorre, P. Bassereau, B. Goud, J.-B. Manneville, and B. Antonny. Arfgap1 generates an arf1 gradient on continuous lipid membranes displaying flat and curved regions. *The EMBO Journal*, 29:292–303, 2010. 19

[6] A. Anantharam, M. A. Bittner, R. L. Aikman, E. L. Stuenkel, S. L. Schmid, D. Axelrod, and R. W. Holz. A new role for the dynamin gtpase in the regulation of fusion pore expansion. *The EMBO Journal*, 22(11):1907–1918, 2011. 28, 127

[7] M. I. Angelova, S. Soléau, Ph. Méléard, F. Faucon, and O. Bothorel. Preparation of giant vesicles by external ac electric fields. kinetic and applications. *Progress in Colloid and Polymer Science*, 88:127–131, 1992. 15

[8] L. Bagatolli and P. B. Sunil Kumar. Phase behavior of multicomponent membranes: Experimental and computational techniques. *Soft Matter*, 5:3234–3248, 2009. 15, 19

[9] P. V. Bashkirov, S. A. Akimov, A. I. Evseev, S. L. Schmid, J. Zimmerberg, and V. A. Frolov. Gtpase cycle of dynamin is couple to membrane squeeze and release, leading to spontaneous fission. *Cell*, 135:1276–1286, 2008. 36, 117, 127, 129

[10] T. Baumgart, S. T. Hess, and W. W. Webb. Imaging coexisting fluid domains in biomembrane models coupling curvature and line tension. *Nature*, 425:821–824, 2003. 22, 123

[11] D. D. Binns, B. Barylko, N. Grichine, M. A. L. Atkinson, M. K. Helms, D. M. Jameson, J. F. Eccleston, and J. P. Albanesi. Correlation between self-association modes and gtpase activation of dynamin. *Journal of Protein Chemistry*, 18(3):277–290, 1999. 30

[12] W. Bleazard, J. M. McCaffery, E. J. King, S. Bale, A. Mozdy, Q. Tieu, J. Nunnari, and J. M. Shaw. The dynamin-related gtpase dnm1 regulates mitochondrial fission in yeast. *Nature Cell Biology*, 1:298–304, 1999. 124

[13] L. Bo and R. E. Waugh. Determination of bilayer membrane bending stiffness by tether formation from giant, thin-walled vesicles. *Biophysical Journal*, 55(3):509 – 517, 1989. 18

[14] J. S. Bonifacino and B. S. Glick. The mechanisms of vesicle budding and fusion. *Cell*, 116:2153–166, 2004. 5

[15] S. Boulant, C. Kural, J.-C. Zeeh, F. Ubelmann, and T. Kirchhausen. Actin dynamics counteract membrane tension during clathrin-mediated endocytosis. *Nature Cell Biology*, 13:1–10, 2011. 128, 130

[16] P. B. Canham. The minimum energy of bending as a possible explanation of the biconcave shape of the human red blood cell. *Journal of Theoretical Biology*, 26(1):61–76, 1970. 13

[17] K. Carvalho, L. Ramos, C. Roy, and C. Picart. Giant unilamellar vesicles containing phosphatidylinositol(4,5)bisphosphate: Characterization and functionality. *Biophysical Journal*, 95:4348–4360, 2008. 15

[18] B. Chang-Ileto, S. G. Frere, R. B. Chan, S. V. Voronov, A. Roux, and G. Di Paolo. Synaptojanin 1-mediated pi(4,5)p(2) hydrolysis is modulated by membrane curvature and facilitates membrane fission. *Developmental Cell*, 20(2):205–218, 2011. 130

[19] J. S. Chappie, S. Acharya, M. Leonard, S. L. Schmid, and F. Dyda. G domain dimerization controls dynamin's assembly-stimulated gtpase activity. *Nature*, 465:435–440, 2010. 32

[20] J. S. Chappie, S. Acharya, Y.-W. Liu, M. Leonard, T. J. Pucadyil, and S. L. Schmid. An intramolecular signaling element that modulates dynamin function in vitro and in vivo. *Molecular Biology of the Cell*, 20:3561–3571, 2009. 28

[21] J. S. Chappie, J. A. Mears, S. Fang, M. Leonard, S. L. Schmid, R. A. Milligan, J. E. Hinshaw, and F. Dyda. A pseudoatomic model of the dynamin polymer identifies a hydrolysis-dependent powerstroke. *Cell*, 147:209–222, 2011. 35

[22] A. Chen, E. Leikina, K. Melikov, B. Podbilewicz, M. M. Kozlov, and L. V. Chernomordik. Fusion-pore expansion during syncytium formation is restricted by an actin network. *Journal of Cell Science*, 121:3619–3628, 2008. 128

[23] Y.-J. Chen, P. Zhang, E. H. Egelman, and J. E. Hinshaw. The stalk region of dynamin drives the constriction of dynamin tubes. *Nature Structural and Molecular Biology*, 11(6):574–575, 2004. 32

[24] M. Chircop, B. Sarcevic, M. R. Larsen, C. S. Malladi, N. Chau, M. Zavortink, C. M. Smith, A. Quan, V. Anggono, P. G. Hains, M. E. Graham, and P. J. Robinson. Phosphorylation of dynamin ii at serine-764 is associated with cytokinesis. *Biochimica et Biophysica Acta (BBA) - Molecular Cell Research*, 1813(10):1689 – 1699, 2011. 28

[25] Y. A. Chizmadzhev, P. I. Kuzmin, D. A. Kumenko, J. Zimmerberg, and F. S. Cohen. Dynamics of fusion pores connecting membranes of different tensions. *Biophysical Journal*, 78(5):2241 – 2256, 2000. 128

[26] S. Cipolat, O. Martins de Brito, B. Dal Zilio, and L. Scorrano. Opa1 requires mitofusin 1 to promote mitochondrial fusion. *PNAS*, 101(45):15927–15932, 2004. 28

[27] O. Cremona, G. Di Paolo, M. R. Wenk, A. LÃ$\frac{1}{4}$thi, W. T. Kim, K. Takei, L. Daniell, Y. Nemoto, S. B. Shears, R. A. Flavell, D. A. McCormick, and P. De Camilli. Essential role of phosphoinositide metabolism in synaptic vesicle recycling. *Cell*, 99(2):179 – 188, 1999. 4, 8

[28] D. Cuvelier, P. Chiaruttini, P. Bassereau, and P. Nassoy. Pulling long tubes from firmly adhered vesicles. *Europhysics Letters*, 71(6):1015–1021, 2005. 18

[29] J. Dai and M Sheetz. Membrane tether formation from blebbing cells. *Biophysical Journal*, 77(6):3363–3370, 1999. 130

[30] H. Damke, T. Baba, D. E. Warnock, and S. L. Schmid. Induction of mutant dynamin specifically blocks endocytic coated vesicle formation. *The Journal of Cell Biology*, 127:915–934, 1994. 25, 26, 116

[31] D. Danino, K.-H. Moon, and J. E. Hinshaw. Rapid constriction of lipid bilayers by the mechanochemical enzyme dynamin. *J. Struct. Biol.*, 147:259–267, 2004. 29, 32, 35, 36, 47

[32] R. F. M. de Almeida, A. Fedorov, and M. Prieto. Sphingomyelin/phosphatidylcholine/cholesterol phase diagram: Boundaries and composition of lipid rafts. *Biophysical Journal*, 85(4):2406 – 2416, 2003. 19

[33] I. Derényi, F. Jülicher, and J. Prost. Formation and interaction of membrane tubes. *Physical Review Letters*, 88(88):238101, 2002. 17

[34] H.G. Döbereiner, J. Käs, D. Noppl, I. Sprenger, and E. Sackmann. Budding and fission of vesicles. *Biophysical Journal*, 65(4):1396 – 1403, 1993. 22

[35] Y. A. Domanov, S. Aimon, G. E. S. Toombes, M. Renner, F. Quemeneur, A. Triller, M. S. Turner, and P. Bassereau. Mobility in geometrically confined membranes. *PNAS*, 108(31):12605–12610, 2011. 19

[36] J. B. Doyon, B. Zeitler, J. Cheng, A. T. Cheng, J. M. Cherone, Y. Santiago, A. H. Lee, T. D. Vo, Y. Doyon, J. C. Miller, D. E. Paschon, L. Zhang, E. J. Rebar, P. D. Gregory, F. D. Urnov, and D. G. Drubin. Rapid and efficient clathrin-mediated endocytosis revealed in genome-edited mammalian cells. *Nature Cell Biology*, 13(3):331–337, 2011. 26

[37] E. Evans and D. Needham. Physical properties of surfactant bilayer membranes: thermal transitions, elasticity, rigidity, cohesion and colloidal interactions. *The Journal of Physical Chemistry*, 91(16):4219–4228, 1987. 11

[38] E. Evans and W. Rawicz. Entropy-driven tension and bending elasticity in condensed-fluid membranes. *Phys. Rev. Lett.*, 64:2094–2097, Apr 1990. 14, 15, 16

[39] K. Faelber, Y. Posor, S. Gao, M. Held, Y. Roske, D. Schulze, V. Haucke, F. NoÃ©, and O. Daumke. Crystal structure of nucleotide-free dynamin. *Nature*, 477:556–560, 2011. 28

[40] S. M. Ferguson, G. Brasnjo, M. Hayashi, M. Wölfel, C. Collesi, S. Giovedi, A. Raimondi, L.-W. Gong, P. Ariel, S. Paradise, E. O'Toole, R. Flavell, O. Cremona, G. Miesenböck, T. A. Ryan, and P. De Camilli. A selective activity-dependent requirement for dynamin 1 in synaptic vesicle endocytosis. *Science*, 316:570–574, 2007. 26, 34

[41] S. M. Ferguson and P. De Camilli. Dynamin, a membrane-remodelling gtpase. *Nature Reviews Molecular Cell Biology*, 2012. 28

[42] M. G. J. Ford, S. Jenni, and J. Nunnari. The crystal structure dynamin. *Nature*, 477:561–566, 2011. 28

[43] A. Fotin, Y. Cheng, N. Grogorieff, T. Walz, S. C. Harrison, and T. Kirchhausen. Structure of an auxilin-bound clathrin coat and its implications for the mechanism of uncoating. *Nature*, 432:649–653, 2004. 8

[44] A. Fotin, Y. Cheng, P. Sliz, N. Grigorieff, S. C. Harrison, T. Kirchhausen, and T. Walz. Molecular model for a complete clathrin lattic from electron cryomicroscpy. *Nature*, 432:573–579, 2004. 7

[45] H. Gao, D. Kadirjan Kalbach, J. E. Froehlich, and K. W. Osteryoung. Arc5, a cytosolic dynamin-like protein from plants, is part of the chloroplast division machinery. *PNAS*, 100(7):4328–4333, 2003. 28

[46] N. C. Gauthier, M. A. Fardin, P. Roca-Cusachs, and M. P. Sheetz. Temporary increase in plasma membrane tension coordinates the activation of exocytosis and contraction during cell spreading. *PNAS*, 108(35):14467–14472, 2011. 128

[47] C. G. Giraudo, C. Hu, D. You, A. M. Slovic, E. V. Mosharov, D. Sulzer, T. J. Melia, and J. E. Rothman. Snares can promote complete fusion and hemifusion as altenative outcomes. *Journal of Cell Biology*, 170(2):249–260, 2005. 127

[48] E. S. Gold, D. M. Underhill, N. S. Morrissette, J. Guo, M. A. McNiven, and A. Aderem. Dynamin 2 is required for phagocytosis in macrophages. *Journal of Experimental Medicine*, 190(12):1849–1856, 1999. 28

[49] C. Gu, S. Yaddanapudi, A. Weins, T. Osborn, J. Reiser, M. Pollak, J. Hartwig, and S. Sever. Direct dynamin actin interactions regulate the actin cytoskeleton. *The EMBO Journal*, 29:3593–3606, 2010. 28

[50] J. Guizetti and D. W. Gerlich. Escrt-iii polymers in membrane neck constriction. *Trends in Cell Biology*, 22(3):133 – 140, 2012. 124

[51] O. Haller, P. Staeheli, and G. Kochs. Interferon induced mx proteins in antiviral host defense. *Biochimie*, 89:812–818, 2007. 28

[52] M. Hayashi, A. Raimondi, E. O'Toole, S. Paradise, C Collesi, O. Cremona, S. M. Ferguson, and P. De Camilli. Cell- and stimulus-dependent heterogeneity of synaptic vesicle endocytic recycling mechanisms revealed by studies of dynamin 1-null neurons. *PNAS*, 105:2175–2180, 2008. 27, 34

[53] V. Heinrich and R. Waugh. A piconewton force transducer and its application to measurement of the bending stiffness of phospholipid membranes. *Annals of Biomedical Engineering*, 24:595–605, 1996. 18

[54] W. Helfrich. Elastic properties of lipid bilayers - theory and possible experiments. *Zur Naturforchung*, 28:693–7034, 1973. 13, 14

[55] W. Helfrich and R. M. Servuss. Undulations, steric interaction and cohesion of fluid membranes. *Nuovo Cimento*, 3D:137–151, 1984. 14

[56] J. R. Henley, E. W. A. Krueger, B. J. Oswald, and M. A. McNivem. Dynamin-mediated internalization of caveolae. *Journal of Cell Biology*, 141:85–99, 1998. 28

[57] W. M. Henne, E. Boucrot, M. Meinecke, E. Evergren, Y. Vallis, R. Mittal, and H. T. McMahon. Fcho proteins are nucleators of clathrin-mediated endocytosis. *Science*, 328:1281–1284, 2010. 6

[58] J. E. Heuser and R. G. W. Anderson. Hypertonic media inhibit receptor-mediated endocytosis by blocking clathrin-coated pit formation. *Journal of Cell Biology*, 108:389–400, 1989. 130

[59] J. E. Heuser and T. S. Reese. Structural changes after transmitter release at the frog neuromuscular junction. *Journal of Cell Biology*, 88:564–580, 1981. 9

[60] J. E. Hinshaw. Dynamin and its role in membrane fission. *Annual Review of Cell and Developmental Biology*, 12:737–519, 2000. 28

[61] J. E. Hinshaw and S. L. Schmid. Dynamin self-assembles into rings suggesting a mechanism for coated vesicle budding. *Nature*, 374(6518):190–192, 1995. 29, 32

[62] V. W. Hsu and J.-S. Yang. Mechanisms of cop1 vesicle formation. *FEBS Letters*, 583(23):3758 – 3763, 2009. 5

[63] J. H. Hurley and P. I. Hanson. Membrane budding and scission by the escrt machinery: it's all in the neck. *Nature*, 11:556–566, 2010. 124, 125

[64] T. Itoh, K. S. Erdmann, A. Roux, B. Habermann, H. Werner, and P. De Camilli. Dynamin and the actin cytoskeleton cooperatively regulate plasma membrane invagination by bar and f-bar proteins. *Developmental Cell*, 9:791–804, 2005. 28, 36, 129, 130

[65] D. Jensen and R. Schekman. Copii-mediated vesicle formation at a glance. *Journal of Cell Science*, 124:1–4, 2011. 5

[66] W. J. Jockusch, G. J. K. Praefcke, H. T. McMahon, and L. Lagnado. Clathrin-dependent and clathrin-independent retrieval of synaptic vesicles in retinal bipolar cells. *Neuron*, 46(6):869–878, 2005. 9

[67] N. Kahya, D. Scherfeld, K. Bacia, B. Poolman, and P. Schwille. Probing lipid mobolity of raft-exhibiting model membranes by fluorescence correlation spectroscopy. *Journal of Biological Chemistry*, 278(30):28109–28115, 2003. 19

[68] E. Karatekin, J. Di Giovanni, C. Iborra, J. Coleman, B. O'Shaughnessy, M. Seagar, and J. E. Rothman. A fast, single-vesicle fusion assay mimics physiological snare requirements. *PNAS*, 107(8):3517–3521, 2010. 127

[69] W. T. Kim, S. Chang, L. Daniell, O. Cremona, G. Di Paolo, and P. De Camilli. Delayed reentry of recycling vesicles into the fusion-competent synaptic vesicle pool in synaptojanin 1 knockout mice. *PNAS*, 99(26):17143–17148, 2002. 8

[70] K. Kinosita, R. Yasuda, H. Noji, S. Ishiwata, and M. Yoshida. F1-atpase: A rotary motor made of a single molecule. *Cell*, 93:21–24, 1998. 122

[71] J. H. Koenig and K. Ikeda. Disappearance and reformation of synaptic vesicle membrane upon transmitter release observed under reversible blockage of membrane retrieval. *J. Neurosci.*, 9:3844–3860, 1989. 25

[72] C. A. Konopka, J. B. Schleede, A. R. Skop, and S. Y. Bednarek. Dynamin and cytokinesis. *Traffic*, 7:239–247, 2006. 28

[73] G. Koster, M. VanDuijn, B. Hofs, and M. Dogterom. Membrane tube formation from giant vesicles by dynamic association of motor proteins. *PNAS*, 100(26):15583–15588, 2003. 18

[74] M. M. Kozlov, H. T. McMahon, and L. V. Chernomordik. Protein-driven membrane stresses in fusion and fission. *Trends in Biochemical Sciences*, 35(12):699–706, 2010. 12

[75] Y. Kozlovsky and M. M. Kozlov. Stalk model of membrane fusion: Solution of energy crisis. *Biophysical Journal*, 82(2):882 – 895, 2002. 127

[76] Y Kozlovsky and M. M. Kozlov. Membrane fission: Model for intermediate structures. *Biophysical Journal*, 85(1):85–96, 2003. 22, 35, 127, 128

[77] R. Kwok and E. Evans. Thermoelasticity of large lecithin bilayer vesicles. *Biophysical Journal*, 35(3):637 – 652, 1981. 15, 16

[78] T. Lang. Snares proteins and membrane rafts. *The Journal of Physiology*, 585:693–698, 2007. 128

[79] T. Lang, D. Bruns, D. Wenzel, D. Riedel, P. Holroyd, C. Thiele, and R. Jahn. Snares are concentrated in cholesterol-dependent clusters that define docking and fusion sites for exocytosis. *The EMBO Journal*, 20(9):2201–2213, 2001. 128

[80] E. Lee and P. De Camilli. Dynamin at actin tails. *PNAS*, 99(1):161–166, 2002. 28

[81] M. C. S. Lee, L. Orci, S. Hamamoto, E. Futai, M. Ravazzola, and R. Schekman. Sar1p n-terminal helix initiates membrane curvature and completes the fission of a copii vesicle. *Cell*, 122(4):605–617, 2005. 6

[82] M. Lenz, D. J. G. Crow, and J.-F. Joanny. Membrane buckling induced by curved filaments. *Phys. Rev. Lett.*, 103:038101, 2009. 125

[83] M. Lenz, J. Prost, and J.-F. Joanny. Mechanochemical action of the dynamin protein. *Physical Review E*, 78:011911, 2008. 34, 47

[84] M. Leonard, B. D. Song, R. Ramachandran, and S. L. Schmid. Robust colorimetric assays for dynamin's basal and stimulated gtpase activities. *Methods in Enzymology*, 404:490–503, 2005. 32

[85] F. Li, F. Pincet, E. Perez, W. S. Eng, T. J. Melia, J. E. Rothman, and D. Tareste. Energetics and dynamics of snarepin folding across lipid bilayers. *Nature Structural and Molecular Biology*, 14(10):890–896, 2007. 127

[86] Reinhard Lipowsky. Budding of membranes induced by intramembrane domains. *Journal de Physique II*, 2(10):1825–1840, 1992. 22

[87] B. Marks, M. H. B. Stowell, Y. Vallis, I. G. Mills, A. Gibson, C. R. Hopkins, and H. T. McMahon. Gtpase activity of dynamin and resulting conformation change are essential for endocytosis. *Nature*, 410:231–235, 2001. 32, 34, 116

[88] D. Marsh. Elastic curvature constants of lipid monolayers and bilayers. *Chemistry and Physics of Lipids*, 144:146–159, 2006. 16

[89] L. Mathivet, S. Cribier, and P. F. Devaux. Shape change and physical properties of giant phospholipid vesicles prepared in the presence of an ac electric field. *Biophysical Journal*, 70:1112–1121, 1996. 15

[90] H. T. McMahon and E. Boucrot. Molecular mechanism and physiological functions of clathrin-mediated endocytosis. *Nature Reviews, Molecular Cell Biology*, 12(8):517–533, 2011. 7, 8

[91] J. A. Mears, L. L. Lackner, S. Fang, E. Ingermann, J. Nunnari, and J. E. Hinshaw. Conformational changes in dnm1 support a contractile mechanism for mitochondrial fission. *Nature Structural and Molecular Biology*, 18(1):20–27, 2011. 124

[92] S. Meeusen, J. M. McCaffery, and J. Nunnari. Mitochondrial fusion intermediates revealed in vitro. *Science*, 305:1747–1752, 2004. 127

[93] C. J. Merrifield, M. E. Feldman, L. Wan, and W. Almers. Imaging actin and dynamin recruitment during invagination of single clathrin-coated pits. *Nature Cell Biology*, 4(9):691–698, 2002. 26

[94] T. Misaka, T. Miyashita, and Y. Kubo. Primary structure of a dynamin-related mouse mitochondrial gtpase and its distribution in brain, subcellular localization, and effect on mitochondrial morphology. *Journal of Biological Chemistry*, 277:15834–15842, 2002. 28

[95] N. Mohandas and E. Evans. Mechanical properties of the red cell membrane in relation to molecular structure and genetic defects. *Annual Review of Biophysics and Biomolecular Structure*, 23:787–818, 1994. 16

[96] S. Morlot, M. Lenz, J. Prost, J.-F. Joanny, and A. Roux. Deformation of dynamin helices damped by membrane friction. *Biophysical Journal*, 99(11):3580–3588, 2010. 122, 124

[97] H. Noji, R. Yasuda, M. Yoshida, and K. Kinosita. Direct observation of the rotation of f1 atpase. *Nature*, 386:299–302, 1997. 122

[98] S. Pautot, B. J. Frisken, and D. A. Weitz. Engineering asymmetric vesicles. *PNAS*, 100(19):10718–10721, 2003. 131

[99] S. Peel, P. Macheboeuf, N. Martinelli, and W. Weissenhorn. Divergent pathways lead to escrt-iii-catalyzed membrane fission. *Trends in Biochemical Sciences*, 36(4):199 – 210, 2011. 6

[100] R. M. Perera, R. Zoncu, L. Lucast, P. De Camilli, and D. Toomre. Two synaptojanin 1 isoforms are recruited to clathrin-coated pits at different stages. *PNAS*, 103(51):19332–19337, 2006. 8

[101] T. R. Powers, G. Huber, and R. E. Goldstein. Fluid-membrane tethers: Minimal surfaces and elastic boundary layers. *Phys. Rev. E*, 65:041901, Mar 2002. 17

[102] G. J. K. Praefcke and H. T. McMahon. The dynamin superfamily: Universal membrane tubulation and fission molecules? *Nature Reviews. Molecular Cell Biology*, 5:133–147, 2004. 28

[103] T. Pucadyil and S. L. Schmid. Real-time visualization of dynamin-catalyzed membrane fission and vesicle release. *Cell*, 135:1263–1275, 2008. 36, 37, 117, 129

[104] T. J. Pucadyil and S. L. Schmid. Supported bilayers with excess membrane reservoir: A template for reconstituting membrane budding and fission. *Biophysical Journal*, 99:517–525, 2010. 36

[105] A. Raimondi, S. M. Ferguson, X. Lou, M. Armbruster, S. Paradise, S. Giovedi, M. Messa, N. Kono, J. Takasaki, V. Cappello, E. O'Toole, T. A. Ryan, and P. De Camilli. Overlapping role of dynamin isoforms in synaptic vesicle endocytosis. *Neuron*, 70(6):1100–1114, 2011. 26

[106] R. Ramachandran, T. J. Pucadyil, Y.-W. Liu, S. Acharya, M. Leonard, V. Lukiyanchuk, and S. L. Schmid. Membrane insertion of the pleckstrin homology domain variable loop 1 is critical for dynamin-catalyzed vesicle scission. *Molecular Biology of the Cell*, 20:4630–4639, 2009. 124

[107] D. Raucher and M. P. Sheetz. Characteristics of a membrane reservoir buffering membrane tension. *Biophysical Journal*, 77(4):1992–2002, 1999. 20

[108] W. Rawicz, K. C. Olbrich, T. J. McIntosh, D. Needham, and E. Evans. Effect of chain length and unsaturation on elasticity of lipid bilayers. *Biophys. J.*, 79(1):328–339, 2000. 16, 17

[109] W. Rawicz, B. A. Smith, T. J. McIntosh, S. A. Simon, and E. Evans. Elasticity, strength, and water permeability of bilayers that contain raft microdoamin-forming lipids. *Biophys. J.*, 94:4725–4736, 2008. 16, 19

[110] N. Ringstad, H. Gad, P. Löw, G. Di Paolo, L. Brodin, O. Shupliakov, and P. De Camilli. Endophilin/sh3p4 is required for the transition from early to late stages in clathrin-mediated synaptic vesicle endocytosis. *Neuron*, 24:143–154, 1999. 7

[111] A. Roux and B. Antonny. The long and short of membrane fission. *Cell*, 135(7):1163 – 1165, 2008. 129

[112] A. Roux, N. Biais, and P. Bassereau. Import-export dans la cellule. *Pour la Science*, pages 46–52, 2007. 6

[113] A. Roux, G. Cappello, J. Cartaud, J. Prost, B. Goud, and P. Bassereau. A minimal system allowing tubulation with molecular motors pulling on giant liposomes. *PNAS*, 99:5394–5399, 2002. 18

[114] A. Roux, D. Cuvelier, P. Nassoy, J. Prost, P. Bassereau, and B. Goud. Role of curvature and phase transition in lipid sorting and fission of membrane tubules. *The EMBO Journal*, 24:1537.1545, 2005. 22, 124

[115] A. Roux, G. Koster, M. Lenz, B. Sorre, J.-B. Manneville, P. Nassoy, and P. Bassereau. Membrane curvature controls dynamin polymerization. *PNAS*, 107(9):4141–4146, 2010. 19, 29, 32, 114

[116] A. Roux, K. Uyhazi, A. Frost, and P. De Camilli. Gtp-dependent twisting of dynamin implicates constriction and tension in membrane fission. *Nature*, 441:528–531, 2006. 36, 47

[117] P. G. Saffman and M. Delbrück. Brownian motion in biological membranes. *PNAS*, 72(8):3111–3113, 1975. 19

[118] D. M. Schlossman, S. L. Schmid, W. A. Braell, and J. E. Rothman. An enzyme that removes clathrin coats: purification of an uncoating atpase. *Journal of Cell Biology*, 99:723–733, 1984. 8

[119] O. Schmidt and D. Teis. The escrt machinery. *Current Biology*, 22(4):R116 – R120, 2012. 124

[120] M. J. Schnitzer and S. M. Block. Kinesin hydrolyses one atp per 8 nm step. *Nature*, 388:386 – 390, 1997. 121

[121] U. Seifert, K. Berndl, and R. Lipowsky. Shape transformations of vesicles: Phase diagram for spontaneous-curvature and bilayer-coupling models. *Physical Review A*, 44(2):1182–1202, 1991. 13

[122] U. Sever, H. Damke, and S. L. Schmid. Garrotes , springs , ratchets , and whips : Putting dynamin models to the test. *Traffic, year = 2000, volume = 1, pages = 385-392,*. 34

[123] R. Shlomovitz, N. S. Gov, and A. Roux. Membrane-mediated interactions and the dynamics of dynamin oligomers on membrane tubes. *New Journal of Physics*, 13:065008, 2011. 123

[124] H. S. Shpetner and R. B. Vallee. Identification of dynamin, a novel mechanochemical enzyme that mediates interactions between microtubules. *Cell*, 59(3):421–432, 1989. 25

[125] H. S. Shpetner and R. B. Vallee. Dynamin is a gtpase stimulated to high levels of activity by microtubules. *Nature*, 355(6362):733–735, 1992. 25

[126] D. P. Siegel. The gaussian curvature elastic energy of intermediates in membrane fusion. *Biophysical Journal*, 95(11):5200–5215, 2008. 17, 21

[127] D. P. Siegel and M. M. Kozlov. The gaussian curvature elastic modulus of n-monomethylated dioleoylphosphatidylethanolamine: Relevance to membrane fusion and lipid phase behavior. *Biophysical Journal*, 87:366–374, 2004. 21

[128] B. Sinha, D. Köster, R. Ruez, P. Gonnord, M. Bastiani, D. Abankwa, R. V. Stan, G. Butler Browne, B. Vedie, L. Johannes, N. Morone, R. G. Parton, G. Raposo, P. Sens, C. Lamaze, and P. Nassoy. Cells respond to mechanical stress by rapid disassembly of caveolae. *Cell*, 144(3):402–413, 2011. 20

[129] V. Slepnev and P. De Camilli. Accessory factors in clathrin-dependent synaptic vesicle endocytosis. *Nature reviews. Neuroscience*, 1(3):161–172, 2000. 6

[130] B. Sorre, A. Callan-Jones, J.-B. Manneville, P. Nassoy, J-F. Joanny, J. Prost, B. Goud, and P. Bassereau. Curvature-driven lipid sorting needs proximity to a demixing point and is aided by proteins. *PNAS*, 106:5622–5626, 2009. 19

[131] B. Sorre, A. Callan-Jones, J. Manzi, B. Goud, J. Prost, P. Bassereau, and A. Roux. Nature of curvature coupling of amphiphysin with membranes depends on its bound density. *PNAS*, 109:173–178, 2011. 19

[132] M. H. B. Stowell, B. Marks, P. Wigge, and H. T. McMahon. Nucleotide-dependent conformational changes in dynamin: evidence for a mechanochemical molecular spring. *Nat. Cell. Biol.*, 1:27–32, 1999. 29, 32

[133] T. C. Südhof and J. E. Rothman. Membrane fusion: Grappling with snare and sm proteins. *Science*, 323:474–477, 2009. 6

[134] D. Suen, K. Norris, and R. Youle. Mitochondrial dynamics and apoptosis. *Genes and Development*, 22:1577–1590, 2008. 28

[135] A. Sundborger, C. Soderblom, O. Vorontsova, E. Evergren, J. E. Hinshaw, and O. Shupliakov. An endophilin-dynamin complex promotes budding of clathrin-coated vesicles during synaptic vesicle recycling. *Journal of Cell Science*, 124:133–143, 2010. 129

[136] S. Svetina, B. Zeks, R. E. Waugh, and R. M. Raphael. Theoretical analysis of the effect of the transbilayer movement of phospholipid molecules on the dynamic behavior of a microtube pulled out of an aspirated vesicle. *European Biophysics Journal*, 27:197–209, 1998. 17

[137] Sharon M Sweitzer and Jenny E Hinshaw. Dynamin undergoes a gtp-dependent conformational change causing vesiculation. *Cell*, 93(6):1021–1029, 1998. 29, 32

[138] K. Takei, P. S. McPherson, S. L. Schmid, and P. De Camilli. Tubular membrane invaginations coated by dynamin rings are induced by gtpγs in nerve terminals. *Nature*, 374:186–190, 1995. 34

[139] M. J. Taylor, D. Perrais, and C. J. Merrifield. A high precision survey of the molecular dynamics of mammalian clathrin-mediated endocytosis. *PLoS Biology*, 9:e1000604, 2011. 8, 9, 26, 129

[140] M. R. Terebiznik, O. V. Vieira, S. L. Marcus, A. Salde, C. M. Yip, W. S. Trimble, T. Meyer, B. B. Finlay, and S. Grinstein. Elimination of host cell ptdins(4,5)p(2) by bacterial sigd promotes membrane fission during invasion by salmonella. *Nature Cell Biology*, 4(10):166–113, 2002. 117

[141] H. M. Thompson, A. R. Skop, U. Euteneuer, B. J. Meyer, and M. A. McNiven. The large gtpase dynamin associates with the spindle midzone and is required for cytokinesis. *Current Biology*, 12(24):2111 – 2117, 2002. 28

[142] A. Tian and T. Baumgart. Sorting of lipids and proteins in membrane curvature gradients. *Biophysical Journal*, 96(7):2676–2688, 2009. 19

[143] P. L. Tuma and C. A. Colins. Activation of dynamin gtpase is a result of positive cooperativity. *Journal of Biological Chemistry*, 269(49):30842–30847, 1994. 30, 32

[144] E. Ungewickell, H. Ungewickell, S. E. H. Holstein, R. Lindner, K. Prasad, W. Barouch, B. Martini, L. E. Greene, and E. Eisenberg. Role of auxilin in uncoating clathrin-coated vesicles. *Nature*, 378:632–635, 1995. 8

[145] R. D. Vale. The molecular motor toolbox for intracellular transport. *Cell*, 112(4):467 – 480, 2003. 6

[146] A. M. van der Bliek and E. M. Meyerowitz. Dynamin-like protein encoded by the drosophila shibire gene associated with vesicular traffic. *Nature*, 351:411–414, 1991. 25, 34

[147] G. van Meer, D. Voelker, and G. Feigenson. Membrane lipids: where they are and how they behave. *Nature reviews. Molecular cell biology*, 9(2):112–24, 2008. 4, 5

[148] K. Visscher, M. J. Schnitzer, and S. M. Block. Single kinesin molecules studied with a molecular force slamp. *Nature*, 400(6740):184–189, 1999. 122

[149] D. E. Warnock, J. E. Hinshaw, and S. L. Schmid. Dynamin self-assembly stimulates its gtpase activity. *The Journal of Biological Chemistry*, 271(37):22310–22314, 1996. 32, 117

[150] R. Waugh and E.A. Evans. Thermoelasticity of red blood cell membrane. *Biophysical Journal*, 26(1):115 – 131, 1979. 15

[151] R E Waugh. Surface viscosity measurements from large bilayer vesicle tether formation. ii. experiments. *Biophys. J.*, 38(1):29–37, April 1982. 18

[152] P. Wigge and H. T. McMahon. The amphiphysin family of proteins and their role in endocytosis at the synapse. *Trends in Neurosciences*, 21(8):339 – 344, 1998. 7

[153] P. Wigge, Y. Vallis, and H. T. McMahon. Inhibition of receptor-mediated endocytosis by the amphiphysin sh3 domain. *Current Biology*, 7(8):554–560, 1997. 8

[154] K. Wilsbach and G. S. Payne. Vps1p, a member of the dynamin gtpase family, is necessary for golgi membrane protein retention in saccharomyces cerevisiae. *The EMBO Journal*, 12(8):3049–3059, 1993. 28

[155] T. Wollert, C. Wunder, J. Lippincott-Schwartz, and J. H. Hurley. Membrane scission by the escrt-iii complex. *Nature*, 458(7235):172–177, 2009. 125

[156] T. Yamashita, T. Hige, and T. Takahashi. Vesicle endocytosis requires dynamin-dependent gtp hydrolysis at a fast cns synapse. *The Journal of Biological Chemistry*, 271(37):22310–22314, 1996. 9

[157] P. Zhang and J. Hinshaw. Three-dimensional reconstruction of dynamin in the constricted state. *Nature Cell Biology*, 3(10):922–926, 2001. 29, 35